NON-LINEAR DEFORMATION OF ROCKS

A thesis submitted to the
University of London
(Imperial College of Science and Technology)

for the degree of
Doctor of Philosophy in the Faculty of Engineering

by

Arabinda Lochan Tamuly Phukan, B.Sc.(Engg.)

Imperial College
January, 1968

BIBL. LOND. UNIV.

ABSTRACT

An extensive survey of the deformation problems in the field of rock mechanics is presented. The deformation of most rocks is non-linear and has an irreversible component. This non-linearity and irreversibility may arise from a macro-fissure system in what is inherently a linear elastic rock or it may be intrinsic to a porous micro-fissured rock such as a sandstone. The results of a series of tests carried out to investigate the intrinsic non-linearity of a relatively homogeneous sandstone are presented. To study the deformation of the specimens, they have been loaded cyclically in compression under confining pressures of 0, 150 and 500 p.s.i. The degree of non-linearity varies with the porosity as does the energy dissipation under cyclic loading. Compressibility is found to be essentially path independent and the relationship between compressibility and the total principal stress constitutes a real material property. The real behaviour of sandstone is more complex than that considered in current theories of composite media. The effects of wetting indicate greater non-linearity, hysteresis and residual strains on unloading for a given porosity and pressure.

The finite element method is described and extended to take into account material non-linear properties. Stresses in a non-linear flexibly loaded half-space were computed using the finite element method and a variety of non-linear material

laws. Results reveal a correspondence with results of field plate bearing tests and the vertical stresses agree remarkably well with the classical linear solution. The horizontal and shear stresses differ more.

A lumped parameter model proposed by Ang and Harper (1963) is used to compute stresses and displacements in an excavation problem and the development of plastic regions due to increments of self weight are recorded. This model is found to be efficient and simple for elastic solutions, but must be used with considerable caution when accounting for plastic behaviour.

TABLE OF CONTENTS

		Page
ABSTRACT		1
TABLE OF CONTENTS		3
CHAPTER 1 - INTRODUCTION		6
1.1	Field of Rock Mechanics	6
1.2	Non-Linear Behaviour of Rocks	8
1.3	Numerical Methods of Solution	11
1.4	Contents of this Thesis	13
CHAPTER 2 - BOUNDARY VALUE PROBLEMS OF INTEREST IN ROCK MECHANICS		15
2.0	Introduction	15
2.1	Outline of Deformation Problems	16
2.2	Ideal Constitute Equation	19
2.3	Real Behaviour of Rocks	21
2.4	Methods of Solution	24
CHAPTER 3 - ORIGIN AND EVIDENCE FOR NON-LINEAR BEHAVIOUR OF ROCKS		26
3.0	Introduction	26
3.1	Analysis of Non-linear Behaviour	27
3.1.1	Open cracks	28
3.1.2	Closed cracks (loading)	32
3.1.3	Closed cracks (unloading)	35
3.2	Effects of Cracks on the Compressibility of rocks	37
3.2.1	Spherical pores	39
3.2.2	Narrow cracks	40
3.3	Effect of Cracks in Rocks on Poisson's Ratio	42
3.4	Discussion of Non-Linear Analysis	46
CHAPTER 4 - EXPERIMENTAL STUDIES OF DEFORMATION OF A SANDSTONE		50
4.0	Preparation and Description of Specimens	50
4.1	Method of Determining Porosity of Rocks	52
4.2	Experimental Apparatus	55
4.2.1	Introduction	55

4.2.2	Uniaxial compression test frame	55
4.2.3	Triaxial test apparatus	56
4.2.4	Measurement of strain	57
4.2.5	Checking of gauge factor	58
4.3	Experimental Procedure	60
4.4	Discussion of Test Results	62
4.4.1	Dry tests	62
4.4.2	Wet tests	74

CHAPTER 5 - FINITE ELEMENT METHOD 78

5.0	Introduction	78
5.1	Basis of the Finite Element Method	79
5.2	The Displacement Method	81
5.3	Stiffness Matrix of the Element	82
5.4	Assemblage of Stiffness Matrix of the Element and Formulation of Equilibrium Equations at Each Nodal Point	88
5.5	Results Obtainable from the Solution of the Equilibrium Equations	91
5.6	Method of Solution of Equilibrium Equation	91
5.7	Over-Relaxation Factor and Error Criteria	93
5.8	Influence of Mesh Size	94
5.9	Stress Ambiguity	95
5.10	Layered System	98

CHAPTER 6 - SOLUTION OF A BOUNDARY VALUE PROBLEM BY THE FINITE ELEMENT METHOD USING NON-LINEAR STRESS-STRAIN RELATIONS 99

6.0	Introduction	99
6.1	Non-Linear Analysis by the Finite Element Method	101
6.2	Formulation of the Problem and Method of Solution	103
6.3	Discussion of Results	106
6.3.1	Results of model 1 and model 2	107
6.3.2	Results of model 3	109
6.3.3	Results of model 1 with varying Poisson's ratio	110
6.4	Practical Aspects of Non-Linear Solution .	111

CHAPTER 7 - STRESSES IN AN EXCAVATION USING A LUMPED PARAMETER MODEL 114

7.0	Introduction	114
7.1	Description of Lumped Parameter Model . .	116
7.2	Formulation of the Problem	119

7.2.1 Elastic stress-strain relation 119
7.2.2 Yield criterion 120
7.2.3 Plastic stress-strain relationship 120
7.3 Boundary Conditions 122
7.4 Equations of Equilibrium 123
7.5 Procedure for the Solution of the Problem 124
7.6 Discussion of Results 125

CHAPTER 8 - CONCLUSIONS 129

APPENDIX A Sliding after Crack Close 133

APPENDIX B Compressibility as a Function of Rock Composition 135

APPENDIX C Derivation of Stiffness for an Arbitrarily Oriented Triangular Element 137

APPENDIX D Computer Programme: Finite Element Method 143

APPENDIX E Numerical Method of Computation: Lumped Parameter Model 146

ACKNOWLEDGEMENTS 150

REFERENCES 151

CHAPTER 1

INTRODUCTION

1.1 FIELD OF ROCK MECHANICS

"Rock mechanics is the theoretical and applied science of the mechanical behaviour of rock; it is that branch of mechanics concerned with the response of the rock to the force fields of its physical environment."*

This definition, given by a group of workers in rock mechanics emphasizes the field of rock mechanics. Only recently a considerable effort has been made in many countries to obtain a better knowledge of mechanical properties and characteristics of rocks and to develop a proper science of rock mechanics. The knowledge in this field is applicable to such different branches as civil engineering, mining engineering and geophysics. It is beyond the scope of this study to elaborate all the problems which can be included in the field of rock mechanics. Morgenstern (1965), Judd (1964), Obert and Duvall (1967) illustrate the various problems which are studied in the field of rock mechanics. As we are mainly interested in the civil engineering side, some of the problems where the application of rock mechanics is possible, are mentioned in the following paragraph.

---

* Definition by the Committee on Rock Mechanics, National Academy of Science in Rock Mechanics Research, Publication 1466, National Academy of Science, National Research Council, Washington, D.C., 1966.

The development of new techniques in concrete technology and metallurgy allow higher permissible stresses for civil engineering structures. Hence rocks are being subjected to ever increasing loads and stresses. For example, the design stresses in concrete of arch dams are now far greater than the design stresses used twenty years ago. In foundation engineering, designers are tending to transfer their heavy superstructural and foundation loads to piles which may be taken down to rock where it occurs at an economic depth below ground level. In hydro-electric projects, higher heads require that pressure tunnels, surge chambers, the foundations for penstocks and power house be designed to meet a new and greater range of pressures. Many applications of rock mechanics to such problems require a knowledge of the deformation properties of rocks. Indeed, the stress level in problems mentioned above, is seldom high enough to produce failure of most intact rocks although the strength along pre-existing discontinuities may be a controlling factor. These deformation problems are further discussed in the following chapter.

Thus the development of the field of rock mechanics will undoubtedly help the civil engineer to design their structures economically. Various authors like Jaeger (1964), Serafim (1964, 1965), Isaacson (1962) have contributed to the application of rock mechanics in the design of dams, the linings of pressure tunnels and so on. Further

knowledge of the mechanical properties of rocks under different conditions will certainly contribute to the rational design of these structures.

1.2 NON-LINEAR BEHAVIOUR OF ROCKS

The linear theory of elasticity is commonly used in solving rock deformation problems. However, it is well known that the stress-strain behaviour of rocks is non-linear. This non-linearity is particularly noticeable in the low stress range and therefore is of considerable importance in civil engineering design.

It is helpful to classify the nature of the non-linearity into two groups. If a specimen say, unweathered granite or basalt is tested in the laboratory a linear stress-strain relation may provide an adequate representation of its mechanical behaviour up to the stress level at which micro-cracking is initiated. However, in the field the rock may be jointed and faulted. Its response in bulk to loading under these conditions is likely to be non-linear. This will be called extrinsic non-linearity. On the other hand, if a specimen of sandstone is tested in the laboratory it will often display a non-linear stress-strain curve even at stress levels too low to cause local failure. This behaviour will be called intrinsic non-linearity. In nature, it may also be fissured and its response to loading will then be due to both intrinsic and extrinsic non-linearity. This distinction

between intrinsic and extrinsic non-linearity is essentially a matter of scale. There is no implication here that the physical basis need differ in the two cases. Intrinsic non-linearity is however studied more easily and if a clear understanding of it is obtained it should be possible to predict, at least qualitatively, how the pattern of joints and similar discontinuities in a rock mass alters its deformation properties.

The non-linear behaviour of rock under low stress has been noted before. For example, Nishihara (1957) reported the results of uniaxial compression tests at low stresses on a series of rocks and observed that in general the stress-strain relation was curved showing increasing stiffness with increasing strain and displayed hysteresis on unloading. Moreover, when the stress had been completely removed, it was observed that the strain had not fully recovered. The non-linearity was rightly attributed to the influence of cracks and pores in the specimen. In discussing the irrecoverable strain, Nishihara considered two alternative explanations, and concluded that the set of the specimen was due to the viscoelastic properties of rock giving retarded elastic rebound. This explanation was favoured over one invoking intercrystalline friction because the experimental evidence for a wet sandstone specimen revealed almost complete time-dependent recovery. Nishihara suggested that permanent plastic strain would occur at stress levels higher than that

used in the tests that he described.

The influence of pores and cracks on the elastic properties of a rock has recently received detailed theoretical consideration by Walsh (1965). As a model, Walsh considered an isotropic linear elastic solid filled with a low concentration of planar elliptical cracks and he derived a relation between the apparent Young's modulus for the model with cracks in terms of the Young's modulus and Poisson's ratio of the uncracked material and the average crack length. Since the cracks close under increasing compressive stress, the material becomes stiffer. Walsh also showed that even when the applied stress is high enough to close all the cracks, the modulus may still not be that of the uncracked material because of the possibility of frictional sliding at the faces of cracks. Another important result that emerged from this study is that cracks which have slid do not immediately slide in the opposite sense upon decrease of stress and hence the initial slope of the unloading curve should be comparable with the Young's modulus of the uncracked material. These considerations will be given a more elaborate treatment in Chapter 3.

Various authors such as Handin (1953), Griggs (1936), Birch (1942), Fatt (1955), Turner et al (1953), Robertson (1955), have studied the deformation characteristics of rocks at high to moderate pressure and temperature such as exists at relatively great depths below the surface of the earth and most of the experimenters recorded the inelastic

behaviour of rocks in the low stress level. But there is hardly any detailed investigation to study the non-linear behaviour of rocks in the low stress level which is of considerable importance to civil engineering problems. Therefore one of the primary objects of this research programme is to investigate intrinsic non-linearity of rock like sandstone at different conditions and to determine the parameters that influence the non-linear behaviour. It is also possible to investigate the applicability of the theoretical considerations of Walsh and others. This will help to formulate a representative non-linear stress-strain relation for rock in the low stress range which could be used to solve boundary value problems. This experimental study is presented in Chapter 4.

1.3 NUMERICAL METHODS OF SOLUTION

The various numerical methods of solution of plane and axisymmetric boundary value problems can be categorized as one of two types.

(i) Methods that depend directly on, or are suggested by variational techniques. This approach is based directly on the use of calculus of variations. With the aid of certain minimum principles which characterize the equilibrium states of an elastic body, the field equations of the body are derived in terms of approximate functions. Examples of this method are: the Ritz method, the Galerkin method.

The use of these methods, however, is seriously hampered by certain limitations. The choice of approximating functions in the approximate solution is governed by the shape of the region and by the form of the boundary condition. Furthermore, even if such functions can be found, the extent of the computations may become prohibitive.

(ii) Numerical methods which depend on the idea of discretization of the continuous body. The most universal of such numerical methods is the method of finite differences. In this method the governing differential equation is replaced by an approximate difference equation thus reducing the problem of solving a partial differential equation to solving a system of algebraic equations. The main disadvantage of the finite difference method is that it gives numerical values for the unknown functions at a set of discrete points instead of approximating functions defined over a region.

The finite element method offers a compromise between the above two approaches in the sense that

(a) approximating functions are defined over a region instead of at a point, while

(b) the problem is reduced to the solution of a system of algebraic equations.

The basic concept of the finite element analysis is that a continuum (or solid) is replaced by an assemblage of a finite number of elements interconnected only at the element model points. With this idealization, a problem in continuum

or solid mechanics is transformed into a related problem for an articulated structure to which standard methods of structural analysis can be applied. It is important to note that the replacement of a contimuum or a solid by an equivalent assemblage of articulated elements is a physical approximation and does not involve a mathematical approximation at this initial stage. In this sense, the finite element method differs from the finite difference method which is an approximate mathematical representation of the governing differential equations of the solid (Rashid, 1964).

In this study the finite element method is used to obtain solutions with a non-linear stress-strain relation to common configurations as engineering interest. Such solutions could, of course, also be used directly in the design of structures that interact with rock.

1.4 CONTENTS OF THIS THESIS

The research work reported in this thesis may be divided broadly into three main parts. The first part is concerned with the analysis of different deformation problems in civil engineering and the treatment of mathematical models which may be conveniently used to explain the behaviour of rock containing different structural defects. The second part of the thesis is the experimental studies of the deformation of a sandstone at room temperature and at a stress level which is considered not to induce any cracks

inside the sample. The third part is devoted to the numerical analysis of boundary value problems by the finite element method using non-linear stress-strain relationships. An extensive survey of the computational work involved is illustrated and the author's computer programme is presented. Further, a lumped parameter model developed by Ang and Harper (1963) is presented to study the stress configuration behind vertical excavation due to self weight.

CHAPTER 2

BOUNDARY VALUE PROBLEMS OF INTEREST IN ROCK MECHANICS

2.0 INTRODUCTION

Problems in Rock Mechanics can be classified into two major groups:

1) deformation problems

2) failure problems

This chapter is devoted to a commentary on only deformation problems.

Knowledge of both deformations and stresses are required for a complete solution of problems such as the foundation and abutments behaviour of dams, design of unlined or lined pressure tunnels, and other deformation problems. To calculate the deformations and stresses induced by different loading conditions, various rock properties and other factors are necessary. Many authors (Rocha, 1964; Serafim et al, 1964; Judd, 1964; Moody, 1964; Lauffer et al, 1961; Lang, 1964; Deere, 1967; Cook et al, 1964; Morgenstern, 1967) have presented valuable information for the analysis of deformation problems.

Rock is a product of its own history. As such, it is a formidable task to account for all the features of the behaviour of a rock mass. Generally, simplified conditions have to be assumed or applied for practical utilization of various theoretical and experimental methods both in laboratory

and field in order to compute the displacements and stresses that the rock mass or interacting complex will exhibit under the various boundary conditions.

The most rational approach to the design of a rock mass or of a structure interacting with a rock mass would be based upon displacements. Either local or overall displacements limit the utility of the engineering structure and are therefore the fundamental design criteria. The major aim of all design calculations is essentially the limitation or control of the displacements of the rock mass. Moreover, the displacements can be measured directly in the field. The control and measurement of stresses may be regarded as an indirect approach to the displacements and failure may be considered as an extreme displacement condition. Therefore almost all problems in rock engineering are reducible to the prediction of displacements or stresses (Morgenstern, 1967). Further, various authors (Hayashi, 1964; Zienkiewicz and Gerstner, 1960, 1961; Rocha, 1964; Moody, 1964) illustrated the effect of deformability of rocks on the design of various structures. Thus deformation analyses are of primary interest in the field of rock mechanics.

2.1 OUTLINE OF DEFORMATION PROBLEMS

The deformation problems encountered in the field of rock mechanics of civil engineering interest can be classified into the following groups:

(i) the foundation and abutment of various types of dams such as arch dam, gravity dam and so on.

(ii) Tunnelling - lined or unlined tunnels of various shapes

(iii) Excavation - open or underground.

The main interest in the analysis of deformation problems of type (i) is to determine deformation under both static and dynamic loadings for the conditions of zero and full reservoir loading. In type (ii) problems, primary attention is paid to the stresses on the rock surface exerted by the various loading conditions such as the hydrostatic pressure of water in case of a pressure tunnel for the hydro-electric scheme. Generally stresses and displacements are both given priority in the analysis of type (iii) deformation problems.

The factors which govern the analysis of deformation problems are the mechanical properties of intact rock and the rock mass as a whole, the natural state of stress inside the rock mass and the change of stress pattern due to the various engineering works. The mechanical properties of rock mass are greatly influenced by the geological aspects such as joints, faults, bedding planes etc. The natural stresses in the rock mass may be the result of active tectonic forces or the residual state after the termination of some geological process. Excavation open or underground during construction disturbs the equilibrium of stresses and displacements occur

which tend to close the opening. The magnitude of these displacements depend upon: (a) geometry of the excavation; (b) magnitude of the initial stress and (c) properties of rock itself. The factors mentioned above must be known before a complete deformation analysis can be done.

The mechanical properties of intact rocks can be determined in the laboratory. Laboratory studies are discussed in chapter 4. Out of all mechanical properties, the modulus of elasticity or the modulus of deformation and poisson's ratio are of primary concern in deformation analyses.

Much has been accomplished in the fields to measure the behaviour of rock mass, the initial state of stress and the change of stress pattern from various measuring techniques and field tests. Various authors (Hast, 1958; Merrill, 1960; Obert et al, 1962; Alexander, 1960; Cook, 1967; Ortlepp and Cook, 1964; Serafim, 1964; Potts, 1964) have described the merits and demerits of different field measurement techniques such as plate bearing tests, flat jack testing, bore hole instruments, stress-relief techniques, seismic methods and so on. It is beyond the scope of these studies to go into details of above techniques. As it is clear that the initial stresses will particularly influence the ultimate deformations in the deformation problems of type (ii) and (iii), the only way to get some information for the analysis is to use stress-relief techniques or bore hole deformation methods to measure the initial stresses in the rock mass.

Various assumptions and considerations have to be taken into account for such measurements (Roberts, 1967).

The field observations and the laboratory studies are used to formulate the theoretical analysis of deformation problems. Such an analysis requires the equation of equilibrium for an element of the rock mass and the constitutive equation governing the material behaviour.

2.2 IDEAL CONSTITUTE EQUATION

It is already emphasized that the ideal deformation analysis would predict, in principle, both stresses and displacements of all points composing a rock structure for the duration of its life and various type of loading that the rock must endure. And a representative constitutive equation governing the material behaviour has to be known to accomplish this task. Generally rock is assumed to be an ideal elastic material and rock properties are taken to be homogeneous and isotropic. Such assumptions permit the use of the ideal equations of linear elasticity or prepared solutions based on it. A commonly applied solution is that of the problem of Boussinesq, which considers the effect of a vertical point load on the surface of a semi-infinite, homogeneous, isotropic, linearly elastic half space. The expressions for stress are in a convenient algebraic form which can be found in most books on elastic theory (e.g. Timoshenko and Goodier, 1951; Love, 1944). Moreover the well known bi-harmonic equation

$$\frac{\partial^4 \phi}{\partial x^4} + 2\frac{\partial^4 \phi}{\partial x^2 \partial y^2} + \frac{\partial^4 \phi}{\partial y^4} = 0$$

or $$\nabla^4 \phi = 0 \qquad (2.1)$$

where ϕ the Airy stress function, is used for the solution of deformation problems.

The stresses are given by

$$\sigma_x = \frac{\partial^2 \phi}{\partial y^2}$$

$$\sigma_y = \frac{\partial^2 \phi}{\partial x^2} \qquad (2.2)$$

and $$\tau_{xy} = -\frac{\partial^2 \phi}{\partial x \partial y}$$

The development of equations (2.1) and (2.2) which govern the elastic stress distribution in two dimensional problems in plane stress and plane strain may be found in standard works of theory of elasticity (e.g. Timoshenko and Goodier, 1951). Several authors (Zienkiewicz, 1945; Rydzewksi, 1960; Zienkiewicz and Gerstner, 1960, 1961; Bishop, 1952; Dibiagio, 1966) have used equation (2.1) for the solution of deformation problems of type (i) and type (iii) mentioned in the previous section. Lame's classical solution (1852) for hollow cylinder submitted to uniform pressure on the inner and outer surfaces is generally taken as an ideal equation for the solution of deformation problems of type (ii) (Moody, 1964). The assumptions that rock

properties are linear elastic, have the advantage of simplicity and lead to problems which are soluble with relative ease by a variety of means. For complex boundaries, photoelastic techniques are used in the laboratory as well as in the field for the determination of stresses for deformation problems (Robert, 1964; Robert et al, 1962; Hawkes and Holister, 1964; Hiramatsu et al, 1957; Hoek, 1964). A study of real rock properties reveals that linear elasticity is seldom a realistic representation.

2.3 REAL BEHAVIOUR OF ROCKS

The use of linear elasticity for the solution of various deformation problems is contradicted by the real behaviour of rocks. From the many static measurements 'in situ' of deformation from tests using pressure plates, flat jacks, hydraulic pressure chambers which are reported by various authors (Serafim et al, 1961; Link, 1964; Lane, 1964; Rocha, 1964) it may be seen that the behaviour of the rock mass is non-linear. Moreover rock behaves differently on loading and unloading. The properties of the rock mass are also non-homogeneous and anisotropic and these characteristics greatly depend on geological factors. Some of the results of 'in situ' tests on rock mass are shown in figures (2.1) to (2.3). The results indicate the significant features of non-linearity, hysteresis and irrecoverable strain on unloading. The shape, slope and other features of the

hysteresis loops and the envelope curve can vary considerably with different types of rock and even in the same rock, with the nature of joint pattern, whether the joints are initially open or closed, nature of joint surface, joint filling material and other characteristics. However, certain features such as the slope of the envelope curve increases as the rock mass is composed of more intact rocks with fewer geological discontinuities. Rock types may be excepted from this more complex behaviour. It is found that many of the rocks encountered in the deep mines of South Africa exhibit elastic stress-strain behaviour prior to brittle failure (Cook, 1967).

Sometimes it is observed that load-deformation curves as reported in figures (2.1) to (2.3) are dependent on time. A typical deformation-time relation is shown in figure (2.4). It is beyond the scope of the thesis to go into detail about creep phenomena. It can only be noted that such studies will help to predict the long term stability of various rock structures.

Some of the laboratory studies of rocks by Nishihara (1957), Walsh (1965) and Phillips (1948) show also that the real behaviour of many rocks corresponds with the results observed in field tests. An analysis of the real behaviour of intact rocks is made in the following chapter.

Since rocks do not, in general, behave elastically, the deformation of rocks is partly elastic (reversible), partly plastic (permanent) in nature. The deformation

modulus determined by the 'secant moduli', is usually taken in the design of rock structures as opposed to the 'modulus of elasticity' or 'Young's modulus' (Link, 1964). The interactions between the rocks and concrete of the structure are of interest in the deformation problems like the behaviour of foundation and abutments of dams and the design of tunnel lining. In such cases, the deformability of rocks not only changes the stresses in the rock mass, but also in the concrete of the structure itself. It is impossible to lay down fixed rules on how far the behaviour of such structures is influenced by the deformability of rocks, since this influence depends on numerous parameters, among which the rigidity of the structure, geological aspects of rock mass and so on. Authors (Rocha, 1964; Hayashi, 1964) reported numerous model studies on the effect of deformability on the structure of arch dam. It was concluded by Rocha (1964) that the state of stress in the concrete of the dam varies in function of the ratio of the deformation modulus of rock (E_R) and the modulus of concrete (E_C). Figure (2.5) illustrates one such study. Further, it was noted that the influence of $\frac{E_R}{E_C}$ is little for values above 1, which seldom occur in practice, the same being true for ratios comprised between 1 and $\frac{1}{4}$. For values below $\frac{1}{8}$, the influence of $\frac{E_R}{E_C}$ grows very important and for values below $\frac{1}{16}$, the behaviour and even the overall conceptions of structure are basically dependent on the foundations. For the design of tunnel

lining, Moody (1964) reported that for the ratio of $\frac{E_R}{E_C}$ equal to 1, up to 90% of the load may be expected to be taken by the rock and when the ratio is equal to .1, 60% of the load may be absorbed by the rock. Interesting result also presented by Zienkiewicz and Gerstner (1961) on the effect of deformability on the stresses of concrete gravity dam. They reported that the variation of the ratio of $\frac{E_R}{E_C}$ has no effect on the distribution of stresses on the upper portion of the dam and only near the base there are significant departures. When the ratio $\frac{E_R}{E_C}$ is less, the compressive stresses in the downstream side is reduced, but the tensile stresses increase in the upstream area. The reverse happens when the ratio $\frac{E_R}{E_C}$ increases. This point is of considerable importance showing that a softer foundation is beneficial in reducing the dangerous tensions which govern the design of gravity dams.

2.4 METHOD OF SOLUTION

Common solutions of deformation problems make use of the linear theory of elasticity. It has already been observed that the use of such classical solutions is often unrepresentative of the real behaviour of the material. The real behaviour of the rock mass is also too complicated to be useful, and a deformation analysis can only be carried out using an approximate representation of the material behaviour. With the recent development of digital

computers, more powerful methods of solution can incorporate a better representation of material behaviour (Zienkiewicz et al, 1967; Clough et al, 1965). When the scale of discontinuities in the rock mass is small in comparison to the whole rock mass, the medium can be represented by a continuum for which methods of analysis such as the finite element method, finite difference methods can be used to solve the various deformation problems encountered. The finite element method is found to be a specially powerful tool which enables even non-linear behaviour of the material to be considered. This discrete method is also used for the solution of the deformation problems for the material having elastic-plastic behaviour (Reyes, 1966). Moreover, solutions based on plasticity are also used for such problems (Jaeger, 1961). The finite element method is fully discussed in chapter 5 and chapter 6.

CHAPTER 3

ORIGIN AND EVIDENCE FOR NON-LINEAR BEHAVIOUR OF ROCKS

3.0 INTRODUCTION

Many authors like Adams and Williamson (1923), Handin (1957), Zisman (1933), Nishihara (1957), Brace (1963) and Walsh (1965) have reported the results of various tests on rocks in the laboratory and they observed the non-linear behaviour of rocks at low stress levels. Further, Link (1964), Lane (1964), Rocha(1964), Serafim et al (1964) presented at the 8th Internation Congress on Large Dams many results from field tests on rock masses. It was also evident from the field results that the behaviour of rocks is characterized by non-linear stress-strain relations and hysteresis. In addition to the non-linear behaviour and hysteresis, the hysteresis loop often does not close at zero stress. By analogy with behaviour under pressure (Birch, 1961), the non-linear behaviour can be attributed to the cracked state of rocks. At low stress, cracks are open; as stress is raised cracks are closed and the rocks become stiffer; that is Young's modulus increases with stress. A stage is reached where no change in stiffness due to crack closure occurs, after which the stress-strain curve is found to be linear. The hysteresis observed in the stress-strain relation can also be explained by the presence of cracks and the effect of friction between the crack surfaces. Although

cracks may be closed under compression, some sliding motion of opposing crack faces is still possible. This motion is hindered by friction and it is easy to show qualitatively that this friction causes a hysteresis loop found for rocks. The diminution of hysteresis for hydrostatic compression is also reasonable, for here there is a lesser tendency for frictional sliding (Walsh, 1965).

The presence of non-linearity and hysteresis in the elastic compression of rocks raises the interesting question of how elastic constants like Young's modulus and Poisson's ratio depend on the cracked state of rocks. In this chapter an analysis of the non-linear characteristics of rocks is presented with a mathematical model developed by Walsh (1965). The elastic properties, Young's modulus, Poisson's ratio and compressibility are treated by investigating analytically the properties of an elastic continuum filled with cracks of various shape which will explain the effects of such cracks on the behaviour of natural rocks.

3.1 ANALYSIS OF NON-LINEAR BEHAVIOUR

A model is used for rock which is assumed to be elastic and isotropic material. Such a model is an idealization for most rocks, which are collections of grains individually exhibiting elastic, anisotropic behaviour. Although deformation on the scale of individual grains is decidedly anisotropic, behaviour of a large group of grains may be considered

isotropic if the grains have no preferred orientation. Obviously, the cracks, which play an important role in deformation, must also have a random orientation if the rock is to be isotropic.

If the effect of cracks is to be qualitatively determined, the shape of the cracks must be specified. In the present analysis, cracks are assumed to be represented by narrow elliptical slits, the width of the crack (in the plane of the crack) being equal to the length. The assumption of plane stress or plane strain, which greatly simplifies the analysis, is considered to be an adequate first approximation to actual cracks in rocks.

The modulus for a body containing many cracks is found by separating the body into regions, each of which contains one crack. The reactions of each region to the applied load are then found and combined to give the overall reaction. The boundary condition assumed is that stress in each region is equal to that of the body as a whole. The effect of different types of cracks are analysed in the following sections.

3.1.1 Open cracks

A general expression for the effect of porosity due to open cavities of any shape or concentration upon Young's modulus is first found by using the reciprocal theorem (Timoshenko and Goodier, 1951;). The reciprocal theorem

states that, for a body acted upon separately by two states of stress, the work done by the first state of stress acting upon the deformation produced by the second state is equal to the work done by the second state of stress acting upon the deformation produced by the first state. Considering a porous cylindrical body of length L and cross section area A_t (Figure 3.1) stressed by an external uniaxial stress σ' and also stressed by a uniform stress σ'_u.

The work done by σ' acting through the deformation produced by σ'_u

$$= \sigma' \delta'_u A_t \tag{3.1}$$

Since each element undergoes a uniform compression the displacement

$$\delta'_u = \frac{\sigma'_u \cdot L}{E} \tag{3.2}$$

where E is the intrinsic Young's modulus.

So the work done (W) by σ' is from equation (3.1)

$$W = \frac{\sigma' \cdot \sigma'_u \cdot A_t \cdot L}{E} \tag{3.3}$$

The stress σ'_u does work against both the external displacement δ'_o and the displacement δ'_i of the boundary of the cavity. The displacement δ'_o can be written in terms of the effective Young's modulus E_{eff} for the porous body as $\frac{\sigma' L}{E_{eff}}$.

Work done by σ'_u through displacement δ'_o

$$= \frac{\sigma'_u \cdot \sigma' A_t \cdot L}{E_{eff}} \tag{3.4}$$

Resolving the displacement δ'_i to the direction of σ'_u and calling the displacement parallel to σ' as u' and the component of crack surface area normal to σ' as dA_x, the work done by σ'_u on the displacement

$$= -\oint \sigma'_u \, u \, dA_x \tag{3.5}$$

From the reciprocal theorem, we get from equations (3.3), (3.4) and (3.5)

$$\frac{\sigma' \cdot \sigma'_u \cdot A_t \cdot L}{E} = \frac{\sigma'_u \cdot \sigma'}{E_{eff}} \cdot A_t \cdot L$$

$$-\oint \sigma'_u \, u \, dA_x$$

or $$\frac{1}{E_{eff}} = \frac{1}{E} + \frac{1}{v} \oint \frac{u}{\sigma'} dA_x \tag{3.6}$$

where $v = A_t \cdot L$

Equation (3.6) provides a means for calculating the effective modulus for any porous body for which the displacements at the cavity boundary due to an externally applied stress σ' can be found.

Multiplying equation (3.6) by $\frac{\sigma'^2 v}{2}$ we get

$$\frac{\sigma'^2 v}{2E_{eff}} = \frac{\sigma'^2}{2E} \cdot v + \frac{\sigma}{2} \oint u dA_x \tag{3.7}$$

The term on the left is the strain energy (W_{eff}) due

to an external uniaxial stress σ' acting on a porous body and the first term on the right is the strain energy (W_s) if the body contains no pores. The last term thus can be considered as the increase in strain energy (W_c) due to the presence of cavities. That is,

$$W_{eff} = W_s + W_c \tag{3.8}$$

and

$$W_c = \frac{\sigma}{2} \oint u \, dA_x$$

Griffith (1924) and others have derived expressions for the strain energy for an infinite body containing a crack by calculating the work done by the external stress acting through the external displacements. Moreover Walsh (1965) using complex variable methods developed by Stevenson (1945) derived the strain energy due to the presence of an inclined narrow elliptical crack in a body under plane stress or plane strain. He gave for plane stress

$$W_c = \frac{2\pi c^3 \sigma'^2}{E} \sin^2\beta \tag{3.9a}$$

The total strain energy W_c is found by summing equation (3.9a) over the total number of cracks N. So, we get

$$W_c = \frac{2\pi \sigma'^2}{E} \sum_N c^3 \sin^2\beta \tag{3.9b}$$

Assuming that the effect of the existing collection of N cracks of various lengths is the same as the effect

produced by N cracks each having an average length $\bar{c}$.

The summation of equation (3.9b) can be evaluated by integrating over the range of orientations. Assuming each crack differs in orientation by the solid angle $d\alpha$ where $d\alpha = \frac{4\pi}{N}$, the integration over all the orientation gives from equation (3.9b),

$$W_c = \frac{2\pi\sigma'^2 N\bar{c}^3}{3E} \tag{3.9c}$$

Through equations (3.7), (3.8) and (3.9c), we get

$$\frac{1}{E_{eff}} = \left(1 + \frac{4\pi N\bar{c}^3}{3V}\right) /E \tag{3.10}$$

Taking average volume of a region $\bar{v}$ where $N\bar{v} = V$, we get from equation (3.10)

$$\frac{1}{E_{eff}} = \frac{1}{E}\left(1 + \frac{4\pi\bar{c}^3}{3\bar{v}}\right) \qquad \text{(plane stress)} \tag{3.11}$$

For plane strain conditions, Walsh (1965) derived

$$W_c = \frac{2\pi\sigma'^2 N\bar{c}^3}{3E}\ (1-m^2) \tag{3.12}$$

So for plane strain one finds from equations (3.7), (3.8) and (3.12)

$$\frac{1}{E_{eff}} = \frac{1}{E}\left[1 + \frac{4\pi}{3}(1-m^2)\frac{\bar{c}^3}{\bar{v}}\right] \qquad \text{(plane strain)} \tag{3.13}$$

3.1.2 Closed cracks (Loading)

A general expression for the effective modulus of a

body of volume v which contains a single closed crack oriented at an angle β to the vertical can be found by using the reciprocal theorem as above. When a crack has closed, a shear stress τ_f and a normal stress σ_x are imposed on the crack faces, figure (3.2). Applying the reciprocal theorem, we get

$$\sigma' \delta_u' A_t + \oint \tau \delta_f dA = \sigma_u' A_t \delta_o' \qquad (3.14)$$

where dA is an element area of crack surface and δ_f is the relative displacement of crack faces. Since $\delta_u' = \frac{\sigma' u}{E} \cdot L$ and $\delta_o' = \frac{\sigma L}{E_{eff}}$, equation (3.14) can be written as

$$\frac{1}{E_{eff}} = \frac{1}{E} + \oint \frac{\tau \delta_f dA}{\sigma' u \sigma' v} \qquad (3.15)$$

We have

$$\sigma_x = \sigma_u \mathrm{Cos}^2\beta$$
$$\tau = \sigma_u \mathrm{Sin}\beta \mathrm{Cos}\beta$$

and hence from equation (3.15)

$$\frac{1}{E_{eff}} = \frac{1}{E} + \oint \frac{\mathrm{Sin}\beta \mathrm{Cos}\beta \, \delta_f dA}{\sigma' v} \qquad (3.16)$$

Applying the same analysis used in the open crack case above, the strain energy (W_c) associated with a closed crack which undergoes sliding is given by

$$W_c = \frac{\sigma'}{2} \sin\beta \cos\beta \oint \delta_f dA \qquad (3.17)$$

Assuming that the crack is closed for σ_n small compared to σ' and $\tau = \mu\sigma_n$, where μ is the friction coefficient, Walsh (1965) arrived at the following solution

$$W_c = \frac{2\pi c^3 \sigma'^2 \sin\beta \cos\beta (\sin\beta \cos\beta - \mu \sin^2\beta)}{E} \qquad (3.18)$$

To find the total contribution to the strain energy of all the cracks, equation (3.18) is integrated, not over all orientations but over only those orientations for which sliding is possible. The appendix (A) shows that the sliding displacement δ_f is proportional to the difference between the applied shear stress on a plane parallel to the crack and the frictional shear stress. Thus, for sliding to take place $\delta_f > 0$ or from equation (A 3.12) (for $\sigma_c \ll 0$)

$$\sin\beta(\cos\beta - \mu \sin\beta) > 0$$

or

$$\tan\beta < 1/\mu \qquad (3.19)$$

So sliding occurs only for crack orientation up to the 'friction angle' $\tan^{-1}(1/\mu)$. Now the total strain energy due to cracks under plane stress is given by

$$W_c = \frac{2\pi \bar{c}^3}{E} \sigma'^2 \int_0^{\tan^{-1}(1/\mu)} \sin\beta \cos\beta (\sin\beta . \cos\beta - \mu \sin^2\beta) . N\cos\beta \, d\beta$$

or

$$W_c = \frac{2\pi \bar{c}^3 \sigma'^2}{15E}\left[\frac{2+3\mu^2+2\mu^4}{(1+\mu^2)^{3/2}} - 2\mu\right] \qquad (3.20)$$

From equations (3.16) and (3.20), we get the effective modulus in the linear portion of the loading cycle for low crack concentration

$$\frac{1}{E_{eff}} = \frac{1}{E}\left[1 + \frac{4\pi \bar{c}^3}{15\bar{v}}\left\{\frac{2+3\mu^2+2\mu^4}{(1+\mu^2)^{3/2}} - 2\mu\right\}\right]$$

(plane stress) (3.21)

$$\frac{1}{E_{eff}} = \frac{1}{E}\left[1 + \frac{4\pi \bar{c}^3(1-m^2)}{15\bar{v}}\left\{\frac{2+3\mu^2+2\mu^4}{(1+\mu^2)^{3/2}} - 2\mu\right\}\right]$$

(plane strain) (3.22)

3.1.3 Closed crack (Unloading)

In appendix (A), it is shown that sliding occurs when the applied shear stress τ is greater than the frictional shear stress τ_f on the crack surface. Let us assume that these shear stresses have the values τ' and τ_f' when unloading begins. As soon as unloading begins, the direction of τ_f changes as shown in figure (3.3). We can see that for sliding in the opposite sense to occur, the reduction in applied stress $\Delta\sigma'$ must be sufficient to overcome a frictional stress of magnitude $2\tau_f'$. The reduction in applied stress $\Delta\sigma'$ results in reductions in applied shear stress and frictional shear stress $\Delta\tau$ and $\Delta\tau_f$. It is clear from figure (3.4), sliding can occur only on

satisfying the inequality,

$$\Delta\tilde{\tau} + \Delta\tilde{\tau}_f - 2\tilde{\tau}_f' > 0 \tag{3.23}$$

The parameters of equation (3.23) can be related to the stress σ'' at which unloading begins and to the decrease in applied stress $\Delta\sigma'$ by using the analysis in appendix (A), we get

$$\begin{aligned} \Delta\tilde{\tau} &= \Delta\sigma' \mathrm{Sin}^2\beta \\ \Delta\tilde{\tau}_f &= \mu\Delta\sigma' \mathrm{Sin}\beta\,\mathrm{Cos}\beta \\ \tau'_f &= \mu\sigma' \mathrm{Sin}\beta\,\mathrm{Cos}\beta \end{aligned} \tag{3.24}$$

From equation (3.23) and (3.24) we get

$$\frac{\Delta\sigma'}{\sigma''} > \frac{2\mu\tan\beta}{1+\mu\tan\beta} \tag{3.25}$$

The equation (3.25) shows that except for $\mu = 0$ and $\beta = 0$, the right hand side is greater than æro. Since μ must be greater than zero and since cracks oriented at $\beta = 0$ do not decrease the effective modulus, the conclusion can be made that cracks do not decrease the modulus because of sliding when the unloading cycle is begun. Thus the modulus during the initial stages of unloading is equal to the value obtained if the body contains no cracks. The slight strain remaining in the sample when the applied stress is removed entirely can be explained by noting that, according to the argument above, cracks which initially closed with a slight compression

due to internal stresses would not necessarily return to the same state at zero load.

3.2 EFFECT OF CRACKS ON THE COMPRESSIBILITY OF ROCKS

In the previous sections, the effect of various types of cracks on the modulus of elasticity is analysed. To illustrate further the non-linear behaviour of rocks, the compressibility of rocks (K) is treated in terms of homogeneous material having different pores. During the studies of deformation of rocks, many authors have observed that the compressibility of rocks is not constant, but varies with pressure and the type of test (Adams and Williamson, 1923; Zisman, 1933). Compressibility of samples jacketed with material impervious to the pressurizing medium usually decreases markedly with increasing pressure, whereas compressibility of unjacketed rocks is nearly constant*.

Such behaviour is explained by saying that 'solid rock' is not solid at all but contains many small fissures. These flaws in the rock structure decrease the apparent moduli until reapplication of pressure to jacketed samples closes the flaws and makes the rock stiffer. When the rock sample is not jacketed, the fluid is free to enter most of the pores, the cracks have little tendency to close, and

---

* Actually, compressibility of single crystals and other non-porous solids changes slightly with pressure by a few per cent in 10 kb which we are ignoring at low stress levels (Clark, 1966).

measurement reflects the deformation of the rock grains, which are nearly perfectly elastic. The presence of flaws and their closing under pressure was first suggested by Adams and Williamson (1923) and offers qualitative explanation for the initial change in the elastic moduli with pressure. This is discussed further in chapter 4.

A model as explained in the previous section is taken to evaluate theoretically the effects of cracks on the compressibility of rocks.

The compressibility of porous elastic material (K_{eff}) can be derived in terms of compressibility of solid material (K_s) and the rate of change of porosity (n) with external pressure (p). Considering a body whose external boundaries enclose a volume (V) containing cavities of total volume (V_c). Chree (1892) shows, using the reciprocal theorem, that the decrease in volume of the solid material $\triangle(V-V_c)$ due to an increase in pressure $\triangle p$ is given by $K_s \triangle pV$. In differential form

$$d(V-V_c) = K_s V dp$$

or

$$\frac{dV}{Vdp} = K_s + \frac{dV_c}{Vdp} \qquad (3.26)$$

Assuming small strains so that V may be considered constant, the last term of equation (3.26) is the rate of decrease of porosity with external pressure. Using the

convention that an increase in porosity is positive, we get from equation (3.26)

$$K_{eff} = K_s - \frac{dn}{dp} \tag{3.27}$$

Equation (3.27) is based on the requirement that the crystalline framework of the rock be linearly elastic and is independent of the shape or total volume of the pores.

3.2.1 Spherical pores

The simple case of a body containing spherical cavities is taken to illustrate equation (3.27). Consider the body to be separated into irregularly shaped regions, each containing one pore and each having the same porosity. Assuming that the distance between pores is great enough so that the stress at the boundary of each region is very nearly the same as that at the boundary of the body. Change in the volume (v_c) of a small cavity due to the application of pressure (P) at the boundary of the body, can be determined from Lame's solution for thick walled spheres (Timoshenko and Goodier, 1951) by approximating the region by a sphere of volume (v') equal to that of the region. The tangential stress ($\sigma_{\theta\theta}$) at the boundary of the cavity (from Lame's solution) can be expressed in the following form

$$\sigma_{\theta\theta} = -\left(\frac{3P}{2}\right)\left(1 - \frac{v_c}{v'}\right)^{-1} \tag{3.28}$$

The tangential strain is $e_{\theta\theta} = (1-m)\frac{\sigma_{\theta\theta}}{E}$, and the

volumetric strain $\frac{\Delta v_c}{v_c} = 3e_{\theta\theta}$.

Thus, the fractional change in volume of the cavity for a differential change in pressure is

$$\frac{dv_c}{v_c} = -\frac{9}{2}\frac{dP}{E}\frac{1-m}{1-\frac{v_c}{v'}}$$

The rate of change of porosity with pressure is

$$\frac{dn}{dP} = \frac{dv_c}{v'dP} = -\frac{9(1-m)}{2E}\frac{n}{1-n} \qquad (3.29)$$

From equations (3.27) and (3.29), we get

$$K_{eff} = K_s\left(1 + \frac{3}{2}\frac{1-m}{1-2m}\cdot\frac{n}{1-n}\right) \qquad (3.30)$$

$$\left(\text{Taking } K_s = \frac{3(1-2m)}{E}\right)$$

3.2.2 Narrow cracks

The effect of a random distribution of narrow cracks upon the compressibility of an elastic body is treated as in the spherical case, by first dividing the body into regions, each of which contains one crack.

Rearranging the equation (3.21) into the following form

$$K_{eff} = \frac{\left(K_s VPdP + PdV_c\right)}{VPdP}$$

or for a single region

$$K_{eff} = \left(K_s v'pdp + pdv_c \right) / v'pdp \qquad (3.31)$$

The first term in the numerator on the right hand side is the strain energy associated with the region if there is no crack and the second term is the increase in strain energy dW_c due to the crack. The increase in strain energy due to cracks of different shape has been calculated for several cases - the penny-shaped crack by Sack (1946) and the elliptical crack in plane stress and plane strain by Griffith (1920). For very narrow cracks of half-length and half-depth c, with uniform pressure p on the region boundary, the expressions are

$$\begin{aligned} dW_c &= K_s \frac{16(1-m^2)c^3}{9(1-2m)} pdp && \text{(penny-shaped)} \\ dW_c &= K_s \frac{4\pi(1-m^2)c^3}{3(1-2m)} pdp && \text{(plane strain)} \\ dW_c &= K_s \frac{4\pi c^3}{3(1-2m)} pdp && \text{(plane stress)} \end{aligned} \qquad (3.32)$$

For total number of regions (N) and defining an average crack length $\bar{c}$, where $N\bar{c}^3 = \sum_N c^3$ and for an average volume $\bar{v}$, where $N\bar{v} = V$, the effective compressibility is found to be, from equations (3.31) and (3.32)

$$\begin{aligned} K_{eff} &= K_s \left(1 + \frac{16}{9} \frac{(1-m^2)\bar{c}^3}{(1-2m)\bar{v}} \right) && \text{(penny-shaped)} \\ K_{eff} &= K_s \left(1 + \frac{4\pi}{3} \frac{(1-m^2)c^{-3}}{(1-2m)\bar{v}} \right) && \text{(plane strain)} \\ K_{eff} &= K_s \left(1 + \frac{4\pi\ \bar{c}^3}{3(1-2m)\bar{v}} \right) && \text{(plane stress)} \end{aligned} \qquad (3.33)$$

The equation (3.33) shows that the compressibility of porous elastic material is higher than the compressibility of the solid material. But the real behaviour of sandstone studied in the laboratory indicates that after a certain stress level the compressibility of the porous elastic material is equal to its solid material. A better model is necessary to account the complex behaviour of porous elastic material. This is discussed further in chapter 4.

3.3 EFFECT OF CRACKS IN ROCKS ON POISSON'S RATIO

The model used for the determination of the effect of cracks and pores on the Young's modulus and compressibility is taken also to find the effect of cracks in rocks on Poisson's ratio. In view of the non-linear deformation characteristics of rock, it is necessary to define 'Poisson's ratio' (Walsh, 1965) in the strain increment form as

$$m_{eff} = - d\varepsilon_{Lat}/d\varepsilon_{long} \qquad (3.34)$$

Since

$$E_{eff} = \frac{d\sigma'}{d\varepsilon_{long}}$$

we get from equation (3.34)

$$m_{eff} = - E_{eff} \left(d\varepsilon_{lat}/d\sigma' \right) \qquad (3.35)$$

Now, the increase in lateral strain $d\varepsilon_{lat}$ due to an increase in stress $d\sigma'$ is found by using the reciprocal

theorem. Consider a body containing pores and cracks in contact to be subjected separately to two applied stresses. The first is a uniaxial compression in the x direction applied to the exterior of the body. The second is equal compression in y and z directions applied to the exterior and interior surfaces of the body so that the solid part is under uniform biaxial lateral compression. These stresses are illustrated in figure (3.5). For simplicity, the stresses and displacements in the z direction are omitted and only one void and one closed crack are shown. Considering the porous body to be a cube of unit dimensions, external forces and displacements may be replaced by stresses and strains. By visualizing figure (3.5) in three dimensions, we see that the uniaxial stress $d\sigma'$ produces a uniform displacement $d\epsilon$ of the y and z faces, a displacement of $d\delta$ of the boundary of a pore, and a displacement of $d\delta_f$ of the boundary of a crack. The only displacement of interest produced by the uniform biaxial stress $d\sigma_u'$ is the displacement $d\epsilon_u$ of the x face. The displacement $d\delta$ is neither normal to the pore boundary nor parallel to the direction of $d\sigma'$. $d\delta_y$ and $d\delta_z$ are assumed as the components of $d\delta$ in the y and z directions and dA_y and dA_z are taken as the normal components of a pore surface element. The stress $d\sigma_u'$ acting on the crack surfaces is decomposed into components normal and parallel $(d\tau_u)$ to the crack surface. The component $d\tau_u$ is of interest and this for a crack at

angle β to the x direction is found from Mohr's circle to be

$$d\tilde{\tau}_u = \text{Sin}\beta\,\text{Cos}\beta\, d\sigma_u$$

From the reciprocal theorem, the work done by the uniform biaxial stress $d\sigma_u'$ is

$$2\varepsilon_{long} d\sigma'_u - \oint d\delta_y d\sigma'_u dA_y - \oint d\delta_z d\sigma'_u dA_z + \oint d\delta_f \text{Sin}\beta\,\text{Cos}\beta\, d\sigma_u' dA \qquad (3.36)$$

where dA is a differential element of crack surface area. The work done by $d\sigma'$ acting through displacement $d\varepsilon_u$ is $d\sigma' d\varepsilon_u$. Equating the two, we get

$$d\sigma' d\varepsilon_u = 2\varepsilon_{long} d\sigma'_u - \oint d\delta_y dA_y - \oint d\delta_z d\sigma'_u dA_z + \oint d\delta_f \text{Sin}\beta\,\text{Cos}\beta\, d\sigma'_u dA \qquad (3.37)$$

From elasticity theory,

$$d\epsilon_u = -2(m/E) d\sigma'_u \qquad (3.38)$$

From equations (3.35), (3.37) and (3.38) we get

$$\frac{2m_{eff}}{E_{eff}} = \frac{2m}{E} + \oint \frac{(d\delta_y dA_y + d\delta_z dA_z)}{d\sigma'} + \oint \frac{d\delta_f \text{Sin}\beta\,\text{Cos}\beta\, dA}{d\sigma'} \qquad (3.39)$$

For a body of volume V with many voids and cracks, equation (3.39) becomes

$$\frac{2m_{eff}}{E_{eff}} = \frac{2m}{E} - \sum \oint \frac{(d\delta_y dA_y + d\delta_z dA_z)}{V d\sigma'} + \sum \oint \frac{d\delta_f \text{Sin}\beta \, \text{Cos}\beta \, dA}{V d\sigma'} \qquad (3.40)$$

From equation (3.6) and (3.16), the effective Young's modulus for a porous material of the type considered here is given by

$$\frac{1}{E_{eff}} = \frac{1}{E} + \sum \oint \frac{d\delta_x dA_x}{V d\sigma'} + \sum \oint \frac{d\delta_f \text{Sin}\beta \, \text{Cos}\beta \, dA}{V d\sigma'} \qquad (3.41)$$

From equation (3.40) and (3.41), we get

$$\frac{1-2m_{eff}}{E_{eff}} = \frac{1-2m}{E} + \frac{1}{V} \sum \oint \frac{d\delta_x dA_x + d\delta_y dA_y + d\delta_z A_z}{d\sigma'}$$

The summation term is the rate of change of the volume V_c of all cavities with stress, i.e.

$$\frac{1-2m_{eff}}{E_{eff}} = \frac{1-2m}{E} + \frac{1}{V} \frac{dV_c}{d\sigma'} \qquad (3.42)$$

The rate of change of the volume of the cavities with uniaxial stress is one third that under hydrostatic pressure:

$$\frac{dV_c}{d\sigma'} = \frac{1}{3} \frac{dV_c}{dp} \qquad (3.43)$$

We have from equation (3.26)

$$K_{eff} = K - \frac{dV_c}{Vdp} \tag{3.44}$$

From equations (3.42), (3.43) and (3.44) we get

$$\frac{3(1-2m_{eff})}{E_{eff}} = K_{eff} \tag{3.45}$$

The relationship between the effective elastic constants in equation (3.45) is identical with that for solid isotropic elastic bodies as might be predicted. The initial value of Poisson's ratio m_o can thus be calculated from the initial value of compressibility K_o and Young's modulus E_o as follows

$$m_o = \frac{1}{2}(1 - E_o K_o/3) \tag{3.46}$$

It is already shown in equation (3.11) and (3.3) that the initial Young's modulus (E_o) and compressibility (K_o) can be obtained from the relation

$$E_o = E\left[1 - \frac{4\bar{\pi}}{3}\frac{N\bar{c}^3}{V}\right]$$

and

$$K_o = K\left[1 + \frac{4\bar{\pi}}{3(1-2m)}\frac{N\bar{c}^3}{V}\right] \tag{3.47}$$

3.4 DISCUSSION OF NON-LINEAR ANALYSIS

From the above analysis, it is clear that the behaviour

of rocks is greatly influenced by the presence of cracks. Analysis of the effect of closing of cracks, the effect of relative motion of the crack surfaces due to sliding and the conditions under which the sliding takes place explains the deformation characteristics of the model which appears to correspond with the behaviour of many real rocks.

Equations (3.11) and (3.13) illustrate that Young's modulus for an elastic solid containing cracks is less than that for an identical solid without cracks. The cracks close under increasing compressive stress causing an increase in modulus. During the loading cycle, sliding of crack surfaces past each other may take place after a crack has closed. Thus Young's modulus in the linear portion of a stress-strain curve after cracks have closed, expressed analytically by equations (3.21) and (3.22), is still less than that for an equivalent uncracked solid.

Equation (3.25) shows that cracks which have undergone sliding do not immediately slide in the other sense when the load is reduced. Therefore, the unloading Young's modulus calculated from the initial unloading curve is found to be higher than the Young's modulus calculated from the linear portion of the stress-strain curve. The above facts have been further supported by the experimental studies in chapter 4.

From the model studies, Walsh (1965) further suspected that strain in the unloading cycle can be retained through

friction at crack surfaces. This was tested by him with vibration at stages in the unloading cycle, while the sample was still loaded. He found that the strain in the sample had fallen at constant stress (figure 3.6) to nearly the same value as obtained in the loading cycle. Apparently the additional energy of the vibration was sufficient to overcome the friction at crack surfaces. The usual hysteresis loop can sometimes be almost eliminated by this procedure. Some of the test results reported by Nishihara (1957) and Mogi (1959) on sandstone and marble give additional support to the results analysed.

To evaluate the theoretical expressions arrived at requires the 'average' crack concentration as expressed in the parameters $\bar{c}$ and $\bar{v}$. Such information is not available, so the accuracy of predicted magnitudes of reduction in modulus due to cracks cannot be determined on an absolute basis. However, the behaviour of the model as discussed above can be compared in a qualitative way with the behaviour of natural rocks.

From equation (3.33), it is observed that the compressibility of rocks with different cracks varies as the cube of the average crack length. So the compressibility of rocks is strongly affected by the pressure of long cracks. Moreover, the effective compressibility in the case of plane stress and plane strain differ by $(1-m^2)$ (equation 3.33) and the results in both cases will differ by about 10%.

Such a difference is negligible in comparison with the overall level of approximation in the analysis.

CHAPTER 4

EXPERIMENTAL STUDIES OF DEFORMATION OF A SANDSTONE

4.0 PREPARATION AND DESCRIPTION OF SPECIMENS

The material tested was Bunter Sandstone*. Right cylindrical specimens of $1\frac{1}{2}$" diameter were produced from quarried blocks of sandstone by use of a standard coring machine with a single core bit. The bit was of the impregnated diamond type and to reduce the possibility of bit damage, drilling was begun at medium speed until the bit was seated, after which the vertical alignment was checked and a higher rate of revolution was utilized until the drilling was completed. It was necessary to maintain a constant bit pressure to produce a smooth-sided straight specimen. The cores were then cut to the final length of approximately 3 inches with a diamond cutter fitted on a lathe. The ends of the trimmed cores were then ground plane

---

* Blocks of Bunter Sandstones were supplied by British Industrial Sand Ltd. from Moneystone Quarry, Oakamoor, Staffordshire. The sandstone deposit is known geologically as the First Grit. This bed forms extensive outcrops to the north of the river Churnet disappearing under over-lying limestone, and to the south the bed dips away under over-lying shales. The bed has a maximum thickness of some 120 ft.; this thickness tapers away northwards across the outcrop. A typical chemical analysis is:

SiO_2 = 98.5%
Fe_2O_3 = 0.035%
Cr_2O_3 = 0.0006%
Al_2O_3 = 0.9%
CaO = Trace
Na_2O) + K_2O) = 0.5%
Loss of ignition = 0.2%
(Smith, 1965)

A study of several thin sections indicated an average grain size of 0.2 mm.

and perpendicular to the long axis using a rotary carburandum wheel. End parallelism to an accuracy of .004 inches, as determined with a 4 inch micrometer, was taken as acceptable. During the cutting, the blade was cooled with water which means that all specimens tested have undergone at least two periods of wetting, one during drilling and one during cutting.

The specimens thus prepared were then dried in an oven at 105°C for 24 hours. The porosities of the dry specimens were determined by the method described in a later section and the specimens were numbered as a means of control.

The cylindrical specimens of $1\frac{1}{2}$" diameter and 3 inch in length were then checked for homogeneity and isotropy by measuring the compressional wave velocity in orthogonal directions. No significant differences ($\pm$ 5%) were observed in any of the specimens. It should be noted that this test does not preclude the existence of local variations of stiffness within the specimen. It is however sufficiently sensitive to pick out major departures from homogeneity and isotropy that are persistent through the specimen.

The compressional wave velocity was determined along the axis of the cylindrical specimen and perpendicular to the axis of the specimen, using a commercially available device for testing concrete (Cawkell UCT2). In this apparatus a barium titanate trandsucer is excited to emit ultrasonic pulses in the compressional mode at a repetition rate equal to the mains frequency. The frequency content of the pulse can be varied

by use of crystals with differing resonant frequencies. The pulses, after transmission through the sample of known length, are detected by an identical transducer to that used for the transmission. The detected signal is displayed on a cathode ray tube, on which a series of time markers (10 μ sec.) are being generated. It is a simple matter to adjust the time instant of transmission on the cathode ray tube trace, make an allowance for the previously measured transducer delay and read off the time of travel of a compressional wave in the sample. The compressional wave velocity of the specimens were obtained and the results are shown in figure (4.3b). As anticipated, (Viksne et al, 1961) the velocity decreases with increasing porosity. The apparatus has also been used in the study of longitudinal velocities in a clay by Morgenstern and Taylor-Smith (1964) and in rocks by Ganguli and Banerjee (1960).

4.1 METHOD OF DETERMINING POROSITY OF ROCKS

The porosity of a natural aggretate of solid grains such as sandstone is governed by grain size distribution, angularity of the grains, colloidal content and degree of compaction. Generally various gas expansion methods (Taliaferro et al,(1937), MacGee (1926)), have been used to determine the porosity of ceramic materials. In this study as well, apparatus has been constructed to find the porosity of the dry specimens using the pressure (P) - volume (V) relationship of gas such as air

expressed by Boyle's law (PV = constant). As there is hardly any change of temperature at the pressure at which the air was expanded, the correction factor for the pressure-volume relationship expressed by Charle's law may be neglected.

Figure (4.1) shows a diagrammatic sketch of the apparatus used to determine the porosity of a dry specimen. The specimen was connected to a mercury manometer. Initially, the pressure in the void space (V_S) of the specimen and the void space (V_O) over the left-hand side of the manometer were both atmospheric. The left and right hand limbs of the manometer were at B and A respectively. The specimen was then surrounded by a rubber membrane and sealed between the top and bottom caps with O rings so that no air could flow into the specimen. The right hand limb of the manometer was lowered to C. The left hand limb dropped to D so that there was a pressure decrease (ΔP) in the closed off pore space and an associated volume increase (ΔV) both which were readily measured. From Boyle's law, we have,

$$P_A (V_S + V_O) = (P_A - \Delta P)(V_S + V_O + \Delta V)$$

or

$$V_S = \frac{P_A \Delta V}{\Delta P} - V_O - \Delta V \qquad (4.1)$$

where V_S = the volume of air in the specimen

V_O = the initial volume of air between the specimen and the manometer

ΔV = the change in volume of air due to decrease in

pressure ΔP.

P_A denotes the atmospheric pressure and ΔP is the decrease in pressure in the sealed void space.

In our measurements, ΔP was usually equal to $P_A/2$ and then V_S is given by (from equation 4.1)

$$V_S = \Delta V - V_O \qquad (4.2)$$

Since V_S is volume of voids in the specimen, this volume divided by the bulk volume of the specimen and multiplied by 100, may be considered the true porosity expressed as a percentage.

For the purpose of comparison, equivalent porosities determined by 48 hour water absorption tests were also determined. Since one hour water absorption tests are sometimes used as a classification index (Hamrol, 1957; Mayer, 1963), these values, called the alteration index, were also determined. Figure (4.2) illustrates the relationship between the porosities and alteration index obtained by the above methods. Though there is a good correlation between the alteration index and porosity obtained by the air expansion method, the range of values given by the former is small and, therefore, is not sensitive enough to take these values as an index of comparison. The values given by the 48 hour water absorption tests are also less sensitive. It is observed from the relationship, that the 48 hour water absorption method gave values about 2% less. This is undoubtedly due to not obtaining complete saturation. Further reference

to porosity will mean that found by the air expansion method.

4.2 EXPERIMENTAL APPARATUS

4.2.1 Introduction

Important advances and refinements of apparatus have developed in testing techniques during the past decades. In particular, the triaxial apparatus has been improved considerably. An extensive survey of the apparatus and testing techniques used in the field of rock mechanics has been given in several recent symposia (A.S.T.M., 1965; A.S.T.M., 1966). Bishop and Henkel (1962) give a detailed description of triaxial apparatus for the testing of soils. Bridgman (1923), Griggs (1936), Handin and Hager (1957), Wilhemi and Somerton (1967) and others have designed different types of apparatus to study the deformation of rocks under high pressure and temperature. Any detailed discussion of the apparatus designed by the various authors mentioned above, is beyond the scope of the thesis. It is most convenient to study many different aspects of rock deformation using triaxial apparatus which has axi-symmetric stress conditions.

4.2.2 Uniaxial Compression Test Frame

A photograph of the loading frame used for the uniaxial compression tests is shown in figure (4.3). The apparatus is designed for an allowance maximum load of 5 tons and the capacity of the proving ring used was 5000 lbs. It may be noted that the loading is manual.

4.2.3 Triaxial Test Apparatus

The equipment used in the triaxial tests consisted basically of a triaxial cell, hydraulic pressure maintainers, instrumentation neccessary to measure the stress and strains involved and a loading frame to apply the axial loads. The apparatus used in these investigations is similar to that described by Bishop and Henkel (1962) and only slight modification has been made to take the terminals of the strain gauges fixed on the specimens out of the cell. The figure (4.4a) indicates the different parts of the triaxial cell and the arrangement for the triaxial testing using confining pressures of 150 p.s.i. The triaxial cell consisted of a stainless steel cylinder $7\frac{1}{2}$ inches in length, machined from 4 inch O.D. stainless steel tubing. The wall thickness of the tubing available was $\frac{3}{8}$ inch and the ends of the cylinder were machined on the inside to fit O-ring grooves for standard $\frac{1}{4}$ inch thick tube (Webb, 1966). A cap of $1\frac{1}{2}$ inch diameter and 1 inch length was fitted to the recess of the pedestal which was screwed through the base of the cell. This was the main modification made to take out the terminals of the strain gauges fixed on the specimen, figure (4.4b).

To use a confining pressure of 500 p.s.i. in the triaxial testing of the specimens, a high pressure generator system as developed by Skinner (1968) was adopted. Figure (4.4c) shows diagrammatically the arrangement of the high pressure system. To generate the high pressure the pump was started which gave

oil pressure and this oil pressure was kept constant at the required value with the help of an Amsler constant pressure spring loaded valve. This oil pressure was fed to a Budenburg dead weight pressure tester to measure the pressure supplied to the triaxial cell.

The self compensating mercury control device (Bishop and Henkel, 1962) was used to hold the cell pressure constant for the tests carried out at a confining pressure of 150 p.s.i. Figure (4.4d).

The hydraulic pressures were measured on a Bourden-tube pressure gauge. The axial load was applied to the specimen manually and the load was measured by a high tensile proving ring with a total load capacity of 6000 lbs. A photograph of the triaxial apparatus with the proving ring is shown in figure (4.4e).

4.2.4 Measurement of Strain

Longitudinal and transverse strains of the specimens were measured by means of PLS-10* electrical resistance strain gauges cemented to the test specimens. Two strain gauges were mounted on the middle third and diametrically opposite each other along the length of the sample. A second pair

---

* PLS-10, polyester gauge of nominal gauge length 10 mm., nominal gauge width 1.5 mm., nominal resistance 120 Ω, gauge factor 2.07, base dimension 25 x 4 mm., is a type of resistance wire strain gauge which is composed of a grid of resistance wire and its supporting base is impregnated with polyester resin. The gauges were cemented to the specimens with P-2 adhesive and PS adhesive. Gauges and cement were supplied by Tokyo Sokki Kenkywjo Co. Ltd., Japan.

was mounted circumferentially in the middle of the sample to measure lateral strains. The two pairs of gauges were usually connected in parallel giving an average result. The strains were generally recorded by the strain indicator* in a full bridge circuit, figure (4.5). However, it is necessary occasionally to read all gauges independently as a check on the homogeneity of deformation. Temperature compensation gauges were mounted on a dummy core.

For the wet tests, special precautions had been taken to make the strain gauges moisture proof on all sides by coating them with a thin layer of P-2 adhesive and PS adhesive. P-2 adhesive helped setting in a brief time and PS adhesive made the gauges moisture proof. A photograph of a dry sample and a wet sample with the strain gauges is shown in figure (4.6).

4.2.5 Checking of gauge factor

The gauge factor of the strain gauges as supplied by the manufacturer has been checked with respect to whether the

---

* All strain measurements were made with either a Peekel strain indicator or a Budd strain indicator. These instruments are suitable for static determination and employ the null point method of measurement. In the Peekel type, two independent input circuits are provided and there are three independent circuits in the Budd type. These may be connected to two arm or four arm Wheatstone bridges and switched in as required. A channel switch balance unit is provided with the Budd strain indicator and this helps to read strain gauges in ten different channels independently. The Peekel strain indicator is designed for a fixed gauge factor of 2 and it is therefore necessary to correct readings according to the gauge factor of the strain gauges supplied by the manufacturing firm. The gauge factor for the Budd indicator is adjustable.

gauge factor is relatively constant under loading and unloading using a Lamb's roller extensometer. Lamb's roller extensometer consists of two elements which are readily clamped on opposite sides of the test piece. Each element is a complete extensometer in itself and may be used separately. But by using the two elements, the mean extension of the specimen is obtained, thus averaging any unequal strains due to non-axial loading or lack of homogeneity. Each element consists of two hardened and lapped steel plates having a knife edge on each; between these plates a hardened and lapped steel roller is inserted in such a way that as the specimen elongates the plates move relatively to each other, giving the roller a small rotatory movement which is strictly proportional to the extension. Each roller carries a mirror; the angular movement of which is measured by a telescope and scale. The telescope fitted with cross wires throws a beam of light on to one mirror which is reflected from the other mirror to a scale. The extension is given by the following expression,

$$e = \frac{c \cdot x}{D + \frac{1}{2} a}$$

where e = extension

x = scale reading

a = distance between mirrors

d = mean diameter of the rollers

$c = d/4$, a constant for each pair of rollers

D = distance between mirror and scale

The strains given by the extensometer and the gauges

during various loadings were recorded and the gauge factor was calculated. The ratio of the gauge factor calculated to the gauge factor supplied under various strains is plotted in figure (4.7) for the dry and wet tests. It was found that for all tests the gauge factor is sensibly constant. Moreover, for tests on dry specimens the value supplied by the manufacturer is correct. In case of wet specimens, the actual strains appear underestimated by about 5%. Since reproducibility is probably not attainable within this accuracy, the test data to be presented will not be corrected for it.

4.3 EXPERIMENTAL PROCEDURE

In order to study the deformation characteristics of sandstone both dry and wet specimens were subjected to loading, unloading and reloading under uniaxial compression as well as triaxial compression using confining pressures of 0, 150 p.s.i. and 500 p.s.i. A series of unconfined compression tests was also carried out to find the maximum compressive strength of Bunter sandstone and the results are shown in figure (4.8). They reveal a significant decrease in strength with increasing porosity.

The experimental procedure on the dry and wet specimens is best described by dividing the tests into three groups: (1) Uniaxial compression test; (2) Triaxial test using confining pressure of 150 p.s.i. and (3) Triaxial test using confining pressure of 500 p.s.i. In all tests loading was not carried

beyond an axial differential stress of 2200 p.s.i. because it was desired that no new crack be induced in the specimen. This stress was a quarter of the unconfined compressive strength of the material. There were eight cycles of loading on each test with an increasing stress increment for each cycle of approximately 275 p.s.i. The rate of loading on all tests maintained essentially constant and the duration of a complete test was about three hours.

In the uniaxial compression test, the specimens with a representative range of porosity were subjected to cyclic loading and unloading. Stress and strains were recorded at approximately 100 p.s.i. increments.

In the case of the tests performed under a confining pressure of 150 p.s.i., the specimens were jacketed with a rubber membrane and the ends were sealed with O rings. They were then placed on the base of the pedestal of the triaxial cell and the leads of the strain gauges were taken out of the cell. The initial readings of the axial and lateral strain gauges were recorded. Then the cell was filled with water and hydrostatic pressure up to 150 p.s.i. was applied in increments of 25 p.s.i. At each increment the strain gauge readings were noted. The axial load was increased manually in steps of approximately 100 p.s.i. and the cyclic load history described previously was carried out. As before, the maximum compressive stress permitted on any sample was 2200 p.s.i.

The procedure for testing the specimens under confining

pressure of 500 p.s.i. was the same as that described in the previous paragraph. It may be noted that the several precautions had to be taken to prevent the leakage of water from the cell along the terminals of the strain gauges. The holes along the side of the base of the cell were sealed with plasticine and covered with a thin copper plate.

For the wet tests, the samples were kept under water for 48 hours.

4.4 DISCUSSION OF TEST RESULTS

4.4.1 Dry tests

The test results which were obtained from uniaxial compression are plotted in figures (4.9) to (4.12). These results extend over a range of porosity from 10.0 to 16.6%*. The results of the triaxial tests using confining pressures of 150 p.s.i. and 500 p.s.i. are shown in figures (4.13) to (4.19). Some of these have also been duplicated. For the sake of clarity of presentation, not all cycles are shown in the figures.

In order to compare the mechanical behaviour of specimens with each other, it is best to use a non-mechanical parameter and since the behaviour of sandstone is closely linked to the structure of the void space, porosity was chosen as an index of

---

* More tests than are presented here have been carried out in this porosity range. They are not presented here since they provide no new information being repeats at porosities already quoted.

comparison. The results plotted in figures (4.9) to (4.12) illustrate that the degree of curvature of the virgin loading portion of the stress-strain curves varies with their porosity. The slope of the stress-strain curve for unloading is not the same as the loading cycle and the axial strain does not return to zero when the load is completely removed. As such, the three significant features of the stress-strain curves are non-linearity, hysteresis and the irrecoverable strain on unloading. All these characteristic features increase with increasing porosity.

The non-elastic behaviour of the specimens as indicated in the uniaxial compression tests, is also observed from the triaxial tests of specimens of a confining pressure of 150 p.s.i. The results indicate the relationship between porosity and the curvature of the stress-strain curve as well; but it is not so dominant as in the uniaxial tests. The triaxial tests using 500 p.s.i. as the confining pressure reveal that the specimens behave almost linearly after the first cycle of loading, there is practically no hysteresis and negligible residual strain after deviatoric loading.

In the figures which pertain to the confined tests, plots are given which show the variation of both axial and lateral strain with increasing confining pressure. These relationships are generally non-linear. The near identity of axial and lateral strains during hydrostatic loading supports the isotropic behaviour of the sandstone noted earlier. The

other plot in these figures shows the variation of lateral strain with axial strain over the complete load history. Some hysteresis and irreversibility may be noted in their relationship.

Restricting consideration to the loading portion of the stress-strain curves obtained from the various tests, it is of interest to investigate the data within the framework of non-linear elasticity. The values of the tangent modulus of compressibility (K), were calculated at different stress levels and the relationship between K and the sum of the principal stresses (σ) is indicated in figures (4.20) and (4.21). It has been observed that the compressibility of the jacketed specimens decreases rapidly as σ increases. K remains sensibly constant after a certain range of σ. Adams and Williamson (1923), Zisman (1933) and others have observed the same phenomena with many other rocks and minerals though generally at much higher pressures. They commented that the compressibility of jacketed specimens approaches asymptotically the compressibility of unjacketed specimens at high pressure. In the case of tests on crystalline rocks, these observations are consistent with the idea that a certain degree of porosity is associated with cracks along grain boundaries and that the large initial decrease in compressibility with pressure is due to the closing of these cracks (Birch, 1938).

From the samples tested under the three groups of cell pressure, it is possible to isolate two families of tests with

porosities of approximately 12% and 15%. In the case of the 15% family, data are available from all these tests paths while only 2 tests paths are available for the 12% family. The variation of K with $\bar{\sigma}$ for the three stress paths applied to samples with a porosity of about 15% is shown in figure (4.21). It is noted that within the accuracy and reproducibility of rock testing a path-independent behaviour is found and the relationship between K and $\bar{\sigma}$ constitutes a real material property. To further support this finding, similar data for the 12% family is given in figure (4.20). Regrettably, only two comparable specimens were available in this case.

It would indeed be surprising if, in the case of the confined tests, no effect in the change of compressibility occurred at the onset of deviatoric loading. Figures (4.22) and (4.23) show that the compressibility increases at this stage and hence the behaviour does in fact deviate from the path-independence noted above. This is due to the anisotropic response of crack closure. Generally, the effect is less than that shown in these figures and it disappears after a small deviatoric loading. While this constitutes a qualification to the conclusions described in the previous paragraph, it is not severe enough to negate the proposition that at a given porosity, there is a unique relationship between tangent compressibility and average principal stress.

The variations of K with log $\bar{\sigma}$ for the 12% and 15% families are shown in figures (4.24) and (4.25). While

there is some scatter in the data which is mainly attributable to the natural variation in the material and small scatter in the porosities, a straight line may be drawn through the data points as indicated. Over the stress range under consideration the compressibility converges on the value for quartz (Clark, 1966). The variation of K with $\bar{\sigma}$ takes the form

$$K = a - b \, \text{Log} \bar{\sigma} \qquad (4.3)$$

For the sandstone tested here, the slope of the line is closely related to the porosity of the specimen. Lines based on smoothed data and from uniaxial compression tests where families are not available are given in figure (4.26) for the full range of porosity. An increase in porosity coincides with a steeper slope of more compressible behaviour. Of particular interest is the convergence of <u>all</u> of the lines to the compressibility of quartz at a particular value of $\bar{\sigma}$ ($\bar{\sigma}_p$). It is expected that this value of $\bar{\sigma}$ will vary from rock to rock since it undoubtedly reflects the stiffness of the cementing material and the internal geometry. The termination of the compressible behaviour at the magnitude of the dominant mineral for increasing $\bar{\sigma}$ constitutes the end of only the first phase of a loading process to destruction. As $\bar{\sigma}$ increases more stress will be generated in the cementing material and cyrstal grains which, even under an all round pressure, would lead to structural breakdown and an enhanced compressibility. Whether the new structure subsequent

loading would display a compressibility converging upon that of quartz is not known at present.

It is of interest to note that at $\overline{\sigma}_p$, we have specimens with significantly different porosities each displaying essentially the same compressibility. This has implications for current theories of composite media which permit the calculations of material properties from those of any two phases composing the medium. The theories which deal with an elastic medium containing holes are applicable to our case (MacKenzie, 1950; Hashin, 1959; Holliday, 1966). For porosities greater than zero, these relations invariably predict moduli less than that of the host medium which vary with porosity. This conflicts with the observation of compressibility at or above $\overline{\sigma}_p$ which is <u>equal</u> to the host medium and is <u>independent</u> of porosity. The real behaviour of sandstone is clearly more complex than that considered in current theories of composite media. It seems that as the average stress is increased, deformation in the cementing matrix occurs until sufficient contacts between quartz grains are established to take all the applied stress. Since no new cracks are established, the cementing matrix must be relatively ductile and observations on the modulus of rigidity support this. Hence, at or above $\overline{\sigma}_p$, but below the hydrostatic pressure required to crack the matrix, the sandstone behaviour is dominated by the properties of quartz with respect to compressibility and by the properties of the cementing material and pore structure with respect to rigidity.

At least a three phase model is necessary to account for these features.

The values of the tangent modulus of rigidity (G) are also calculated from the loading portion of the stress-strain curves and they are plotted against $\bar{\sigma}$ in figures (4.27) to (4.29). During the uniaxial tests, it is found that as $\bar{\sigma}$ is increased, G also increases up to a stress level, $\bar{\sigma}$, of about 1600 p.s.i. after which G becomes constant. The same relationship between G and $\bar{\sigma}$ is also observed with the triaxial tests using a confining pressure of 150 p.s.i. The data from the triaxial tests with the confining pressure of 500 p.s.i. show that G is constant for the range of $\bar{\sigma}$ investigated. Wilhemi and Somerton (1967), observed the same phenomena on Bandra, Berea and Boise sandstone under different high confining pressure. In their case, as the confining pressure was increased the value of G also increased and they associated this with an increased strength of the samples.

The variation of G with $\bar{\sigma}$ for the 15% family is given in figure (4.28). It appears that the stress path now has some influence but it is of the same order as the natural variability of G at a given porosity. The constant value of G which is obtained at higher stresses is plotted against porosity in figure (4.30) for the different confining pressures. The influence of confining pressure is not clearly defined.

The variation of G with $\bar{\sigma}$ given in figures (4.27)

to (4.29) is much less than that of K. Certainly above $\sigma \geq 1600$ p.s.i., a material behaviour characterised by a non-linear K and a constant G is representative. Indeed, to a first approximation, this would be an acceptable characterisation over the whole loading range. Finite element calculations are, of course, not limited to such restrictions.

With the preceeding observations, it may be concluded that the non-linear stress-strain relationship of sandstone is controlled mainly by the compressibility of the material until the compressibility of quartz is reached. At this stage the rigidity of the sandstone is about one tenth that of quartz so that the transmission of shear is controlled mainly by the cement matrix and pore structure. Further loading would at some stage initiate intergranular fracture. Porosity is the main factor that effects the characteristic features of non-linearity, hysteresis and irrecoverable strain on unloading of sandstone at low stress level. As the confining pressure is increased, the rock tends to behave more as a linear elastic material. This explanation was first suggested by Adams and Williamson (1923) and later Walsh and Brace (1965; 1967) investigated in detail the effects of the structural defects such as cracks and pores on the behaviour of rocks. It is observed during the uniaxial stress that at low stress the slope of the stress-strain curve is relatively low. An increase in the axial stress closes some of the cracks and the rocks become stiffer. So

beyond a certain stress level, the stress-strain curve for initial loading becomes approximately linear due to closure of the cracks with a high aspect ratio which are readily deformed. This closure stress varies with porosity as shown in figure (4.31). In some cases it may be possible to represent the non-linear deformation of a sandstone by using a bi-linear hysteretic model with the change in slope at this closure stress.

The deformation of the specimens has been further analysed in order to explore the non-linear behaviour, by determining their energy dissipation properties under cyclic loading. If an element is at a given set of stresses and is subjected to unloading, the material properties during unloading will depend upon the amount of recoverable strain energy. For the tests reported here, the energy dissipated in each cycle of loading and unloading was computed from the stress-strain relation of each specimen. Results are shown in figures (4.32a) and (4.33a), where the specific energy dissipation, the energy dissipated per unit volume (inch-pounds per cu. inch) is plotted against the maximum stress level of the cycle. The linearity of the relationship over most of the stress range is particularly interesting. The departure from linearity at high stresses in one case may be associated with the onset of new cracks if it is assumed that the linear increase of dissipation with stress is due to slip on pre-existing cracks. It would be expected that for a given

confining pressure higher porosity specimens would be more dissipative and hence the slope of the stress-dissipation relation, which we call the dissipation factor, would decrease with increasing porosity. This has been observed for the tests reported here and the relation is shown in figure (4.32b). The application of confining pressure of 150 p.s.i. has little effect on the alteration of the stress-strain characteristic of the sample, as a result of which, the energy dissipation in each cycle of loading and unloading is comparable with the uniaxial tests. The relationship between the dissipation factor and the porosity observed from both series of tests is plotted in figure (4.32b) and the results confirm this point. The use of higher confining pressure (500 p.s.i) virtually eliminates the energy dissipation. It is likely that the cracks close and the normal pressure across them increases to such an extent that there is hardly any relative motion possible between the crack walls by the sliding of one face past the other. Hence there can be hardly any energy dissipation under these conditions of high confining pressure and low deviatoric loading.

A few specimens were retested uniaxially about 6 months later in order to investigate the influence of elastic recovery of the set whose presence was suggested by Nishihara (1957). Their stress-strain curve on loading was much closer to the penultimate loading curve in the earlier test than to the initial loading curve. An example is given in figure

(4.34). This suggests that the time effects were slight and is not in accord with Nishihara's observations. If specimens with a set after unloading are subjected to vibration, some of the set is relieved (Walsh, 1965). Typically, four minutes of vibration produced 25 μ strain longitudinal expansion and 20 μ strain transverse expansion in the cases where this influence was investigated. The influence of vibration is probably to reduce the normal pressure on some locked cracks and allow slip to take place. The existence of the residual strain suggests that it is seldom possible to re-use specimens in experiments designed to study their deformation properties.

The non-linear deformation of sandstone is illustrated more clearly in figure (4.35), where the tangent modulus from the uniaxial tests is plotted against stress for a range of porosities. Figure (4.35b) shows the variation of tangent Poisson's ratio for the same tests. The variation of tangent modulus with stress could be fitted with, say, a power function. In any case, in any attempt to solve a boundary value problem one is likely to use a piece-wise linear approximation to the real data.

Walsh (1965) suggested that the tangent unloading modulus would be higher than the tangent loading modulus at the same stress level. This is corroborated in figure (4.36) which shows both unloading tangent modulus and Poisson's ratio plotted against the stress level for the same tests.

In discussing the influence of cracks in the uniaxial compression of rocks, Walsh (1965) also observed that the elastic modulus calculated from sonic velocities would correspond to some average slope of the stress-strain loop representing the dynamic loading. If this were so, the dynamic modulus should be closer to the tangent unloading modulus than the initial tangent loading modulus. Since, in our case, velocities were determined with no static stresses applied it is necessary to compare the dynamic modulus with the tangent moduli at zero stress. The static moduli were obtained by extrapolation in figures (4.35) and (4.36) to zero stress and are shown plotted against porosity in figure (4.37a). The variation in compressional wave velocity with porosity is shown in figure (4.37b). The dynamic modulus is given by the formula

$$E_D = \frac{V^2 \rho \ (1+m)(1-2m)}{144\ g(1-m)}$$

Since only the wave velocity (V) and density of the specimens (ρ) were known, it was necessary to assume the value of Poisson's ratio (m) in order to compute the dynamic Young's modulus. The dynamic Poisson's ratio for most rocks falls between 0.15 and 0.35 (Morgenstern, 1965; Fairhurst, 1963; Judd, 1964). Calculations have been carried out for values of Poisson's ratio equal to 0.15, 0.20 and 0.35 and the resulting variation of dynamic Young's modulus with porosity are shown in figure (4.37a). The correspondence

with the unloading modulus is particularly good. Indeed, values obtained with Poisson's ratio equal to 0.20 fit the static unloading values almost perfectly.

4.4.2 Wet Tests

The wet tests of samples with a range of porosity from 11.0% to 16.3% were investigated in the three groups of cell pressure as indicated in the previous section and the results are plotted in similar ways as the dry tests for comparison. The results of the uniaxial compression tests are shown in figures (4.38) to (4.40). Figures (4.41) to (4.43) illustrate the results obtained during the triaxial tests using confining pressures of 150 p.s.i. and 500 p.s.i.

The results plotted in figures (4.38) to (4.40) show also the three significant features of the stress-strain curves - non-linearity, hysteresis and irrecoverable strain on unloading. As before all these characteristic features increase with increasing porosity. In comparison with the dry tests, the results of the wet tests presented in the above figures show greater non-linearity, hysteresis and residual strain for a given confining pressure and porosity. Behaviour similar to that observed during the uniaxial tests, is also observed in the triaxial tests of specimens at a confining pressure of 150 p.s.i. and 500 p.s.i. as shown in figures (4.41) to (4.42). The use of confining pressure of 500 p.s.i. which brought a major change in the stress-strain relationship

of the dry samples, has much less influence on the behaviour of the wet samples although this observation is based on only one test. For a given confining pressure and porosity, it appears that both energy dissipation and irrecoverable strain are increased when specimens are wetted.

The relationship between K and σ for the wet tests is illustrated in sigures (4.44) and (4.45). Like the dry tests, the compressibility of the jacketed wet specimens decreases rapidly as σ increases. K remains sensibly constant after a certain range of σ. The figures illustrate also that the wet samples were more compressible initially than the dry tests. It is important to note that the path-independent behaviour which is found during the dry tests of the samples, is not observed in the case of wet tests. The above conclusion is made from only two comparable specimens having the same porosity of about 15.0%, which had been tested under confining pressures of 0 and 150 p.s.i. The uniaxial test results given in figure (4.40) show that the sample failed after the application of only 1400 p.s.i. load and the sample was also incompressible prior to failure. As a result no unique relationship between K and σ can be found. However, more extensive tests on wet samples must be performed before clear conclusions can be drawn.

Figure (4.46) illustrates the variation of K with log σ for the different test results. The compressibility of each sample tested also converges on the value of quartz;

but the unique result of the dry tests, the convergence of all the lines to the compressibility of quartz at a particular stress level, is not observed here. Though there is high initial compressibility of the wet samples, the slope of the lines gradually becomes less steep than the dry specimens for a given confining pressure and porosity. The slope of the line like the dry tests, is closely related to the porosity of the sample and equation (4.3) can be fitted to the above results.

The values of G are also calculated from the loading portion of the stress-strain curves and figure (4.47) indicates the relationship between G and σ for the different tests. Like results of dry tests, G increases up to a stress level as σ increases during the uniaxial tests. But G is found to be constant during the triaxial tests with confining pressures of 150 p.s.i. and 500 p.s.i. The range of values of G during the wet tests is much less than that of the dry tests.

The non-linear deformation of the wet samples has been further analysed also by finding out the energy dissipation properties and it is observed that the wet specimens were more dissipative and there is some departure from the linear relationship, figures (4.48) and (4.49). The relationship between the dissipation factor and the porosity from uniaxial tests and triaxial tests is plotted in figure (4.48b). The results indicate greater energy dissipation than the dry tests.

A possible explanation of such behaviour will be, the crystal grains are becoming detached at their grain boundaries during wetting, as a result of which there is more internal friction between the grain boundaries or the crack surfaces. Hence greater energy dissipation and non-elastic behaviour will be exhibited. Moreover, the compressive strength of the wet samples was greatly reduced and some of the specimens failed after the fifth cycle of loading (about 1600 p.s.i.). Colback (1965) studied the weakening influence of moisture on the compressive strength of rock and he suggested that it was due to the reduction of molecular cohesive strength of the material. The data presented here shows that the presence of moisture weakens the intergranular bonds.

CHAPTER 5

FINITE ELEMENT METHOD

5.0 INTRODUCTION

The 'finite element method' is a general method of structural analysis in which a continuum (or solid) is replaced by a finite number of elements interconnected at a finite number of nodal points or nodes. With this idealisation, a problem in continuum or solid mechanics is transformed into a related problem for an articulated structure to which the standard matrix method of structure analysis can be applied.

From the historical standpoint, Clough (1960) first introduced the term 'the finite element' and he presented the triangular and rectangular plate elements in plane stress analysis. However, in 1941 Hrennioff illustrated the idea of approximating a continuum by the assembly of a finite number of discrete structural members. The analogy was not correct and from the practical point of view, it was not possible to solve a large number of equations at that time. Gradually the development of high speed digital computers motivated renewed and more extensive development of numerical methods. Argyris (1954; 1955) provided the most general approach to the computer analysis of structures. Turner, Clough, Martin and Topp (1956) introduced the methods of calculating stiffness influence coefficients. Martin (1961) presented a more direct approach for the calculation of

stiffness of a triangular element in a plane stress problem of elasticity. Finally Wilson (1963), de Veubeke (1964; 1965), Clough (1965) and Zienkiewicz (1967) presented the finite element procedure, its applications and different practical solutions of engineering problems.

Thus, the finite element method involves not only the new idea of structural approximation of the continuum, but also the use of two or three dimensional elements. Using such elements, the structural idealisation is obtained merely by dividing the original continuum into segments of approximate sizes and shapes, all the material properties of the original system being retained in the individual elements. This capacity for treating arbitrary material properties is one of the principal attributes of the finite element method.

5.1 BASIS OF THE FINITE ELEMENT METHOD

There was some criticism at the time of the early application of the finite element method because of its apparent lack of a sound theoretical basis. However, theoretical studies by de Veubeke (1964; 1965), Jones (1964) have now shown that the finite element technique can be developed in terms of variational considerations. From this standpoint, the finite element technique can be classified into three categories:

(i) The displacement models: This method is based on parametric displacement fields ensuring compatibility of

deformations both internal to the elements and across their boundaries; but does not satisfy equilibrium across element boundaries. It is generally known as the displacement method or the direct stiffness method.

(ii) The equilibrium models: These models based on stress fields satisfy internal equilibrium and continuous stress transmission but not compatibility.

(iii) Mixed models called 'Hybrid' which do not necessarily satisfy either compatibility or equilibrium.

This classification identifies the basis of the displacement models as the principle of variation of total potential energy and that of equilibrium models as the principle of variation of complementary energy (de Veubeke, 1965). A general formulation for the mixed models in which both stresses and displacements can be varied independently was described by Jones (1964).

De Veubeke (1964) proved that the displacement and equilibrium models, respectively, yield lower and upper bounds on influence coefficients, i.e. a displacement solution underestimates the generalized displacements while an equilibrium solution overestimates them.

The equilibrium method is generally not used due to its difficulty in forming the stress functions. In practice, the usual method the displacement models is utilized with minimum size of elements to approach the true representation.

5.2 THE DISPLACEMENT METHOD

In this study the displacement or the direct stfffness method has been used. Briefly, the method involves the following steps:

(i) Structural idealization.

(ii) Evaluation of the stiffness matrix of the individual elements which is expressed in any convenient co-ordinate system.

(iii) Superposition of the individual element stiffnesses contributing to each nodal point in order to generate the stiffness matrix of the system or the total assemblage nodal stiffness matrix.

(iv) Formulation and solution of the equilibrium equations at each nodal point consistent with the imposed loads or displacements in order to find the nodal displacements.

(v) Calculation of the stresses in the elements from the computed nodal displacements.

These steps can be applied directly if the material is elastic because the stiffness matrix which depends on the elastic constants and on the geometry of the assemblage only is constant. The entire prescribed loads can therefore be applied to obtain the nodal displacements, from which the stresses and strains in the elements can be computed.

However, if the elastic constants of the material are not constant at different stress levels or in other words the behaviour of the material is a non-linear one, a new

stiffness matrix based on the current stress levels in the elements must be computed. In this study a method has been developed to handle the non-linear material properties and it is discussed in the following chapter.

The procedure for generating the stiffness matrix of a configuration consisting of triangular elements which are the most convenient ones in our studies, is well documented (Clough (1965), Zienkiewicz (1967)). The whole procedure is briefly recorded here merely for completeness. Notations and technique generally those of Clough (1965) have been adopted.

5.3 STIFFNESS MATRIX OF THE ELEMENT

The first step in the development of the stiffness matrix of a typical element in the displacement analysis is to assume a general form of the displacement functions subject to the requirement that they are continuous throughout each element as well as across the boundaries. These functions can be quite arbitrary in general. But a linear displacement function has been used in most studies. This linear displacement field is defined in terms of $U(x, y)$ and $V(x, y)$ by equations of the following form

$$U = \alpha_1 + \alpha_2 X + \alpha_3 Y \tag{5.1}$$

$$V = \alpha_4 + \alpha_5 X + \alpha_6 Y \tag{5.2}$$

in which U, V are the generalized displacements, α_1, α_2, α_3, α_4, α_5, α_6 are the constants and X, Y are the co-ordinates.

The geometry of a typical triangular element is defined in figure (5.1). This linear displacement field for the element has the results that the U and V displacements at the nodes completely specify the configuration of the deformed element. Moreover, by maintaining the continuity of the nodal displacements in the assembled system, continuity across the boundaries is automatically satisfied. Hence the assumed displacement function conforms to the requirement of complete compatibility.

Each node of the triangle (in plane deformation) has two degrees of freedom, the displacement in the x and y directions respectively. Therefore for the whole triangular element, there are six degrees of freedom; hence six generalized constants because it is desirable but not essential that the number of unknown coefficients in the assumed displacement functions be equal to the total number of degrees of freedom of the element.

From figure (5.1) introducing successively, the nodal co-ordinates into the set of expressions (5.1) and (5.2), the generalized constants can be expressed in terms of the nodal displacements and the geometry of the element. Thus

$$\begin{bmatrix} U_i \\ U_j \\ U_k \\ V_i \\ V_j \\ V_k \end{bmatrix} = \begin{bmatrix} 1 & X_i & Y_i & 0 & 0 & 0 \\ 1 & X_j & Y_j & 0 & 0 & 0 \\ 1 & X_k & Y_k & 0 & 0 & 0 \\ 0 & 0 & 0 & 1 & X_i & Y_i \\ 0 & 0 & 0 & 1 & X_j & Y_j \\ 0 & 0 & 0 & 1 & X_k & Y_k \end{bmatrix} \begin{bmatrix} \alpha_1 \\ \alpha_2 \\ \alpha_3 \\ \alpha_4 \\ \alpha_5 \\ \alpha_6 \end{bmatrix} \qquad (5.3)$$

in which U_i, V_i etc. refer to the nodal displacements and X_i, Y_i etc. refer to the nodal co-ordinates as shown in figure (5.1), or in symbolic form

$$[\delta] = [A][\alpha]$$

or

$$[\alpha] = [A^{-1}][\delta] \qquad (5.4)$$

The strains within the element (assumed to be uniform) can be obtained from the assumed displacement field, equation (5.1) and equation (5.2), by considering the basic definitions of strain.

$$\begin{bmatrix} \epsilon_x \\ \epsilon_y \\ \gamma_{xy} \end{bmatrix} = \begin{bmatrix} \frac{\partial u}{\partial x} \\ \frac{\partial v}{\partial y} \\ \frac{\partial v}{\partial x} + \frac{\partial u}{\partial y} \end{bmatrix} = \begin{bmatrix} 0 & 1 & 0 & 0 & 0 & 0 \\ 0 & 0 & 0 & 0 & 0 & 1 \\ 0 & 0 & 1 & 0 & 1 & 0 \end{bmatrix} \begin{bmatrix} \alpha_1 \\ \alpha_2 \\ \alpha_3 \\ \alpha_4 \\ \alpha_5 \\ \alpha_6 \end{bmatrix} \qquad (5.5)$$

or in symbolic form

$$[\epsilon] = [B][\alpha] \tag{5.6}$$

or

$$[\epsilon] = [B][A^{-1}][\delta] \tag{5.6a}$$

The stress can be expressed in terms of the strain using the stress-strain relations of the material (assuming plane strain)

$$\begin{bmatrix} \sigma_x \\ \sigma_y \\ \tau_{xy} \end{bmatrix} = \frac{E(1-m)}{(1+m)(1-2m)} \begin{bmatrix} 1 & \frac{m}{1-m} & 0 \\ \frac{m}{1-m} & 1 & 0 \\ 0 & 0 & \frac{1-2m}{2(1-m)} \end{bmatrix} \begin{bmatrix} \epsilon_x \\ \epsilon_y \\ \tau_{xy} \end{bmatrix} \tag{5.7}$$

in which E is Young's modulus and m is Poisson's ratio or in symbolic form

$$[\sigma] = [D][\epsilon]$$

or

$$[\sigma] = [D][B][\alpha] \tag{5.8}$$

Substituting equation (5.6a)

$$[\sigma] = [D][B][A^{-1}][\delta] \tag{5.9}$$

The specific elastic characteristics of the finite element material are represented by this stress-strain matrix $[D]$.

The stiffness matrix of the element is then obtained by introducing a virtual displacement and applying the principle of virtual work (Clough (1965)). The internal virtual work dw_1 of any differential volume dv of the element is given by the product of the actual stress σ and the virtual strain $\bar{\epsilon}$ through which they move

$$dw_1 = \bar{\epsilon}^T \sigma \, dv \qquad (5.10)$$

The substitution of equations (5.6) and (5.8) into equation (5.9) yields

$$dw_1 = \bar{\alpha}^T B^T D B \alpha \, dv \qquad (5.11)$$

in which $\bar{\alpha}$ represents the virtual generalized co-ordinate displacements associated with $\bar{\epsilon}$. The internal virtual work

$$w_1 = \bar{\alpha}^T \left[\int_{Vol} B^T D B \, dv \right] \alpha \qquad (5.12)$$

($\bar{\alpha}$ and α are extracted from the integral because they are independent of x and y co-ordinates).

The external work associated with the virtual generalized displacement $\bar{\alpha}$ is given by

$$w_E = \bar{\alpha}^T \beta \qquad (5.13)$$

where β represents the generalized force components.

Introducing a unit value of the virtual displacement components in sequence, from the principle of virtual work, it follows that

$$w_E = w_I$$

and

$$\beta = \left[\int_{vol} B^T D B dv \right] \alpha$$

or

$$\beta = K \alpha \tag{5.14}$$

By definition $[K]$ is the (6 x 6) stiffness matrix for the triangular element and is given by

$$K = \int_{vol} B^T D B dv \tag{5.15}$$

To get the relation between the nodal forces and the nodal displacements, the stiffness matrix of the element is transformed to the nodal point stiffness, $\bar{K}$ with the standard co-ordinate transformation in which the transformation matrix $[A^{-1}]$ relates the generalized co-ordinates α to the nodal point co-ordinates δ as shown in equation (5.4). Thus nodal point stiffness,

$$\bar{K} = [A^{-1}]^T [K] [A^{-1}] \tag{5.16}$$

The steps leading to the value of K or $\bar{K}$ are seen

to be purely standard matrix multiplication with the exception of the required inversion in equation (5.4). A general expression is obtained in appendix C for the nodal point stiffness of the triangular element and this expression has been used directly for the calculation of the nodal point stiffness from the geometry of the element and the elastic parameters avoiding the long process of matrix multiplication and inversion.

5.4 ASSEMBLAGE OF STIFFNESS MATRIX OF THE ELEMENT AND FORMULATION OF EQUILIBRIUM EQUATIONS AT EACH NODAL POINT

After obtaining the stiffness matrix for the elements, superposition of the individual element stiffness contributing to each nodal point is done and the equilibrium equation is generated at each nodal point to get the relation of nodal point forces and nodal displacements.

In this study the continuum is idealized as shown in figure (5.2). For simplicity, the assemblage of the stiffness matrix at any nodal point and the equilibrium equations are formulated by the following procedure.

For any nodal point A, figure (5.2), the forces applied in the X direction and Y direction are (say) F and G respectively and let us assume f and g are the internal forces in an element in the direction of X and Y respectively.

By definition

$$\begin{bmatrix} f_i \\ f_j \\ f_k \\ g_i \\ g_j \\ g_k \end{bmatrix} = \begin{bmatrix} K_{11} & K_{12} & K_{13} & K_{14} & K_{15} & K_{16} \\ K_{21} & K_{22} & K_{23} & K_{24} & K_{25} & K_{26} \\ K_{31} & K_{32} & K_{33} & K_{34} & K_{35} & K_{36} \\ K_{41} & K_{42} & K_{43} & K_{44} & K_{45} & K_{46} \\ K_{51} & K_{52} & K_{53} & K_{54} & K_{55} & K_{56} \\ K_{61} & K_{62} & K_{63} & K_{64} & K_{65} & K_{66} \end{bmatrix} \begin{bmatrix} U_i \\ U_j \\ U_k \\ V_i \\ V_j \\ V_k \end{bmatrix} \qquad (5.17)$$

where K_{11} .... K_{66} are the nodal point stiffness coefficients obtained from the equation (5.16).

The equilibrium equation at the nodal point A in the U and V directions are

$$F = f_j^K + f_k^L + f_k^M + f_j^N + f_i^P + f_i^Q \qquad (5.18)$$

$$G = g_j^K + g_k^L + g_k^M + g_j^N + g_i^P + g_i^Q \qquad (5.19)$$

in which the subscript refers to the nodes and the power refers to the element.

From equation (5.17) we have

$$\begin{aligned} F = {} & K_{21}^K U_i^K + K_{22}^K U_j^K + K_{23}^K U_k^K + K_{24}^K V_i^K + K_{25}^K V_j^K \\ & + K_{26}^K V_k^K + K_{31}^L U_i^L + K_{32}^L U_j^L + K_{33}^L U_k^L + K_{34}^L V_i^L \\ & + K_{35}^L V_j^L + K_{36}^L V_k^L + K_{31}^M U_i^M + K_{32}^M U_j^M + K_{33}^M U_k^M \\ & + K_{34}^M V_i^M + K_{35}^M V_j^M + K_{36}^M V_k^M + K_{21}^N U_i^N + K_{22}^N U_j^N \end{aligned}$$

$$+ K^N_{23}\, U^N_k + K^N_{24}\, V^N_i + K^N_{25}\, V^N_j + K^N_{26}\, V^N_k + K^P_{11}\, U^P_i$$
$$+ K^P_{12}\, U^P_j + K^P_{13}\, U^P_k + K^P_{14}\, V^P_i + K^P_{15}\, V^P_j + K^P_{16}\, V^P_k$$
$$+ K^Q_{11}\, U^Q_i + K^Q_{12}\, U^Q_j + K^Q_{13}\, U^Q_k + K^Q_{14}\, V^Q_i + K^Q_{15}\, V^Q_j$$
$$+ K^Q_{16}\, V^Q_k \qquad (5.20)$$

From compatibility condition, we obtain

$$U_1 = U^K_i = U^L_i \quad ; \quad V^K_i = V^L_i = V_1$$
$$U_2 = U^K_k = U^N_i \quad ; \quad V^K_k = V^N_i = V_2$$
$$U^K_j = U^L_k = U^M_k = U^N_j = U^P_i = U^Q_i = U_3$$
$$V^K_j = V^L_k = V^M_k = V^N_j = V^P_i = V^Q_i = V_3$$
$$U_4 = U^L_j = U^M_i \quad ; \quad V^L_j = V^M_i = V_4$$
$$U_7 = U^N_k = U^P_k \quad ; \quad V^N_k = V^P_k = V_7$$
$$U_6 = U^P_j = U^Q_k \quad ; \quad V^P_j = V^Q_k = V_6$$
$$U_5 = U^M_j = U^Q_j \quad ; \quad V^M_j = V^Q_j = V_5 \qquad (5.21)$$

From equation (5.20) we have

$$F = (K^K_{21} + K^L_{31})\, U_1 + (K^K_{22} + K^L_{33} + K^M_{33} + K^N_{22} + K^P_{11}$$
$$+ K^Q_{11})\, U_3 + (K^K_{23} + K^N_{21})\, U_2 + (K^L_{32} + K^M_{31})\, U_4$$
$$+ (K^M_{32} + K^Q_{12})\, U_5 + (K^N_{23} + K^P_{13})\, U_7 + (K^P_{12} + K^Q_{13})$$
$$U_6 + (K^K_{24} + K^L_{34})\, V_1 + (K^K_{25} + K^L_{36} + K^M_{36} + K^N_{25}$$
$$+ K^P_{14} + K^Q_{14})\, V_3 + (K^K_{26} + K^N_{24})\, V_2 + (K^L_{35} + K^M_{34})$$
$$V_4 + (K^M_{35} + K^Q_{15})\, V_5 + (K^N_{26} + K^P_{16})\, V_7 + (K^P_{15}$$
$$+ K^Q_{16})\, V_6$$

or $$F = UU\ U_1 + U_0\ U_3 + U_L\ U_2 + UUR\ U_4 + UR\ U_5 + UDL\ U_7 + UD\ U_6 + VU\ V_1 + V_0\ V_3 + V_L\ V_2 + VUR\ V_4 + VR\ V_5 + VDL\ V_7 + D_D\ V_6 \qquad (5.22)$$

Similarly we get

$$G = UU'\ U_1 + U_0'\ U_3 + U_L'\ U_2 + UUR'\ U_4 + UR'\ U_5 + UDL'\ U_7 + UD'\ U_6 + VU'\ V_1 + V_0'\ V_3 + VL'\ V_2 + VUR'\ V_4 + VR'\ V_5 + VDL'\ V_7 + VD'\ V_6 \qquad (5.23)$$

The convenient way to obtain the superposition of the nodal stiffness coefficients U_0 ... VD and U_0' ... VD' in the equations (5.22) and (5.23) has been recorded in the appendix D describing the computational analysis.

5.5 RESULTS OBTAINABLE FROM THE SOLUTION OF THE EQUILIBRIUM EQUATIONS

From the equilibrium equations (5.22) and (5.23) formed at each nodal point, the nodal displacements in the directions of X and Y are obtained. And by using equation (5.9) or directly the equation (A5.13), the stresses in the elements can be computed.

5.6 METHOD OF SOLUTION OF EQUILIBRIUM EQUATION

For most practical problems, equations (5.22) and (5.23) represent a system of several hundred equations. The

major difficulties which are encountered in a direct solution of such a large set of equations are that a big storage is required and the time of solution is increased enormously with the number of equations. For these reasons, an iterative method has to be used to solve such a large number of simultaneous equations. It has been found that the well known Gauss-Seidel over-relaxation iteration procedure is best suited to tackle such equations.

In this study the digital computer IBM 7090 has been used to solve these equilibrium equations by the Gauss-Seidel method. The Gauss-Seidel procedure is merely a systematic relaxation technique for solving the linear equations (Varga 1962; Khabaza, 1963; Faddeeva, 1959). The set of equilibrium equations to be solved at each nodal point can be written in the form

$$X_1 = \frac{1}{a_{11}} \left(b_1 - a_{12}X_2 - a_{13}X_3 \cdots\cdots - a_{1n}X_n \right)$$

$$X_2 = \frac{1}{a_{22}} \left(b_2 - a_{21}X_1 - a_{23}X_3 \cdots\cdots - a_{2n}X_n \right) \qquad (5.24)$$

$$X_n = \frac{1}{a_{nn}} \left(b_n - a_{n1}X_1 \cdots\cdots - a_{nn-1}X_{n-1} \right)$$

An initial approximation to the solution is taken as

$$X_1 = \frac{b_1}{a_{11}} \quad , \quad X_2 = \frac{b_2}{a_{22}} \quad \cdots\cdots \quad X_n = \frac{b_n}{a_{nn}}$$

The next approximation is obtained by substituting these approximations into the right hand side of equations (5.24). The process is continued until successive approximations for all unknown are within some preset tolerance.

5.7 OVER-RELAXATION FACTOR AND ERROR CRITERIA

The rate of convergence of the Gauss-Seidel procedure can be greatly accelerated by the use of an over-relaxation factor (Lehman, 1960). After each iteration, the change in the displacement of a nodal point is calculated and then the over-relaxation factor is applied.

Suppose after S cycles of iteration, the change in displacement (r) at any nodal point n

$$\Delta r_n^{(S)} = r_n^{(S)} - r_n^{(S-1)} \tag{5.25}$$

The new displacement of nodal point n is then determined from the following equation

$$r_n^{(S+1)} = r_n^{S} + \beta \Delta r_n^{S} \tag{5.26}$$

where β is the over-relaxation factor.

The rate of convergence for a particular solution depends greatly on the selection of the over-relaxation factor. It has been shown in figure (5.3) how the convergence of a particular solution in the study has been obtained with the minimum number of iterations. Moreover, it has been found

in our solutions that the over-relaxation factor between 1.5 - 1.6 gives the best convergence.

In the solution of a given problem, the main error lies in the solution of the simultaneous equations (equations (5.22) and (5.23)) to determine the nodal displacement. By experimenting with different tolerable relative errors, it has been concluded that a relative error of $.5 \times 10^{-3}$ gives good results. The number of iterations required to reduce the relative error depends on the characteristics of the problem, mesh size and the boundary conditions.

The influence of error on the results is investigated by a flexible strip loading case on a homogeneous material with assumed elastic properties. When the error is reduced from 10^{-3} to 10^{-5}, there is hardly any change in results (up to the third decimal point). But the number of iterations is increased enormously which can be seen from figure (5.3) in which the relationship between the error and the iteration is plotted. Even with the optimum over-relaxation factor of 1.5, it took approximately 100 iterations to get the results within the relative error of 10^{-3}, whereas an accuracy of 10^{-5} is obtained with about 300 iterations. So, for the efficient numerical solution of a problem, the preset tolerance to get the convergence has to be examined properly.

5.8 INFLUENCE OF MESH SIZE

In order to investigate the influence of mesh size

on the accuracy of results, the author solved a flexible strip loading problem in an elastic medium with different mesh sizes. The three different mesh sizes are denoted A, B and C, figure (5.4). The mesh size 'A' consists of elements of uniform area. The mesh size 'B' and mesh size 'C' are made of graded elements. But the mesh size 'C' contains more nodal points at the regions of high stress gradient in comparison with mesh size 'B'. Figure (5.5) shows the vertical stresses obtained at the centre line of the loading by the use of different mesh sizes and the results are compared with the elastic solution. It is observed from the results that there is hardly any difference between the results of mesh size 'C' and the elastic solution. Thus as the mesh size is refined, the results converge to the true solution. It may be noted that the computer programme developed can be used for as many nodal points as desired.

5.9 STRESS AMBIGUITY

Equation (5.9) can be used for the determination of stresses in the element. This equation can be written as

$$\{\sigma\} = [S]\{U\}$$

where $\{\sigma\} = \begin{Bmatrix} \sigma_x \\ \sigma_y \\ \tau_{xy} \end{Bmatrix}$ = stresses in element

$$\{U\} = \begin{Bmatrix} U_i \\ U_j \\ U_k \\ V_i \\ V_j \\ V_k \end{Bmatrix} = \text{nodal displacements for triangle}$$

$[S]$ = the so-called stress matrix and depends on nodal co-ordinates, Young's modulus and Poisson's ratio.

Since stresses and strains are constant within any given triangle, discontinuities in these terms will occur across common edges of adjacent triangles. Hence ambiguity arises in interpreting stress data and plotting results. The computed nodal point displacements are unambiguous, but considerable difficulties may be encountered in plotting and evaluating stresses at a point unless a very fine mesh is used. Moreover, the stress ambiguity cannot be removed in the stiffness finite element method. But various methods may be developed to get nodal point stresses. Wilson (1963) suggested a 'weighted average' method which can be used to determine nodal point stresses. The method involves the following calculations to determine the three components of stress at point i figure (5.6).

$$\sigma_x = \frac{1}{S_x} \sum_n \frac{a^{(n)}}{a^{(n)}+b^{(n)}} \sigma_x^{(n)}$$

$$\sigma_y = \frac{1}{S_y} \sum_n \frac{b^{(n)}}{a^{(n)}+b^{(n)}} \sigma_y^{(n)}$$

$$\tau_{xy} = \frac{1}{N} \sum_n \tau_{xy}^{(n)}$$

where

$$a^{(n)} = \left| X_k^{(n)} + X_j^{(n)} - 2X_i \right|$$

$$b^{(n)} = \left| Y_k^{(n)} + Y_j^{(n)} - 2Y_i \right|$$

$$S_x = \sum \frac{a^{(n)}}{a^{(n)}+b^{(n)}}$$

$$S_y = \sum \frac{b^{(n)}}{a^{(n)}+b^{(n)}}$$

The summation is performed on all N elements connected at nodal point i.

Generally (Zienkiewicz, 1967) the stresses are assumed to concentrate at the centroid of each triangle from which the nodal point stresses are calculated. The author has applied the method of averaging the element stresses of all stresses connected to the nodal point. Figure (5.7) shows a typical nodal point 'A' and the stresses at the nodal point 'A' are obtained by taking the average stresses contributed by the elements 1, 2, 3 and 4. Such averaging gives better results than the methods mentioned above. Recently Argyris (1965) has suggested the introduction of three more nodal points on the sides of the triangle and a linearly varying strain distribution in the element. This will produce better

results than the elements with constant strain and stress, particularly in the case of problems involving large stress gradients.

5.10 LAYERED SYSTEM

A two layered problem under a flexible strip loading figure (5.8a) has been solved. The elastic properties assumed are shown in the figure. The stresses obtained at different points are compared with the closed form solution given by Lemcoe (1060). From Fig. (5.8b) it can be observed that there is a great difference in results, especially at the interface of two layers. It can only be commented that this finite element technique (displacement method) does not give good results in the solution of such interface problems. Higher order approximations are necessary. Alternatively, a finely graded mesh on the interface will give more sensible results.

CHAPTER 6

SOLUTION OF A BOUNDARY VALUE PROBLEM BY THE FINITE ELEMENT METHOD USING NON-LINEAR STRESS-STRAIN RELATIONS

6.0 INTRODUCTION

It has already been mentioned that the solution of most boundary value problems with non-linear material properties, is virtually impossible using classical methods. However, the development of the finite element method and other methods of analysis using digital computers now makes the solution of non-linear problems tractable. The finite element method which is discussed in the previous chapter, is extended in this chapter to the considerations of non-linear problems. A boundary value problem is formulated and solved with assumed non-linear material properties. The assumption of the material properties is guided by the observations discussed in chapter 4.

Clough (1965) has commented on the extension of the finite element method to treat non-linear material properties. Further, Clough and Woodward (1967) showed that the incremental construction history can be conveniently accounted together with the effect of non-linear properties. Wilson (1964) suggested two possible solution techniques called a step-by-step procedure and a trial and error procedure which may be used for the finite element analysis of two-dimensional structures with non-linear behaviour. The step-by-step

procedure involves the replacing of the non-linear analysis by the sum of a sequence of piece-wise linear analyses, each subjected to a small increment of load. In the trial and error procedure, the equilibrium position of a structure subjected to a given set of loads may be determined by a trial and error procedure. In this case the structure is solved repeatedly until the final geometry and stresses agree with the assumed geometry and stresses. A similar trial and error process is applicable with non-linear material properties.

King (1965) and Raphael and Clough (1965) used the incremental procedure mentioned above for the analysis of temperature and creep effects in the construction of concrete gravity dams. Another method is used by Reyes (1965) for the determination of stresses around underground openings where the material behaviour is elastic-plastic. This method also involves the incremental process. But for the plastic range the yield condition of perfectly plastic material as given by Drucker and Prager (1952) is utilized. This yields a stress-strain relationship in the plastic range from which the stress-strain matrix, D*, may be expressed as a function of the current stress components. Zienkiewicz and Cheung (1966) listed the three ways of using the finite element method in rock mechanics to consider non-linear behaviour for a uniaxial situation. These were noted earlier

---

* Equation (5.8) in the previous chapter.

by Argyris (1965) and are:

(i) direct iterative process

(ii) incremental-initial strain process

(iii) incremental-varying elasticity process.

In the first approach, it is assumed that the stress-strain relationships are unique and that, therefore, a hypothetical set of elastic (secant) constants can be associated with every value of stress. This method is similar to the trial and error procedure mentioned above. In the second process, the load is applied incrementally with the initial elastic properties which are kept constant throughout the process. Figure (6.3c) illustrates this method in which the non-linear relationship is replaced by the elastic-plastic behaviour. The inelastic strains are found for each increment and these are used to find the stress increment for the next increment of loading. The third method is the same as method (ii), but the elastic properties are allowed to vary in each increment of loading.

The author's approach to the solution of non-linear problems is the 'step-by-step' procedure with the direct iterative technique. A computer programme is developed for the solution of an example of this type of problem and without any major changes this programme may be used for other problems.

6.1 NON-LINEAR ANALYSIS BY THE FINITE ELEMENT METHOD

Clough (1965; 1967), Wilson (1964), Argyris (1965),

Zienkiewicz and Cheung (1967) have all considered the extension of the finite element method to treat non-linear problems. Non-linearity due to geometric changes and the material behaviour, both can be treated in this method. This can be further elucidated from the equation (5.16), mentioned in the previous chapter. This relation

$$F(\text{force}) = A^{-1^T} K A^{-1} u \qquad (\text{displacement})$$

(in matrix form)clearly illustrates how the above two factors may be treated in the finite element analysis. For a linear material, the matrix A and K are constant and hence the solution of linear problems is straightforward in the finite element method. For material non-linearity, K is a function of the element properties and in the case of geometric non-linearity, A is a function of geometry. The non-linearity due to geometric changes will not be considered further in this study.

The main relation where the non-linear material properties enters into the finite element method may be indicated by equation (5. 9). In this relation the matrix [D] is the prominent form which has to be generated according to the material behaviour and this matrix [D] ultimately changes the stiffness matrix [K] which can be seen from equation (5.15).

It is assumed at the outset that the non-linear relationship can be approximated by a bi-linear model and

a hypothetical set of elastic (secant) constants can be associated with every value of total stress. A direct iterative process is then as follows,

(i) compile stress distribution based on the initial values of elastic constants.

(ii) a new set of elastic constants is found for each element based on values obtained from (i) when the stress in the elements exceeds the limit at which the change of elastic properties takes place.

(iii) the stages (i) and (ii) are repeated until convergence is obtained.

As a whole, the analysis of non-linear problems by the finite element method on the basis of material non-linearity, is to create a new stiffness matrix for load under which the change of material properties takes place. The method by which the new stiffness is generated in order to solve non-linear problems, is discussed in the following section.

6.2 FORMULATION OF THE PROBLEM AND METHOD OF SOLUTION

A flexible strip loading problem with defined boundary conditions as shown in figure (6.1) is taken as an example to illustrate the use of the finite element method using non-linear material properties. Conditions of plane strain are assumed and the non-linear behaviour of the material under the loads is given by the following models,

(i) Bi-linear model (1) as shown in figure (6.2a)

(ii) Bi-linear model (2) as shown in figure (6.2b)

(iii) Tri-linear model (3) as shown in figure (6.2c)

The assumed values of the elastic constants are indicated in the figures. The magnitude of loading is varied from 500 p.s.i. to 3000 p.s.i. and the stress at which the elastic parameters changes is also noted in figure (6.2).

The first step in using the finite element method is to idealize the continuum with elements which will adequately represent the geometry and provide more detail in the region of larger stress changes. The most commonly used, triangular elements are adopted with their nodal points connected together as illustrated in figure (6.1b). There are altogether 275 nodal points and 392 elements in the mesh which has represented the domain over which the displacements and stresses are to be obtained. Naturally, the smaller the mesh size, the more accurate would be the answer, but this is limited by obvious practical considerations such as the storage available in the computer used and time of execution required for the programme.

With the mesh size shown in figure (6.1b), the problem is fed to the computer IBM 7090 with the appropriate instructions and assumed material properties. This computer programme is discussed in appendix D. The whole process of the finite element technique as mentioned in the previous sections is performed to obtain displacements and stresses

at the nodal points using the step-by-step method with the direct iterative procedure to account for the non-linear material properties. In essence, the material under the load is assumed to behave linearly up to a certain total stress* with stiffness properties in each element defined on the basis of total local stress. The stiffness of the element is re-evaluated on the basis of whether the stress in the element has exceeded the stress at which the elastic properties are assumed to alter before the final results are obtained. So, the analysis involves the following sequence of operations:

(i) determination of the state of stress in the element with the initial elastic parameters.

(ii) formulation of new stiffness matrix on the basis of new elastic parameters as determined from stresses calculated in (i).

(iii) the final solution for displacements and stresses at the required nodal points.

The basis on which the new elastic parameters are assigned to the elements can be explained from figure (6.3). The compressibility (K) which is a function of total stress, is assumed to vary as shown in figure (6.3a) and (6.3b), whereas the modulus of rigidity (G) is taken to be independent of total stress. This hypothesis seems to be quite reasonable from the experimental studies discussed in

---

* This term is used in chapter 4 to correlate the non-linear behaviour.

chapter 4. According to the state of stress, the elastic parameters are alloted to the elements and the new stiffness is calculated from the new secant moduli mentioned above.

The convergence of a solution using Gauss-Siedel iteration with over-relaxation, has already been discussed in the previous chapter. It can only be mentioned here that the over-relaxation factor of 1.6 is found to be the optimum value for these solutions.

6.3 DISCUSSION OF RESULTS

The magnitudes of the stresses and displacements obtained under the flexible strip loading at different sections mentioned in figure (6.1) using model 1 and model 2 are shown in figures (6.4) to (6.7). The vertical and horizontal displacements of selected points for different surface loads are indicated in figures (6.8) to (6.22). The horizontal, vertical and shear stresses expressed as the percentage of the surface load intensity of 1000 p.s.i. as well as 2000 p.s.i. are illustrated in figures (6.23) to (6.28). The results obtained from the linear elastic solution are plotted also in the above figures. In a similar way, the results obtained by using model 3 are plotted in figures (6.29) to (6.31). Moreover, model 1 has been studied in further detail, figure (6.34), to see the effect of Poisson's ratio on the distribution of stresses under the loading. The results are given in figures (6.32) to (6.34).

6.3.1 Results of model 1 and model 2.

The vertical displacements of point (1) to point (9) (figure (6.1)) vary with the surface loading as plotted in figures (6.8) to (6.16) and indicate a non-linear behaviour up to approximately a load level of 1500 p.s.i. Then the slopes of the load-displacement lines are parallel to the bounded lines which have been obtained from the linear solutions as mentioned in the figures. The distinct non-linear relation between the vertical displacement and the applied load has an interesting correspondence with results of field plate bearing tests mentioned in chapter 2, and which illustrates the non-linear behaviour of rocks. The maximum non-linear effects are found at the surface where the stress concentration is high and as the influence of stress is reduced, the influence of non-linearity becomes quite negligible. Moreover, the maximum effect of surface loads on the vertical displacement is found to be up to a depth equal to B, after which the vertical displacements are reduced by 50 to 60% of the surface displacements. At distances equal to 2B, the vertical displacements at different depths do not change at all.

The horizontal displacements obtained at the selected points and plotted against the loads in figures (6.17) to (6.22) also show non-linear behaviour. But the results are different from the vertical displacements in the sense that the horizontal displacements under the two models do not

behave well within the bounded lines obtained from the elastic solution. It is seen from figures (6.4) and (6.5) that the non-linear effect is more prominent at depths than at the surface and the horizontal displacement increases up to a depth equal to B. Some of the model tests on dry sand reported by Eggestad (1963) show that the maximum lateral strains occur at a depth of about B near the centre line of loading which clearly agrees with the results obtained in these solutions. The linear solutions do agree to the above findings. Some of the lateral strains obtained by him at different depths are plotted against the loading ratio in figures (6.35) and (6.35). The nature of the relationship obtained between lateral strain and the loading ratio bears an interesting qualitative correspondence with some of the results from the bi-linear model.

The stresses obtained at different depths which are shown in figures (6.23) to (6.28), indicate that the stresses, especially the vertical stresses, are in good agreement with the results predicted by the theory of elasticity. There is about a maximum of 10% difference between the horizontal stresses obtained from these models and the results obtained by the elastic solution. In the case of shear stresses, there is about a maximum difference of 5%. The important result is found that the vertical stresses obtained by using two different models give practically the same results which agree remarkably well with the elastic solution based

on Boussinesq's formula. Some of the field tests reported by Turnbull et al (1961), Plantema(1953), show that the Boussinesq's solution for the vertical stresses is in good agreement with the field measurements. Moreover, the field tests obtained by the Waterways Experimental Station (1951-1954) on different soils arrived at the same conclusion. So, it can be concluded from our results also that the elastic solution can be used for the calculation of vertical stresses which are used for the prediction of settlements. Moreover the close agreement between the results obtained from two different models with varying elastic parameters indicates that the vertical stresses are independent of the stress-strain relation of the material to a reasonable degree of approximation. This accounts, in part, for the success of current methods of predicting settlements in normally consolidated clays.

6.3.2 Results of model 3.

The stresses obtained by using this model figure (6.2c) are plotted in figures (6.29) to (6.31). The results of the vertical stresses compared with the elastic solution further illustrates the good agreement achieved in the previous section. Only the magnitudes of horizontal stresses are about 10% less than the elastic solution at different depths. The values of the shear stresses also agree well with the elastic solution. The computer programme as

developed can be readily extended to any number of components simulating a non-linear curve. The only limitation is one of computation time.

6.3.3 Results of model 1 with varying Poisson's ratio.

Model (1) is used with varying Poisson's ratio in order to investigate the effect of Poisson's ratio on the distribution of stresses at different depths. Figures (6.32) to (6.34) illustrate the results obtained with the surface load of 750 p.s.i. only. The vertical stresses, figure (6.33), at different depths are found to be unaffected with the variation of Poisson's ratio and the results also agree with the elastic solution. The distribution of shear stresses at different depths (figure (6.34)) shows that there is hardly any effect of Poisson's ratio. But the variation of Poisson's ratio has a great influence on the distribution of horizontal stresses (figure (6.32)). The important result observed in this case, is that when there is no change in Poisson's ratio, the horizontal stress obtained agrees quite well with the elastic solution. The greater is the variation of Poisson's ratio between piece-wise linear steps, the greater is the deviation of results from the solution of elasticity. This can be explained from the fact that in order to maintain the continuity of displacement within the element with bi-linear properties, the horizontal stresses are changed according to the variation of Poisson's ratio. This can be

explained from figure (6.37). Let figure (6.37a) represent position of two elements before the load is applied. After the application of loads, the elements will deform which is indicated in figure (6.37b). If there is greater variation of Poisson's ratio in the material properties, the differential displacements between the elements will be more in comparison to the stage when there is hardly any alteration of Poisson's ratio. Therefore, the element with lesser Poisson's ratio has to pull out to maintain the continuity between the elements.

6.4 PRACTICAL ASPECTS OF NON-LINEAR SOLUTION

From a practical point of view, there are many aspects which should be considered for the solution of non-linear problems. The representation of the material properties and the time of execution of computer programmes, should be noted. It is obvious that as the behaviour of the material is better represented, the results will converge to the actual solution. As there is a limitation to such representation, practical experience and experimental results have to be used to meet practical requirements. In this finite element method, the nature of the mesh size which represents the whole problem, is one of the main factors which should be kept in mind. Within the capacity of the computer available, the mesh size has to be fixed in such a way which will offer more nodal points in the region where the stress gradient is expected

to be high.

The time of execution of different solutions are mentioned in table (6.1). This is greatly influenced by the number of equations to be solved and iterations required to obtain the convergence limit. The number of equations are obviously fixed by the type of mesh size used with boundary conditions at different nodal points. The convergence limit of the solution has to be determined which will give acceptable results. It is already noted, figure (5.3) that as the convergence limit is reduced, the number of iterations increases. So before going into the details of a particular solution, a trial run has to be performed to find the reasonable convergence limit which will offer an acceptable time of execution of the programme and correct results. It is beyond the scope of this study to go into the details of convergence of numerical solutions. From the experience gained here the relationship between the convergence limit and the number of iterations required figure (5.3), will definitely help to fix the acceptable convergence criterion.

TABLE (6.1)

COMPUTATION TIME OF DIFFERENT SOLUTIONS

Type of Solution	Time taken
1) Linear solutions	maximum 5 mins.
2) Non-linear solutions	
a) Bi-linear models	12 mins.
b) Tri-linear model	15 mins.

CHAPTER 7

STRESSES IN AN EXCAVATION USING A LUMPED PARAMETER MODEL

7.0 INTRODUCTION

When a material is subjected to general loading conditions and constraints, it is expected that the highly stressed regions of the material will fail or yield first and as the applied load is increased, the plastic regions may enlarge or new yield regions may be developed. The quantitative analysis or prediction of such progressive yielding of plastic regions in rock or soil under different loading conditions and boundary constraints, is an extremely difficult and analytically unsolved problem of continuum mechanics. In this chapter a numerical method called a lumped parameter model developed by Ang and Harper (1963), is presented to study the stress configuration and development of the plastic region behind a vertical excavation under plane strain conditions due to self weight. The material is assumed to be elastic - perfectly plastic but the method may be applied to materials with other mechanical behaviour.

Many authors (Panek, 1951; Barton, 1954; Roy, 1956; Savin, 1961) reported the analyses of stresses in a continuous medium or in load bearing structural components with various shapes of holes such as semi-circular, V-shaped and elliptical notches. The analyses were generally restricted

to simple uniaxial loading and were not concerned with body forces. Allen and Southwell (1950) noted that the approximate solutions of contained problems of plastic flow were possible through a finite difference determination of a stress function and Schjodt (1958) used such a method with a relatively coarse grid to obtain a solution for an open excavation in an elastic medium with weight. De No (1966) presented a dissertation in which he attempted to compute the plastic flow in a vertical excavation. As will be noted, his approach may be subjected to serious criticism. Finn (1966) also presented some data about the stresses behind a vertical excavation due to self weight. His solution is for an elastic medium and he used a relatively coarse mesh size. Some of his results which are obtained by the finite element method are compared with the present model. Dibiagio (1966) reported a solution for an open trench in an elastic medium with weight computed with finite differences. The same sample problem is solved here with the lumped parameter model and the results are compared. Sturgul and Scheidegger (1967) also presented the finite difference method for the determination of tectonic stresses in the vicinity of a wall in a homogeneous elastic field. Wang and Singh (1965) reported the use of the lumped parameter model as mentioned here, to obtain stress distribution at the bottom of a bore hole for an elastic - perfectly plastic medium. The solution takes into account loads due to the overburden, fluid pressure in the hole due to the circulating

medium and stresses induced by a bit tooth at the hole bottom. They showed also that the development of the yielded region under such stress configuration encountered in rock drilling can be traced.

7.1 DESCRIPTION OF LUMPED PARAMETER MODEL

A lumped parameter model is used as a substitute system in place of a plane continuum. Such a substitution in the physical system is mathematically equivalent to the use of finite difference approximations to governing differential equations (Ang and Harper, 1964).

The discrete model is described symbolically in figure (7.1a). Essentially, it is composed of mass points and stress points that are arranged into a square grid with sides of length, say h. The mass points are located at the corner of the squares and the stress points at the centre. The displacements are defined at mass points, whereas the strains and corresponding stresses are defined only at stress points. The X and Y axes of the model system make an angle of 45° with the centre line or line of symmetry of the physical problem and the boundaries of the model contain mass points only.

This model provides a physical basis for discretization of a plane continuum. In addition, the model satisfies the requirement that the relationships and equations of the model are identically the same as the usual finite difference

approximations to the differential relationships and equations of the corresponding continuum. With such a property, the convergence of a sequence of solutions (corresponding to a decreasing sequence of mesh sizes of the model) toward the true solution of the continuum may be inferred on the basis of mathematical theories relating to the convergence of linear finite difference systems (Courant et al, 1928).

Referring to figure (7.1a), the strain-displacement relationship for a typical stress point "1" can be expressed from the model as follows:

$$\epsilon_{x_1} = \frac{U_a - U_b}{D}$$

$$\epsilon_{y_1} = \frac{V_d - V_c}{D} \qquad (7.1)$$

and

$$\gamma_{xy_1} = \frac{U_d - U_c}{D} + \frac{V_a - V_b}{D}$$

in which ϵ_{x_1}, ϵ_{y_1} and γ_{xy_1} are the strain components at the stress point "1"; U_a, U_b, U_c and U_d are the component of displacements in the X direction at the mass points a, b, c and d respectively; V_a, V_b, V_c and V_d are the component of displacements in the Y direction at the mass points a, b, c and d respectively; D is the diagonal distance between mass points.

These relationships are identically the same as of the finite difference approximation of the differential

relationship

$$\epsilon_x = \frac{\partial u}{\partial x}$$

$$\epsilon_y = \frac{\partial v}{\partial y}$$

and $$\gamma_{xy} = \frac{\partial u}{\partial y} + \frac{\partial v}{\partial x}$$

The normal and shearing forces acting on a regular mass point "1" as shown in figure (7.1b) are related to the stresses defined at the neighbouring stress point as follows:

$$F_x = \sigma_x \cdot D/2$$

$$F_y = \sigma_y \cdot D/2 \qquad (7.2)$$

$$F_{xy} = \tau_{xy} \cdot D/2$$

where F_x, F_y and F_{xy} are the forces. The thickness of the model is taken as unity.

The equations of equilibrium for the forces acting on the mass point "a" in figure (7.1b) in the absence of body forces are

$$F_{x_3} - F_{x_1} + F_{xy_4} - F_{xy_2} = 0$$

and (7.3)

$$F_{y_4} - F_{y_2} + F_{xy_3} - F_{xy_1} = 0$$

Thus with this model, the equations of equilibrium

are found at mass points of the problem at all levels of applied loads and through the appropriate stress-strain relationship (discussed in the later section) and through equation (7.1), the whole problem is transformed into the determination of displacements at all mass points. But it does not satisfy the conditions of compatibility.

7.2 FORMULATION OF THE PROBLEM

The problem with the assumed elastic parameters, geometry and other assumed material constants, is shown in figure (7.2). The material properties assumed in the analysis is elastic - perfectly plastic with zero friction. The constitutive relationships of such material may be conveniently divided into the following parts:

(i) A stress-strain relationship in the elastic range

(ii) a yield criterion for defining the initiation of plastic yielding and

(iii) a stress-strain relationship in the plastic region.

The unloading and relaoding criteria are not considered in the above relation and are not taken into account for the solution of the problem.

7.2.1 Elastic stress-strain relation

Within this elastic range, the material is assumed to follow Hooke's linear relationship and under plane strain conditions, the elastic stresses are expressed as

$$\sigma_x = \frac{E}{(1+m)(1-2m)}\left[(1-m)\epsilon_x + m\,\epsilon_y\right]$$

$$\sigma_y = \frac{E}{(1+m)(1-2m)}\left[(1-m)\epsilon_y + m\,\epsilon_x\right] \qquad (7.4)$$

$$\tau_{xy} = G\,\gamma_{xy}$$

in which E is Young's modulus, m is Poisson's ratio and G is the shear modulus.

7.2.2 Yield criterion

The yield condition known as the Von Mises is used to define the limit of the elastic behaviour and the initiation of plastic straining under all possible combinations of stresses. For a plane strain condition, this criterion, can be expressed as

$$\left(\frac{\sigma_x - \sigma_y}{2}\right)^2 + \tau_{xy}^2 = k^2 \qquad (7.5)$$

where k is the yield stress in simple shear.

It may be noted that the left-hand side of equation (7.5) is identical to the square of the maximum shear stress in the X-Y plane and hence we get

$$T_{max}^{m} = k \qquad (7.6)$$

where T_{max}^{m} is the maximum shear stress.

7.2.3 Plastic stress-strain relationship

During plastic flow, the material is assumed to obey

the stress-strain rate relationship of the Prandtl-Reuss theory (Prager and Hodge, 1951). The theory assumes that in an elastic - plastic deformation there is no plastic volume change and the plastic strain rate is proportional to the deviator stress.

For an elastic - perfectly plastic solid under plane plastic flow, it can be shown that the plastic stress-strain equations expressed in incremental form (after Harper and Ang, 1963) are

$$\begin{aligned}
\Delta\sigma_x &= \Delta\epsilon_x\left[\frac{4G+3K}{3} - \frac{G}{k}\left(\frac{\sigma_x-\sigma_y}{2}\right)^2\right] \\
&\quad + \Delta\epsilon_y\left[\frac{-2G+3K}{3} + \frac{G}{k^2}\left(\frac{\sigma_x-\sigma_y}{2}\right)^2\right] \\
&\quad + \Delta\gamma_{xy}\left[-\frac{G}{k^2}\tau_{xy}\left(\frac{\sigma_x-\sigma_y}{2}\right)\right] \\
\Delta\sigma_y &= \Delta\epsilon_x\left[\frac{-2G+3K}{3} + \frac{G}{k^2}\left(\frac{\sigma_x-\sigma_y}{2}\right)^2\right] \\
&\quad + \Delta\epsilon_y\left[\frac{4G+3K}{3} - \frac{G}{k^2}\left(\frac{\sigma_x-\sigma_y}{2}\right)^2\right] \\
&\quad + \Delta\gamma_{xy}\left[\frac{G}{k^2}\tau_{xy}\left(\frac{\sigma_x-\sigma_y}{2}\right)\right] \qquad (7.7) \\
\Delta\tau_{xy} &= \Delta\epsilon_x\left[\frac{-G}{k^2}\tau_{xy}\left(\frac{\sigma_x-\sigma_y}{2}\right)\right] \\
&\quad + \Delta\epsilon_y\left[\frac{G}{k^2}\tau_{xy}\left(\frac{\sigma_x-\sigma_y}{2}\right)\right] \\
&\quad + \Delta\gamma_{xy}\left[G\left(1 - \frac{\tau_{xy}^2}{k^2}\right)\right]
\end{aligned}$$

in which K is the bulk modulus.

At a yielded stress point, these incremental stresses are added to the stresses at the previous load level to obtain the total stresses.

7.3 BOUNDARY CONDITIONS

By symmetry only half of the physical problem as shown in figure (7.2) need be considered. The following boundary conditions are assumed:

(i) It is assumed that the bottom row of mass points is fixed, i.e.

$$U_{i,j} = V_{i,j} = 0 \quad \text{for} \begin{cases} i = M \\ J = 1, \ \ldots \ N \end{cases}$$

(ii) To simulate the model for a semi-infinite body, it is assumed that the horizontal displacement of the rightmost column of mass points is zero and that the vertical displacement will be equal to the vertical displacement of mass points immediately to the left of this end column.

If these displacements are resolved in the X and Y directions, the boundary conditions on the right-hand edge of the model become (refer figure 7.2)

$$U_{i,j} = \frac{1}{2}\left(U_{i,j-1} + V_{i,j-1} \right)$$

$$V_{i,j} = U_{i,j}$$

$$\text{for} \begin{cases} i = 1, \ \ldots \ M-1 \\ j = N \end{cases}$$

(iii) The boundary conditions on the left edge of the model (from the condition of symmetry) are

$$U_{i,j} = V_{i,j+2}$$

$$V_{i,j} = U_{i,j+2}$$

$$\text{for } \begin{cases} i = M_A, \ \ldots \ M \\ j = 1 \end{cases}$$

7.4 EQUATIONS OF EQUILIBRIUM

In the problem analysed here, the excavation is assumed to have been previously open, the weight of the material is applied to each mass point. Therefore the equations of equilibrium of a typical mass point "a" as noted in equation (7.3), are reformulated as

$$F_{x_3} - F_{x_1} + F_{xy_4} - F_{xy_2} + \frac{\gamma h^2}{\sqrt{2}} = 0$$

and

$$F_{y_4} - F_{y_2} + F_{xy_3} - F_{xy_1} + \frac{\gamma h^2}{\sqrt{2}} = 0 \qquad (7.8)$$

Using equation (7.2) and dividing by D/2, we get

$$\sigma_{x_3} - \sigma_{x_1} + \tau_{xy_4} - \tau_{xy_2} + \gamma h = 0$$

and

$$\sigma_{y_4} - \sigma_{y_2} + \tau_{xy_3} - \tau_{xy_1} + \gamma h = 0 \left(h = D/\sqrt{2}\right) \qquad (7.9)$$

Through equations (7.4) and (7.1), the equations of equilibrium may be expressed in displacements of different mass points.

7.5 PROCEDURE FOR THE SOLUTION OF THE PROBLEM

As shown in figure (7.2), the geometry is replaced by conveniently spaced mass points and stress points. The use of different mesh sizes is discussed in the following section. The method of computation is essentially a step-by-step procedure of determining a set of displacements of mass points for each loading which produce a compatible set of stresses at the stress points and that satisfy the requirements of statical equilibrium, as given by equation (7.9). The self weight of the material at each mass points is increased in small increments and at each load level the displacements of mass points which satisfy the equilibrium equations and boundary conditions, are determined. At each load level, whether any mass point has gone to the plastic range is examined by equation (7.6). The calculations of the stress increments at stress points that are within the elastic range are based on equation (7.4), whereas for regions that have yielded, the stress increments are calculated using equation (7.7). To calculate the stress increment in the plastic range, incremental strains and instantaneous stresses are required. The strains are calculated from the displacements as shown in equation (7.1) and the difference between the total strains of two consecutive loads is taken as the strain increment and the stresses at the last load level are substituted for the instantaneous stresses.

Thus the whole problem is reduced to the problem of

solution of linear equations at each mass points to determine the displacements which satisfy the equilibrium equations (7.9) and boundary conditions noted in section (7.3). These linear equations are solved with the Gauss-Seidel iteration method. The details of the numerical procedure with the computer programme are described in appendix E.

7.6 DISCUSSION OF RESULTS

The problem as illustrated in figure (7.2) is solved with a grid of (28 x 21) mass points. The density of the material is increased from 100 lbs. per cu. ft. by an increment of 2 lbs. per cu. ft. The different density at which the stress points have yielded are noted in figure (7.3). The first yielding developed at the toe of the excavation and as the density increased, the plastic regions spread. Up to the density of 150 lbs. per cu. ft., the development of the plastic region is quite fast. Then the load has to be increased significantly to obtain further spreading of the plastic zone. At the density of 380 lbs. per cu. ft., no equilibrium is obtained and the solution could not be pursued. The maximum shear stress (as percentage of the yield stress) obtained at the end of loading of 370 lbs. per cu. ft., are shown in figure (7.4). An interesting result is the development of a tension region at the upper part of the model, figure (7.2). The development of such tension regions which have reached the plastic zone may produce the critical situation of failure.

This problem has also been solved with a grid of (55 x 41) mass points and practically the same results are obtained as mentioned above.

De No (1966) submitted a report on the development of plastic flow behind a vertical excavation with the same material behaviour as discussed here. In his analysis he assumed that the shear strength of the material increased suddenly at a certain depth so that the material underlying the horizontal surface of the excavation remained elastic. When first yielding occurred at the toe of the excavation, the increment of weight was computed so that the yield condition be again reached at a new stress point. The plastic zone was permitted to develop horizontally and the procedure is repeated in such a way that in every increment of loading the yielding condition was reached in a different stress point at a different row and column until the plastic zone reaches the surface of the model. Therefore the whole procedure of the plastic flow is influenced by the decisions of the programmer.

The problem mentioned in figure (7.2) is solved again with Poisson's ratio of 0.25 and .45. But the regions below the horizontal surface of the excavation are not allowed to yield. The density of the material is increased from 100 lbs./cu. ft. in increments of 10 lbs./cu. ft. The results obtained with Poisson's ratio of 0.25 are shown in figure (7.5) and figure (7.6) shows the results with Poisson's ratio of 0.45. From the above results, it is found that the development

of the plastic zone is greatly influenced by Poisson's ratio. Both results show a tension zone at the top of the model. No equilibrium is reached with a density of 210 lbs./cu. ft. in the case of Poisson's ratio of .25 and a density of 310 lbs./cu. ft. is the critical value for Poisson's ratio of .45. An interesting result with Poisson's ratio of 0.25 is the development of one complete plastic zone at the base of the excavation as shown in figure (7.5). This can be explained from figure (7.7). The strength of the material is constant which is shown by the dotted lines. The maximum shear stress increases with depth and at the region where there is a complete plastic zone, the maximum shear stress exceeds the allowable stress in the material.

A problem considered by Dibiagio (1966) is shown in figure (7.8). He solved the problem with unit weight of the material using the finite difference equations. The same problem is solved here by the lumped parameter model and a comparison of the stresses obtained is shown in figures (7.9) to (7.11). In figures (7.9) to (7.11) stress contours are drawn which illustrate the stress pattern for a portion of the region investigated. The stresses are expressed in dimensionless quantities by expressing them in terms of the unit weight of the material and the grid spacing parameter "h". The figures represent the changes in stress brought about by unloading of the bottom and sides of the excavation. These results are compared with the results obtained by

Dibiagio (1966) and there is no significant difference in the results. The deformed network of grid points due to self weight of 100 lbs. per cu. ft. are portrayed by the displacement grid in figure (7.12). There is sideways displacement of the grid points in the sides of the excavation and the badly deformed grid squares in the vicinity of the corner of the excavation are observed. Such deformation was also reported in the photoelastic study of a vertical slope by means of a gelatine model (La Rochelle, 1960).

Figure (7.13) shows a problem solved by Finn (1966) with the finite element method. The problem was also analysed for the gravity stress field and he tabulated the results of stresses obtained at different points as mentioned in the figure. The same problem is solved with this lumped parameter model. As Finn (1966) used a relatively coarse mesh size, there is a difference in results between the two methods. But the development of tension region is indicated at the upper part by both the methods. The magnitude of the stresses at the boundary in Finn's solution are suspect. Figure (7.14) shows the comparison between the results obtained by the two methods.

CHAPTER 8

CONCLUSIONS

The use of linear elasticity for the solution of various deformation problems is in accord with the real behaviour of rocks. The deformation of most rocks is non-linear and has an irreversible component. This non-linearity and irreversibility may arise from a macro-fissure system in what is inherently a linear elastic rock or it may be intrinsic to a porous micro-fissured rock such as a sandstone.

From the experimental studies of Bunter sandstone at different confining pressures, it may be concluded that the three significant features of the stress-strain relation of such a relatively homogeneous porous rock are non-linearity, hysteresis and the irrecoverable strain on unloading. Porosity is the main factor that influences the non-linear deformation of rock at stress levels which are of primary interest to the Civil Engineer. All these characteristic features increase with increasing porosity. The compressional wave velocity is also found to vary with porosity. All specimens tested came from the same location and therefore the variation in porosity is representative of a natural condition. This variation in porosity has accounted for a variation in rock stiffness of several hundred percent and it demonstrates that sufficient specimens from any site should be tested in order to determine the variation of rock deformation properties.

The behaviour of the sandstone is best interpreted in terms of micro-cracks closing on compression and energy being dissipated by friction due to relative movement along their interface. The model developed by Walsh (1965) can be used to explain qualitatively the deformation characteristics of many rocks and the interesting question of how elastic constants like Young's modulus, Poisson's ratio and compressibility depend on different shapes and types of cracks can be evaluated.

The experiments on the sandstone reveal that the change in compressibility is essentially path independent at low stress level and the relationship between compressibility and the total stress constitutes a real material property. The real behaviour of sandstone is more complex than that considered in current theories of composite media. It may be concluded that the non-linear stress-strain relationship of sandstone is controlled by the compressibility of the material until the compressibility of quartz is reached.

The use of different confining pressures in the experimental studies reveal that when the confining pressure is high enough to close the micro-cracks in the rocks, the stress-strain relationship is linear. The effects of wetting show greater non-linearity, hysteresis and residual strains for given porosity and pressure and the presence of moisture reduces the strength of the material.

The non-linear behaviour of rocks can be approximated by the bi-linear, tri-linear or any suitable models and the

finite element method may be used to solve different boundary value problems with such material behaviour. A method by which the non-linear problems can be solved with the finite element technique is developed. The studies of a flexible strip loading on material having non-linear properties, reveal an interesting correspondence with results of field plate bearing tests and the vertical stresses obtained by using different models give practically the same results which agree remarkably well with the elastic solution based on Boussinesq's formula. But the horizontal and the shear stresses are different. It is concluded that the elastic solution can be used for the prediction of settlements. A computer programme is developed for the solution of non-linear problems and without any major changes this programme can be used for many configurations.

The displacement approach of the finite element method is now well developed whereas the equilibrium model of the finite element (the derivation of stiffness depending on the stress distribution) has to be studied further to get a complete solution of a problem. Pian (1965), Khanna (1966), Marcel and Hayes (1967) considerations of the equilibrium model deserve to be extended for the solution of non-linear problems.

A lumped parameter model developed by Ang and Harper (1963) is found to be a useful numerical approach for the solution of various elastic or non-linear problems. In comparison with the finite difference approach for the solution

of excavation problems with gravity stress fields, this lumped parameter model is found to be efficient and simple. From the practical point of view also, it takes less time for the execution of the computer programme. The use of this model for the studies of the propagation of plastic regions in excavations due to self weight needs further investigation and it would be of interest to couple it with experimental data. Christian's (1966) analysis leading to incremental stress-strain relations for different yield criterions may be extended for the solution of excavation problems as noted.

The development of the computer programmes in this study and other available computational schemes will surely make it possible to use complicated stress-strain relations for the prediction of stresses and displacements under different loads and boundary conditions applied to rock masses. This suggests that laboratory and theoretical research into the stress-strain behaviour of rocks aimed at developing general models is important. The two dimensional studies have to be extended to the three dimensional case to represent the actual conditions in the field. The lumped parameter model approach is only particularly useful for two dimensionsal problems. Some effort has already been spent on extending the finite element method to three dimensions (Argyris, 1965; Zienkiewicz, 1967). Further effort of this nature will make practical the computation of stresses in realistic rock masses.

APPENDIX A

SLIDING AFTER CRACKS CLOSE

A crack which has closed under an applied uniaxial compression σ' can support a normal stress σ_n and a frictional shear stress τ_f. Finding the relative displacement of the crack faces after closing is most easily done by dividing the applied stress by means of Mohr's circle into components normal and parallel to the crack as shown in figure (A3.1).

The stress system of figure (A3.1) can be separated into superposable simple stress system as shown in figure (A3.2). It is seen from the various stress states figure (A3.2) sliding motion at the crack surface is represented by applied shear stress $\tilde{\tau}_{xy} - \tilde{\tau}_f$ and stress free crack surface.

The frictional shear stress τ_f can be related to the normal stress σ_n on the crack surface by the usual law of dry friction

$$\tilde{\tau}_f = \mu \sigma_n \qquad (A3.1)$$

where μ is the coefficient of friction.

The assumption is now made that the crack remains open until the applied stress σ_y normal to the crack reaches a value σ_c. The normal stress σ_n on the crack surface is assumed to increase linearly with σ_y after the

crack has closed, i.e.

$$\sigma_n = \sigma_y - \sigma_c \qquad (A3.2)$$

The equation (A3.1), (A.3.2) and the expressions for τ_{xy} and τ_y are combined to give

$$\tau_{xy} - \tau_f = \sigma \sin\beta(\cos\beta - \mu \sin\beta) + \mu\sigma_n \qquad (A3.3)$$

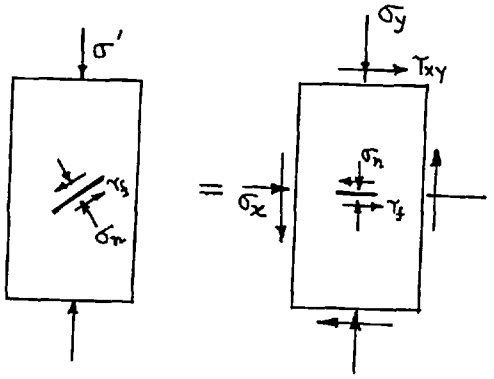


fig. A 3.1

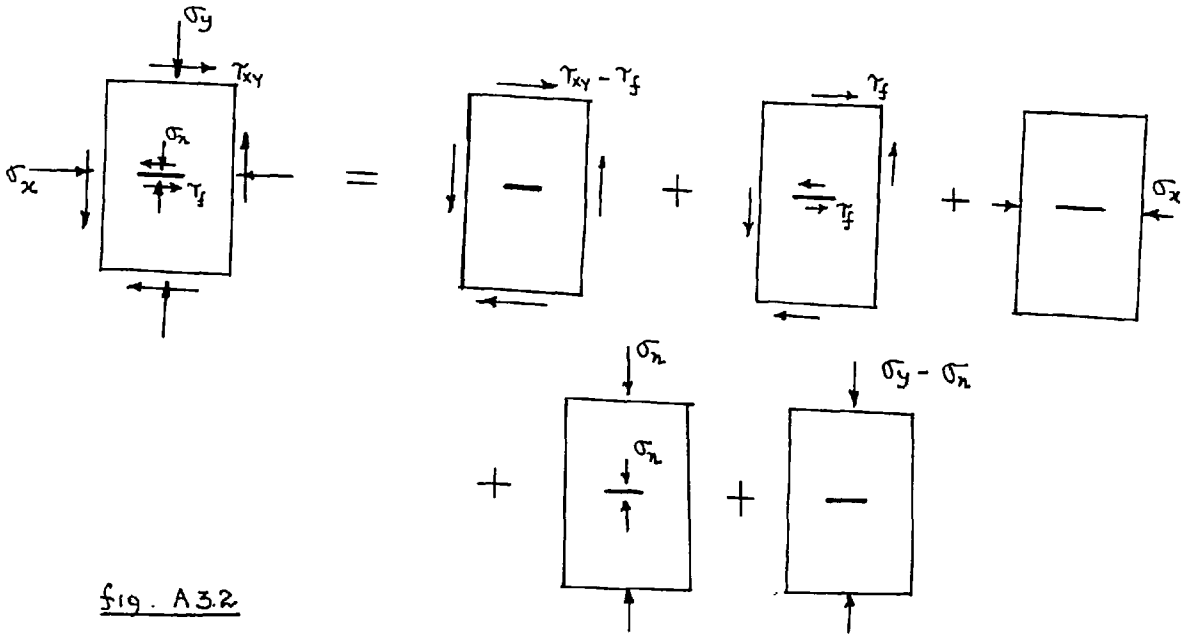


fig. A3.2

APPENDIX B

COMPRESSIBILITY AS A FUNCTION OF ROCK COMPOSITION

We are considering here a mathematical expression which can be obtained to show compressibility as a function of rock composition also.

Chree (1892) showed using reciprocal theorem, that the decrease in volume of the solid material $(V_o - V_c)$, due to an increase in pressure ΔP (external) is given $C_r \Delta P V_o$. In differential form,

$$d(V_b - V_p) = C_r d\sigma V_b$$

where V_b is the bulk volume of the rock material

V_p is the volume of the pores of the rock material

C_r is the grain compressibility

σ is the external pressure

or

$$\frac{dV_b}{V_b d\sigma} = C_r + \frac{dV_p}{V_b d\sigma}$$

or

$$C_b = C_r + \frac{dV_p}{V_p d\sigma} \times \frac{V_p}{V_b}$$

where C_b is the bulk volume compressibility

or

$$C_b = C_r + f \cdot C_p \qquad (A4.1)$$

where f is the porosity of the rock material.

We have

$$C_r = G \cdot C_g + M \cdot C_m \qquad (A4.2)$$

where G = grain content

C_g = grain compressibility

M = intergranular material content

C_m = intergranular material compressibility

and

$$G = (1 - M)$$

or

$$M = 1 + G \qquad (A4.3)$$

From equation (A4.1), (A4.2) and (A4.3) we get

$$C_b = G\, C_g + (1 + G)C_m + f \cdot C_p$$

or

$$C_b = (C_g + C_m)G + C_m + f \cdot C_p \qquad (A4.4)$$

The equation (A4.4) shows that the composition of rock is a great factor on the measurement of compressibility.

APPENDIX C

DERIVATION OF STIFFNESS FOR AN ARBITRARILY ORIENTED TRIANGULAR ELEMENT

The matrix $[A]$ in the final stiffness expression (equation (5.16)) requires to be inverted. This can be done by partioning the matrix so as to exclude as much as possible most of the zeros. Partioning it into a set of (3 x 3) matrix, the matrix $[A]$ symbolically becomes (equation (5.3))

$$[A] = \begin{bmatrix} a_{11} & o \\ o & a_{11} \end{bmatrix} \qquad (A5.1)$$

and

$$[A^{-1}] = \begin{bmatrix} a_{11}^{-1} & o \\ o & a_{11}^{-1} \end{bmatrix} \qquad (A5.2)$$

Thus the matrix $[A]$ is reduced to finding $[a_{11}^{-1}]$. This can easily be evaluated by making use of the principle of matrix inversion by means of the adjoint matrix.

By definition

$$[a_{11}^{-1}] = \frac{\text{Adj } a_{11}^{*}}{\det a_{11}}$$

or

$$[a_{11}^{-1}] = \frac{\text{Adj } a_{11}}{|a_{11}|} \qquad (A5.3)$$

---

* An adjoint matrix is defined as the transposed matrix of its co-factors and $|a_{11}.|$ is obtained by multiplying elements of a_{11} and adj a_{11}.

From equation (A5.1) and through equation (5.3), we have

$$\left[a_{11}\right] = \begin{bmatrix} 1 & X_i & Y_i \\ 1 & X_j & Y_j \\ 1 & X_k & Y_k \end{bmatrix}$$

Co-factors of

$$\left[a_{11}\right] = \begin{bmatrix} (X_jY_k - X_kY_j) & -(Y_k - Y_j) & (X_k - X_j) \\ -(X_iY_k - X_kY_i) & (Y_k - Y_i) & -(X_k - X_i) \\ (X_iY_j - X_jY_i) & -(Y_j - Y_i) & (X_j - X_i) \end{bmatrix} \quad \text{(A5.4)}$$

$$\text{Adj } a_{11} = \begin{bmatrix} (X_jY_k - X_kY_j) & -(X_iY_k - X_kY_i) & (X_iY_j - X_jY_i) \\ -(Y_k - Y_j) & (Y_k - Y_i) & -(Y_j - Y_i) \\ (X_k - X_j) & -(X_k - X_i) & (X_j - X_i) \end{bmatrix} \text{(A5.5)}$$

$$\left|a_{11}\right| = \begin{bmatrix} 1 & X_i & Y_i \\ 1 & X_j & Y_j \\ 1 & X_k & Y_k \end{bmatrix} \begin{bmatrix} (X_jY_k - X_kY_j) & -(X_iY_k - X_kY_i) & (X_iY_j - X_jY_i) \\ -(Y_k - Y_j) & (Y_k - Y_i) & -(Y_j - Y_i) \\ (X_k - X_j) & -(X_k - X_i) & (X_j - X_i) \end{bmatrix}$$

$$= \begin{bmatrix} (X_jY_k - Y_jX_k) & 0 & 0 \\ -X_i(Y_k - Y_j) & & \\ +Y_i(X_k - X_j) & & \\ 0 & (X_jY_k - Y_jX_k) - X_i(Y_k - Y_j) & 0 \\ & +Y_i(X_k - X_j) & \\ 0 & 0 & (X_jY_k - Y_jX_k) - X_i(Y_k - Y_j) \\ & & +Y_i(X_k - X_j) \end{bmatrix} \quad \text{(A5.6)}$$

From equation (A5.5) and equation (A5.6) we get

$$\left[a_{11}^{-1}\right] = \frac{1}{\left[a_{11}\right]} \begin{bmatrix} (X_j Y_k - X_k Y_j) & -(X_i Y_k - X_k Y_i) & (X_i Y_j - X_j Y_i) \\ -Y_{kj} & Y_{ki} & -Y_{ji} \\ -X_{jk} & -X_{ki} & X_{ji} \end{bmatrix} \quad \text{(A5.7)}$$

where $X_{jk} = X_j - X_k$; $Y_{kj} = Y_k - Y_j$

$X_{ki} = X_k - X_i$; $Y_{ki} = Y_k - Y_i$

$X_{ji} = X_j - X_i$; $Y_{ji} = Y_j - Y_i$

$$\left[A^{-1}\right] = \frac{1}{\left[a_{11}\right]} \begin{bmatrix} (X_j Y_k - X_k Y_j) & -(X_i Y_k - X_k Y_i) & (X_i Y_j - X_j Y_i) & 0 & 0 & 0 \\ -Y_{kj} & Y_{ki} & -Y_{ji} & 0 & 0 & 0 \\ -X_{jk} & -X_{ki} & X_{ji} & 0 & 0 & 0 \\ 0 & 0 & 0 & (X_j Y_k - X_k Y_j) & -(X_i Y_k - X_k Y_i) & (X_i Y_j - X_j Y_i) \\ 0 & 0 & 0 & -Y_{kj} & Y_{ki} & -Y_{ji} \\ 0 & 0 & 0 & -X_{jk} & -X_{ki} & X_{ji} \end{bmatrix} \quad \text{(A5.8)}$$

We have element stiffness from equation (5.15)

$$K = \int_{vol} \left[B^T\right] \left[D\right] \left[B\right] \, dv$$

Taking unit thickness

$$K = \left[B^T\right] \left[D\right] \left[B\right] \; * \; \text{Area of the element}$$

$$\text{Area of the element} = \frac{1}{2}\begin{bmatrix} 1 & X_i & Y_i \\ 1 & X_j & Y_j \\ 1 & X_k & Y_k \end{bmatrix}$$

$$= \frac{1}{2}\begin{bmatrix} a_{11} \end{bmatrix}$$

$$K = \begin{bmatrix} B^T \end{bmatrix}\begin{bmatrix} D \end{bmatrix}\begin{bmatrix} B \end{bmatrix} * \frac{1}{2}\begin{bmatrix} a_{11} \end{bmatrix} \qquad \text{(A5.9)}$$

From equation (5.7), putting

$$\lambda = \frac{E(1-m)}{(1+m)(1-2m)}$$

$$\mu = \frac{Em}{(1+m)(1-2m)}$$

and

$$\nu = \frac{E}{2(1+m)}$$

we get

$$\begin{bmatrix} D \end{bmatrix} = \begin{bmatrix} \lambda & \mu & 0 \\ \mu & \lambda & 0 \\ 0 & 0 & \nu \end{bmatrix} \qquad \text{(A5.10)}$$

From equation (A.5.9) we get

$$K = \begin{bmatrix} 0 & 0 & 0 & 0 & 0 & 0 \\ 0 & \lambda & 0 & 0 & 0 & \mu \\ 0 & 0 & \nu & 0 & \nu & 0 \\ 0 & 0 & 0 & 0 & 0 & 0 \\ 0 & 0 & \nu & 0 & \nu & 0 \\ 0 & \mu & 0 & 0 & 0 & \lambda \end{bmatrix} \frac{1}{2}\begin{bmatrix} a_{11} \end{bmatrix} \qquad \text{(A5.11)}$$

Through equation (A5.8) and equation (A5.10) we get the expression for the nodal point stiffness as follows:

$$\bar{K} = \left[A^{-1}\right]^T [K] \left[A^{-1}\right]$$

$$= \frac{1}{2 \cdot [a_{11}]} \times$$

$$\begin{array}{cccccc}
\lambda Y_{kj}^2 + \nu X_{jk}^2 & - & - & - & - & - \\
-\lambda Y_{ki} Y_{kj} + \nu X_{ki} X_{jk} & \lambda Y_{ki}^2 + \nu X_{ki}^2 & - & \text{Symmetrical} & - & - \\
\lambda Y_{ji} Y_{kj} - \nu X_{ji} X_{jk} & -\lambda Y_{ji} Y_{ki} - \nu X_{ji} X_{ki} & \lambda Y_{ji}^2 + \nu X_{ji}^2 & - & - & - \\
\nu Y_{kj} X_{jk} + \mu X_{jk} Y_{ki} & \nu Y_{kj} X_{ki} - \mu X_{jk} Y_{ki} & -\nu Y_{kj} X_{ji} + \mu X_{jk} Y_{ji} & \nu Y_{kj}^2 + \lambda X_{jk}^2 & - & - \\
-\nu Y_{ki} X_{jk} + \mu X_{ki} Y_{kj} & -\nu Y_{ki} X_{ki} - \mu X_{ki} Y_{ki} & \nu Y_{ki} X_{ji} + \mu X_{ki} Y_{ji} & -\nu Y_{ki} Y_{kj} + \lambda X_{ki} X_{jk} & \nu Y_{ki}^2 + \lambda X_{ki}^2 & - \\
\nu Y_{ji} X_{jk} - \mu X_{ji} Y_{kj} & \nu Y_{ji} X_{ki} + \mu X_{ji} Y_{ki} & -\nu Y_{ji} X_{ji} - \mu X_{ji} Y_{ji} & \nu Y_{ji} Y_{kj} - \lambda X_{ji} X_{jk} & -\nu Y_{ji} Y_{ki} - \lambda X_{ji} X_{ki} & \nu Y_{ji}^2 + \lambda X_{ji}^2
\end{array}$$

(A5.12)

From this equation (A5.12), the nodal point stiffness of any element has been calculated directly by putting the co-ordinates of the nodal points and the elastic parameters.

CALCULATION OF STRESS IN AN ELEMENT

From equation (5.9) we have

$$[\sigma] = [D][B][A^{-1}][\delta]$$

Through equation (A5.10), equation (5.6) and equation (A5.8) we can get the stress in an element.

$$\sigma = \frac{1}{[a_{11}]} \begin{bmatrix} -\lambda Y_{kj} & \lambda Y_{ki} & -\lambda Y_{ji} & -\mu X_{jk} & -\mu X_{ki} & \mu X_{ji} \\ -\mu Y_{kj} & \mu Y_{ki} & -\mu Y_{ji} & -\lambda X_{jk} & -\lambda X_{ki} & \lambda X_{ji} \\ -\gamma X_{jk} & -\gamma X_{ki} & \gamma X_{ji} & -\gamma Y_{kj} & \gamma Y_{ki} & -\gamma Y_{ji} \end{bmatrix} \begin{bmatrix} U_i \\ U_j \\ U_k \\ V_i \\ V_j \\ V_k \end{bmatrix} \quad \text{(A5.13)}$$

APPENDIX D

COMPUTER PROGRAMME: FINITE ELEMENT METHOD

The programme which is listed here, is coded in the Fortran language and has been used with the IBM 7090 computer. The maximum mesh size that can be used is governed by the availability of computer storage. The programme listed here is for the solution of the non-linear problem as discussed in chapter 6. The maximum number of nodal points used in this programme is 225 and the maximum number of elements is 398. The programme consists of a main programme and nine subroutines. The programme performs three major tasks in the complete analysis of a problem with two dimensional triangular elements. First, the equilibrium equations for the system are formed from a basic numerical description of the system. Second, this set of equations is solved for the displacements of the nodal points by an iterative procedure. And third, the internal stresses are determined from these displacements. The main sequence of operations of the computer programme is shown in a flow diagram, figure (A6.1).

The following main operations are performed for the solution of the non-linear problem.

(i) All input data are read. All the nodal points are located in the two dimensional array and the elements are numbered with their elastic properties.

(ii) The nodal point stiffness matrix for each element

from equation (5.16) is formulated with the help of the subroutine STFNO.

(iii) The coefficients of the stiffness matrix are formulated with the help of four subroutines FORMU 1 to FORMU 4 according to the position of the nodal points and the equations of equilibrium are formed at all nodal points with their boundary conditions.

(iv) These equilibrium equations are solved by the Gauss-Seidel over-relaxation iteration method until an acceptable error is achieved and the displacements of all nodal points are noted with the element number (subroutine DISPL).

(v) From the nodal point displacements, the stresses are calculated by using the equation (A5.13) in subroutine STRESS. The stresses obtained in each element are checked whether they have exceeded the limit at which the elastic properties change or not. If so, the appropriate elastic properties are alloted to the elements and the operations (ii) to (v) are repeated until convergence to the acceptable error is obtained. The convergence criteria is given in two subroutines called subroutine COMP and subroutine COMPP. The relative error can be found from the following expression

$$\text{relative error} = \left(\frac{\text{New value - old value}}{\text{New value}}\right)$$

(vi) The desired displacements and stresses are printed.

The computer programme thus developed can be used for other cases with minor changes. The programme is listed in figure (A6.2).

FIGURE (A6.1)

FLOW DIAGRAM OF NUMERICAL COMPUTATION

FINITE ELEMENT METHOD

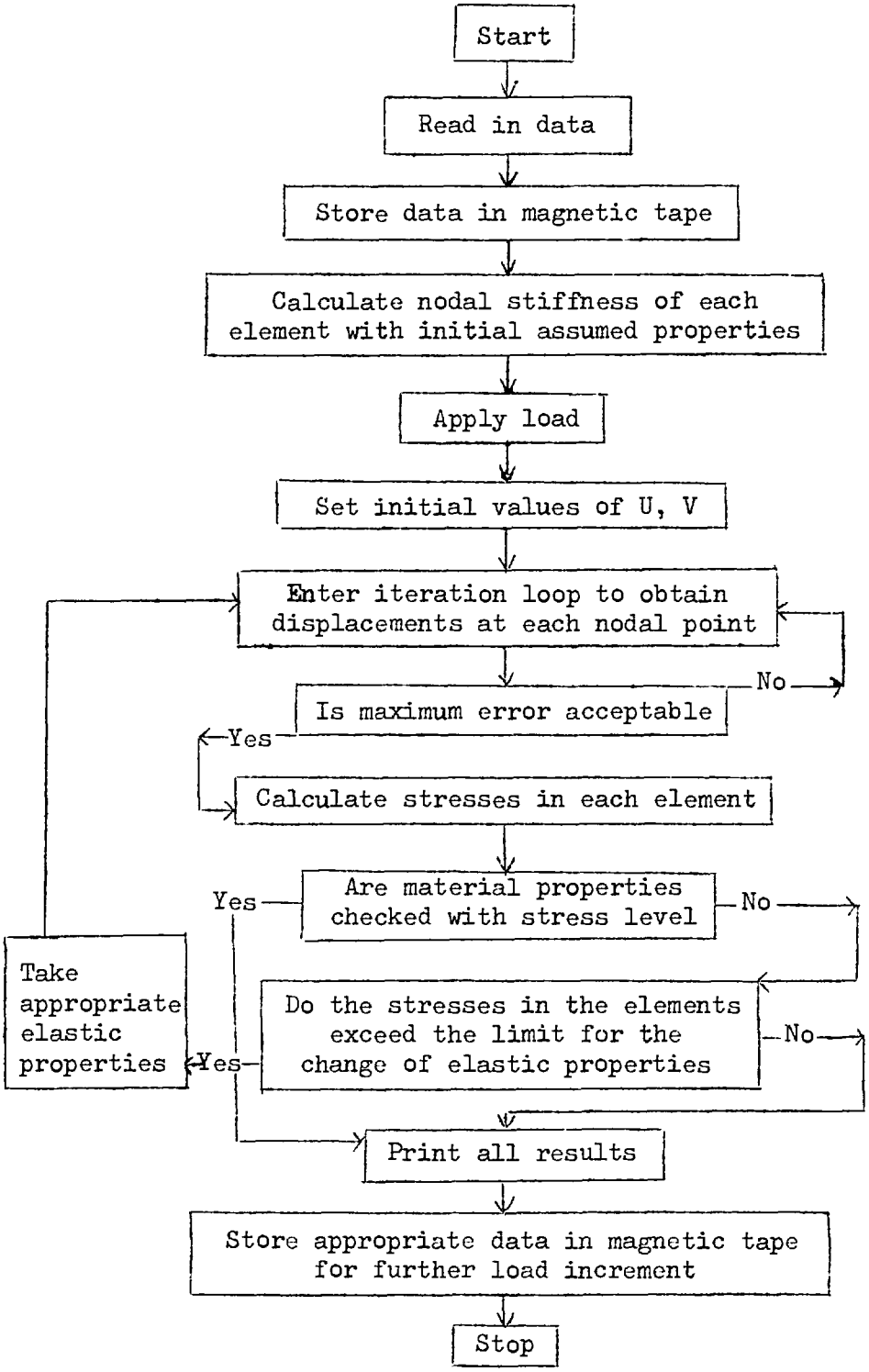


FIG. A6.1

FIG. (A.6.2) LISTING OF THE COMPUTER PROGRAMME: FINITE ELEMENT METHOD

```
C BILINEAR MODEL FOR THE SOLUTION OF NON-LINEAR DEFORMATION OF ROCKS
      COMMON SM(6,2352),E(392),POIS(392),CI,II,JJ,KEY,ITER,MXITER,SITER
     1,W,NA,NB,NC,ND,MA,MB,MC,MD,U(15,15),V(15,15),IK,IN,SS(28,6,1),
     2FL(14),A(3,3),SN(6,6),C,I,J,UO,UL,UR,UU,UUR,UD,UDL,VO,VL,VR,VU,VUR
     3,VD,VDL,BMC,EP,ER,L,DE,U1(15,15),V1(15,15),MITER,LOAD,SSX(392),SSY
     4(392),SSXY(392),SX(392),SY(392),SXY(392),PR,YM
     5 ,BL(392)
      READ(5,11) NO,ITER,MXITER,W,     ER,PR,YM
      READ(5,12) NA,NB,NC,ND,MA,MB,MC,MD
      READ(5,14) FL
   11 FORMAT(3I10, F10.3,F10.5,F10.2,F10.0)
   12 FORMAT(8I9)
   14 FORMAT(11F6.0)
      PRINT90
   90 FORMAT(34H LOAD ON UNIT 85 REEL NUMBER X0334)
      CALL PAUSE
      BMC=1000.
      EP=0.
      SITER=0.
      MITER=0
      LOAD=1
      DO 21 I=1,NB
      DO 21 J=1,NB
      U(I,J)=0.
   21 V(I,J)=0.
      DO 22 I=1,NA
      POIS(I)=.33
   22 E(I)=50000
C CALCULATE NODAL STIFFNESS WITH ALL ELEMENT PROPERTIES
   18 SITER=SITER+1.
      ITER=0
      N=0
      DO 101 L=1,NA
C READ CO-ORDINATES OF NODAL POINTS
      READ(9)((A(I,J),J=1,3),I=1,3)
      AE= A(2,2)*A(3,3)-A(3,2)*A(2,3)-A(1,2)*A(3,3)+A(1,2)*A(2,3)+A(1,3)
     1*A(3,2)-A(1,3)*A(2,2)
      DE=.5/AE
      CALL STFNO(1,1)
      DO 102 M=1,6
      DO 102 NL=1,6
        NN=N+NL
      SM(M,NN)=SN(M,NL)
  102 CONTINUE
      N=N+6
  101 CONTINUE
      REWIND9
      CI=0.
      II=0
      JJ=0
   10 KEY=0
      ITER=ITER+1
      IF(SITER.EQ.2.) GO TO 130
      GO TO 131
  130 WRITE(6,23) ITER,CI,II,JJ
```

```
  23 FORMAT(I10,E16.6,2I10)
131 CI=0.
    I=1
    J=1
    K=4
    L=1
    CALL FORMU1(K,L)
    RY=
   1    (FL(J)-UR*U(I,J+1)-VR*V(I,J+1)-VD*V(I+1,J))/VO
    CALL COMPP(RY)
    K=2
    L=2
    DO 40 J=2,NC
    CALL FORMU2(K,L)
    RX=
   1   (-UL*U(I,J-1)-UR*U(I,J+1)-UD*U(I+1,J)-UDL*U(I+1,J-1)-VO*V(I,J)-
   1VL*V(I,J-1)-VR*V(I,J+1)-VDL*V(I+1,J-1)-VD*V(I+1,J))/UO
    CALL COMP(RX)
    K=K+3
    CALL FORMU2(K,L)
    RY=
   1    (FL(J)-UL*U(I,J-1)-UR*U(I,J+1)-UD*U(I+1,J)-UDL*U(I+1,J-1)-UO*U(
   1I,J)-VL*V(I,J-1)-VR*V(I,J+1)-VD*V(I+1,J)-VDL*V(I+1,J-1))/VO
    CALL COMPP(RY)
    L=L+12
    K=2
 40 CONTINUE
    L=3
 42 I=I+1
    IF(I.EQ.NB) GO TO 43
    K=6
    J=1
    CALL FORMU3(K,L)
    RY=
   1   (-UR*U(I,J+1)-UUR*U(I-1,J+1)-VR*V(I,J+1)-VU*V(I-1,J)-VUR*V(I-1,J
   1+1)-VD*V(I+1,J))/VO
    CALL COMPP(RY)
    L=L+5
    K=K-4
    DO 41 J=2,NC
    CALL FORMU4(K,L)
    RX=
   1   (-UL*U(I,J-1)-UR*U(I,J+1)-UU*U(I-1,J)-UUR*U(I-1,J+1)-UD*U(I+1,J)
   1-UDL*U(I+1,J-1)-VO*V(I,J)-VL*V(I,J-1)-VR*V(I,J+1)-VU*V(I-1,J)-VUR*
   2V(I-1,J+1)-VD*V(I+1,J)-VDL*V(I+1,J-1))/UO
    CALL COMP(RX)
    K=K+3
    CALL FORMU4(K,L)
    RY=
   1   (-UL*U(I,J-1)-UR*U(I,J+1)-UU*U(I-1,J)-UUR*U(I-1,J+1)-UD*U(I+1,J)
   1-UDL*U(I+1,J-1)-UO*U(I,J)-VL*V(I,J-1)-VR*V(I,J+1)-VU*V(I-1,J)-VUR*
   2V(I-1,J+1)-VD*V(I+1,J)-VDL*V(I+1,J-1))/VO
    CALL COMPP(RY)
    L=L+12
```

```
      K=2
   41 CONTINUE
      L=L+7
      GO TO 42
   43 IF(KEY.EQ.0) GO TO 15
      IF(MXITER-ITER) 15,15,10
   15 IB=1
      IC=1
      WRITE(6,100)((U(I,J),J=1,NB),I=1,NB)
      WRITE(6,100)((V(I,J),J=1,NB),I=1,NB)
  100 FORMAT(8E16.7)
      IN=1
      WRITE(6,180)
  180 FORMAT(1HO,10X,2HSX,10X,2HSY,12X,3HSXY,18X,3HPS1,18X,3HPS2,19X,5H
     4THETA)
   17 CALL DISPL(IB,IC)
C  CALCULATE  STRESS OF THE ELEMENTS
      IK=1
      DO 16 ICON=1,MB
      READ(9)((A(I,J),J=1,3),I=1,3)
      DE=  A(2,2)*A(3,3)-A(3,2)*A(2,3)-A(1,2)*(A(3,3)-A(2,3))+A(1,3)*
     1(A(3,2)-A(2,2))
      CALL STRES(IN)
      IK=IK+1
      IN=IN+1
   16 CONTINUE
      IB=IB+1
      IF(IB.EQ.NB) GO TO 114
      IC=1
      GOTO 17
  114 REWIND9
      IF(SITER.EQ.2.) GO TO 115
      IF(EP.EQ.1.) GO TO 18
  115 DO 171  I=1,NO
      XX=(SX(I)-SY(I))/2.
      XY=(SX(I)+SY(I))/2.
      TMAX=SQRT(SXY(I)*SXY(I)+XX*XX)
      PS1=XY+TMAX
      PS2=XY-TMAX
      THETA=28.64789*ATAN(SXY(I)/XX)
  171 WRITE(6,172) SX(I),SY(I),SXY(I),PS1,PS2,TMAX,THETA
  172 FORMAT(7E16.6)
      WRITE(6,190)(E(I),I=1,NO)
  190 FORMAT(10E12.3)
      CALL HOLD(9)
      STOP
      END
```

```
      SUBROUTINE STFNO(I,J)
       COMMON SM(6,2352),E(392),POIS(392),CI,II,JJ,KGY,ITER,MXITER,SITER
     1,W,NA,NB,NC,ND,MA,MB,MC,MD,U(15,15),V(15,15),IK,IN,SS(28,6,1),
     2FL(14),A(3,3),SN(6,6),C,I,J,UO,UL,UR,UU,UUR,UD,UDL,VO,VL,VR,VU,VUR
     3,VD,VDL,BMC,EP,ER,L,DE
      EA=E(L)/(2.*(1.+POIS(L)))
      EB=(E(L)*POIS(L))/(((1.+POIS(L))*(1.-2.*POIS(L))))
      EC=(E(L)*(1.-POIS(L)))/(((1.+POIS(L))*(1.-2.*POIS(L))))
      AB=A(2,2)-A(3,2)
      AC=A(3,2)-A(1,2)
      AD=A(2,2)-A(1,2)
      BB=A(3,3)-A(2,3)
      BC=A(3,3)-A(1,3)
      BD=A(2,3)-A(1,3)
C  FORMULATION OF NODAL   STIFFNESS SN
      SN(I,J)=DE*(EC*BB*BB+EA*AB*AB)
      SN(I+1,J)=DE*(EA*AC*AB-BC*BB*EC)
      SN(I+1,J+1)=DE*(EC*BC*BC+EA*AC*AC)
      SN(I,J+1)=SN(I+1,J)
      SN(I+2,J)=DE*(EC*BD*BB-EA*AD*AB)
      SN(I,J+2)=SN(I+2,J)
      SN(I+2,J+1)=DE*(-EC*BC*BD-EA*AD*AC)
      SN(I+1,J+2)=SN(I+2,J+1)
      SN(I+2,J+2)=DE*(EC*BD*BD+EA*AD*AD)
      SN(I+3,J)=(EA*AB*BB+EB*AB*BB)*DE
      SN(I,J+3)=SN(I+3,J)
      SN(I+3,J+1)=(EA*BB*AC-EB*AB*BC)*DE
      SN(I+1,J+3)=SN(I+3,J+1)
      SN(I+3,J+2)=DE*(-EA*BB*AD+EB*BD*AB)
      SN(I+2,J+3)=SN(I+3,J+2)
      SN(I+3,J+3)=DE*(EA*BB*BB+EC*AB*AB)
      SN(I+4,J)=DE*((-EA*AB*BC)+(EB*AC*BB))
      SN(I,J+4)=SN(I+4,J)
      SN(I+4,J+1)=DE*(-EA*BC*AC-EB*AC*BC)
      SN(I+1,J+4)=SN(I+4,J+1)
      SN(I+4,J+2)=DE*(EA*BC*AD+EB*AC*BD)
      SN(I+2,J+4)=SN(I+4,J+2)
      SN(I+4,J+3)=DE*(-EA*BB*BC+AC*AB*EC)
      SN(I+3,J+4)=SN(I+4,J+3)
      SN(I+4,J+4)=DE*(EA*BC*BC+AC*AC*EC)
      SN(I+5,J)=DE*(EA*AB*BD-EB*AD*BB)
      SN(I,J+5)=SN(I+5,J)
      SN(I+5,J+1)=DE*(EA*BD*AC+EB*AD*BC)
      SN(I+1,J+5)=SN(I+5,J+1)
      SN(I+5,J+2)=DE*(-EA*AD*BD-EB*AD*BD)
      SN(I+2,J+5)=SN(I+5,J+2)
      SN(I+5,J+3)=DE*(EA*BB*BD -EC*AB*AD)
      SN(I+3,J+5)=SN(I+5,J+3)
      SN(I+5,J+4)=DE*(-EA*BD*BC-EC*AC*AD)
      SN(I+4,J+5)=SN(I+5,J+4)
      SN(I+5,J+5)=DE*(EA*BD*BD+EC*AD*AD)
      RETURN
      END
```

```
      SUBROUTINE FORMU1(K,L)
       COMMON SM(6,2352),E(392),POIS(392),CI,II,JJ,KGY,ITER,MXITER,SITER
     1,W,NA,NB,NC,ND,MA,MB,MC,MD,U(15,15),V(15,15),IK,IN,SS(28,6,1),
     2FL(14),A(3,3),SN(6,6),C,I,J,UO,UL,UR,UU,UUR,UD,UDL,VO,VL,VR,VU,VUR
     3,VD,VDL,BMC,EP,ER,L,DE
      UR=SM(K,L+1)
      VO=SM(K,L+3)
      VR=SM(K,L+4)
      VD=SM(K,L+5)
      RETURN
      END
```

```
      SUBROUTINE FORMU2(K,L)
        COMMON SM(6,2352),E(392),POIS(392),CI,II,JJ,KEY,ITER,MXITER,SITER
     1,W,NA,NB,NC,ND,MA,MB,MC,MD,U(15,15),V(15,15),IK,IN,SS(28,6,1),
     2FL(14),A(3,3),SN(6,6),C,I,J,UO,UL,UR,UU,UUR,UD,UDL,VO,VL,VR,VU,VUR
     3,VD,VDL,BMG,EP,ER,L,DE
      UO=SM(K,L)+SM(K-1,L+5)+SM(K-1,L+11)
      UL=SM(K,L-1)
      UR=SM(K-1,L+12)
      UD=SM(K-1,L+6)+SM(K-1,L+13)
      UDL=SM(K,L+1)+SM(K-1,L+7)
      VO=SM(K,L+3)+SM(K-1,L+8)+SM(K-1,L+14)
      VL=SM(K,L+2)
      VR=SM(K-1,L+15)
      VD=SM(K-1,L+9)+SM(K-1,L+16)
      VDL=SM(K,L+4)+SM(K-1,L+10)
      RETURN
      END
```

```
      SUBROUTINE FORMU3(K,L)
      COMMON SM(6,2352),E(392),POIS(392),CI,II,JJ,KEY,ITER,MXITGR,SITER
     1,W,NA,NB,NC,ND,MA,MB,MC,MD,U(15,15),V(15,15),IK,IN,SS(28,6,1),
     2EL(14),A(3,3),SN(6,6),C,I,J,UO,UL,UR,UU,UUR,UD,UDL,VO,VL,VR,VU,VUR
     3,VD,VDL,BMC,EP,ER,L,DE
      VO=SM(K,L+3)+SM(K,L+9)+SM(K-2,L+85)
      VR=SM(K,L+8)+SM(K-2,L+86)
      VU=SM(K,L+1)
      VUR=SM(K,L+2)+SM(K,L+7)
      VD=SM(K-2,L+87)
      UR=SM(K,L+5)+SM(K-2,L+83)
      UUR=SM(K,L-1)+SM(K,L+4)
      RETURN
      END
```

```
      SUBROUTINE FORMU4(K,L)
      COMMON SM(6,2352),E(392),POIS(392),CI,II,JJ,KGY,ITER,MXITGR,SITER
     1,W,NA,NB,NC,ND,MA,MB,MC,MD,U(15,15),V(15,15),IK,IN,SS(28,6,1),
     2FL(14),A(3,3),SN(6,6),C,I,J,UO,UL,UR,UU,UUR,UD,UDL,VO,VL,VR,VU,VUR
     3,VD,VDL,BMC,EP,ER,L,DE
      UO=SM(K,L)+SM(K+1,L+7)+SM(K+1,L+13)+SM(K,L+78)+SM(K-1,L+83)+SM(K-1
     1,L+89)
      UL=SM(K,L+1)+SM(K,L+77)
      UR=SM(K+1,L+12)+SM(K-1,L+90)
      UU=SM(K,L-1)+SM(K+1,L+5)
      UUR=SM(K+1,L+6)+SM(K+1,L+11)
      UD=SM(K-1,L+84)+SM(K-1,L+91)
      UDL=SM(K,L+79)+SM(K-1,L+85)
      VO=SM(K,L+3)+SM(K+1,L+10)+SM(K+1,L+16)+SM(K,L+81)+SM(K-1,L+86)+SM(
     1K-1,L+92)
      VL=SM(K,L+4)+SM(K,L+80)
      VR=SM(K+1,L+15)+SM(K-1,L+93)
      VU=SM(K,L+2)+SM(K+1,L+8)
      VUR=SM(K+1,L+9)+SM(K+1,L+14)
      VD=SM(K-1,L+87)+SM(K-1,L+94)
      VDL=SM(K,L+82)+SM(K-1,L+88)
      RETURN
      END
```

```
      SUBROUTINE STRES(IN)
      COMMON SM(6,2352),E(392),POIS(392),CI,II,JJ,KEY,ITER,MXITER,SITER
     1,W,NA,NB,NC,ND,MA,MB,MC,MD,U(15,15),V(15,15),IK,IN,SS(28,6,1),
     2EL(14),A(3,3),SN(6,6),C,I,J,UO,UL,UR,UU,UUR,UD,UDL,VO,VL,VR,VU,VUR
     3,VD,VDL,BMC,EP,ER,L,DE,U1(15,15),V1(15,15),MITER,LOAD,SSX(392),SSY
     4(392),SSXY(392),SX(392),SY(392),SXY(392),PR,YM
     5 ,BL(392),PR1,BTC,YM1
      EA=(E(IN)*(1.-POIS(IN)))/(((1.+POIS(IN))*(1.-2.*POIS(IN))))
      EB=(E(IN)*POIS(IN))/(((1.+POIS(IN))*(1.-2.*POIS(IN))))
      EC=E(IN)/((2.*(1.+POIS(IN))))
      AB=A(2,2)-A(3,2)
      AC=A(3,2)-A(1,2)
      AD=A(2,2)-A(1,2)
      BB=A(3,3)-A(2,3)
      BC=A(3,3)-A(1,3)
      BD=A(2,3)-A(1,3)
      SX(IN)=
     1     (-EA*BB*SS(IK,1,1)+EA*BC*SS(IK,2,1)-EA*BD*SS(IK,3,1)-EB*AB*SS(
     1IK,4,1)-EB*AC*SS(IK,5,1)+EB*AD*SS(IK,6,1))/DE
      SY(IN)=
     1     (-EB*BB*SS(IK,1,1)+EB*BC*SS(IK,2,1)-EB*BD*SS(IK,3,1)-EA*AB*SS(
     1IK,4,1)-EA*AC*SS(IK,5,1)+EA*AD*SS(IK,6,1))/DE
      SXY(IN)=
     1     (-EC*AB*SS(IK,1,1)-EC*AC*SS(IK,2,1)+EC*AD*SS(IK,3,1)-EC*BB*SS(
     1IK,4,1)+EC*BC*SS(IK,5,1)-EC*BD*SS(IK,6,1))/DE
      IF(SITER.EQ.2.) GO TO 52
      SZ=POIS(IN)*(SX(IN)+SY(IN))
      TS=ABS(SX(IN)+SY(IN)+SZ)
      IF(TS.GT.BTC) GO TO 55
      IF(TS.GT.BMC) GO TO 51
      GO TO 52
   51 POIS(IN)=PR
      ST=ABS(TS/50000.-(TS-1000.)/100000.)
      E(IN)=TS/ST
      EP=1.
      GO TO 52
   55 POIS(IN)=.46
      ST1=ABS((TS-1500.)/100000.+1./60.)
      E(IN)=TS/ST1
      EP=1.
   52 RETURN
      END
```

```
      SUBROUTINE DISPL(I,J)
       COMMON SM(6,2352),E(392),POIS(392),CI,II,JJ,KGY,ITER,MXITER,SITER
     1,W,NA,NB,NC,ND,MA,MB,MC,MD,U(15,15),V(15,15),IK,IN,SS(28,6,1),
     2FL(14),A(3,3),SN(6,6),C,I,J,UO,UL,UR,UU,UUR,UD,UDL,VO,VL,VR,VU,VUR
     3,VD,VDL,BMC,EP,ER,L,DE
       IK=1
  600  SS(IK,1,1)=U(I,J)
       SS(IK,2,1)=U(I,J+1)
       SS(IK,3,1)=U(I+1,J)
       SS(IK,4,1)=V(I,J)
       SS(IK,5,1)=V(I,J+1)
       SS(IK,6,1)=V(I+1,J)
       IK=IK+1
       J=J+1
       SS(IK,1,1)=U(I,J)
       SS(IK,2,1)=U(I+1,J)
       SS(IK,3,1)=U(I+1,J-1)
       SS(IK,4,1)=V(I,J)
       SS(IK,5,1)=V(I+1,J)
       SS(IK,6,1)=V(I+1,J-1)
       IK=IK+1
       IF(IK.EQ.MC) GO TO 601
       GO TO 600
  601  RETURN
       END
```

```
      SUBROUTINE COMP(B)
       COMMON SM(6,2352),E(392),POIS(392),CI,II,JJ,KEY,ITER,MXITGR,SITER
     1,W,NA,NB,NC,ND,MA,MB,MC,MD,U(15,15),V(15,15),IK,IN,SS(28,6,1),
     2EL(14),A(3,3),SN(6,6),C,I,J,UO,UL,UR,UU,UUR,UD,UDL,VQ,VL,VR,VU,VUR
     3,VD,VDL,BMC,EP,ER,L,DE,U1(15,15),V1(15,15),MITER,LOAD,SSX(392),SSY
     4(392),SSXY(392),SX(392),SY(392),SXY(392),PR,YM
     5 ,BL(392)
      C=ABS(1.-U(I,J)/B)
      IF(C.GT.0.00005) KEY=1
      U(I,J)=(B-U(I,J))*W+U(I,J)
      IF(C-CI) 60,60,61
   61 CI=C
      II=I
      JJ=J
   60 RETURN
      END
```

```
      SUBROUTINE COMPP(F)
       COMMON SM(6,2352),E(392),POIS(392),CI,II,JJ,KGY,ITER,MXITER,SITER
     1,W,NA,NB,NC,ND,MA,MB,MC,MD,U(15,15),V(15,15),IK,IN,SS(28,6,1),
     2EL(14),A(3,3),SN(6,6),C,I,J,UO,UL,UR,UU,UUR,UD,UDL,VO,VL,VR,VU,VUR
     3,VD,VDL,BMC,EP,ER,L,DE,U1(15,15),V1(15,15),MITER,LOAD,SSX(392),SSY
     4(392),SSXY(392),SX(392),SY(392),SXY(392),PR,YM
     5 ,BL(392)
       C=ABS(1.-V(I,J)/F)
       IF(C.GT.0.00005) KEY=1
       V(I,J)=(F-V(I,J))*W+V(I,J)
       IF(C-CI) 70,70,71
   71  CI=C
       II=I
       JJ=J
   70  RETURN
       END
```

APPENDIX E

NUMERICAL METHOD OF COMPUTATION:

LUMPED PARAMETER MODEL

The numerical method of solution of the problem as discussed in chapter 7, can be summarized by means of a flow diagram shown in figure (A7.1). Initially ass mass points are in equilibrium under a set of initial displacements (assumed to be zero) with no applied load. The first increment of load is applied at all mass points, thus disturbing the statical equilibrium of the loaded mass points. The Gauss-Seidel iteration method is used to solve the equilibrium equations of each mass point. The following steps are performed for each mass point of the model.

(i) With equation (7.1) and using the current displacements available, the strains of the stress points surrounding a mass point are computed.

(ii) The stresses acting on the mass point are determined by using equation (7.4) for the stress points that are in the elastic region and equation (7.7) for the stress points that are in the plastic region.

(iii) The stresses are added to see whether the equilibrium equations (7.9) for this mass point is satisfied. Generally, the equations (7.9) will not be satisfied and unbalanced stresses in the two co-ordinate directions will result.

(iv) To satisfy the general situation in step (iii), the

mass point is relaxed by giving an additional displacement which is equal to the product of an unbalanced stress and a flexibility of the mass point. Such corrections are performed for the two co-ordinate directions.

(v) Steps (i) to (iv) are repeated for all the other mass points. This constitutes one cycle of computations.

Then the computational cycle is repeated to limited number of iterations which will give reasonable accuracy to satisfy the equilibrium equations (7.9). Then the stresses are calculated at each stress point to see whether any stress point has yielded by equation (7.6) and the necessary information is recorded for the next increment of loading. This constitutes the solution at a particular load level and the entire process is repeated until the whole problem is solved.

A computer programme has been written for this solution and a listing of the programme is given in figure (A7.1). The programme consists of a main programme and two subprogrammes, subroutine elast and subroutine plast. Subroutine elast computes the elastic stresses, residuals and displacements, whereas the subroutine plast computes the incremental stresses. The maximum dimensions in this programme are 28 rows and 21 columns of mass points. The whole programme was run on IBM 7090 and it takes about 12 minutes for 600 iterations to solve a particular load increment. The output from the programme consists of the following data:

(i) parameters and properties of the model

(ii) horizontal and vertical displacements of each mass point

(iii) vertical, horizontal and shear stresses at each stress point

(iv) principal stresses and direction at each stress point

(v) maximum stresses expressed as the percentage of yield stress and the locations of yielded stress points.

All the displacements, normal stresses and locations of yielded stress points are stored in a magnetic tape for use in the next increment of loading.

FLOW DIAGRAM OF NUMERICAL COMPUTATION

LUMPED PARAMETER MODEL

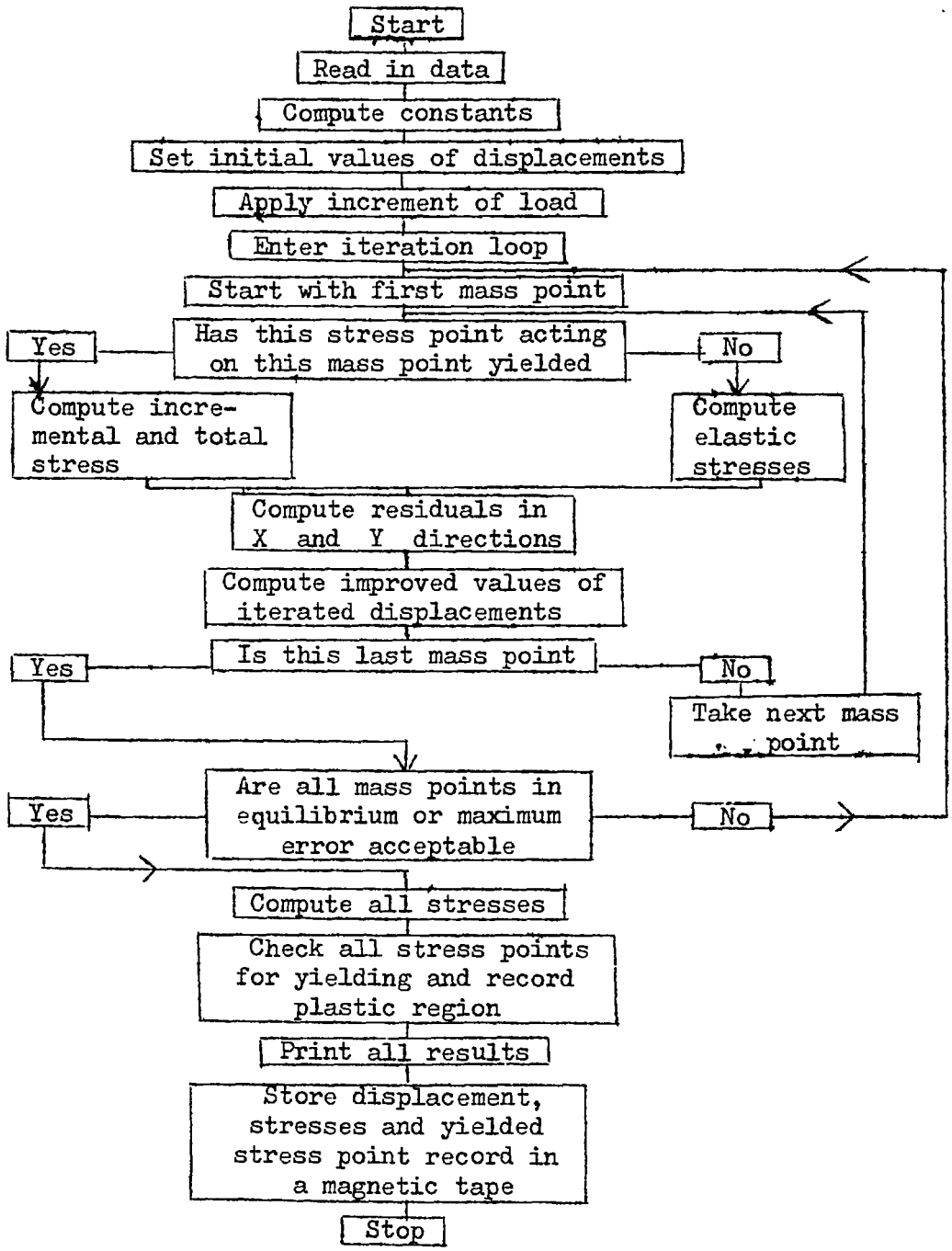


FIG. (A2.1)

FIG. (A7.2) LISTING OF THE COMPUTER PROGRAMME: LUMPED PARAMETER MODEL.

```
C     DETERMINATION OF PLASTIC REGION BY LUMP PARAMETER MODEL(PLANESTRAIN
      COMMON U(28,21),V(28,21),SX(27,20),SY(27,20),TXY(27,20),UU(28,21)
     1,VV(28,21), DX,DY,DXY,                    U1(27,20),V1(27,20),AM,BM,
     2CM,C,WU(12,8),WV(13,20),ITER,MXITER,EP(27,20),AU(5),AV(5),SUMR(900
     1),    ER,NC,P,H,DSX(2,2),DSY(2,2),DTXY(2,2),JL,PP
      READ(5,10)
     1       MA,MB,MC,MD,NA,NB,NC,ND,ME,NE
      READ(5,11) E,XK,ITER,MXITER
      READ(5,12) LPS,ER,POIS,H,ID
   10 FORMAT(10I7)
   11 FORMAT(F10.0,F10.1,2I10)
   12 FORMAT(I10,F10.3,F10.3 ,F10.0,I10)
  840 FORMAT(1H0,9H DENSITY=,I10,5X,7H ERROR=,F10.0,7X,16H POISSONS RATI
     10=,F10.3,5X,14H GRID SPACING=,F10.0)
      DO 51 I=1,28
      DO 51 J=1,21
      U(I,J)=0.
   51 V(I,J)=0.
      DO 200 J=1,20
      DO 200 I=1,27
  200 EP(I,J)=0.
      D=H*SQRT(2.0)
      AM=(E*(1.-POIS))/(D*(1.+POIS)*(1.-2.*POIS))
      BM=(E*POIS)/(D*(1.+POIS)*(1.-2.*POIS))
      CM=E/(2.*(1.+POIS)*D)
      AU(2)=AM+CM
      AU(3)=AU(2)
      AU(4)=AU(2)+CM
      AU(5)=AM
      AU(1)=2.*AU(2)
      AV(1)=AU(1)
      AV(2)=AU(2)
      AV(3)=AU(3)
      AV(4)=AU(2)+AM
      AV(5)=CM
      C=CM/(XK*XK)
   52 P=FLOAT(LPS)
      WRITE(6,840) LPS,ER,POIS,H
      P=P/1728.
      PF=P*H
      PN=.5
      I=MA
      DO 251 J=2,NE
  251 WV(I,J)=PF*PN
        I=1
      DO 260 J=NB,NC
  260 WV(I,J)=PF*PN
        J=NA
      DO 252 I=2,ME
  252 WU(I,J)=PF*PN
      JL=1
    9 ITER=ITER+1
      SUMR(JL)=0.
      CALL ELAST(1,NA,NA,1,1,5)
```

```
      CALL ELAST(I,NB,NC,1,2,2)
      DO 201 I=2,ME
      CALL ELAST(I,NA,NA,2,1,3)
      CALL ELAST(I,NB,NC,2,2,1)
  201 CONTINUE
      CALL ELAST(MA,2,NE,1,2,2)
      CALL ELAST(MA,NA,NA,2,2,4)
      CALL ELAST(MA,NB,NC,2,2,1)
      DO 202 I=MB,MC
      CALL ELAST(I,2,NC,2,2,1)
  202 CONTINUE
      GO TO 811
  810 IF(SUMR(JL).GT.SUMR(JL-1)) GO TO 24
  811 IF(SUMR(JL).LE.ER) GO TO 24
      JL=JL+1
      IF(MXITER-ITER) 24,24,9
   24 WRITE(6,80)(SUMR(I),I=1,ITER)
   80 FORMAT(10E13.6)
      IF(SUMR(ITER).GT.1.0E38) GO TO 825
      LY=LPS
      WRITE(6,211)
  211 FORMAT(1H0,6H   I   J,10X,2HDV,10X,2HDH,10X,2HSV,10X,2HSU,10X,3HPS1,
     1 10X,3HPS2,10X,3HTXY ,10X,5HTHETA,7H  STATE,2HPP)
      JS=NA
      DO 204 I=1,MC
      IF(I-MA) 205,206,206
  206 JS=2
  205 DO 204 J=JS,NC
      IF(I.GE.7) GO TO 208
      IF(EP(I,J)) 208,208,209
  209 CALL PLAST(I,J,5)
      SX(I,J)=SX(I,J)+DX
      SY(I,J)=SY(I,J)+DY
      TXY(I,J)=TXY(I,J)+ DXY
      GO TO 210
  208 SX(I,J)=AM*(U(I+1,J+1)-U(I,J))+BM*(V(I+1,J)-V(I,J+1))
      SY(I,J)=AM*(V(I+1,J)-V(I,J+1))+BM*(U(I+1,J+1)-U(I,J))
      TXY(I,J)=
     1          CM*(U(I+1,J)-U(I,J+1)+V(I+1,J+1)-V(I,J))
  210 DV=(U(I,J)+V(I,J))/1.4142136
      DH=(U(I,J)-V(I,J))/1.414213
      TEMP=(SX(I,J)+SY(I,J))/2.
      SU=TEMP-TXY(I,J)
      SV=TEMP+TXY(I,J)
      A=(SX(I,J)-SY(I,J))/2.
      TMAX=SQRT(TXY(I,J)*TXY(I,J)+A*A)
      PP      =TMAX*100./XK
  701 IF(TMAX-XK) 61,60,60
   60 EP(I,J)=LY
      IF(TMAX.GT.XK) GO TO 820
      GO TO 61
  820 ERR=XK/TMAX
      WRITE(6,821) SX(I,J),SY(I,J),TXY(I,J),ERR,I,J
      SX(I,J)=(SX(I,J)*(1.+ERR)+SY(I,J)*(1.-ERR))/2.
      SY(I,J)=(SX(I,J)*(1.-ERR)+SY(I,J)*(1.+ERR))/2.
```

```
      TXY(I,J)=TXY(I,J)*ERR
      A=(SX(I,J)-SY(I,J))/2.
      TMAX=SQRT(TXY(I,J)*TXY(I,J)+A*A)
      PP=TMAX*100./XK
      WRITE(6,821) SX(I,J),SY(I,J),TXY(I,J),PP,I,J
  821 FORMAT(4E13.6,2I10)
   61 PS1=TEMP+TMAX
      PS2=TEMP-TMAX
      THETA=28.64789*ATAN(-A/TXY(I,J))
      IF(TXY(I,J))212,212,213
  213 IF(A) 214,215,215
  214 THETA=THETA-90.
      GO TO 212
  215 THETA=THETA+90.
  212 WRITE(6,207) I,J,DV,DH,SV,SU,PS1,PS2,TXY(I,J),THETA,EP(I,J),PP
  207 FORMAT(4X,I3,I3,2F14.4,5F11.4,5X,F8.2,2X,2F5.0)
  204 CONTINUE
      DO 54 J=1,16
      DO 54 I=1,14
      UU(I,J)=U(I,J)
   54 VV(I,J)=V(I,J)
      ITER=0
      LPS=LPS+10
      IF(LPS.EQ.ID) GO TO 25
      GO TO 52
   25 REWIND 9
      WRITE(9) ((U(I,J),J=1,16),I=1,14)
      WRITE(9) ((V(I,J),J=1,16),I=1,14)
      WRITE(9) ((SX(I,J),J=1,15),I=1,13)
      WRITE(9) ((SY(I,J),J=1,15),I=1,13)
      WRITE(9)((TXY(I,J),J=1,15),I=1,13)
      WRITE(9) ((EP(I,J),J=1,15),I=1,13)
  825 STOP
      END
```

```
      SUBROUTINE ELAST(I,JS,JE,KE,LE,JK)
       COMMON U(28,21),V(28,21),SX(27,20),SY(27,20),TXY(27,20),UU(28,21)
     1,VV(28,21), DX,DY,DXY,                    UI(27,20),VI(27,20),AM,BM,
     2CM,C,WU(12,8),WV(13,20),ITER,MXITER,EP(27,20),AU(5),AV(5),SUMR(900
     1),    ER,NC,P,H,DSX(2,2),DSY(2,2),DTXY(2,2),JL,PP
       DO 12 J=JS,JE
       DO 5 IA=1,KE
       K=I+1-IA
       DO 5 JA=1,LE
       L=J+1-JA
       IF(EP(I,J))1,1,4
    1  TXY(K,L)=CM*(U(K+1,L)-U(K,L+1)+V(K+1,L+1)-V(K,L))
       DTXY(IA,JA)=0.
       IF(IA-JA) 3,2,3
    2  SX(K,L)=AM*(U(K+1,L+1)-U(K,L))+BM*(V(K+1,L)-V(K,L+1))
       DSX(IA,JA)=0.
       GO TO 5
    3  SY(K,L)=AM*(V(K+1,L)-V(K,L+1))+BM*(U(K+1,L+1)-U(K,L))
       DSY(IA,JA)=0.
        GO TO 5
    4  CALL PLAST(K,L,IA-JA)
       DSX(IA,JA)=DX
       DSY(IA,JA)=DY
       DTXY(IA,JA)=DXY
    5  CONTINUE
       GO TO(10,9,8,7,6),JK
    6  RX=SX(I,J)+DSX(1,1)+.25*P*H
       RY=TXY(I,J)+DTXY(1,1)+.25*P*H
       GO TO 11
    7  RX=SX(I,J)+DSX(1,1)+TXY(I,J-1)+DTXY(1,2)-TXY(I-1,J)-DTXY(2,1)+
     1.75*P*H
       RY=SY(I,J-1)+DSY(1,2)-SY(I-1,J)-DSY(2,1)+TXY(I,J)+DTXY(1,1)+.75*P*
     1H
       GO TO 11
    8  RX=SX(I,J)+DSX(1,1)-TXY(I-1,J)-DTXY(2,1)+WU(I,J)
       RY=          -SY(I-1,J)-DSY(2,1)+TXY(I,J)+DTXY(1,1)  +WU(I,J)
       GO TO 11
    9  RX=           SX(I,J)+DSX(1,1)+TXY(I,J-1)+DTXY(1,2)     +WV(I,J)
       RY=           SY(I,J-1)+DSY(1,2)+TXY(I,J)+DTXY(1,1)     +WV(I,J)
       GO TO 11
   10  RX=SX(I,J)+DSX(1,1)-SX(I-1,J-1)-DSX(2,2)+TXY(I,J-1)+DTXY(1,2)-TXY
     1(I-1,J)-DTXY(2,1)+P*H
       RY=SY(I,J-1)+DSY(1,2)-SY(I-1,J)-DSY(2,1)+TXY(I,J)+DTXY(1,1)-TXY(I-
     11,J-1)-DTXY(2,2) +P*H
   11  SUMR(JL)=SUMR(JL)+ABS(RX)+ABS(RY)
       U(I,J)=U(I,J)+RX/AU(JK)
       V(I,J)=V(I,J)+RY/AV(JK)
   12  CONTINUE
       IF(JE-NC) 14,13,13
   13  U(I,NC+1)=(U(I,NC)+V(I,NC))/2.
       V(I,NC+1)=U(I,NC+1)
   14  IF(JS-2) 15,15,16
   15  U(I,1)=V(I,3)
       V(I,1)=U(I,3)
   16  RETURN
```

END

```
      SUBROUTINE PLAST(K,L,IJ)
       COMMON U(28,21),V(28,21),SX(27,20),SY(27,20),TXY(27,20),UU(28,21)
     1,VV(28,21), DX,DY,DXY,                    U1(27,20),V1(27,20),AM,BM,
     2CM,C,WU(12,8),WV(13,20),ITER,MXITER,EP(27,20),AU(5),AV(5),SUMR(900
     1),    ER,NC,P,H,DSX(2,2),DSY(2,2),DTXY(2,2),JL,PP
       EX=U(K+1,L+1)-U(K,L)-UU(K+1,L+1)+UU(K,L)
       EY=V(K+1,L)-V(K,L+1)-VV(K+1,L)+VV(K,L+1)
       EXY=U(K+1,L)-U(K,L+1)+V(K+1,L+1)-V(K,L)-UU(K+1,L)+UU(K,L+1)-VV(K+1
     1,L+1)+VV(K,L)
       T=(SX(K,L)-SY(K,L))/2.
       TT=T*T
       DXY=(EY-EX)*C*TXY(K,L)*T+EXY*(CM-C*TXY(K,L)*TXY(K,L))
       IF(IJ) 1,2,1
     1 DY=EX*(BM+C*TT)+EY*(AM-C*TT)+EXY*C*TXY(K,L)*T
       IF(IJ-5) 3,2,2
     2 DX=EX*(AM-C*TT)+EY*(BM+C*TT)-EXY*C*TXY(K,L)*T
     3 RETURN
       END
```

ACKNOWLEDGEMENTS

The research work described in this thesis was carried out in the Department of Civil Engineering, Imperial College of Science and Technology, under the supervision of Dr. N. R. Morgenstern.

I am grateful to Dr. Morgenstern for his personal supervision and constant encouragement throughout the period of my work.

I am also grateful to Professor A. W. Skempton and Professor A. W. Bishop for their encouragement in the research programme.

The author wishes to thank his colleagues for their discussions, especially Mr. A. E. Skinner for his assistance in carrying out the experimental work. Messrs. D. Evans and L. Spall helped with the preparation of samples and equipment for which I am truly grateful.

I am much obliged to the Assam State Electricity Board, India, for the financial assistance they provided for the last three years.

Last, but not least, is my wife, whom I am grateful to for being an assistance in many ways throughout the research programme.

REFERENCES

Adams, L. H. and Williamson, E. D. 1923. "The compressibility of minerals and rocks at high pressures". J. Franklin Ins., 195, 475-529.

Allen, D. N. de G. and Southwell, R. 1950. "Relaxation methods applied to engineering problems - XIV plastic straining in two dimensional stress-strain systems". Phil. Tran. Roy. Soc. of London, Series A, 242, London.

Alexander, L. G. 1960. "Field and laboratory tests in rock mechanics". Third Australia-New Zealand Conf. on Soil Mech. and Foundation Eng., pp.161-168.

Ang, A. and Harper, G. N. 1963. "A Numerical Procedure for the Analysis of Contained Plastic Flow Problem". Structural Research Series No. 266, Civil Eng. Studies, Dept. of Civil Eng., University of Illinois.

Ang, A. and Harper, G. N. 1964. "Analysis of contained plastic flow in plane solids". Proc. A.S.C.E., 90, EM5, 397-418.

Argyris, J. H. 1960. "Energy Theorems and Structural Analysis". Butterworths Scientific Publications, London. (Reprinted from Aircr. Eng. 1954-1955).

Argyris, J. H. 1965. "Elasto-Plastic matrix displacement analysis of three dimensional continua". J. Roy. Aero. Soc., 69, 633-635.

Argyris, J. H. 1965. "Triangular elements with linearly varying strain for the matrix displacement method". J. Roy. Aero. Soc., October.

A.S.T.M. 1965-1966. "Testing Techniques for Rock Mechanics". Sp. Tech. Pub. No. 392 & 402, A.S.T.M., Philadelphia.

Banerjee, S., and Ganguli, D. 1960. "A study in the relationship between compressional wave velocity and stress-strain in some rocks". J. Science and Engineering Res., 4, 2, pp.272.

Barton, C. S. 1954. "A method for determining the stress distribution in a plate due to a uniform pressure applied over the boundary of a square hole". Proc. of the Second U.S. Nat. Cong. of Appl. Mech.

Bishop, A. W. 1952. "The stability of earth dams". Ph.D. Thesis, University of London.

Bishop, A. W. and Henkel, D. J. 1962. "The Measurement of Soil Properties in the Triaxial Test". Edward Arnold Ltd., London.

Birch, F. and Bancrof, D. 1938. "The effect of pressure on the rigidity of rocks". J. Geology, 46, 114-141.

Birch, F. 1942. "Handbook of physical constants". Geo. Soc. America Special Pub. 36, pp. 325.

Birch, F. 1961. "The velocity of compressional waves in rocks to 10 kilobars". Part 1, J. Geophy. Research, 65, 1083-1102; Part 2, 66, 2199-2224.

Brace, W. F. 1963. "Brittle fracture of rocks". Int. Conf. on State of Stress in the Earth's Crust, American Elsevier Pub. Company, pp. 110-178, New York.

Brace, W. F. 1965. "Some new measurements of linear compressibility of rocks". J. Geophy. Research, 70, No. 2, 391-398.

Brace, W. F. and Walsh, J. B. 1964. "Elasticity of Rock: A review of some recent theoretical studies". Rock Mechanics and Engineering Geology, Vol. IV/4. 283-297

Bridgman, P. W. 1923. "The compressibility of thirty metals as a function of pressure and temperature". Proc. Am. Acad., 58, 166-242.

Chree, C. 1892. "Changes in the dimensions of elastic solids due to given system of forces". Tran. Cambridge Phil. Soc., 15, 313-337.

Clark, Jr., S. P. 1966. "Handbook of Physical Constants". Geo. Soc. of Am., Mem. 97.

Christian, J. T. 1966. "Two-Dimensional Analysis of Stress and Strain in Soils". Contract report No. 3-129, Civil Eng. Dept., Massachusetts Institute of Technology, Cambridge, Massachusetts.

Clough, R. W. 1960. "The finite element in plane stress analysis". Proc. 2nd A.S.C.E. Conf. on Electronic Computations, Pittsburg, Pa., September.

Clough, R. W. 1965. "The finite element method in structural analysis". Chapter 7 of Stress Analysis, ed. O. C. Zienkiewicz and G. S. Holister, Wiley.

Clough, R. W. and Woodward, R. W., III. 1967. "Analysis of embankment stresses and deformations". Proc. A.S.C.E., 93, SM4, 529-549.

Clough, R. W. and Wilson, E. L. 1963. "Stress analysis of a gravity dam by the finite element method". RILEM Bull., 19, June.

Courant, R. and Friedrichs, K. and Lewy, H. 1928. "Uber die partiellen differenzengleichungen der mathematischen physik". Mathematische Annalen, Vol. 100

Colback, P. S. B. 1965. "The influence of moisture content on the compressive strength of rock". Rock Mechanics Symposium, Toronto.

Cook, N. G. W. 1967. "The design of underground excavations". Proc. Eighth Symp. Rock Mechanics, University of Minnesota.

Coates, D. 1964. "Classification of rocks for rock mechanics". Int. J. of Rock Mechanics and Mining Sciences, 1, 3, 421-429.

De Veubeke, B. F. 1964. "Upper and lower bounds in matrix structural analysis". AGARDograph, 72, 165, Pergamon Press.

De Veubeke, B. F. 1965. "Displacement and equilibrium models in the finite element method". In Stress Analysis, ed. O. C. Zienkiewicz and G. S. Holister, Wiley.

De No, C. L. 1964. "Plastic flow behind a vertical excavation". M.Sc. Thesis, Massachusetts Institute of Technology.

Deere, D. V. 1967. "Geologie considerations". Preprint Advanced Course on Rock Mechanics in Eng. Practice, Swansea.

Dibiagio, E. L. 1966. "Stresses and displacements around an unbraced rectangular excavation in an elastic medium". Ph.D. Thesis, University of Illinois.

Eggestad, A. 1963. "Deformation measurements below a model footing on the surface of dry sand". Proc. European Conf. on Soil Mech. and Found. Eng., Wiesbaden, 1, 233-239.

Faddeeva, V. N. 1959. "Computational Methods of Linear Algebra". Dover Pub., New York.

Fairhurst, C. 1963. "Rock Mechanics". Pergamon Press.

Fatt, L. 1958. "Compressibility of sandstone at low to moderate pressures". A.A.P.G., Vol. 42, 1924.

Finn, W. D. L. 1966. "Static and seismic analysis of slopes". Rock Mechanics and Engineering Geology, Vol. IV/3, 268-277.

Griffith, A. A. 1920. "The phenomena of rupture and flow in solids". Phil. Trans. Roy. Soc. London, A, 221, 163-197.

Griggs, D. T. 1936. "Deformation of rocks under high confining pressure". Jour. Geology, Vol. 44, 541-577.

Hayes, D. J. and Marcel, P. V. 1967. "Determination of upper bounds for problems in plane stress using finite element techniques". Int. J. Mech. Sci., Vol. 9, 245-251.

Handin, J. 1953. "An application of high pressure in geophysics: Experimental rock deformation". Am. Soc. Mech. Eng. Trans., Vol. 75, 315-324.

Handin, J. and Hager, R. V. 1957. "Experimental deformation of sedimentary rocks under confining pressure. Tests on room temperature on dry samples". Am. Ass. Petrol. Geo. Bull., Vol. 41, 1-50.

Handin, J. 1957. "Experimental deformation of rocks and minerals". Second Sym. on Rock Mechanics, Colorado School of Mines.

Hayashi, M. 1964. "Influence of the deformability of the foundations on the stresses in arch dams". Theory of Arch Dams, International Symposium at Southampton Univ., ed. J. Rydzewski, Pergamon Press, 585-602.

Hamrol, A. 1961. "A quantitative classification of the weathering and weatherability of rocks". Proc. 5th Int. Conf. Soil Mechanics and Foundation Eng., Vol. 2, p. 771, Dunod, Paris.

Hashin, Z. 1959. "The moduli of an elastic solid, containing spherical particles of another elastic material". Non-Homogeneity in Elasticity and Plasticity, ed. W. Olszak, Pergamon Press, New York, 463-478.

Hast, N. 1958. "Measurement of rock pressures in mines". Sverige Geologiska Undersökring, Ars. 52, No. 3.

Hawkes, I. and Holister, G. S. 1965. "Photoelastic techniques applied to rock mechanics problems of underground excavations and foundations". Chapter 12 of Stress Analysis, ed. O. C. Zienkiewicz, and G. S. Holister, Wiley.

Hiramatsu, Y., Niwa, Y., and Oka, Y. 1957. "Measurement of stress in the field by the application of photo-elasticity". Tech. Report, Kyoto University, VII, 3, No. 37.

Holliday, L. 1966. "Composite Materials". Elsevier.

Hoek, E. 1964. "Fracture of anisotropic rock". J. South African Inst. Min. Met., 64, 510-518.

Hrennifoff, A. 1941. "Solution of problems in elasticity by the framework method". J. Appl. Mech., 8, 169-175.

Isaacson, E. D. 1962. "Effects of physical characteristics of rock upon stresses induced in the lining of pressure tunnels". Indian Concrete Journal, June.

Jaeger, C. 1961. "Rock mechanics for hydropower engineering". Water Power, Sept. and Oct.

Jaeger, C. 1964. "Rock mechanics and dam design". Water Power, May.

Jones, R. E. 1964. "A generalization of the direct stiffness method of structural analysis". A.I.A.A. Journal, Vol. 2, No. 5, 821-826.

John S. Evans.1967. "The effect of rock deformability on the design of some engineering structures". M.Sc. dissertation, University of London.

Judd, W. R. 1964. "Effects of the elastic properties of rocks on civil engineering design". Engineering Geology Case Histories Numbers 1-5, Geol. Soc. of Am., 163-184.

Khabaza, I. M. 1963. "A Course of Lectures on Matrix Computation". University of London.

Khanna, J. 1966. "Some investigations into the finite element method with special reference to plane stress". University of British Columbia. Ph.D. Thesis.

King, I. P. 1965. "Finite element analysis of two dimensional stress problems with time dependent properties". Ph.D. Thesis, University of California.

Lane, R. G. T. 1964. "Rock foundations. Diagnosis of mechanical properties and treatment". Trans. 8th Int. Congress on Large Dams, Edinburgh, 1, 141-166.

Lauffer, H. and Seeber, G. 1961. "Design and control of linings of pressure tunnels and shafts, based on measurements of the deformability of the rock". Trans. 7th Int. Cong. on Large Dams, Rome, 2, 679-709.

La Rochelle, P. 1960. "The short-term stability of slopes in London clay". Ph.D. Thesis, University of London.

Lame, G. 1852. "Lecons sur la theorie mathematique de l'elasticite". Paris.

Lehman, F. G. 1960. "Simultaneous equations solved by over-relaxation". Proc. A.S.C.E. 2nd Conf. on Electronic Computation, Pittsburgh, Pa., September.

Lemcoe, M. M. 1960. "Stresses in layered elastic solids". Proc. A.S.C.E., Aug. EM4, 1.

Link, H. 1964. "Evaluation of elasticity moduli of dam foundation rock determined seismically in comparison to those arrived at statically". Trans. 8th Int. Cong. on Large Dams, Edinburgh, 1, 833-858.

Lang, T. A. 1964. "Rock mechanics considerations in design and construction". Proc. 6th Sym. on Rock Mechanics, University of Missouri at Rolla, 561-605.

Love, A. E. H. 1944. "A Treatise on the Mathematical Theory of Elasticity". New York.

Martin, H. C. 1961. "Plane elasticity problems and the direct stiffness method". The Trend in Engineering, January, 5-8.

Mackenzie, J. K. 1950. "The elastic constants of a solid containing spherical holes". Proc. Phys. Soc. London, B, 63, 2-11.

Mayer, A. 1963. "Recent work in rock mechanics". Third Rankine Lecture, Geotechnique, Vol. 13, 97-120.

MacGee, A. 1926. "Several gas expansion porosimeters". J. Am. Ceramic Society, Vol. 9, 814.

Merrill, R. H. 1960. "Static stress determinations in salt". U.S. Bur. Mines Rept., April, 38-3.1, July, 30.

Morgenstern, N. R. 1965. "Rock mechanics". Unpublished lectures to soil mechanics postgraduate students at Imperial College, University of London.

Morgenstern, N. R. 1967. "Ultimate behaviour of rock structure". Preprint Advanced Course on Rock Mechanics, University College, Swansea.

Morgenstern, N. R. and Taylor-Smith, D. 1964. "Longitudinal velocities in a clay during plastic compression". Reprint, Review Pure and Applied Geophysics, Vol. 58, 123-128.

Moody, W. T. 1964. "Importance of geological information as a factor in tunnel-lining design". Engineering Geology Case Histories, Numbers 1-5, ed. P. D. Trask, Geol. Soc. America, 155-162.

Mogi, K. 1959. "Experimental study of deformation and fracture of marble". Bull. Earthquake Res. Inst. Tokyo Univ., 37, 155-170.

Nishihara, M. 1957. "Stress-strain relation of rocks". Doshisha Eng. Rev., 8, 32-54.

Obert, L. and Duvall, W. 1967. "Rock Mechanics and the Design of Structures in Rocks". New York, Wiley.

Obert, L., Merrill, R. H. and Morgan, T. A. 1962. "Borehole deformation gauge for determining the stress in mine rock". U.S. Bur. Mines Rept. Invest., 5978, pp.11.

Ortlap, W. D. and Cook, N. G. W. 1964. "The measurement and analysis of the deformation around deep hard-rock excavation". 4th Int. Conf. on Strata Control and Rock Mechanics, 140-150.

Panek, L. A. 1951. "Stresses About Mine Openings in a Homogeneous Rock Body". Edward Brothers Inc., New York.

Phillips, D. W. 1948. "Tectonics of mining". Colliery Engineering, June, 199-202.

Pian, T. H. H. 1965. "Element stiffness matrices for boundary compatibility and for prescribed boundary stresses". Proc. Conf. on Matrix Methods in Structural Mechanics, Wright-Patterson Air Force Base, Dayton, Ohio.

Potts, E. L. J. 1964. "The in situ measurement of rock stress based on deformation measurements". In State of Stress in the Earth's Crust, ed. W. Judd, Elsevier, New York, p. 397.

Prager, W. and Hodge, P. G. 1951. "Theory of Perfectly Plastic Solids". John Wiley and Sons. Inc., New York.

Rashid, Y. R. 1964. "Solution of elasto-static boundary value problems by the finite element method". Ph.D. Thesis, University of California.

Reyes, S. F. 1966. "Elastic-plastic analysis of underground openings by the finite element method". Ph.D. Thesis, University of Illinois.

Rocha,, M. 1964. "Mechanical behaviour of rock foundation in concrete dams". Trans. 8th Int. Cong. on Large Dams, Edinburgh, 1, 785-832.

Rocha, M. 1964. "Statement of the physical problems of the arch dam". Theory of Arch Dam: Int. Sym. at Southampton University, ed. J. Rydzewski, Pergammon Press, 3-22.

Roy, S. K. 1956. "On the biharmonic analysis of stresses around openings in structures in relation to the unlimited stress fields". Proc. 2nd Cong. on Theoretical and Applied Mechanics, New Delhi.

Robert, A. 1964. "Progress in the application of photoelastic techniques to rock mechanics". Proc. 6th Symp. on Rock Mechanics.

Robert, A. 1967. "The measurement of stress in rock masses". Preprint Advanced Course on Rock Mechanics, University College, Swansea.

Robert, A., Emery, C. L., Chakravarty, P. K. and Williams, F. T. 1962. "Photoelastic coating techniques applied to research in rock mechanics". Trans. Inst. Mining Met., Vol. 71, pt. 10, 581-617.

Rydzewski, J. R. 1960. "Stress distribution in gravity dams". Water Power, 12, 6, 239-243, June.

Savin, G. N. 1961. "Stress Concentration Around Holes". Pergammon Press, New York.

Sack, R. A. 1946. "Extension of Griffith's theory of rupture to three dimensions". Proc. Phys. Soc. London, A, 58, 729-736.

Schjødt, R. 1958. "Stresses in an excavation with a vertical wall subjected to its own weight". Proc. of the Brussels Conf. on Earth Pressure Problems, Vol. 1, 89-93.

Serafim, J. L. 1964. "Rock mechanics considerations in the design of concrete dams". In State of Stress in the Earth's Crust, ed. W. Judd, Elsevier, New York, 611-652.

Serafim, J. L. and Lopes, J. J. B. 1961. "In situ shear tests and triaxial tests of foundation rocks of concrete dams". Proc. 5th Cong. Soil Mech. and Found. Eng., Paris, 1, 533-540.

Skinner, A. E. 1968. "The effect of high pore water pressures on the mechanical behaviour of sediments". Ph.D. Thesis, University of London.

Smith, A. R. 1965. Personal communication.

Sturgul, J. R. and Scheidegger, A. E. 1967. "Tectonic stress in the vicinity of a wall". Rock Mechanics and Engineering Geology, Vol. V/2-3, 137-149.

Stevenson, A. C. 1945. "Complex potentials in two-dimensional elasticity". Proc. Roy. Soc. London, A, 184, 129-179.

Taliaferro, Jr., D. B. and Dewees, E. J. 1937. "A method of determining porosity". U.S.B.M. R.I. 3352.

Timoshenko, S. and Goodier, J. N. 1951. "Theory of Elasticity". McGraw-Hill, New York.

Turner, M. J., Clough, R. W., Martin, H. C. and Topp, L. J. 1956. "Stiffness and deflection analysis of a complex structure". J. Aero. Sci., 23, No. 9.

Varga, R. S. 1962. "Matrix Iterative Analysis". Prentice-Hall Inc., New Jersey.

Viksne, A., Berg, J. W. and Cook, K. L. 1961. "Effect of porosity, grain content and cement on compressional wave velocity through synthetic sandstones". Geophysics, 26, 1, 77-84.

Wang, Y. J. and Singh, M. M. 1965. "Stress distribution at the bottom of a borehole by a numerical method". 7th Sym. on Rock Mechanics, The Pennsylvania State University, Pennsylvania, 1, 89-118.

Walsh, J. B. 1965. "The effects of cracks on the compressibility of rock". J. Geophy. Research, 70, 2, 381.

Walsh, J. B. 1965. "The effects of cracks on the uniaxial compression of rocks". J. Geophy. Research, 70, 2, 399.

Walsh, J. B. 1965. "The effects of cracks in rocks on Poisson's ratio". J. Geophy. Research, 70, 20, 5249.

Waterways Experimental Station. 1951-1954. "Investigations of pressures and deflections for flexible pavements". Report 1 and 4, U.S. Corps of Engrs. Tech. Memo, 3-323, Vicksburg, Miss.

Webb, D. L. 1966. "The mechanical properties of undisturbed samples of London clay and Pierre shale". Ph.D. Thesis, University of London.

Wilhemi, B. and Somerton, W. H. 1967. "Simultaneous measurement of pore and elastic properties of rocks under triaxial stress conditions". Soc. of Petrol Engineers Journal, September, 283-294.

Wilson, E. L. 1963. "Finite element analysis of two-dimensional structures". Ph.D. Thesis, University of California.

Zienkiewicz, O. C. 1945. "Classical theories of gravity dam design in the light of modern analytical methods". Ph.D. Thesis, University of London.

Zienkiewicz, O. C. and Cheung, Y. K. 1967. "The Finite Element Method in Structural and Continuum Mechanics". McGraw-Hill, London.

Zienkiewicz, O. C. and Cheung, Y. K. 1966. "Application of the finite element method to problems of rock mechanics". Proc. First Int. Congr. of the Int. Soc. of Rock Mechanics, Vol. 1, 661-666.

Zienkiewicz, O. C., Cheung, Y. K. and Stagg, K. G. 1966. "Stresses in anisotropic media with particular reference to problems of rock mechanics". J. Strain Analysis, Vol. 1, 172-182.

Zienkiewicz, O. C. and Gerstner, R. W. 1960. "A stress function approach to interface and mixed boundary condition problems". Int. J. Mech. Sciences, 2, 93-101.

Zienkiewicz, O. C. and Gerstner, R. W. 1961. "Foundation elasticity effects in gravity dams". Proc. Instn. Civ. Engrs,, 19, 209-216, June.

Zisman, W. A. 1933. "Comparison of the statically and seismically determined elastic constants of rocks". Proc. Natl. Acad. Sci. U.S. 19, 680-686.

Zisman, W. A. 1933. "Compressibility and anisotropy of rocks at and near the earth's surface". Proc. Natl. Acad. Sci. U.S., 19, 666-679.

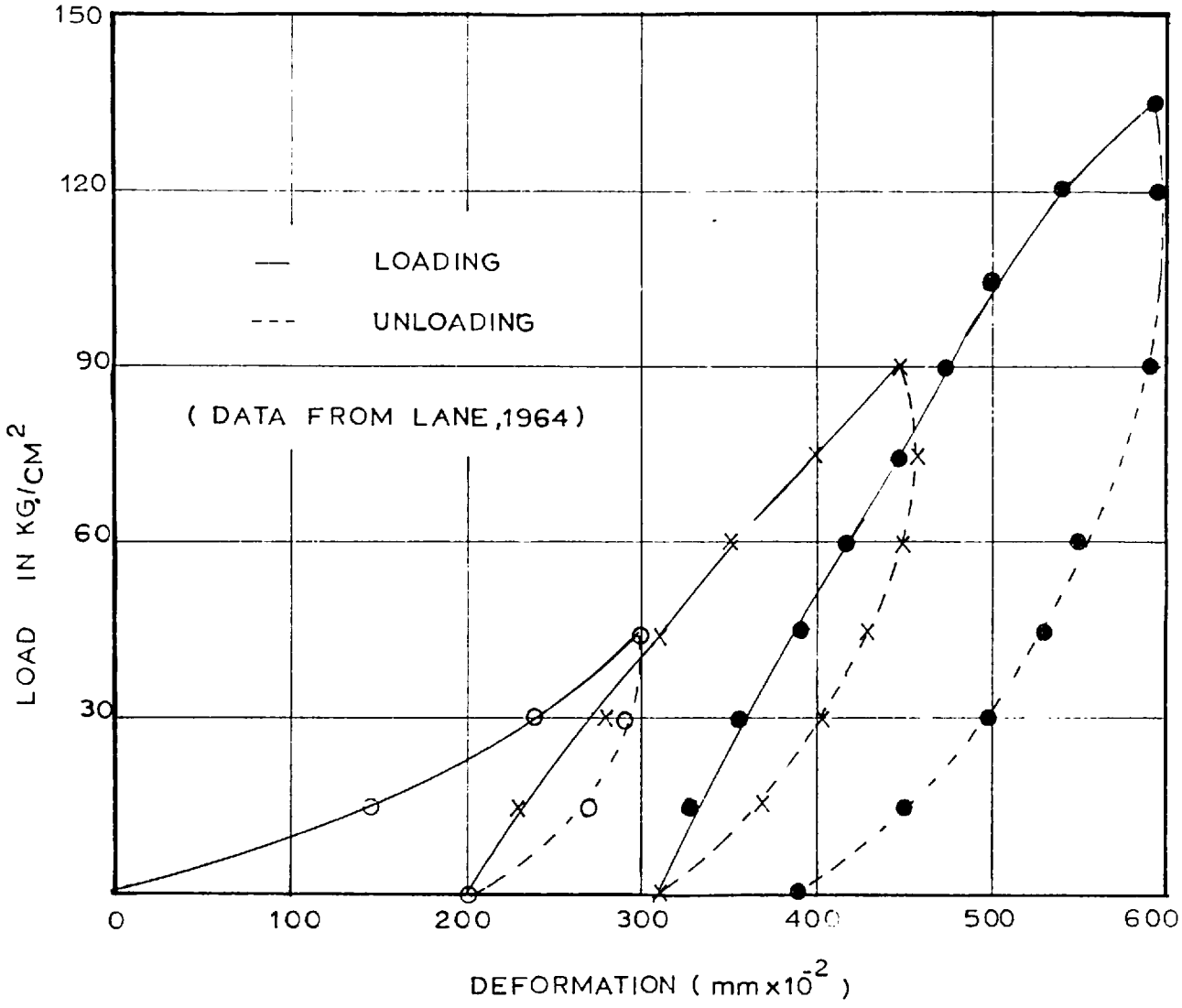

150
120
90
60
30
0
100
200
300
400
500
600
LOADING
UNLOADING
(DATA FROM LANE, 1964)
LOAD IN KG/CM2
DEFORMATION (mm x 10-2)

FIG. 2.1

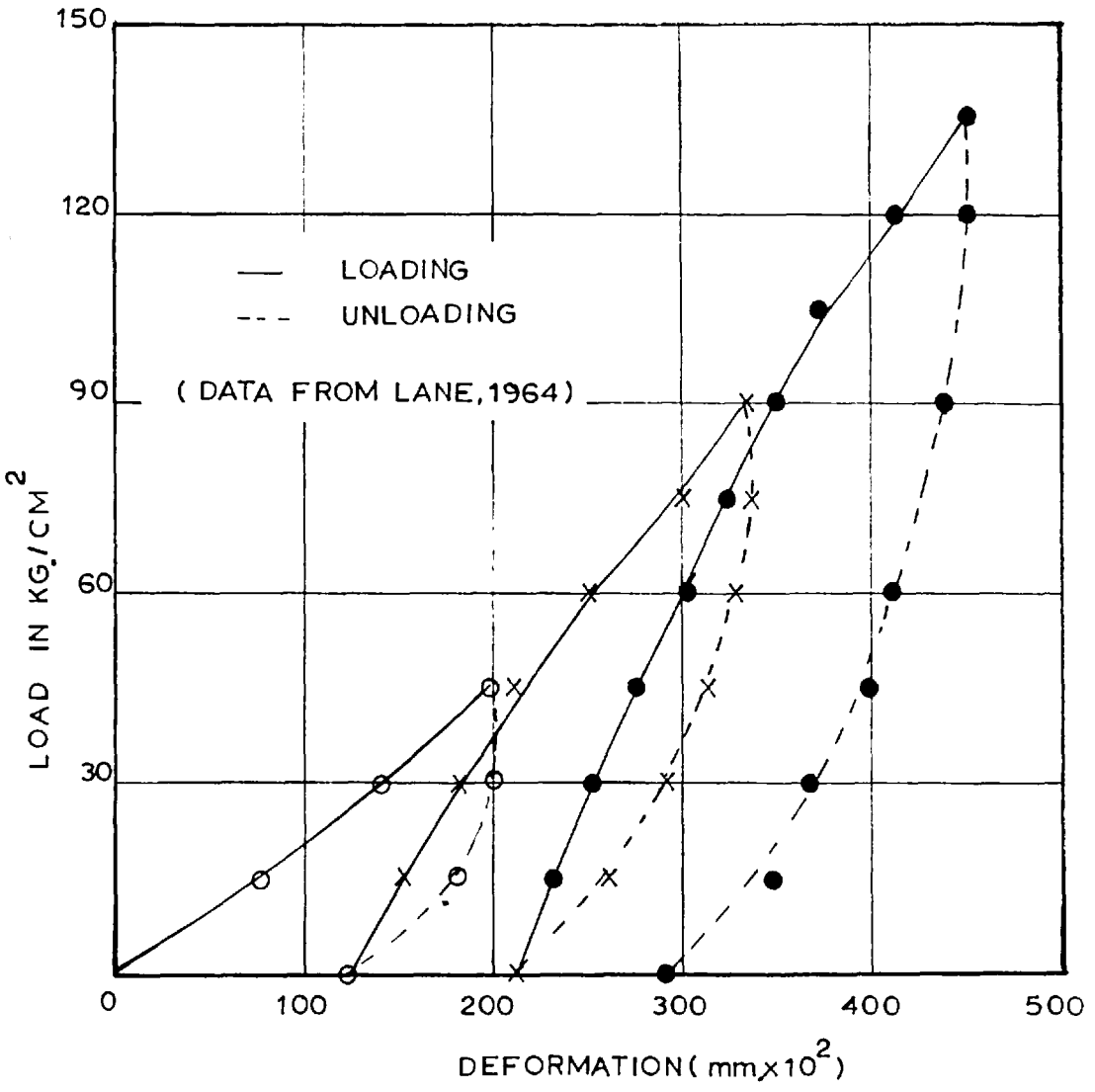

150
120
90
60
30
0
100
200
300
400
500
LOADING
UNLOADING
(DATA FROM LANE, 1964)
LOAD IN KG./CM^2
DEFORMATION (mm x 10^2)

FIG. 2.2

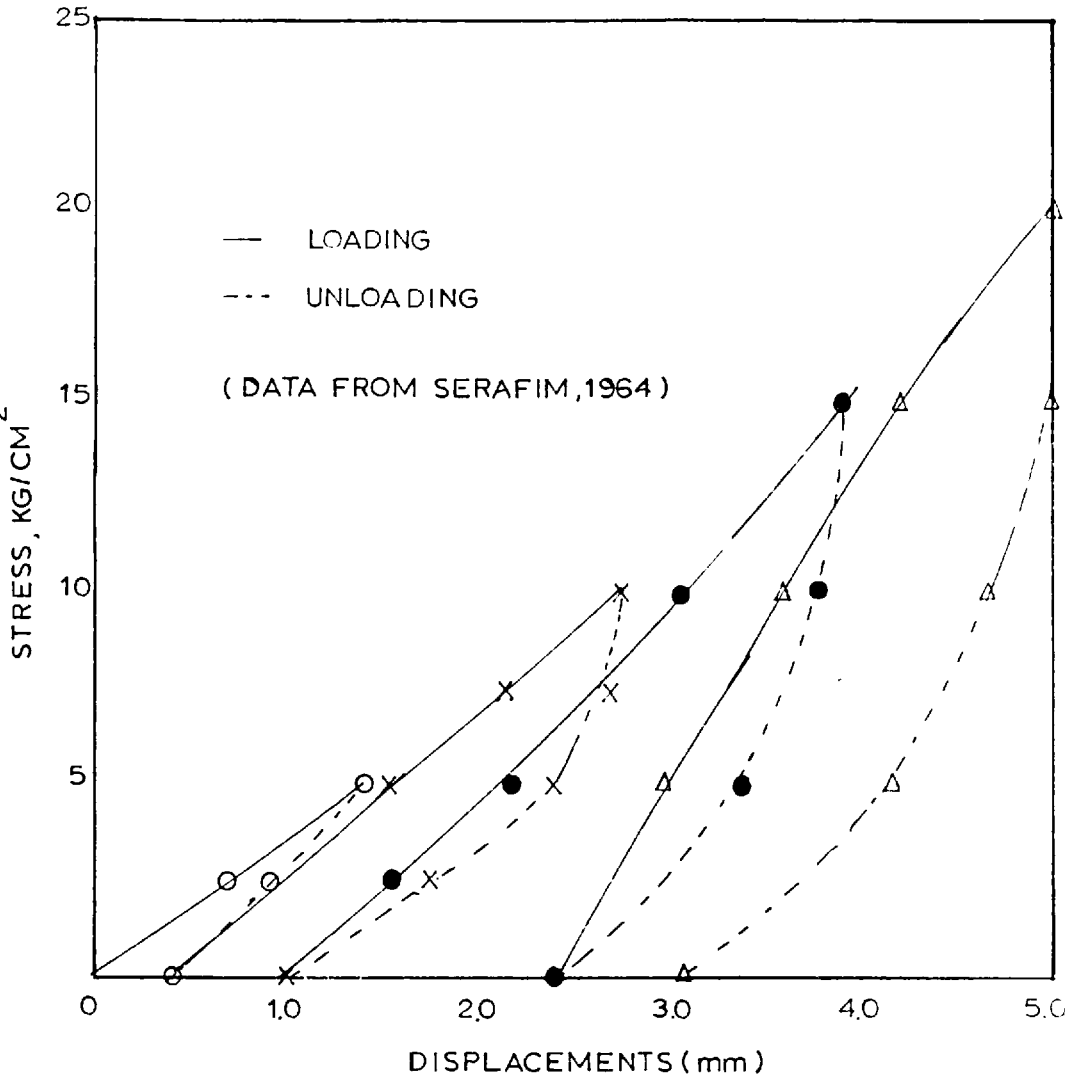

25
20
15
10
5
0
1.0
2.0
3.0
4.0
5.0
LOADING
UNLOADING
(DATA FROM SERAFIM, 1964)
STRESS, KG/CM 2
DISPLACEMENTS (mm)

FIG. 2.3

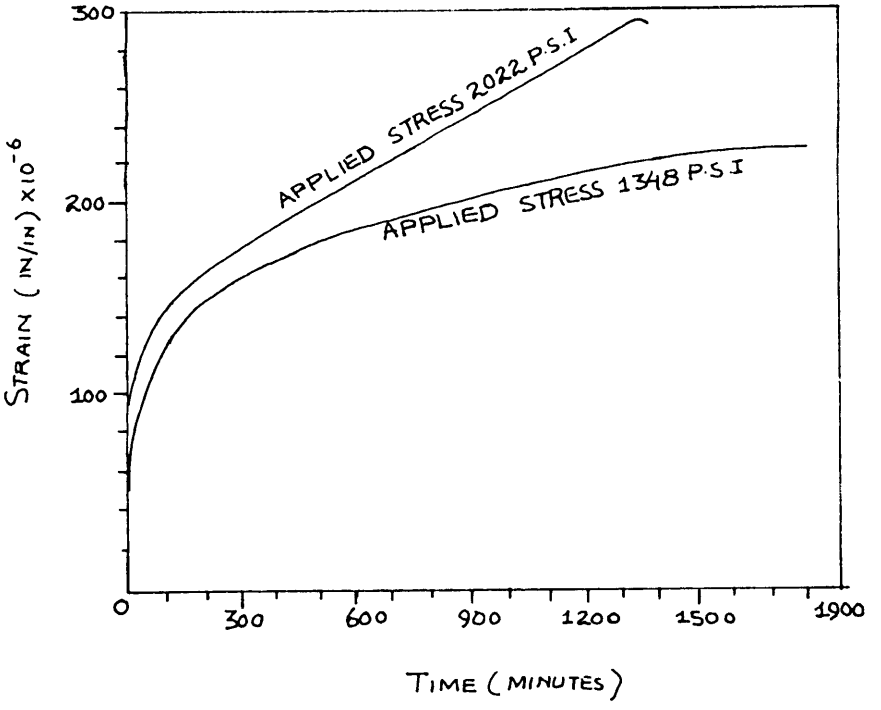
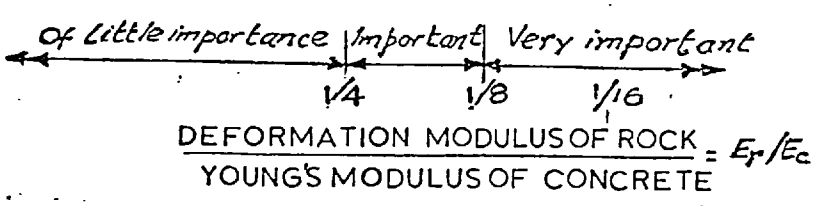
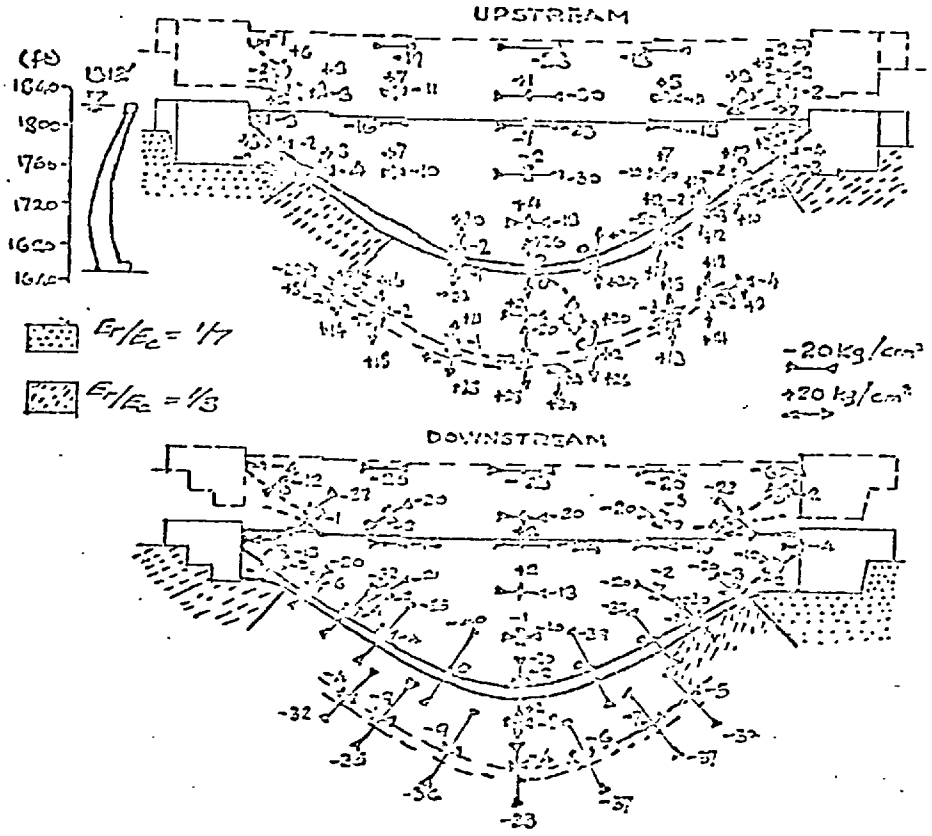


FIG. 24. STRESS STRAIN CURVES FOR STEEP ROCK LAKE IRON ORE UNDER UNIAXIAL STRESS AND ROOM TEMP. (AFTER HARDY, 1959)



(a) Influence of rock deformability on the design of arch dams illustrated qualitatively. (Rocha, 196



(b) Quantitative example of the effect of rock deformability on the design of arch dams. (Rocha, 1964)

FIG. 2.5

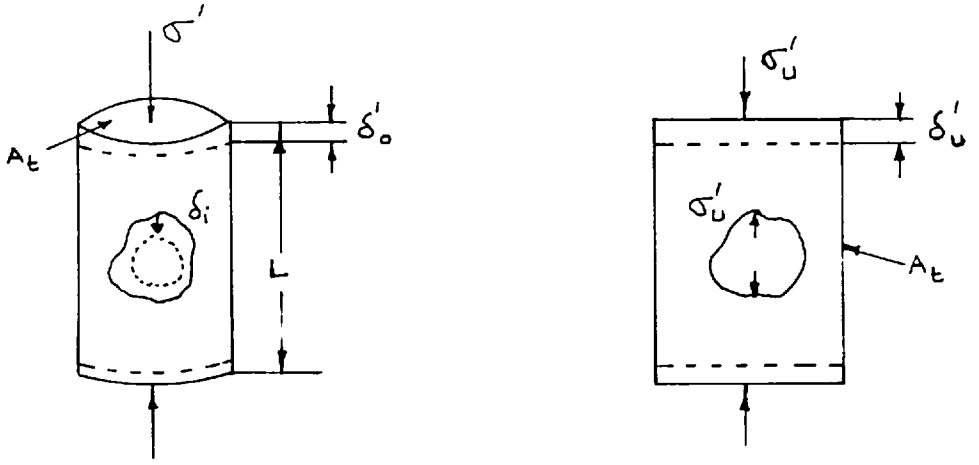


FIG.(3.1) STRESSES FOR APPLYING THE RECIPROCAL THEOREM TO A POROUS BODY

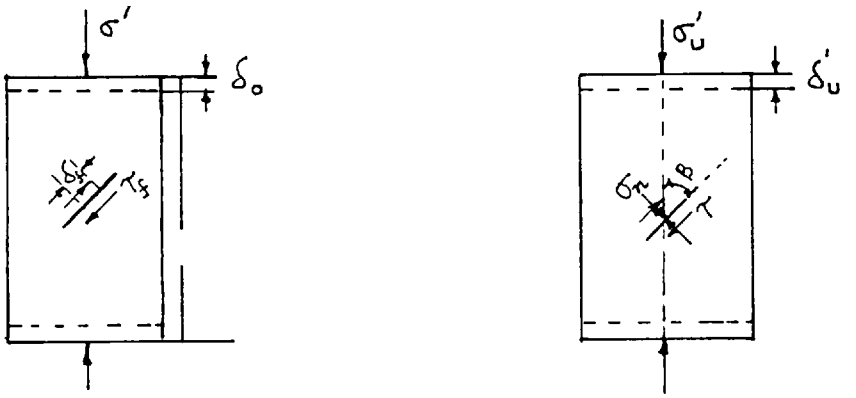


FIG.(3.2) STRESSES FOR APPLYING THE RECIPROCAL THEOREM TO A BODY WITH CLOSED CRACK

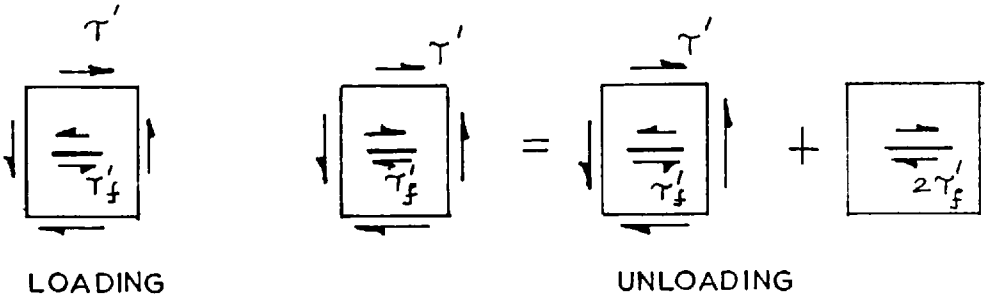


FIG.(3.3) CHANGE IN SHEAR STRESSES AT POINT OF UNLOADING

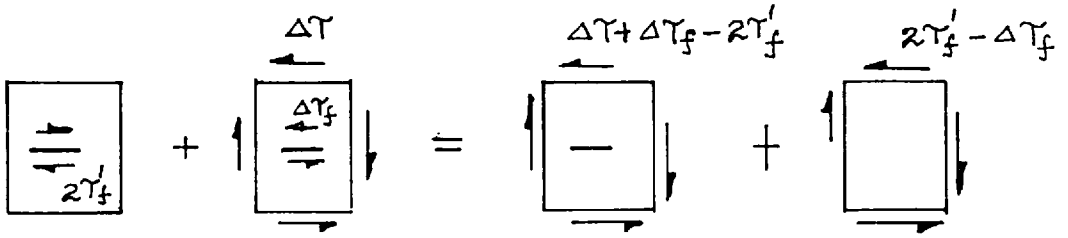


FIG.(3.4) SHEAR STRESS REQUIRED FOR SLIDING DURING UNLOADING CYCLE

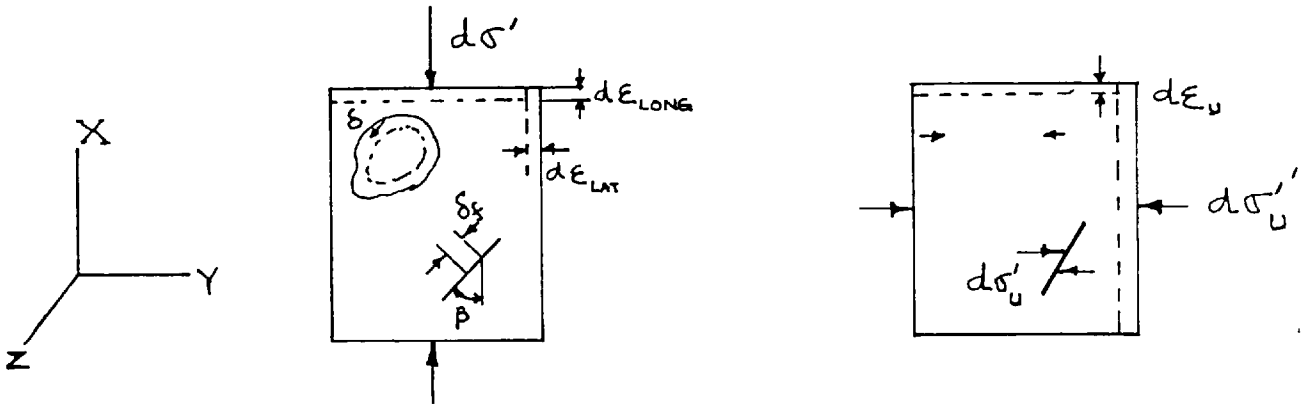

X
Y
Z
dσ'
dε_LONG
dε_LAT
δ
δs
β
dε_u
dσ'_u
dσ'_u

FIG. 3.5

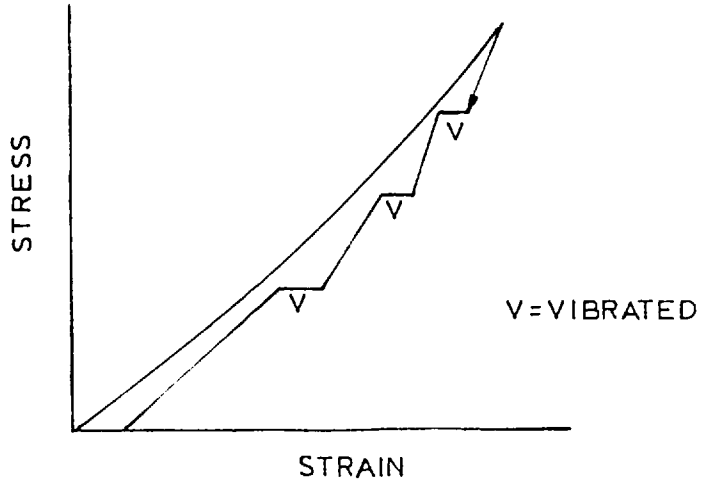
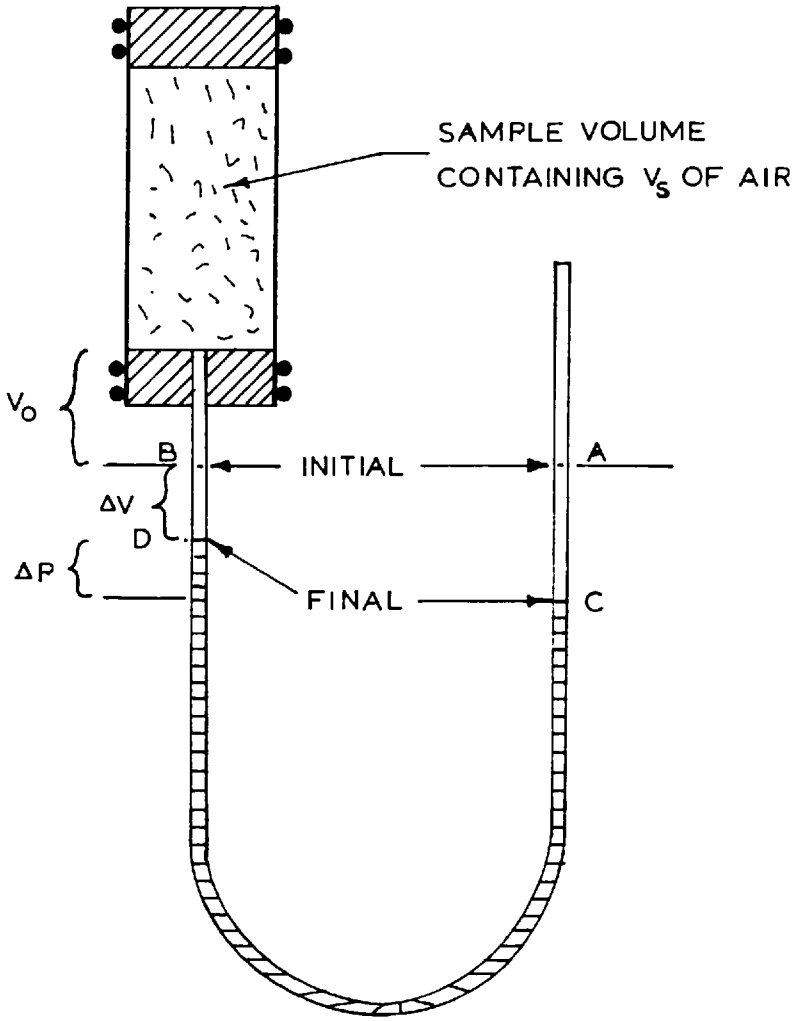
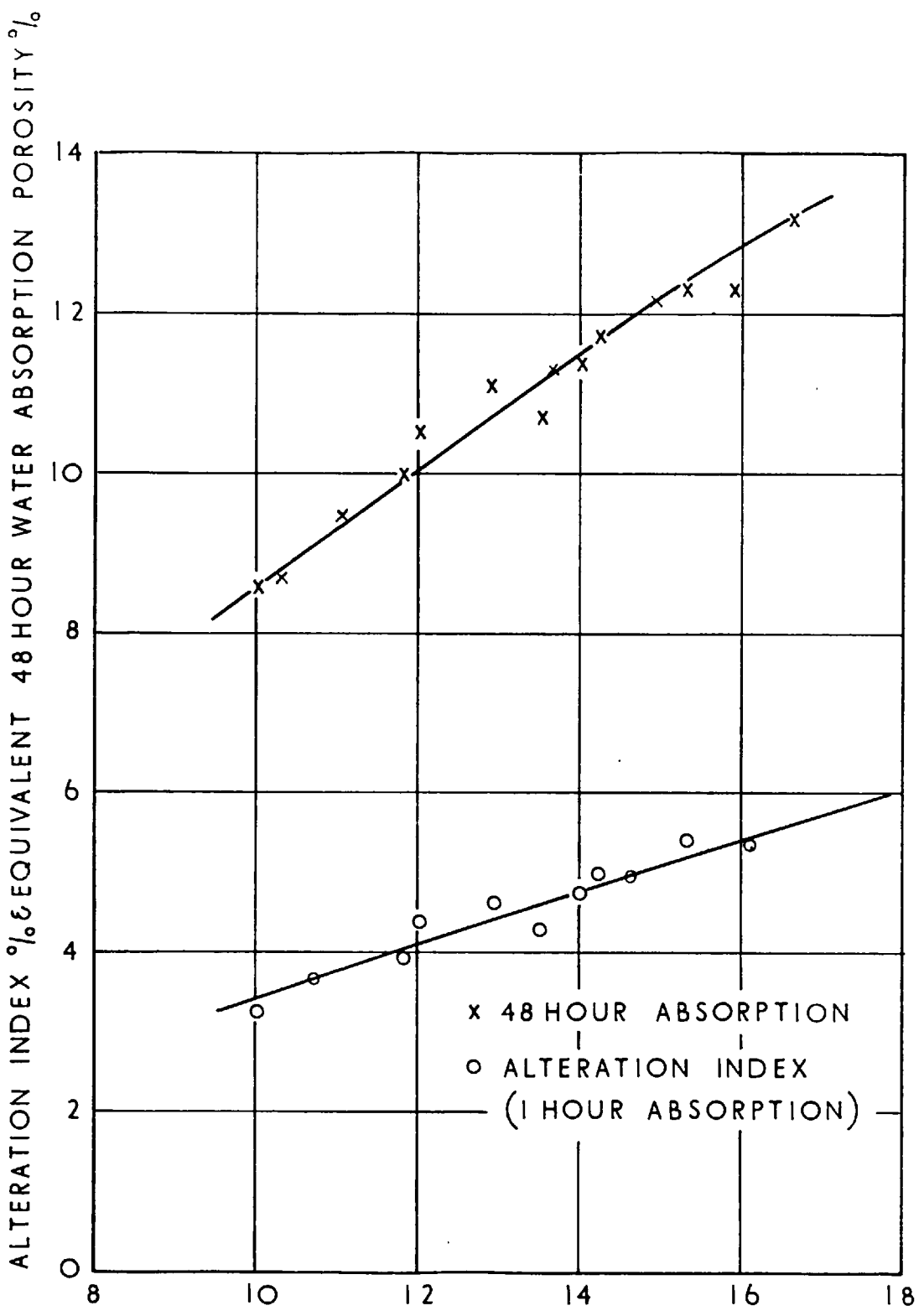

STRESS
STRAIN
V
V
V
V=VIBRATED

FIG. 3.6



POROSITY BY AIR EXPANSION APPARATUS

FIG. 4.1



POROSITY CORRELATION

FIG. 4.2

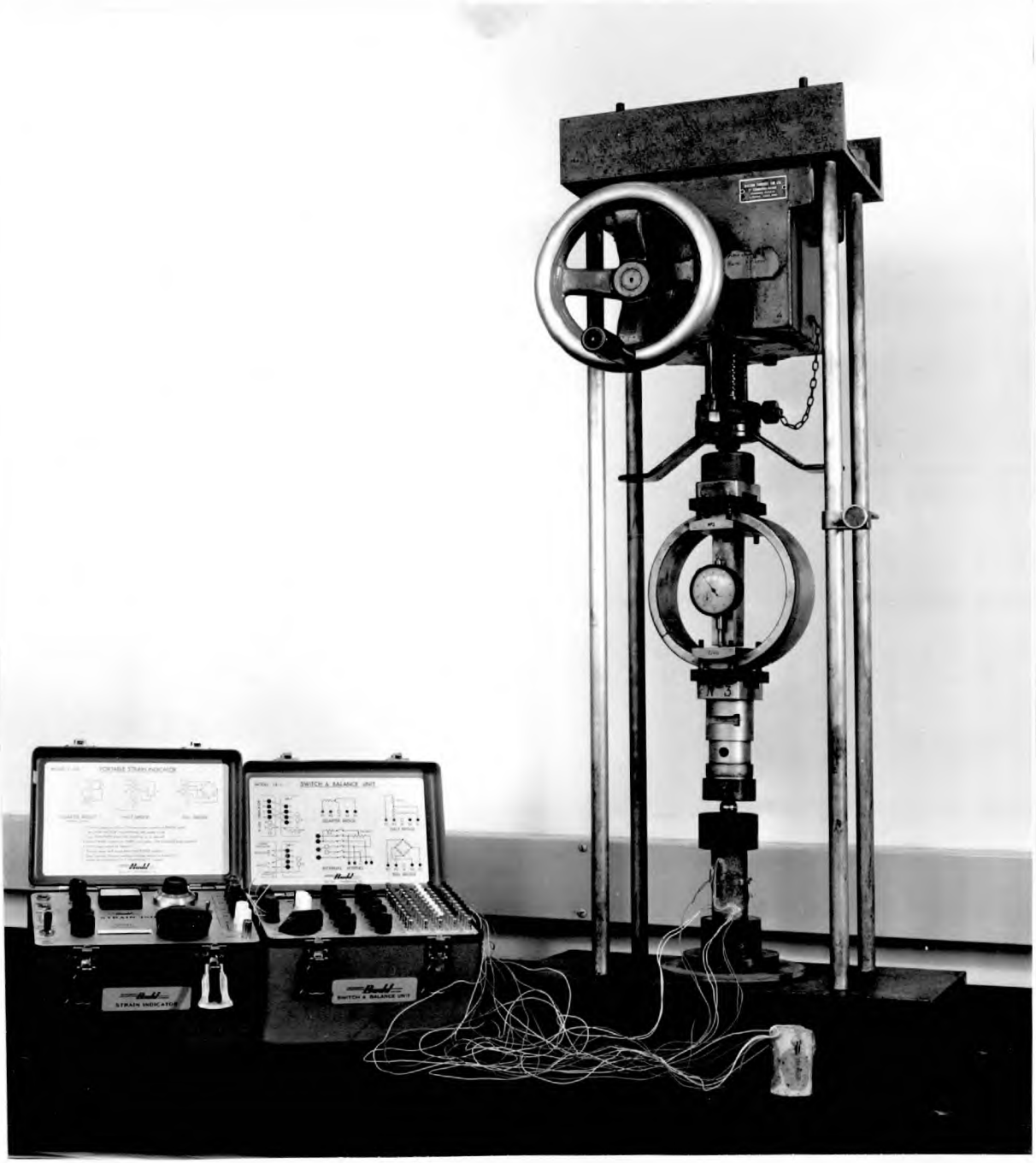
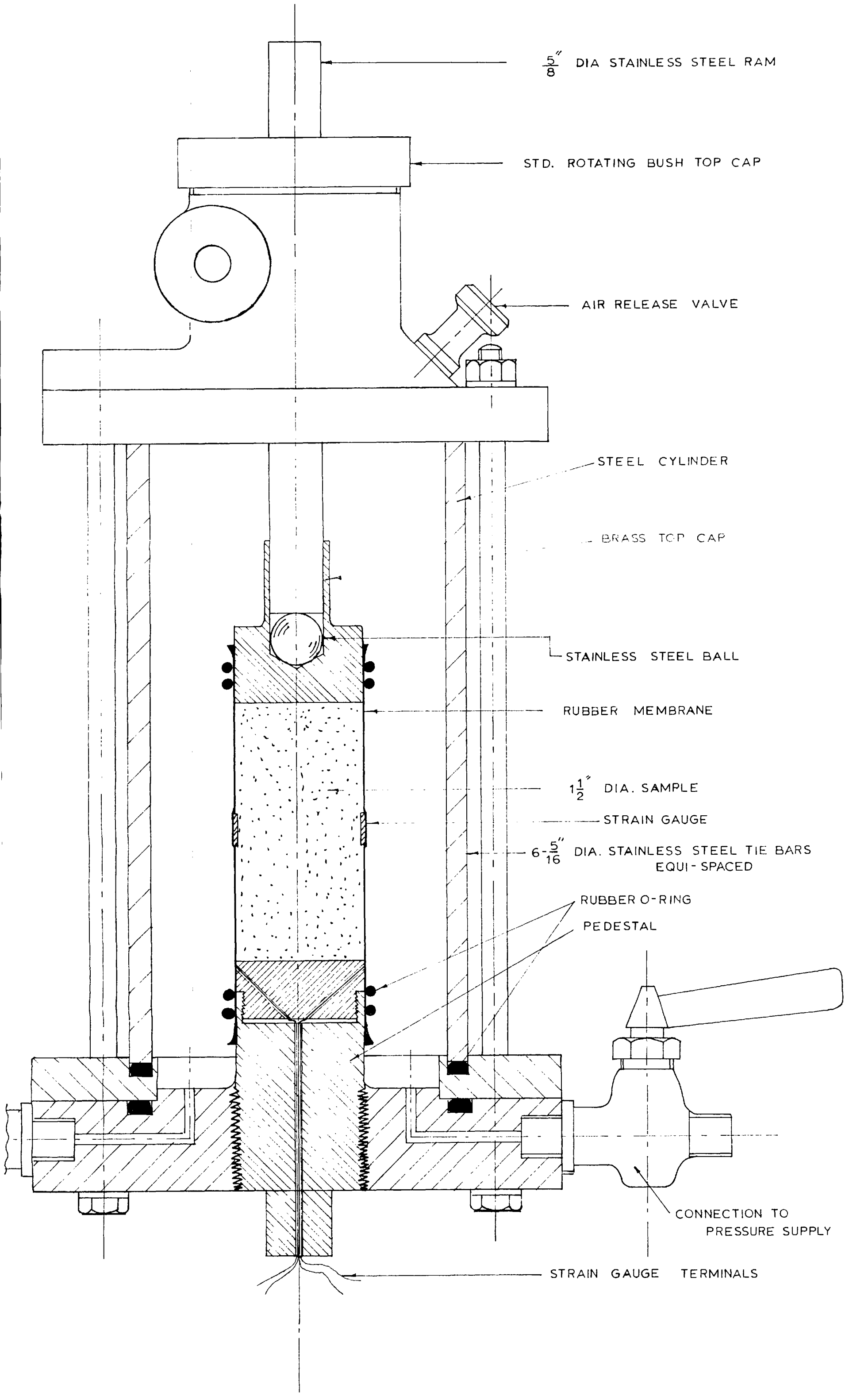


FIGURE (4.3). ARRANGEMENT OF UNIAXIAL TEST FRAME AND STRAIN MEASURING DEVICE

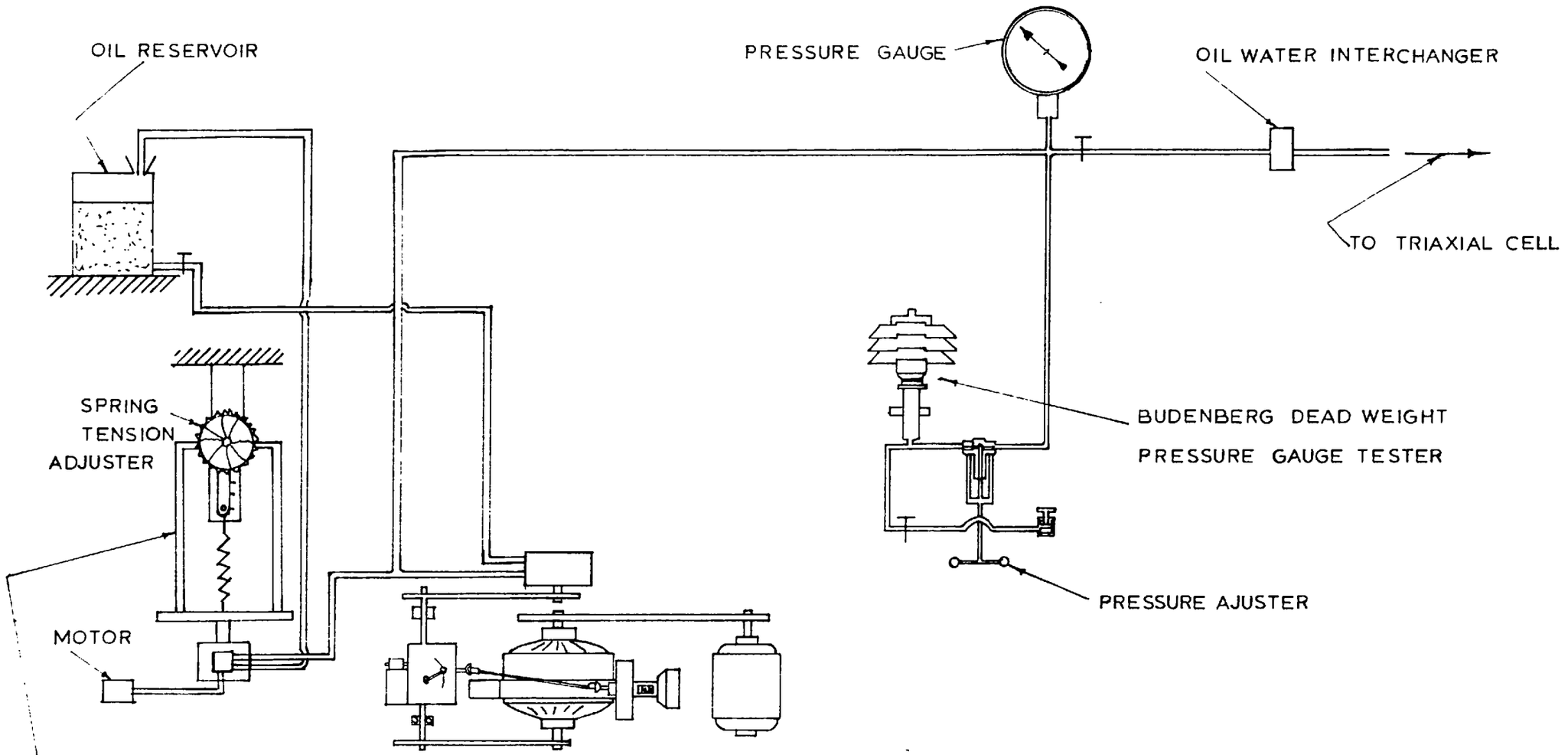


TRIAXIAL COMPRESSION APPARATUS

FIG. 4.4(a)

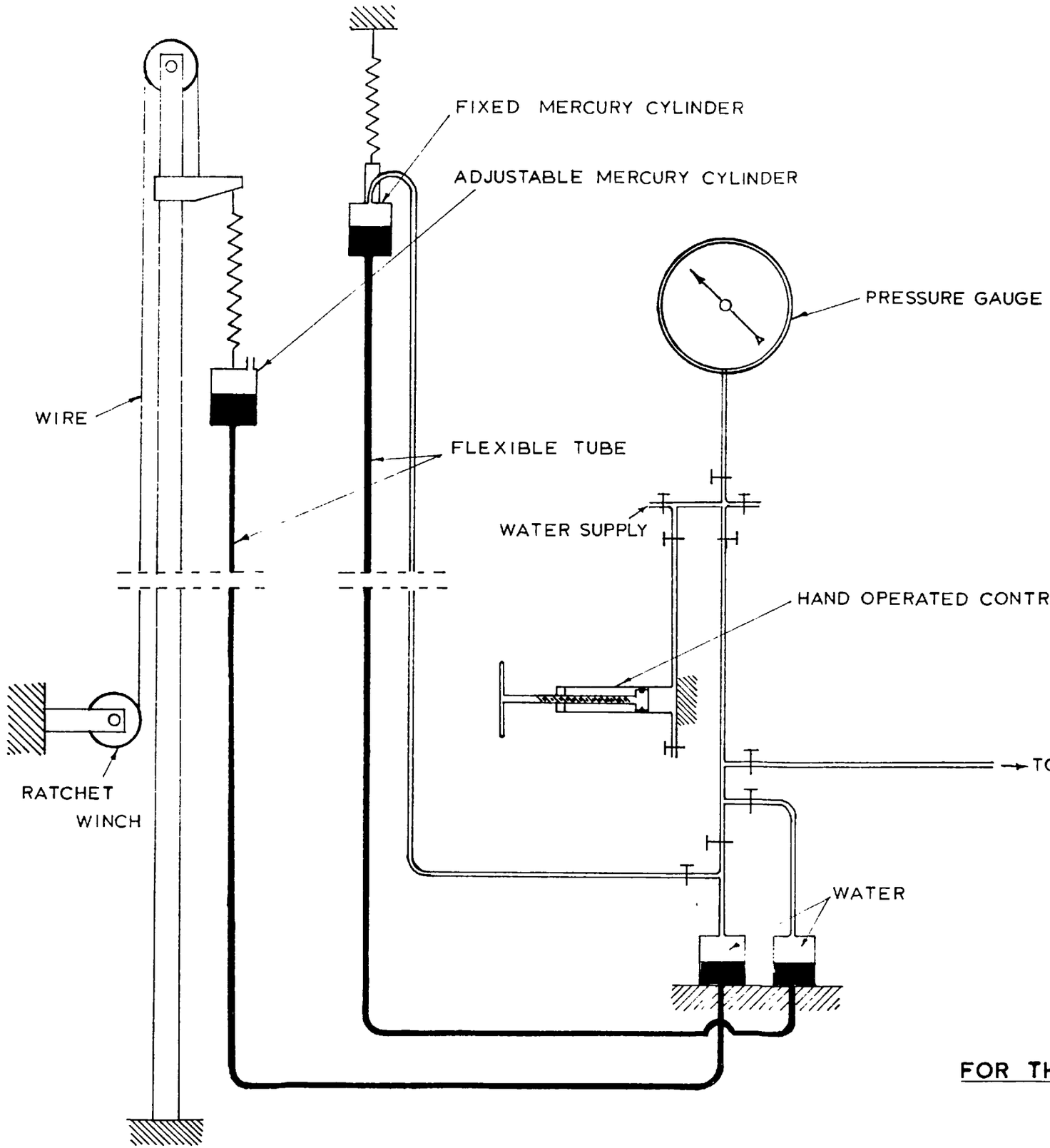


FIGURE (4.4b) SPECIMENS IN POSITION FOR TESTING, THE STRAIN GAUGE LEADS BEING TAKEN OUT THROUGH THE PEDESTAL.



HIGH PRESSURE CONTROL SYSTEM

FIG.4.4(C)



PRESSURE CONTROL SYSTEM

FOR THE TRIAXIAL TESTS USING CONFINING

PRESSURE OF 150 P.S.I

FIG. 4.4(d)

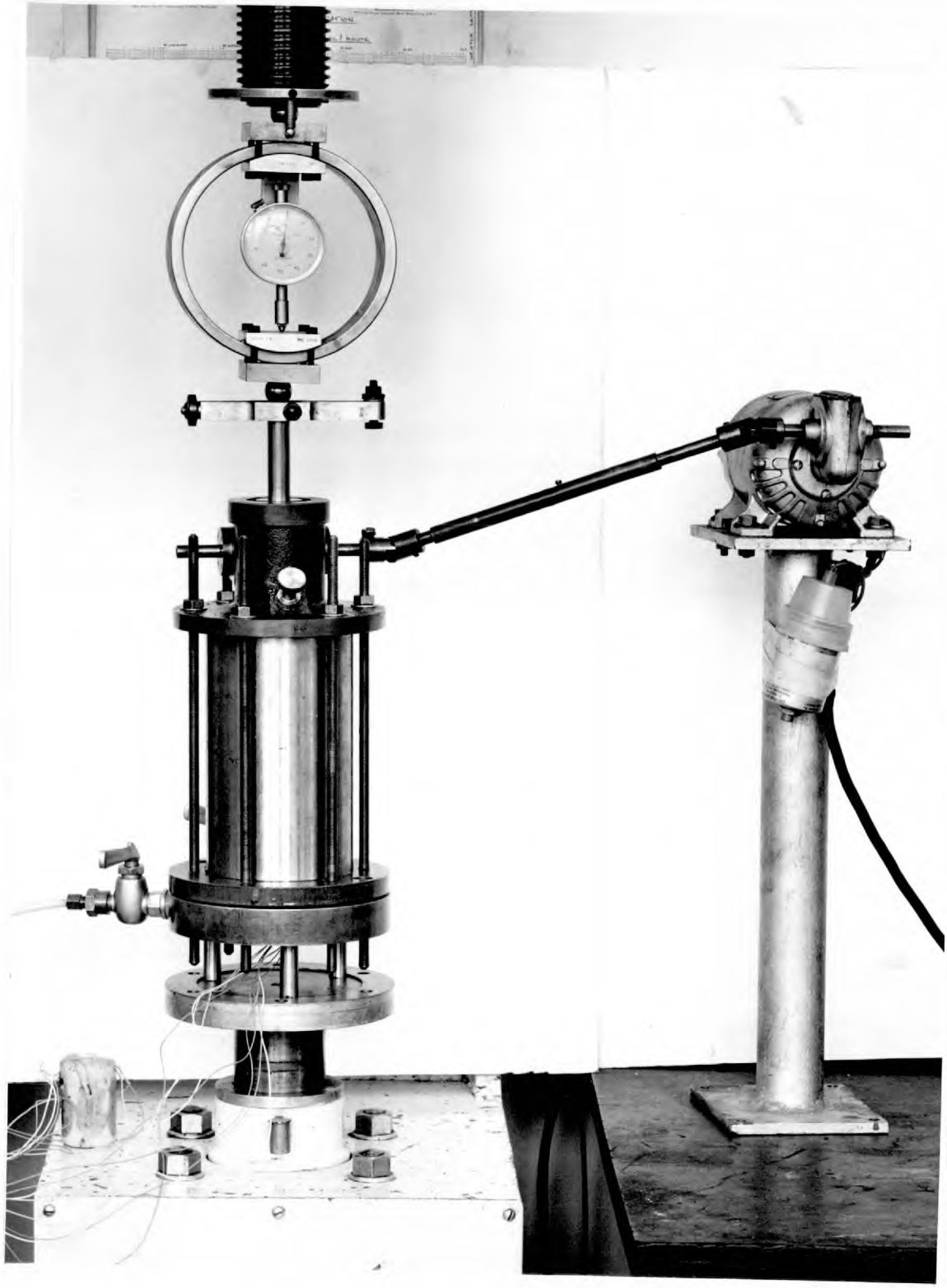
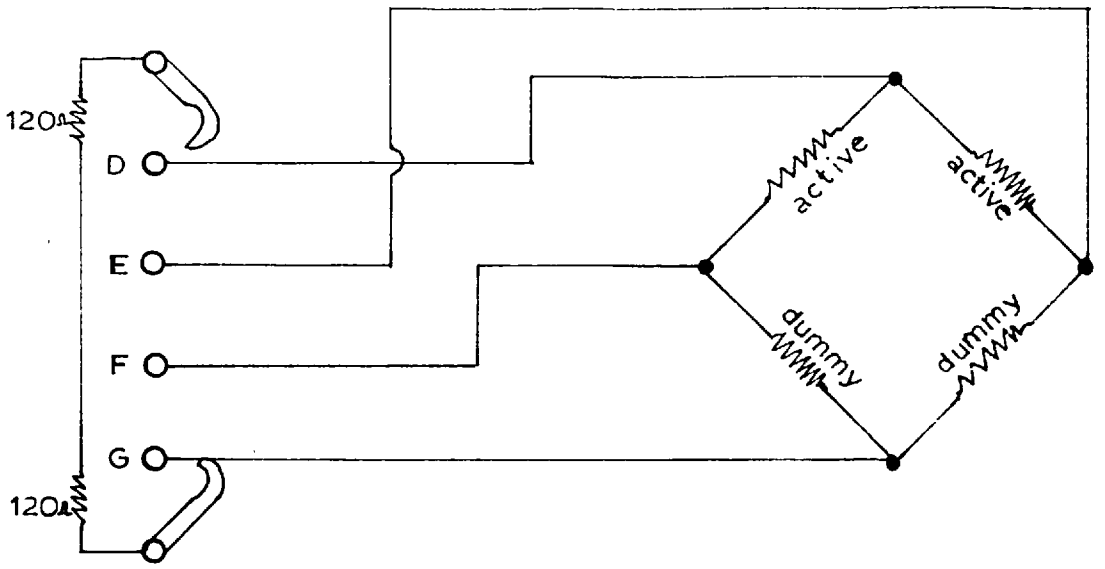
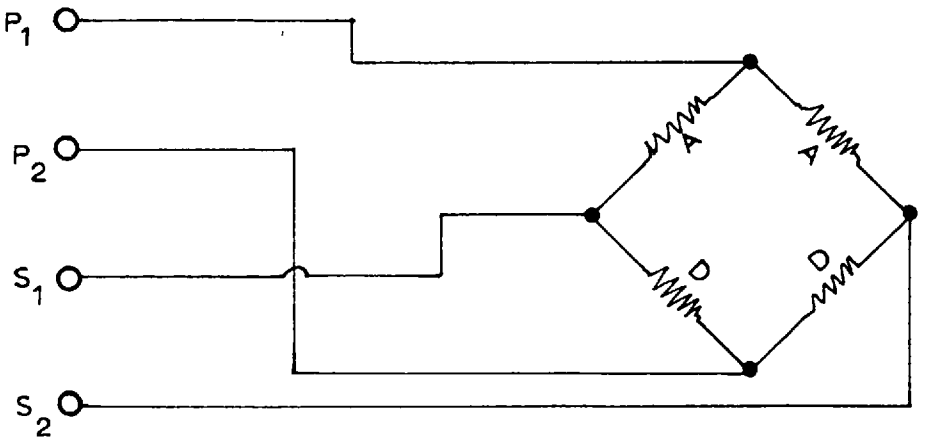


FIGURE (4.4e) ARRANGEMENT OF TRIAXIAL CELL AND PROVING RING IN TEST FRAME



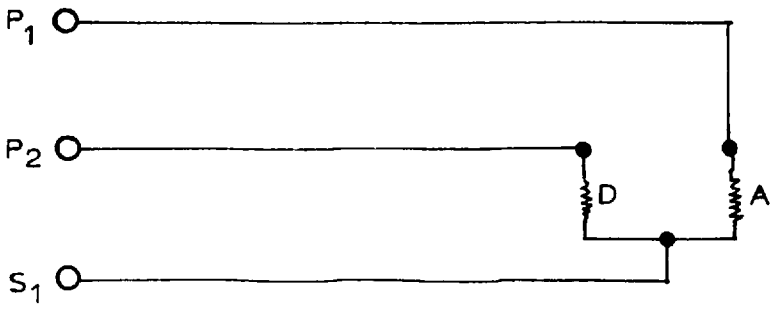
FULL BRIDGE SYSTEM

(PEEKEL-STRAIN INDICATOR)



FULL BRIDGE SYSTEM

(BUDD-STRAIN INDICATOR)



A: ACTIVE GAUGE

D: DUMMY GAUGE

HALF BRIDGE SYSTEM

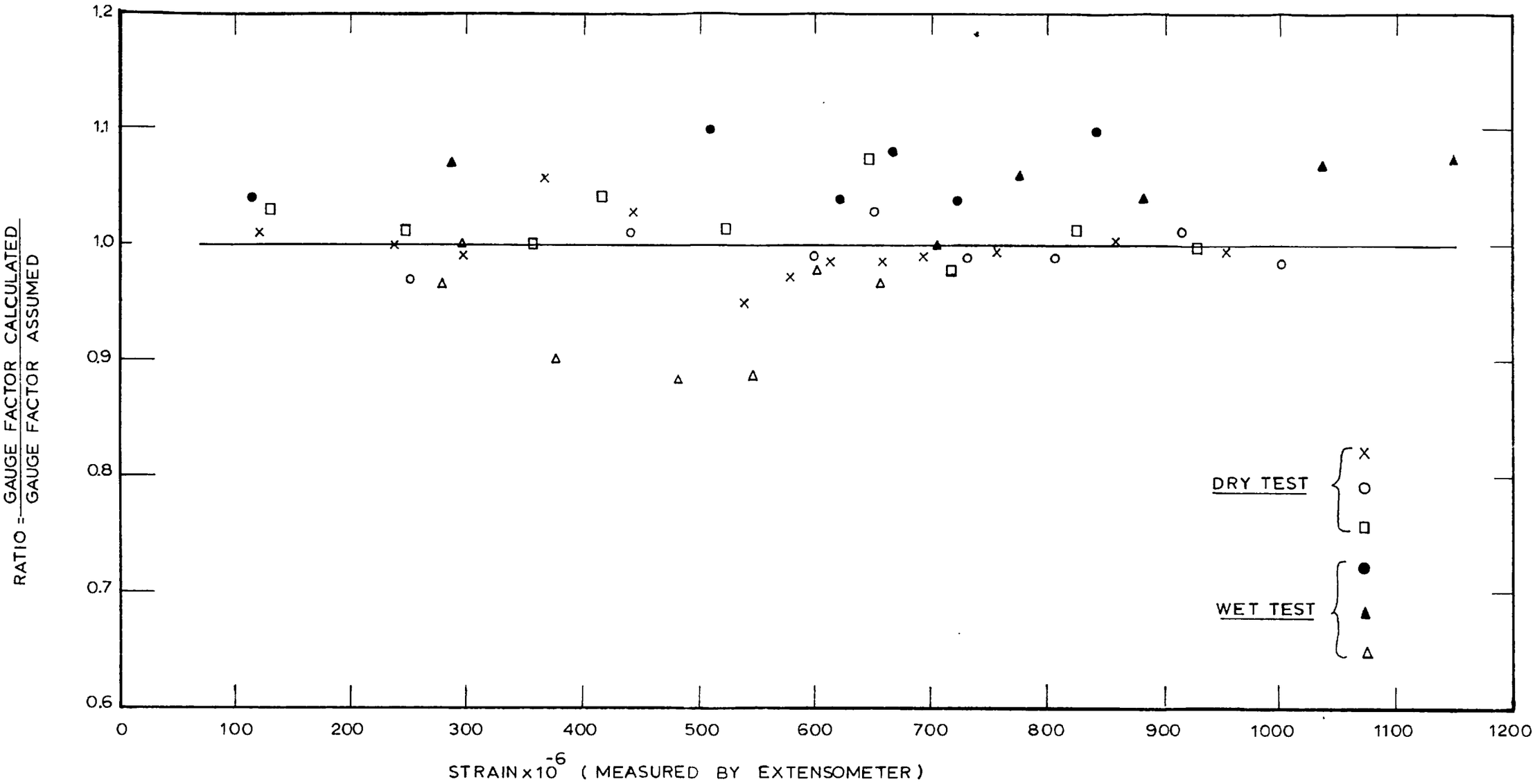
CIRCUIT DIAGRAM

FIG.4.5



For wet test For dry test

FIGURE (4.6) SPECIMENS WITH STRAIN GAUGES ATTACHED



CHECKING OF GAUGE FACTOR OF STRAIN GAUGES BY EXTENSOMETER

FIG. 4.7

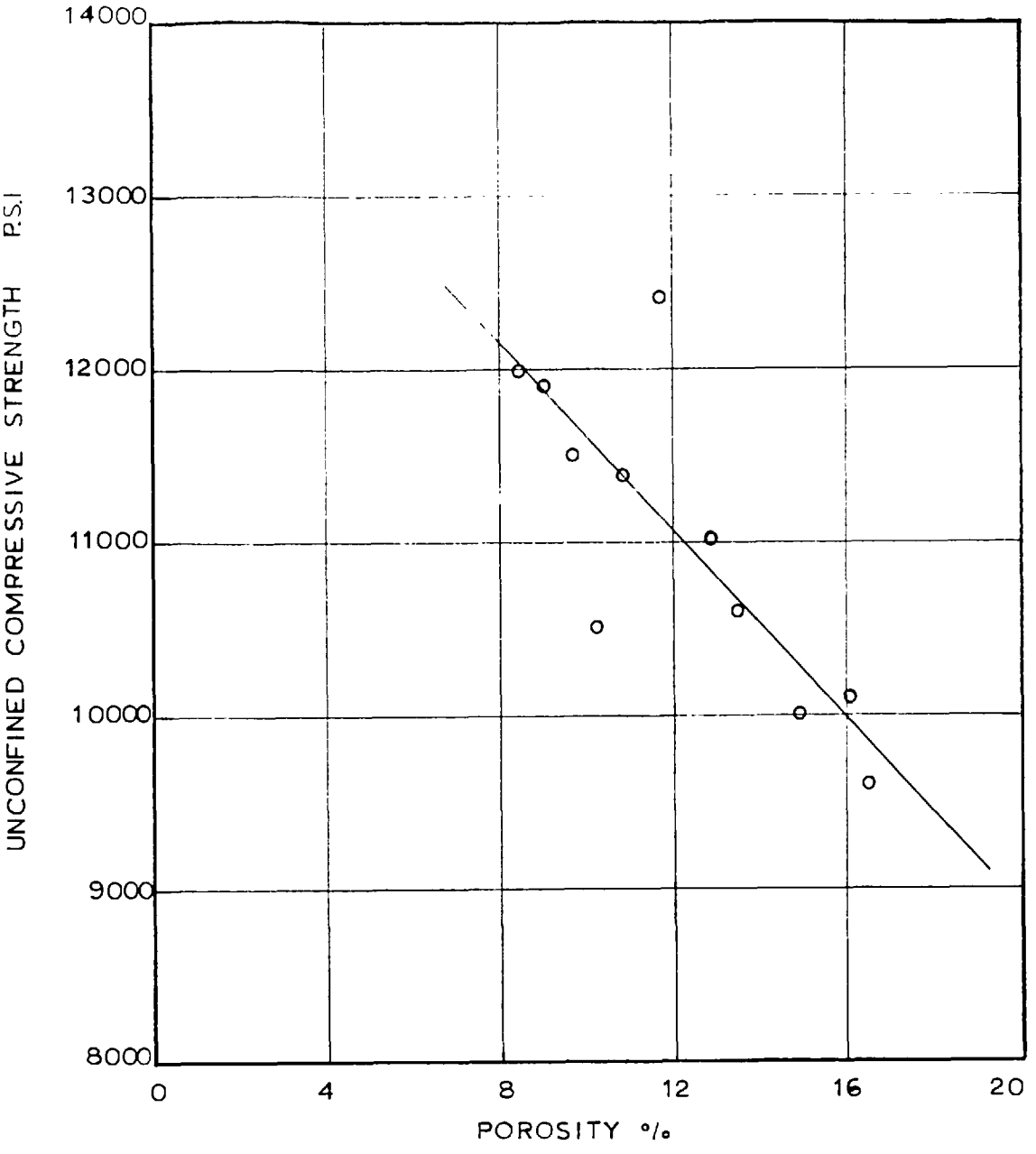
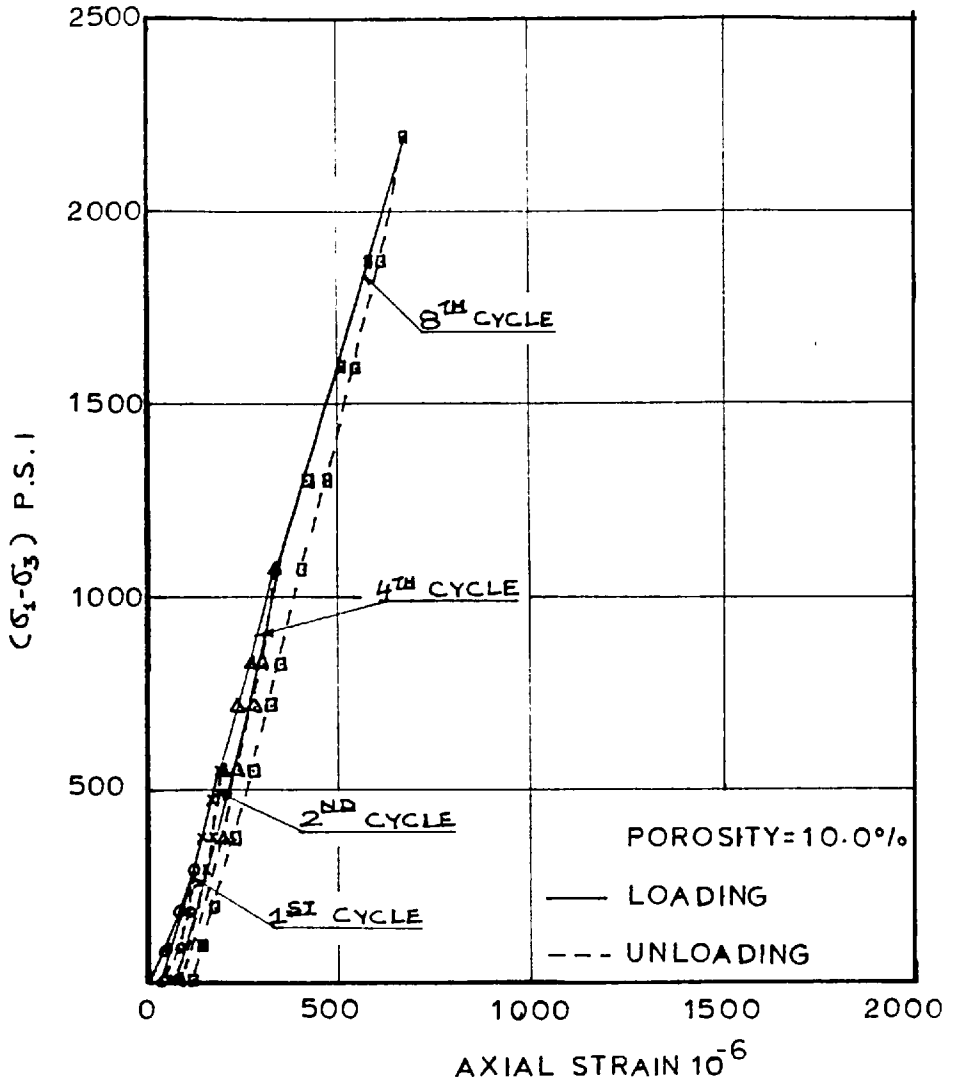
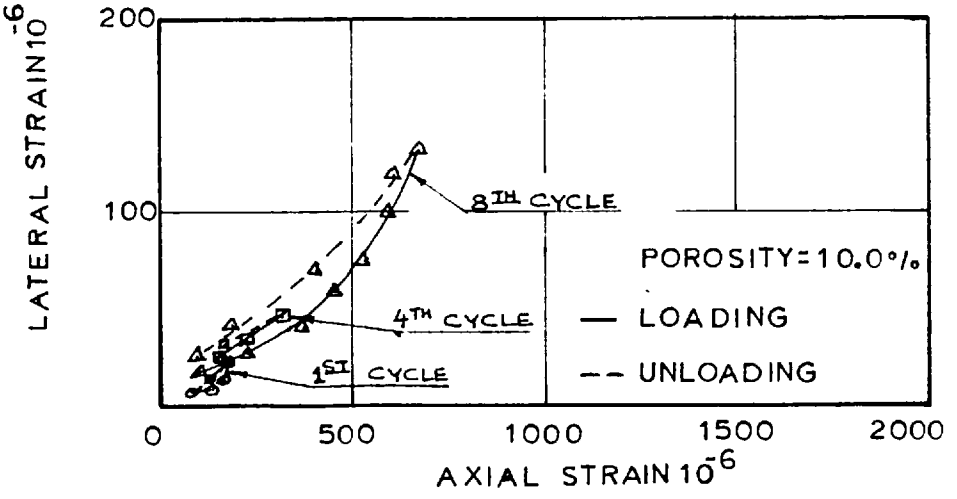

14000
13000
12000
11000
10000
9000
8000
UNCONFINED COMPRESSIVE STRENGTH P.S.I
0
4
8
12
16
20
POROSITY %

FIG.4.8

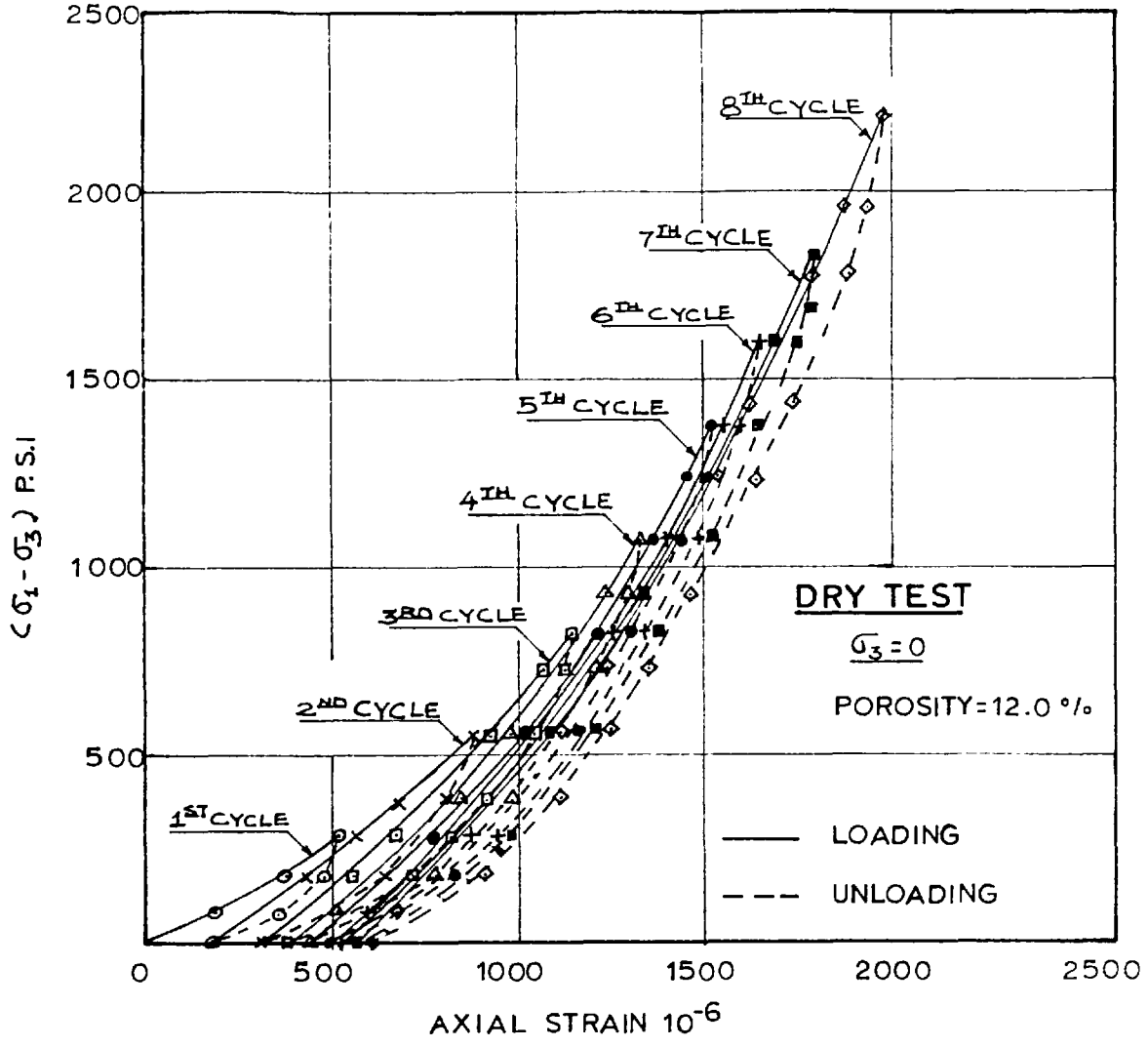




$\sigma_3 = 0$

FIG. 4.9

DRY TEST


2500
2000
1500
1000
500
0
500
1000
1500
2000
2500
$(\sigma_1 - \sigma_3)$ P.S.I
AXIAL STRAIN 10^{-6}
8TH CYCLE
7TH CYCLE
6TH CYCLE
5TH CYCLE
4TH CYCLE
3RD CYCLE
2ND CYCLE
1ST CYCLE
DRY TEST
$\sigma_3 = 0$
POROSITY = 12.0 %
LOADING
UNLOADING

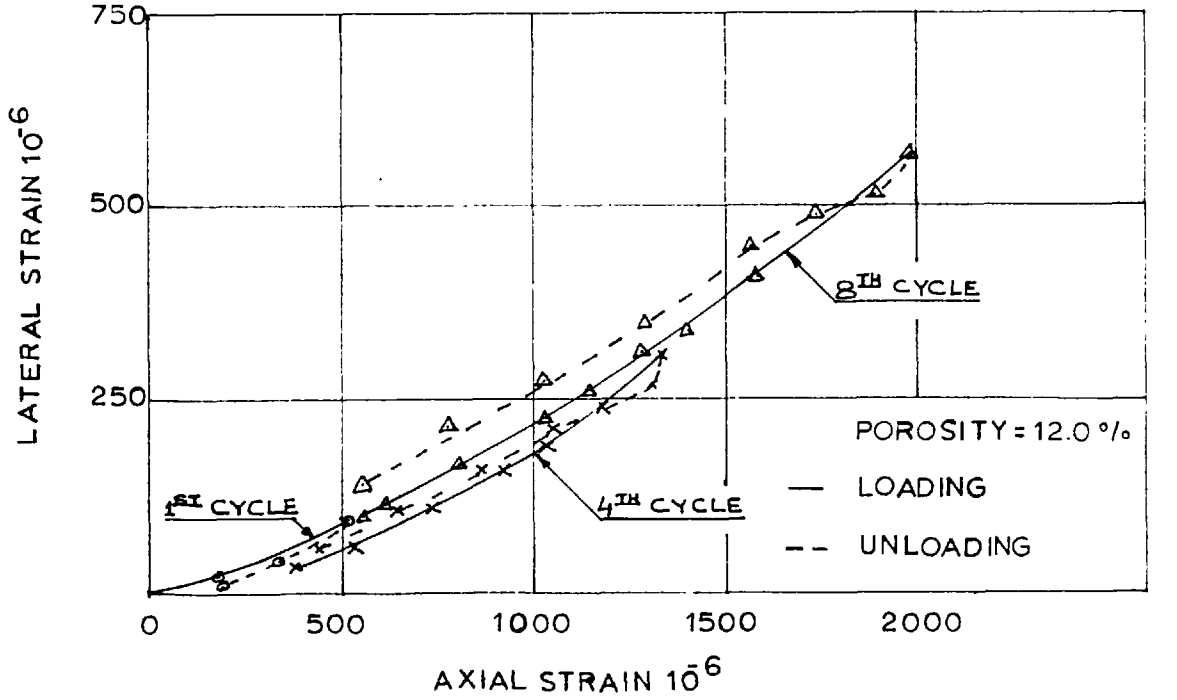
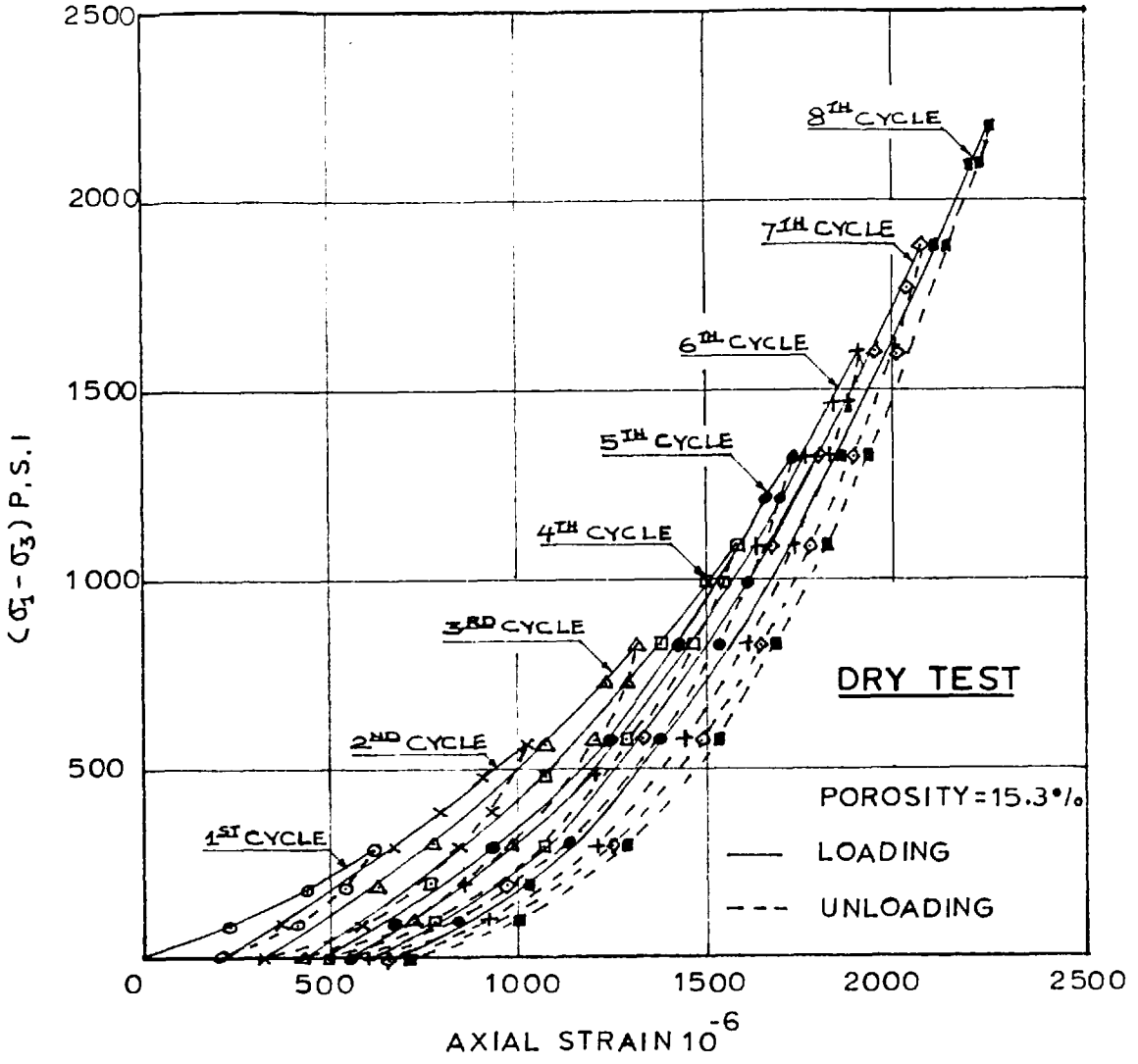
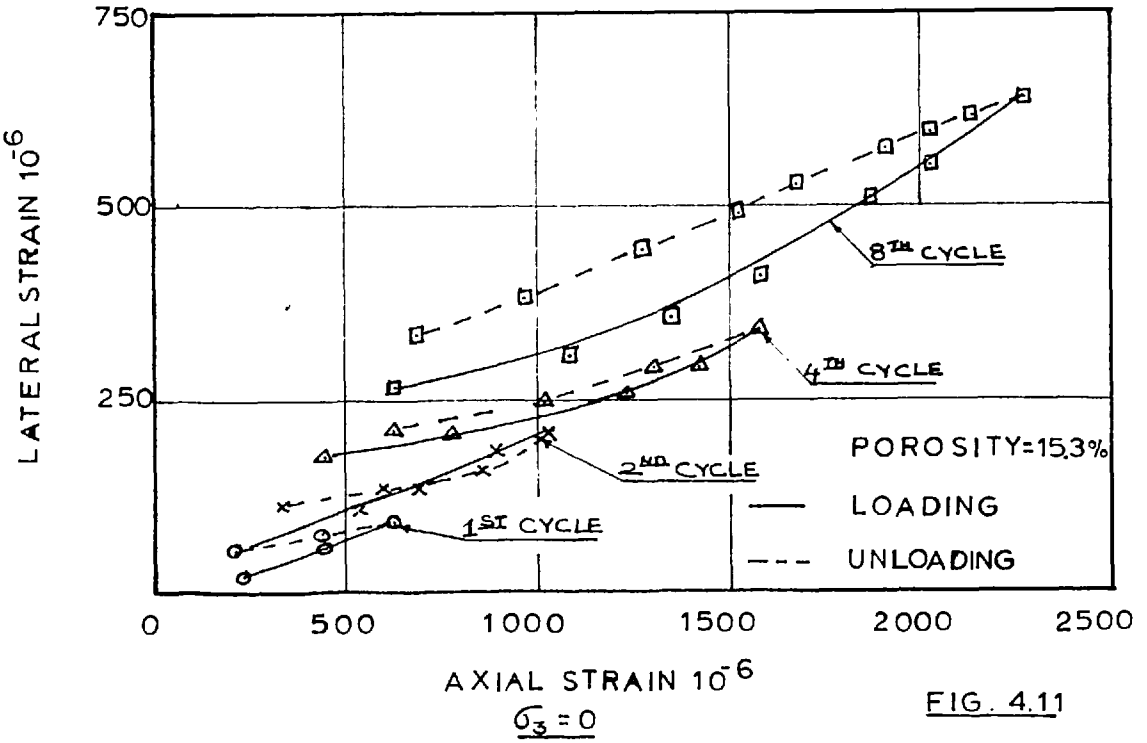

750
500
250
0
500
1000
1500
2000
LATERAL STRAIN 10^{-6}
AXIAL STRAIN 10^{-6}
8TH CYCLE
4TH CYCLE
1ST CYCLE
POROSITY = 12.0 %
LOADING
UNLOADING

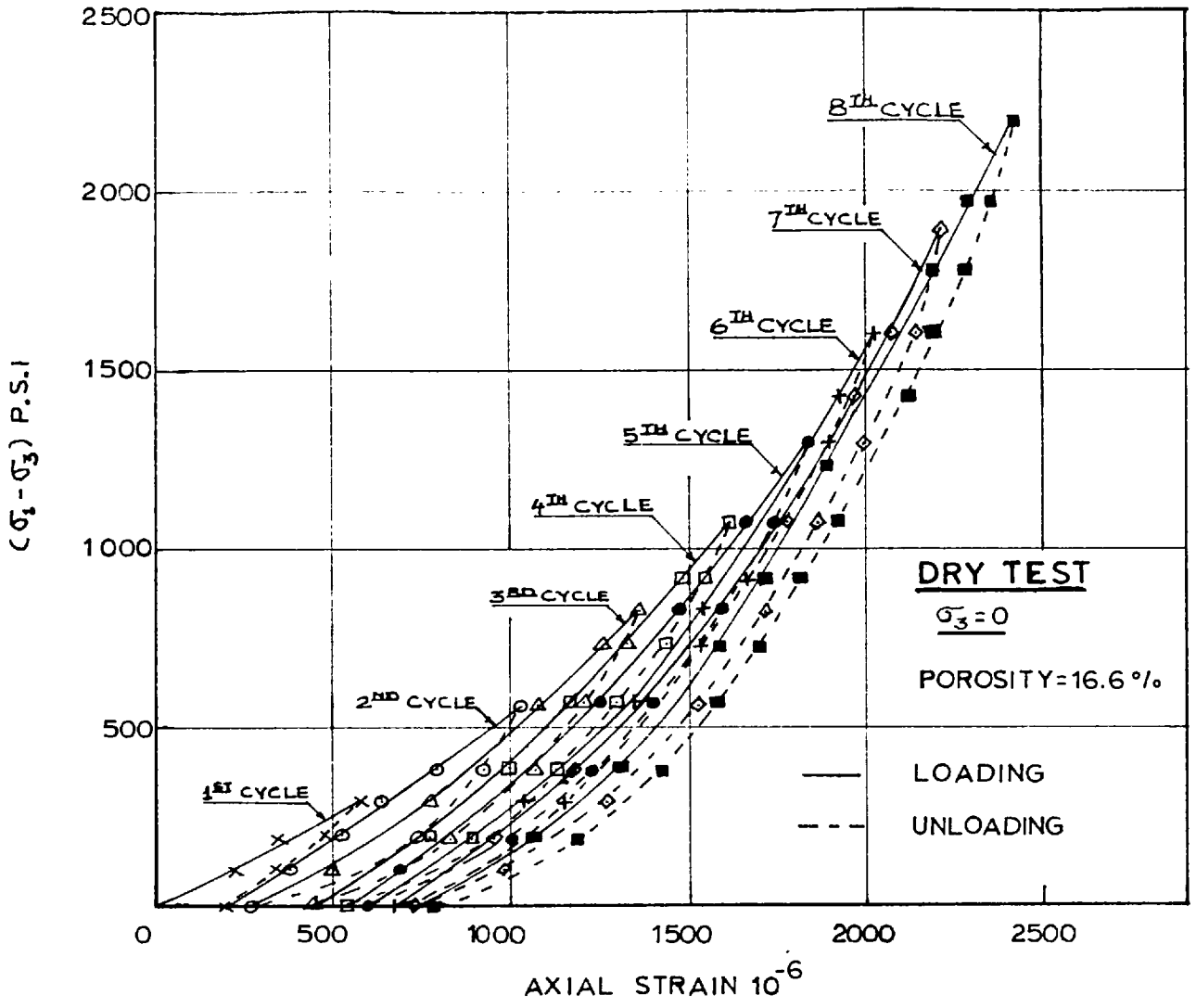
FIG. 4.10





$\sigma_3 = 0$

FIG. 4.11


2500
2000
1500
1000
500
0
500
1000
1500
2000
2500
$(\sigma_1 - \sigma_3)$ P.S.I
AXIAL STRAIN 10^{-6}
8TH CYCLE
7TH CYCLE
6TH CYCLE
5TH CYCLE
4TH CYCLE
3RD CYCLE
2ND CYCLE
1ST CYCLE
DRY TEST
$\sigma_3 = 0$
POROSITY=16.6 %
LOADING
UNLOADING

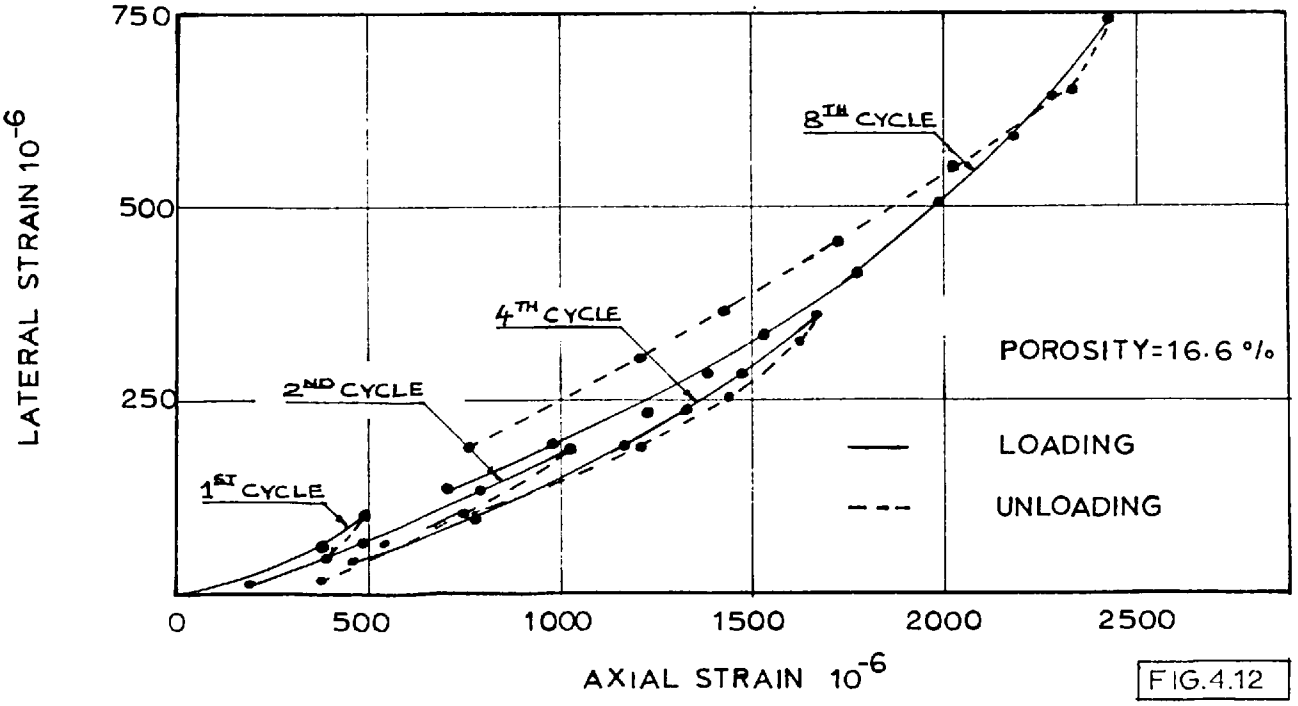
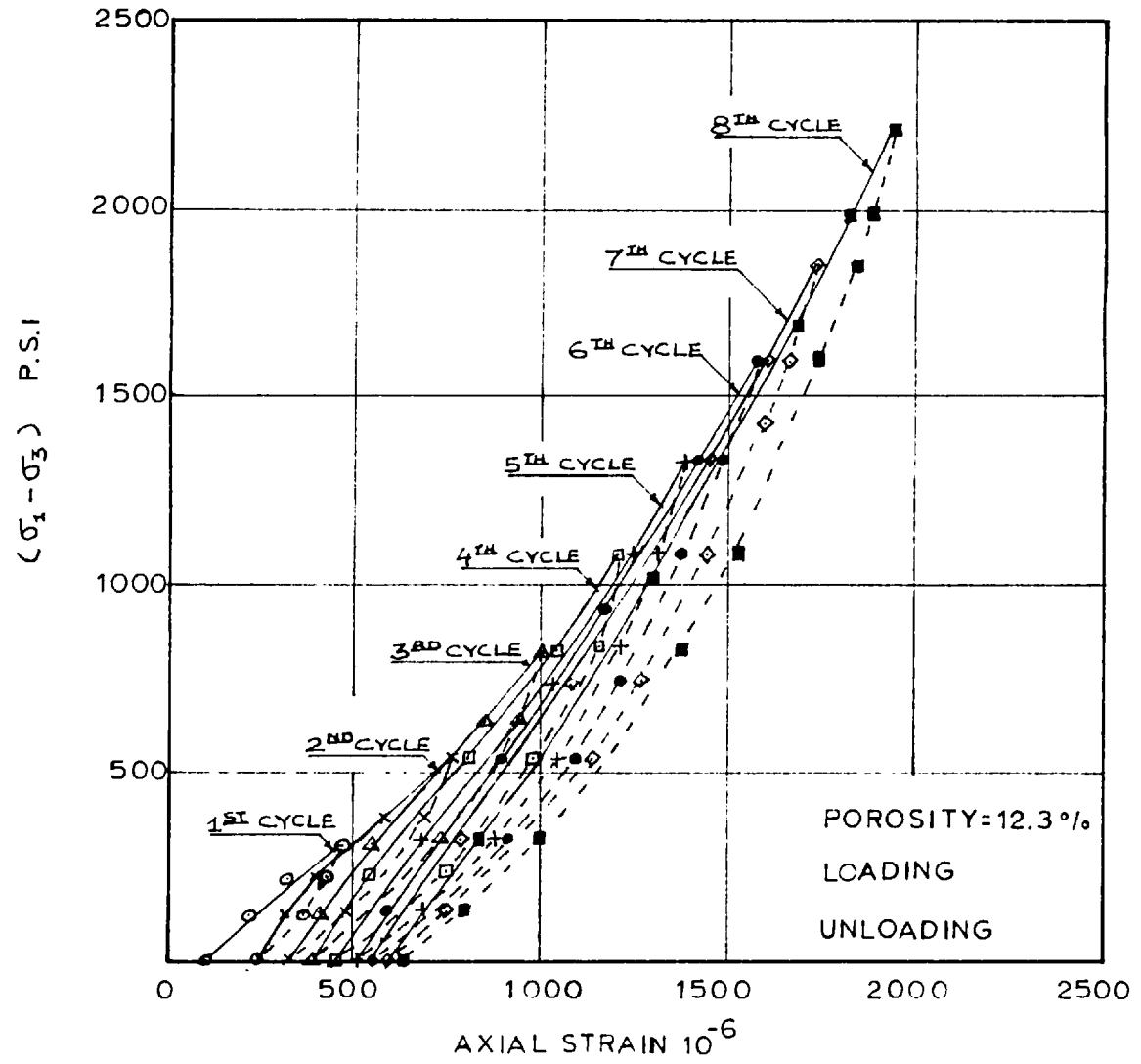
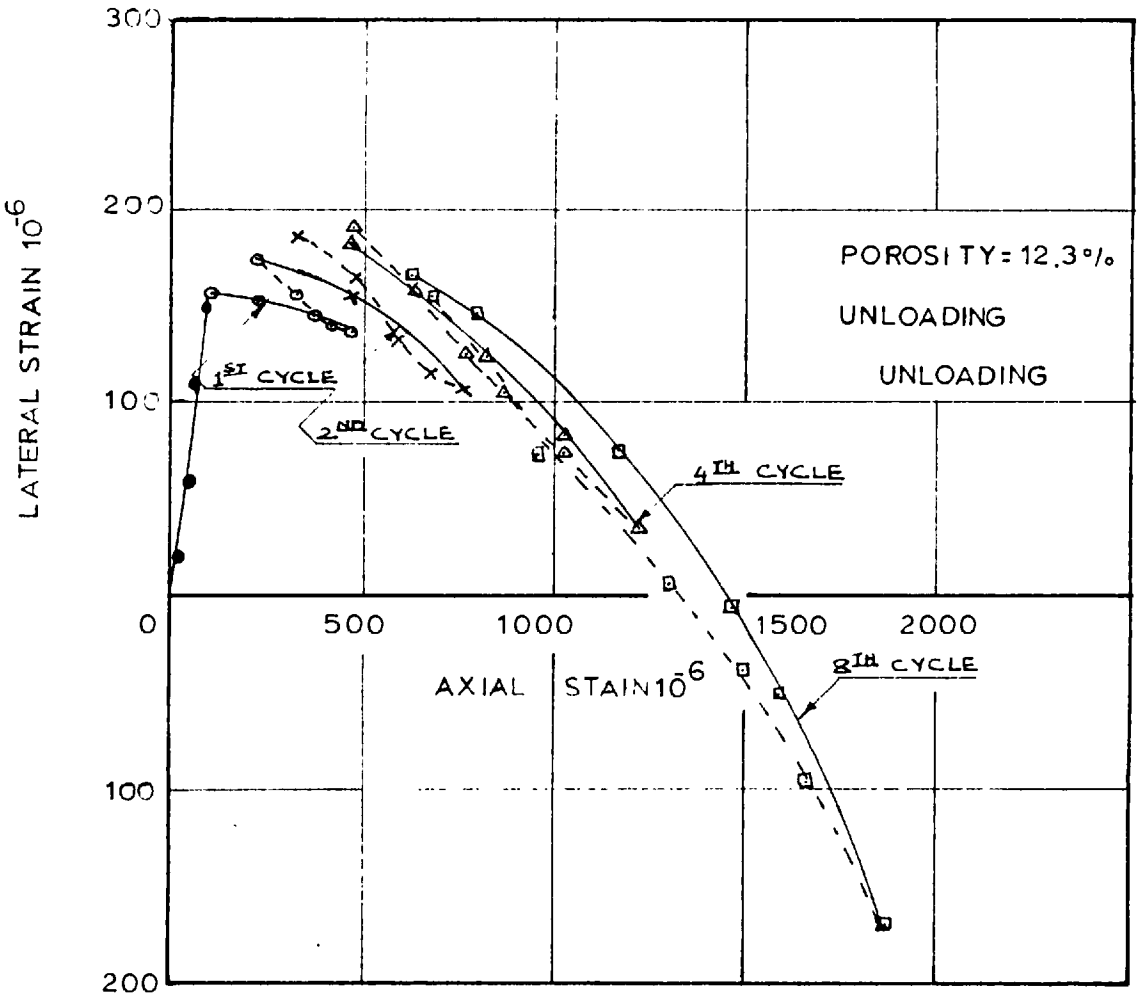
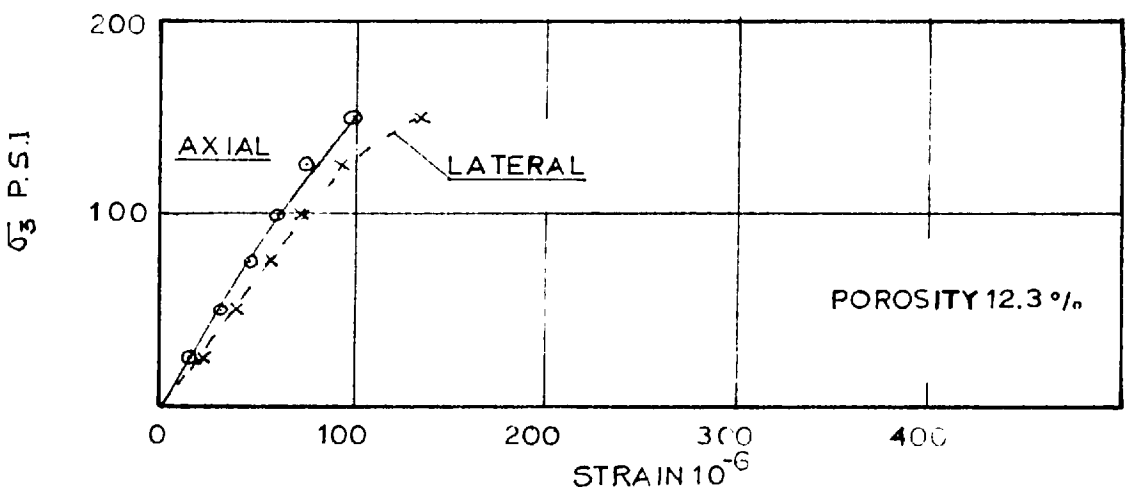

750
500
250
0
500
1000
1500
2000
2500
LATERAL STRAIN 10^{-6}
AXIAL STRAIN 10^{-6}
8TH CYCLE
4TH CYCLE
2ND CYCLE
1ST CYCLE
POROSITY=16.6 %
LOADING
UNLOADING

FIG.4.12



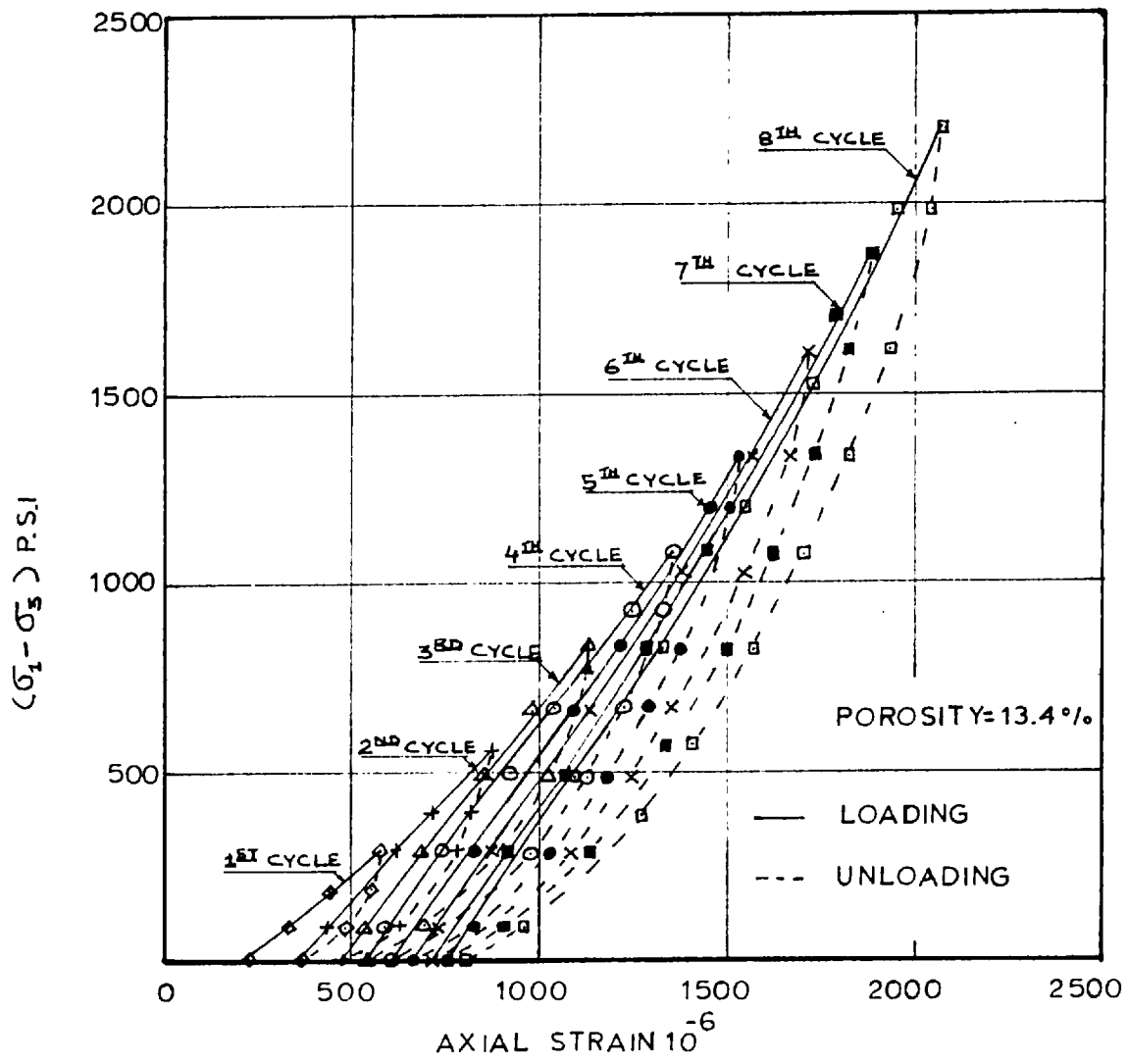


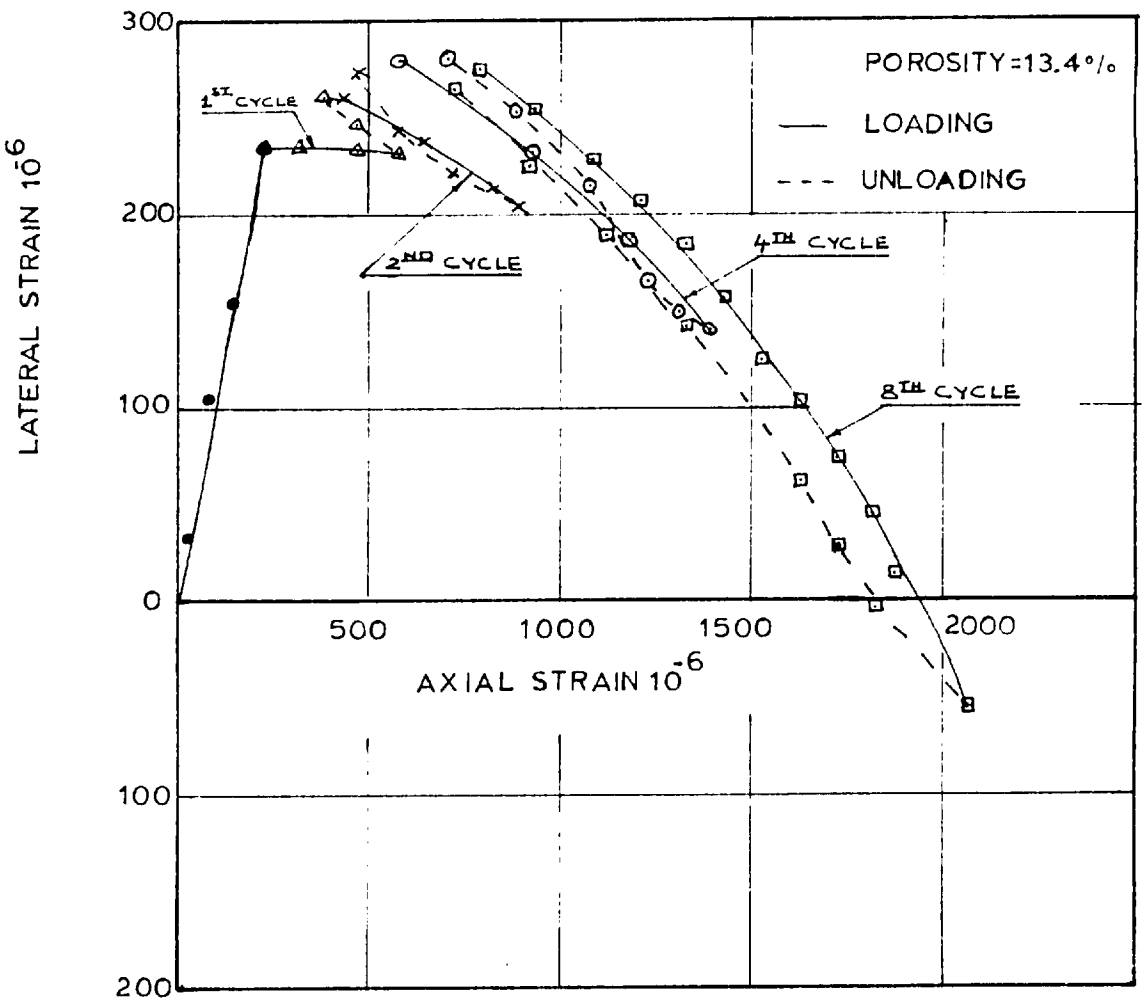


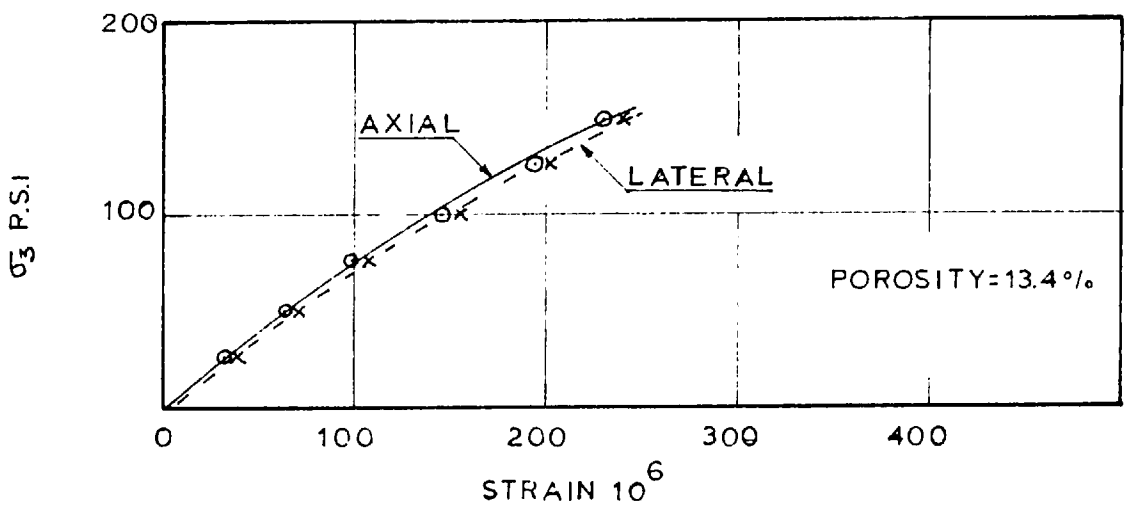
DRY TEST

σ_3 = 150 P.S.I

FIG. 4.13



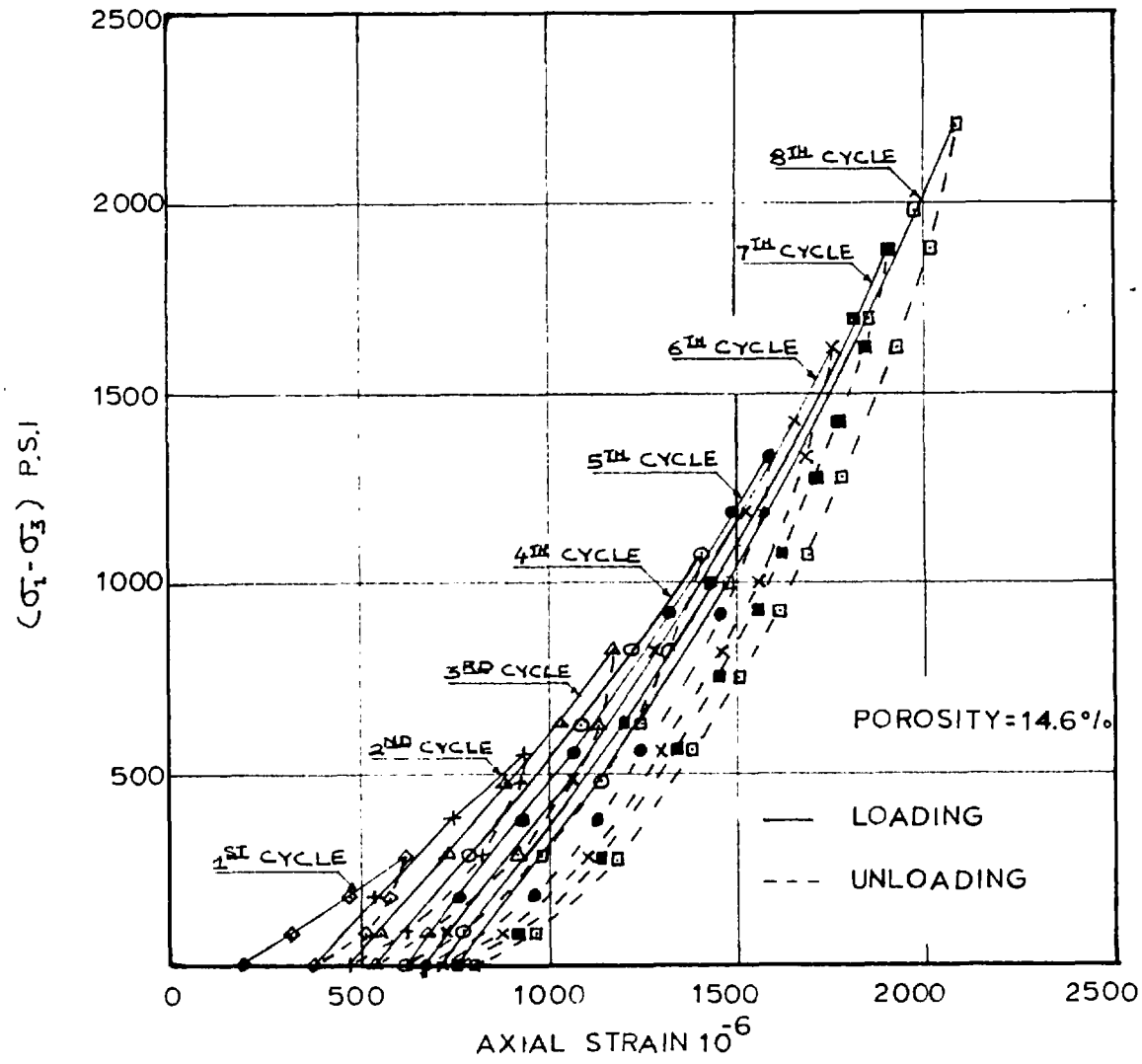


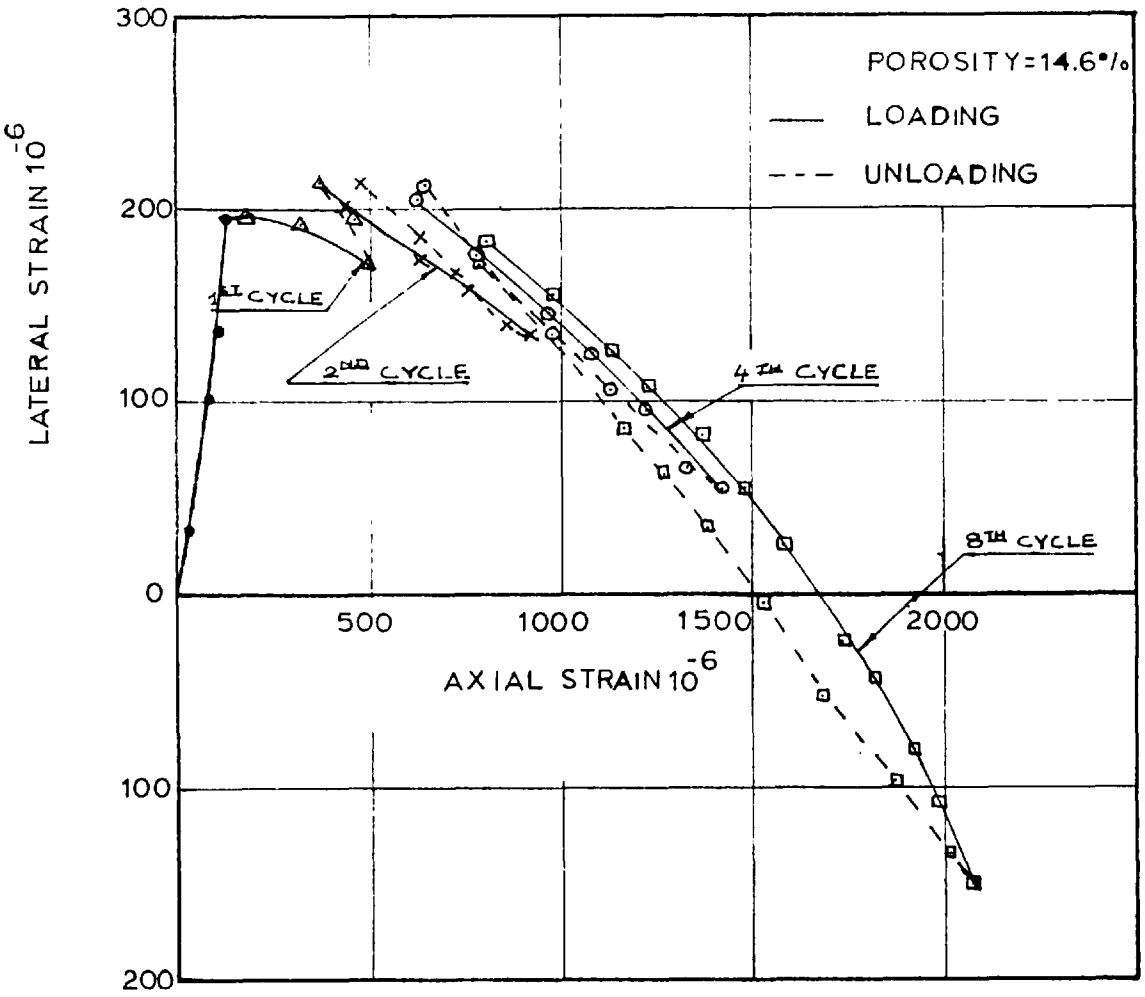


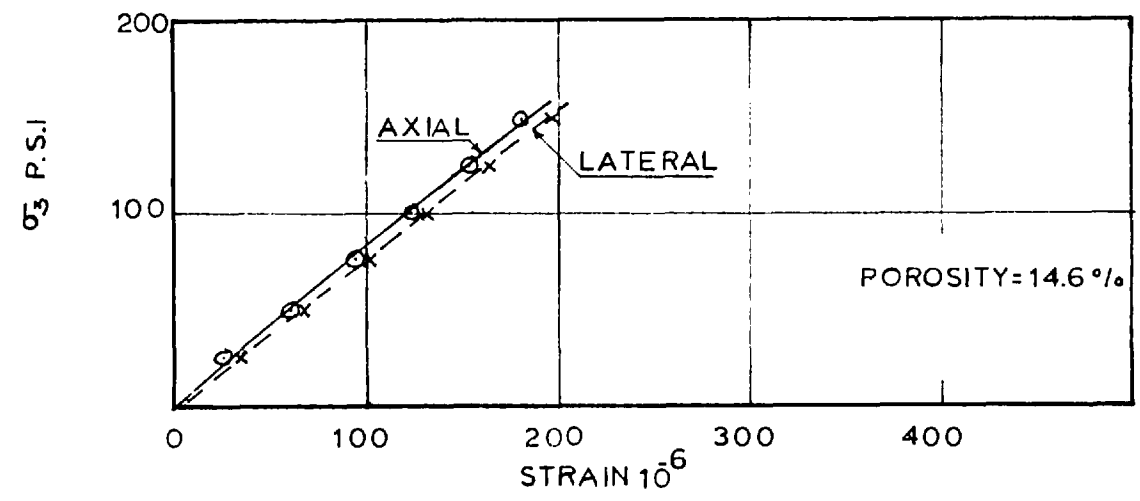
DRY TEST

σ_3 = 150 P.S.I

FIG. 4.14



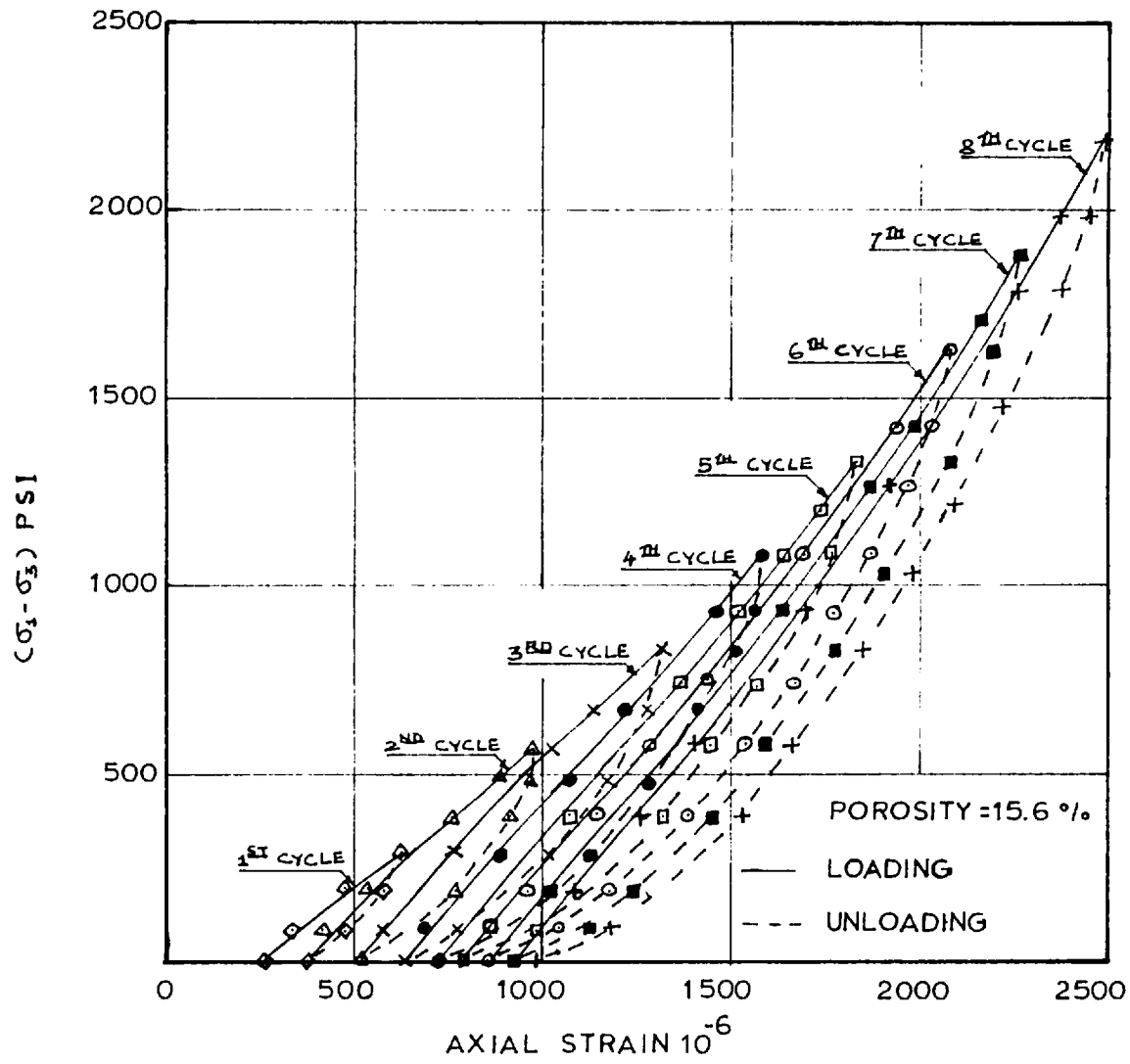


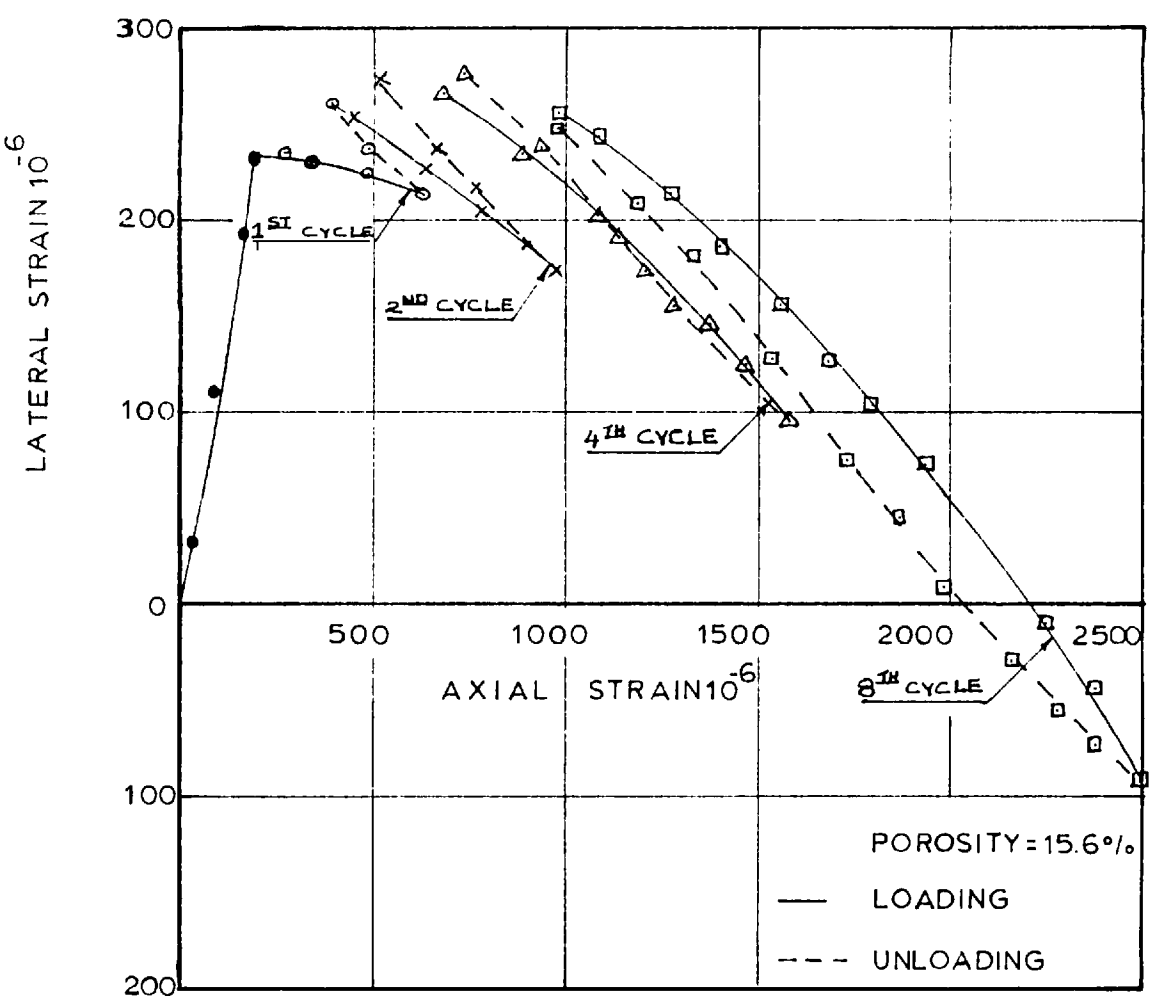


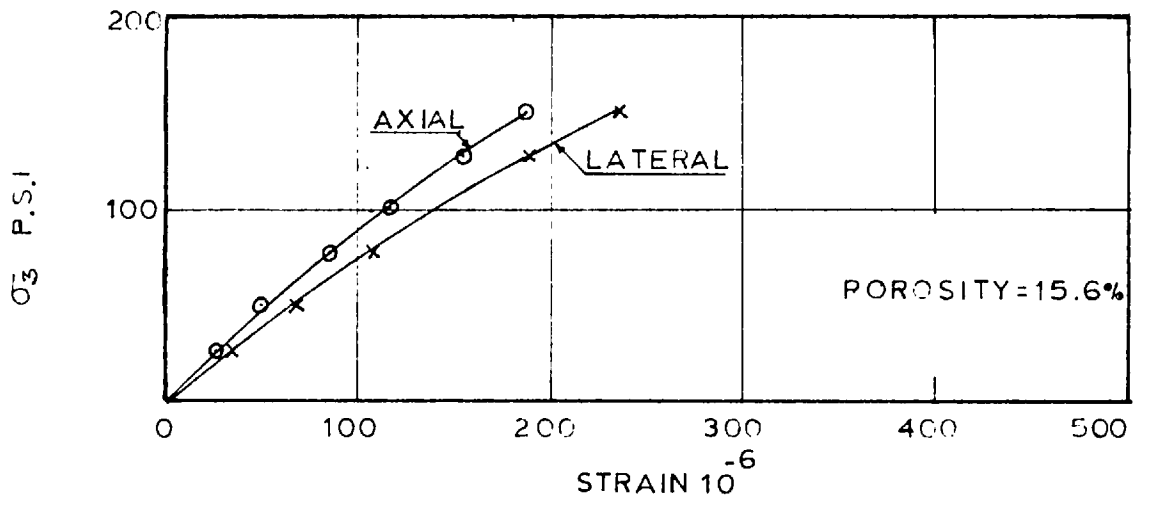
DRY TEST

σ_3 = 150 P.S.I

FIG.4.15



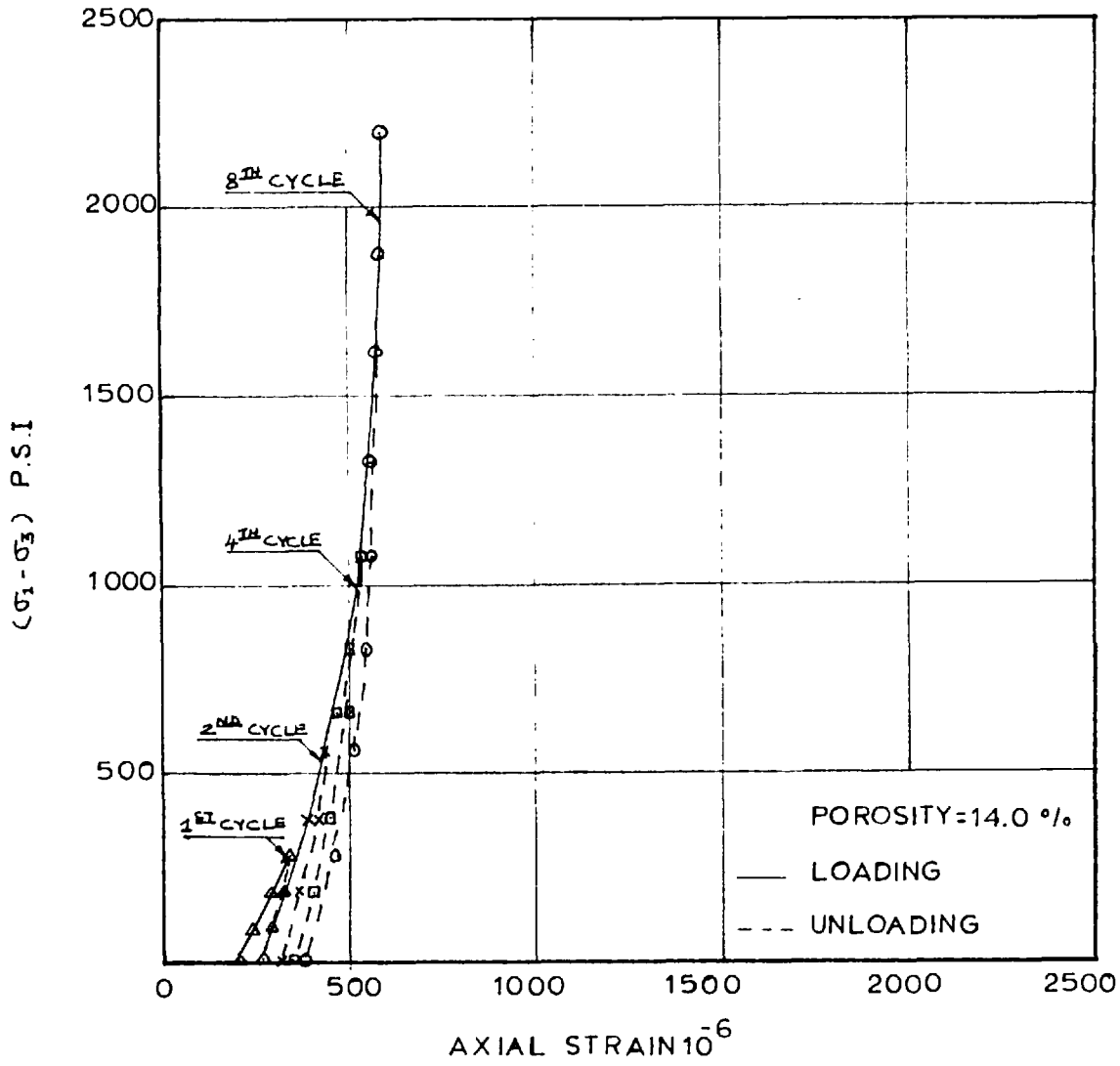


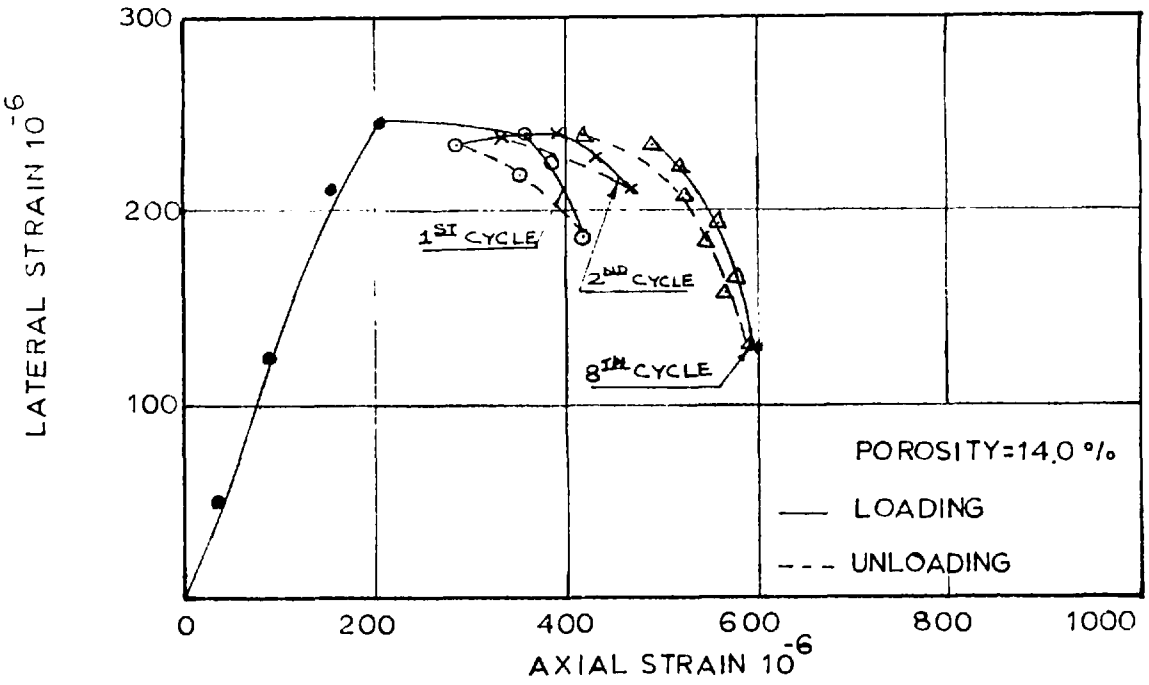


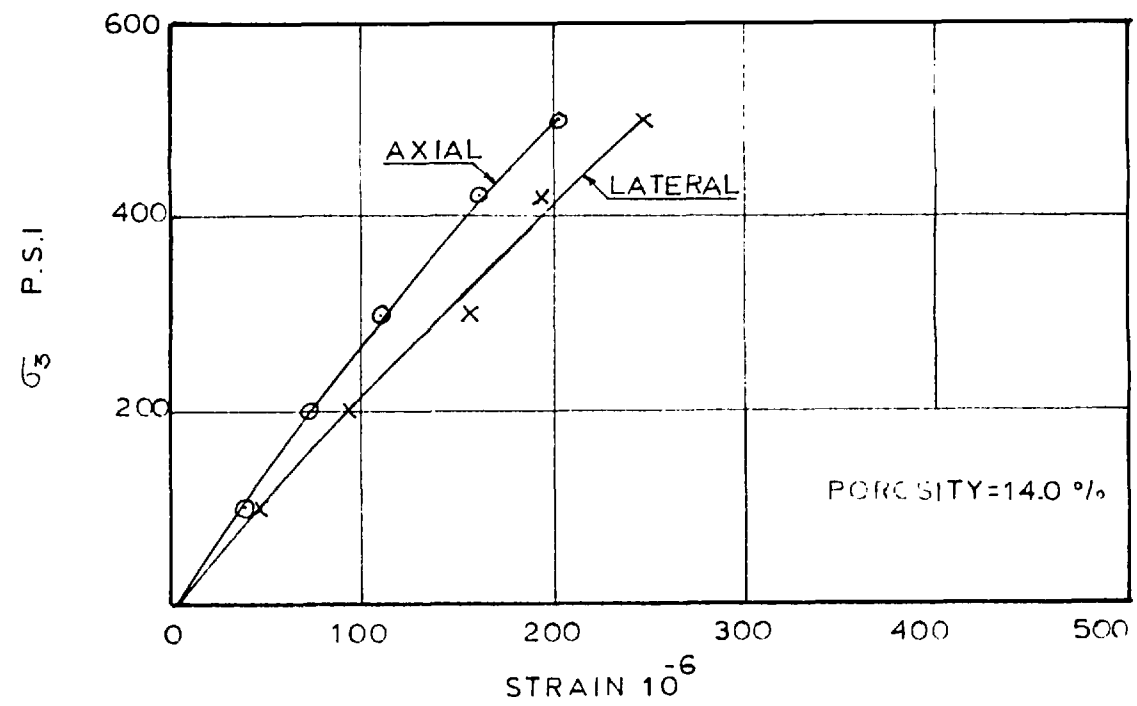
DRY TEST

σ_3 = 150 P.S.I

FIG. 4.16



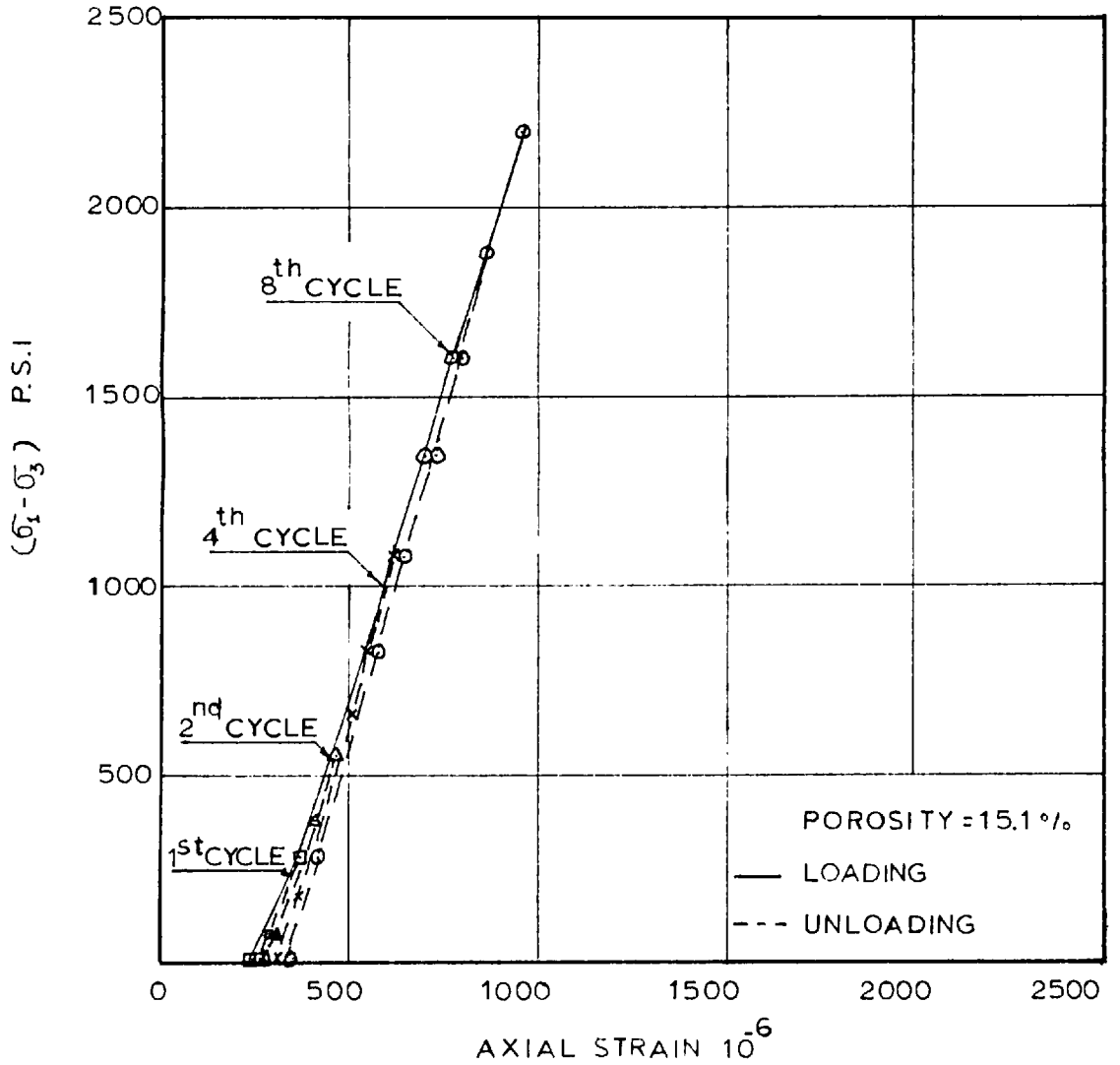


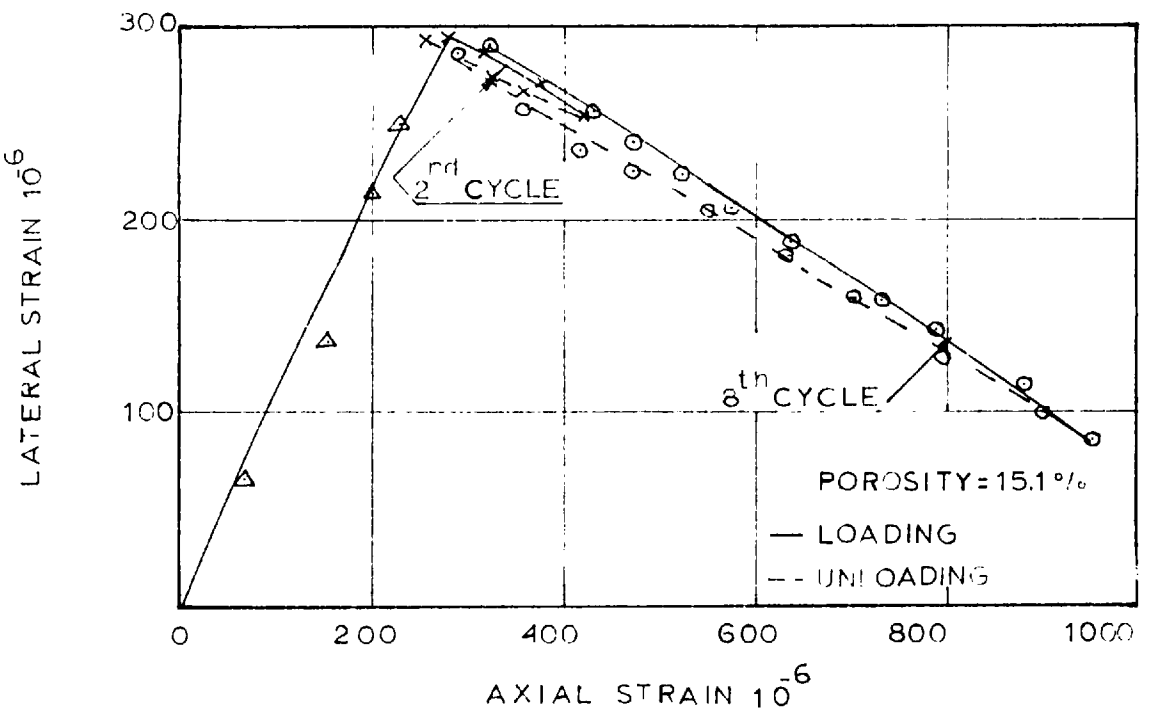


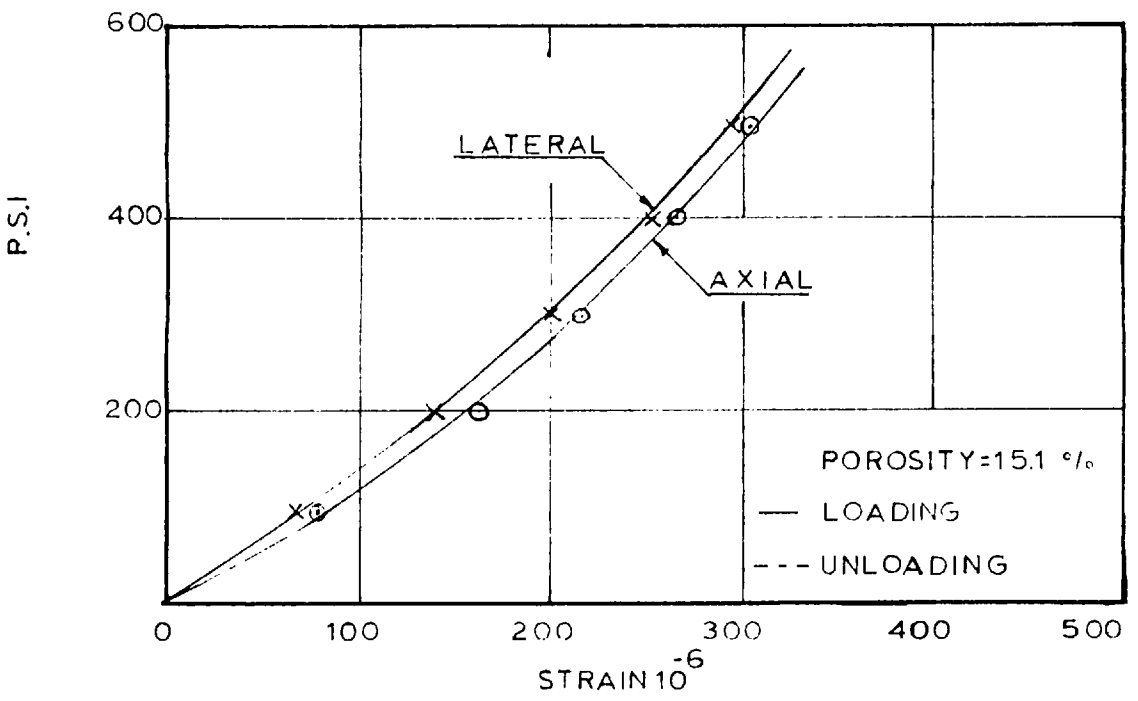
DRY TEST

σ_3 = 500 P.S.I

FIG. 4.17



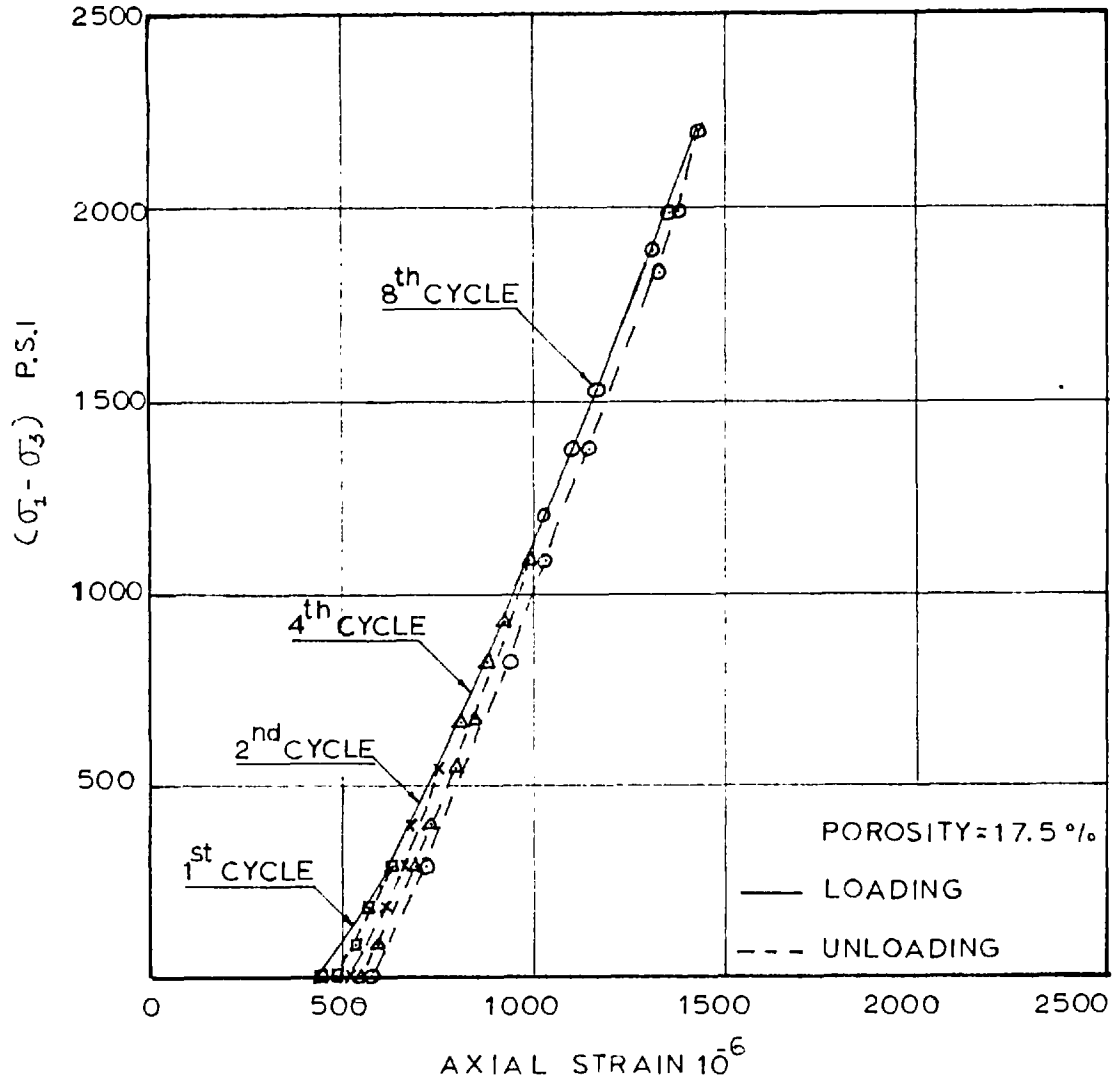


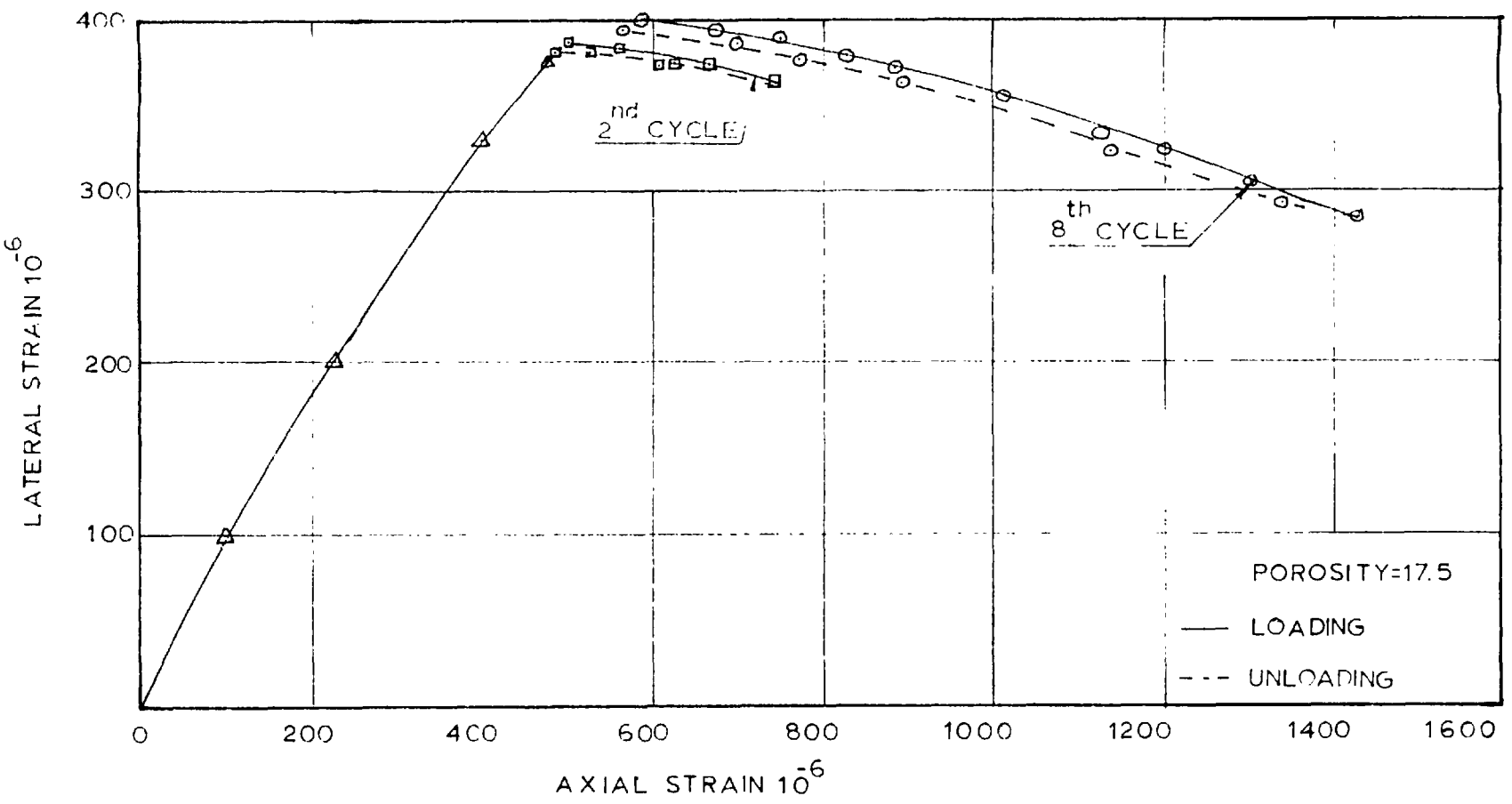


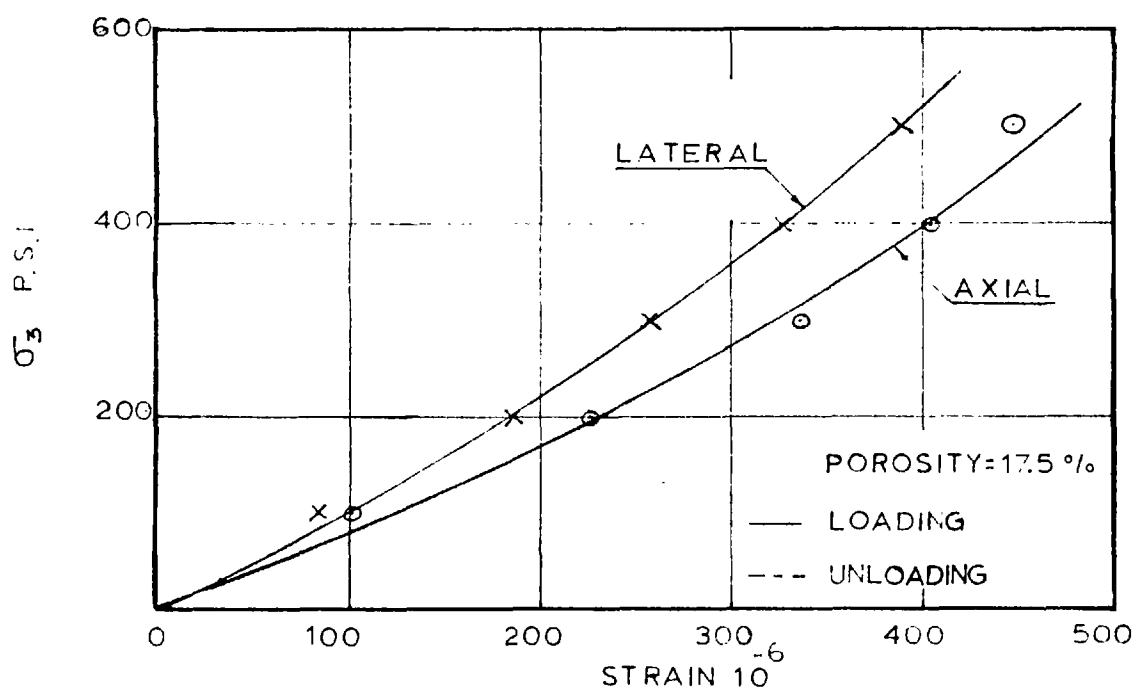
DRY TEST

σ_3 = 500 P.S.I

FIG. 4.18



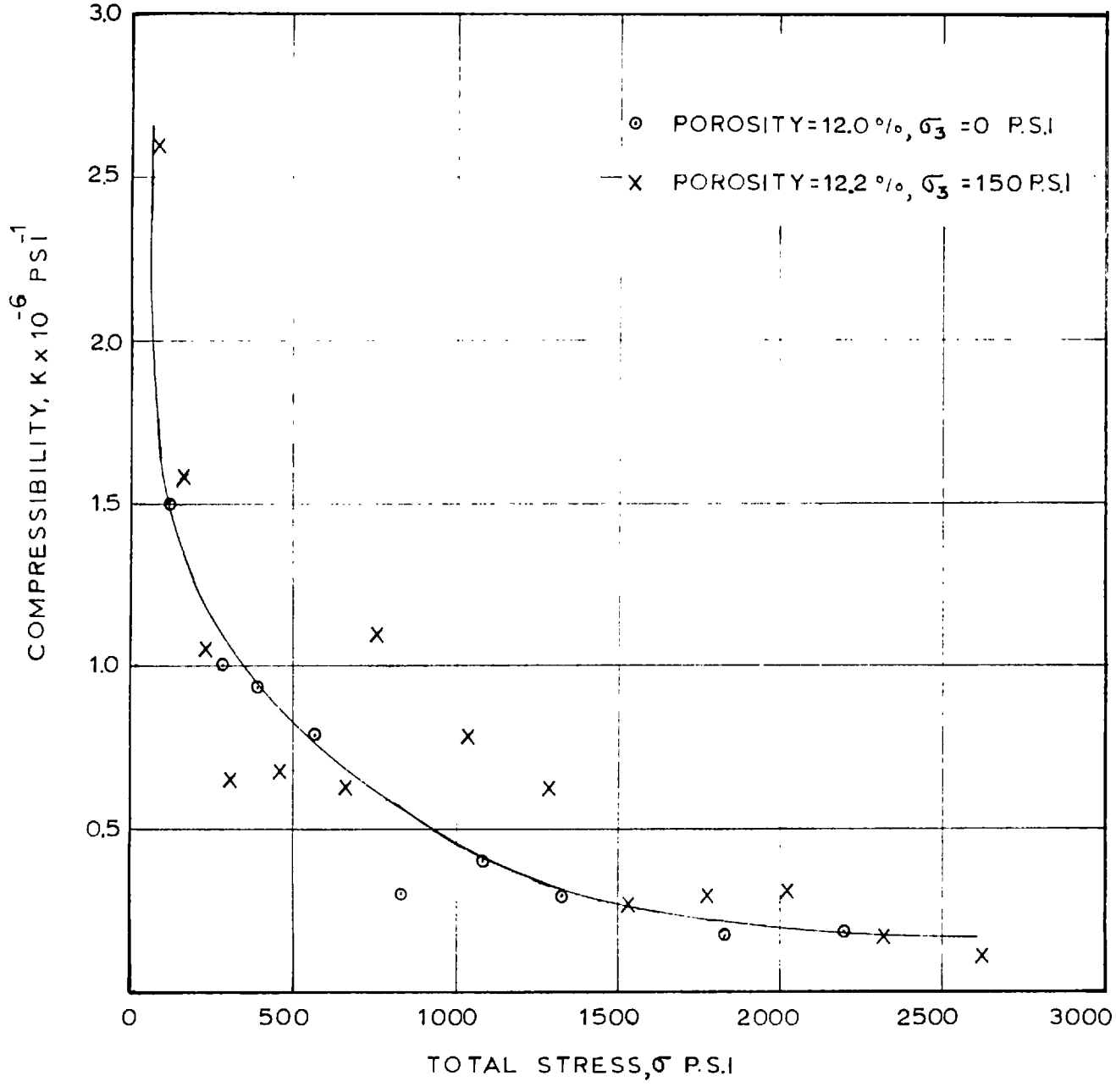




DRY TEST

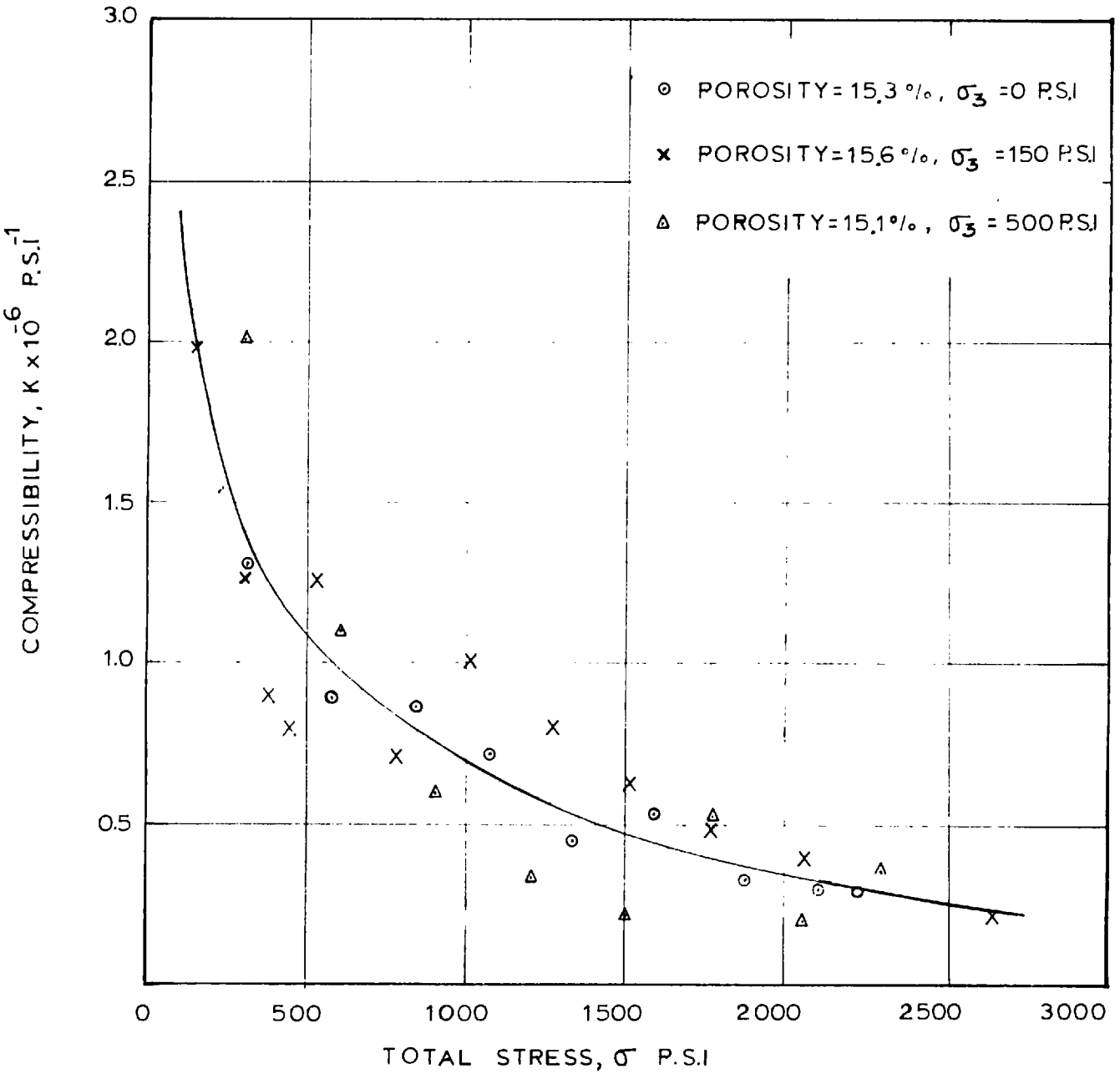
σ_3 = 500 P.S.I

FIG. 4.19



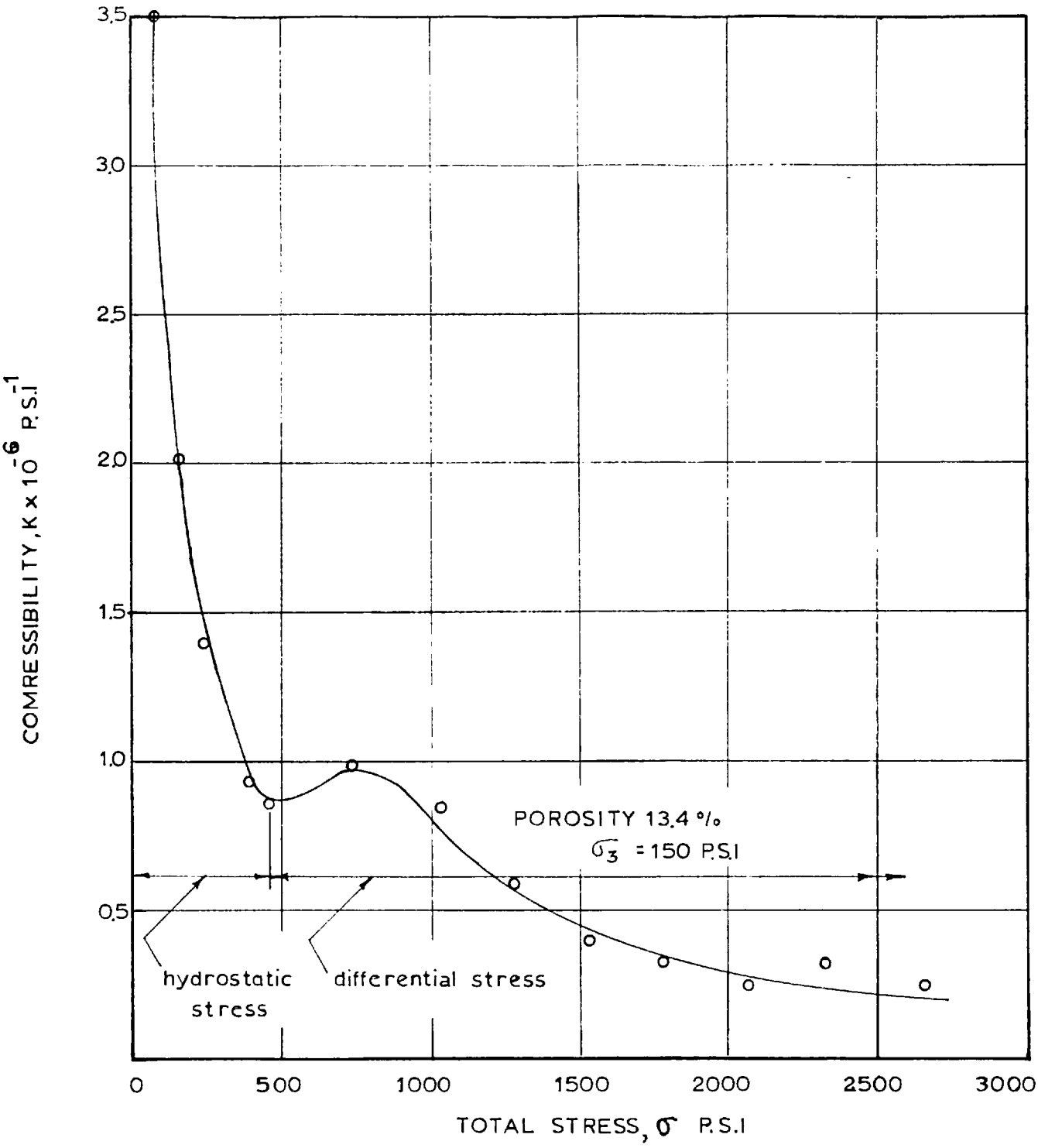
DRY TEST

FIG. 4.20



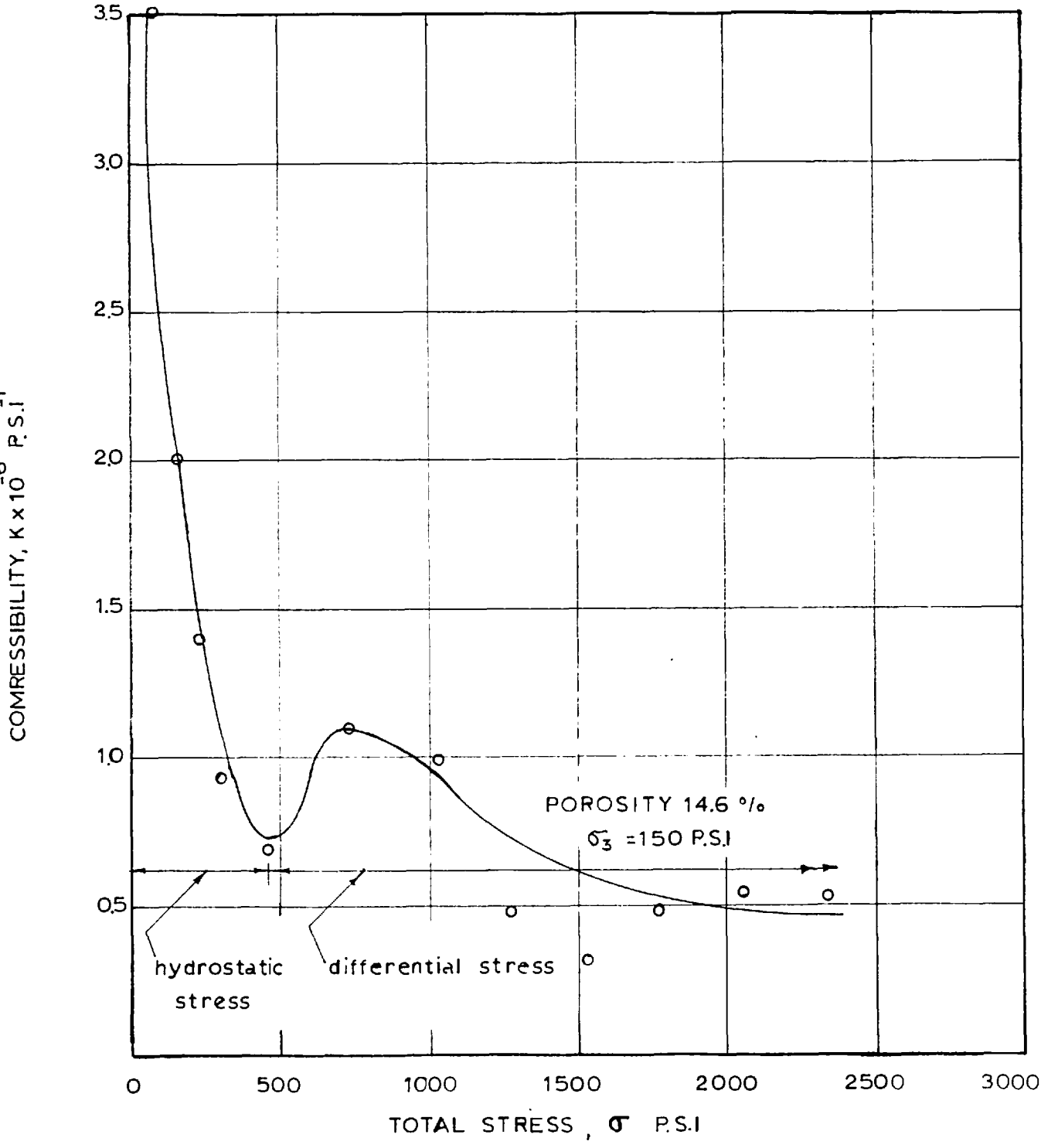
DRY TEST

FIG.4.21



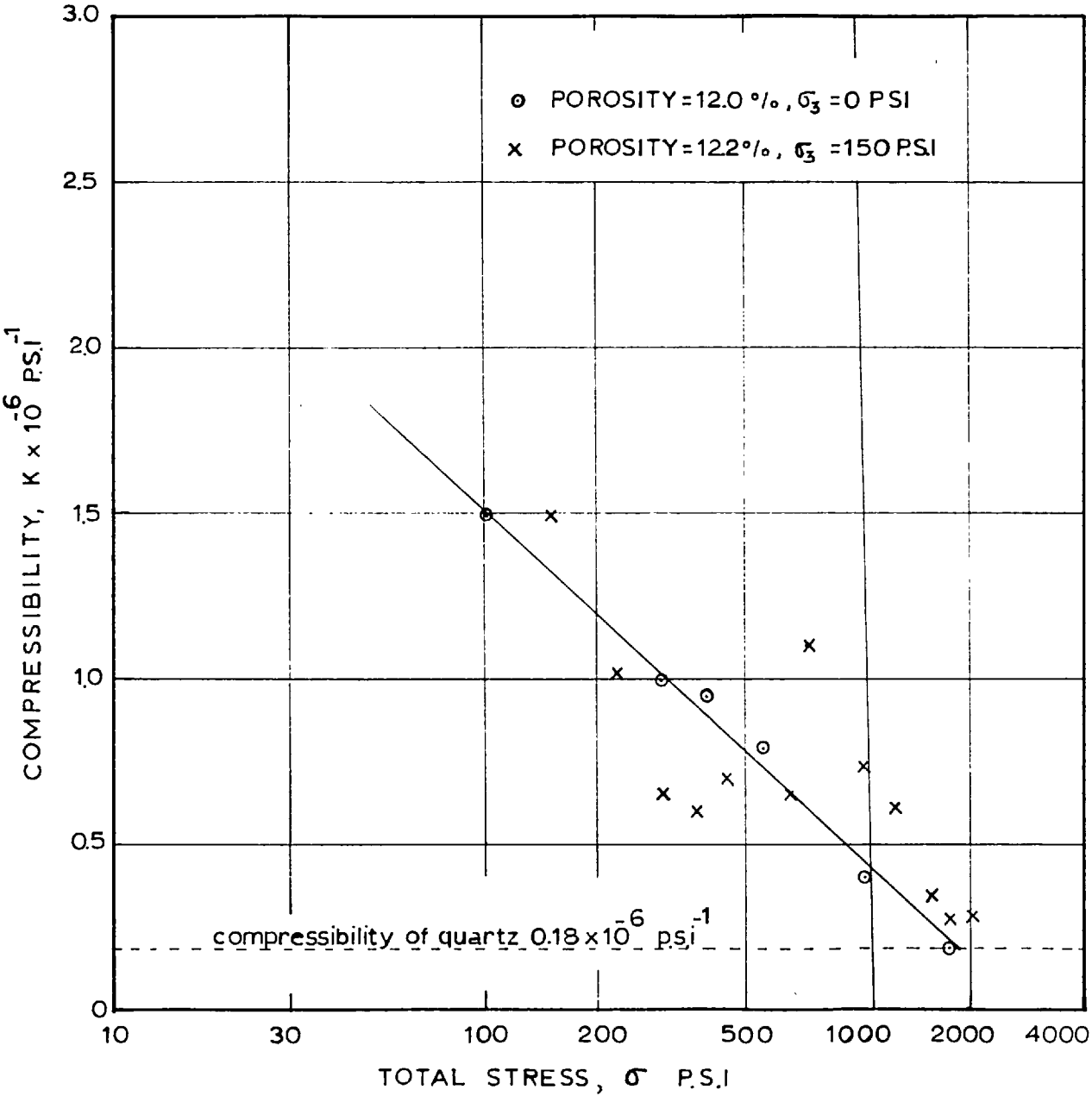
DRY TEST

FIG. 4.22



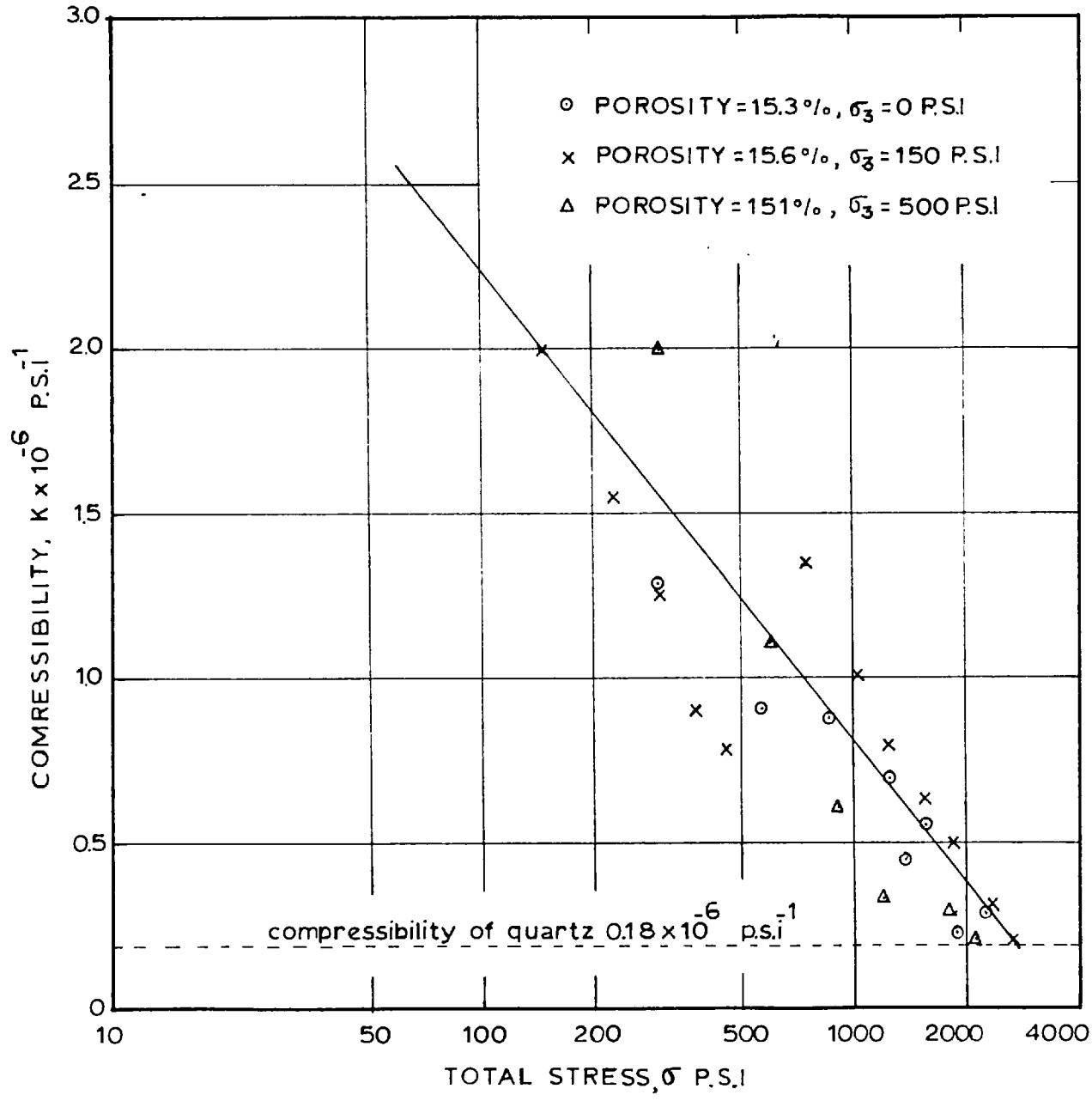
DRY TEST

FIG. 4.23



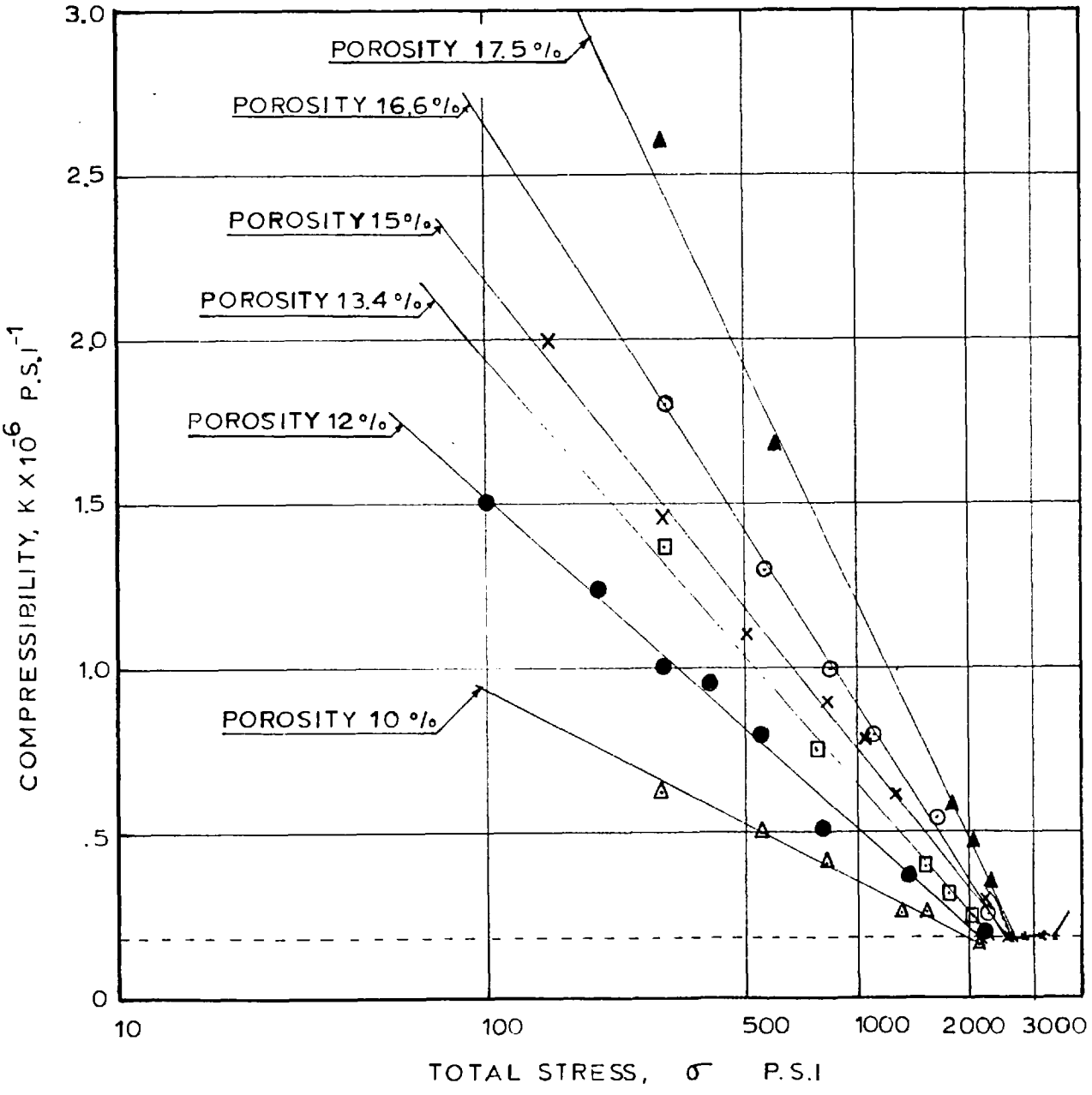
DRY TEST

FIG. 4.24



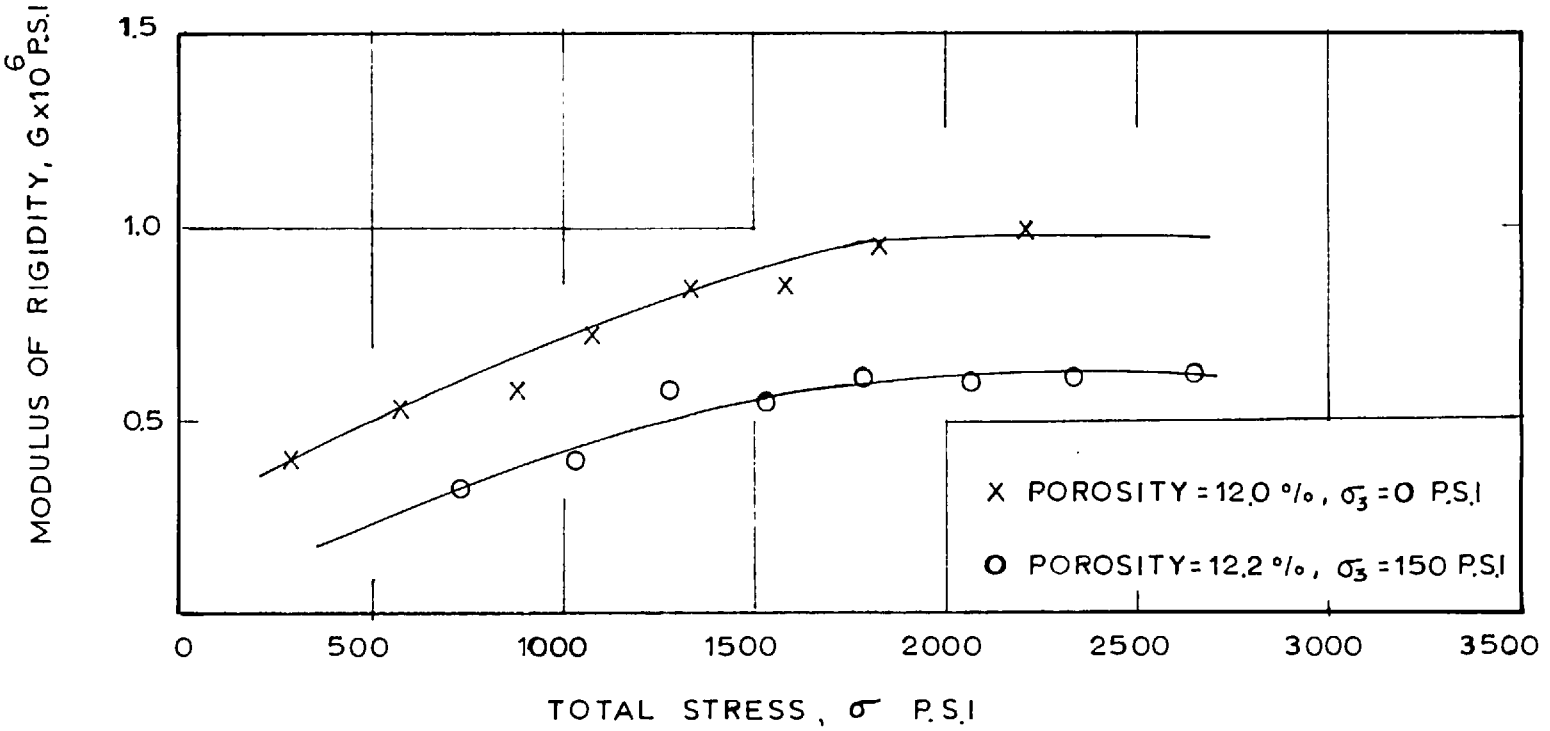
DRY TEST

FIG. 4.25



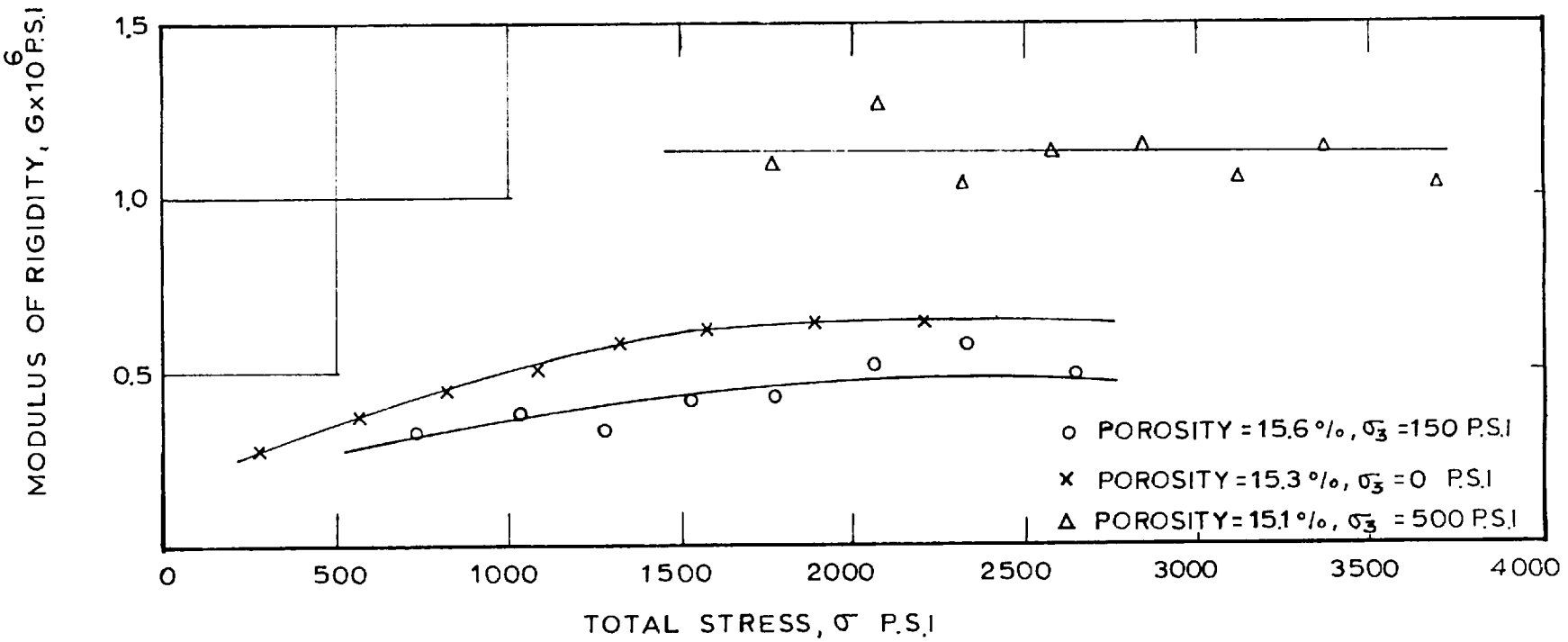
DRY TEST

FIG.4.26



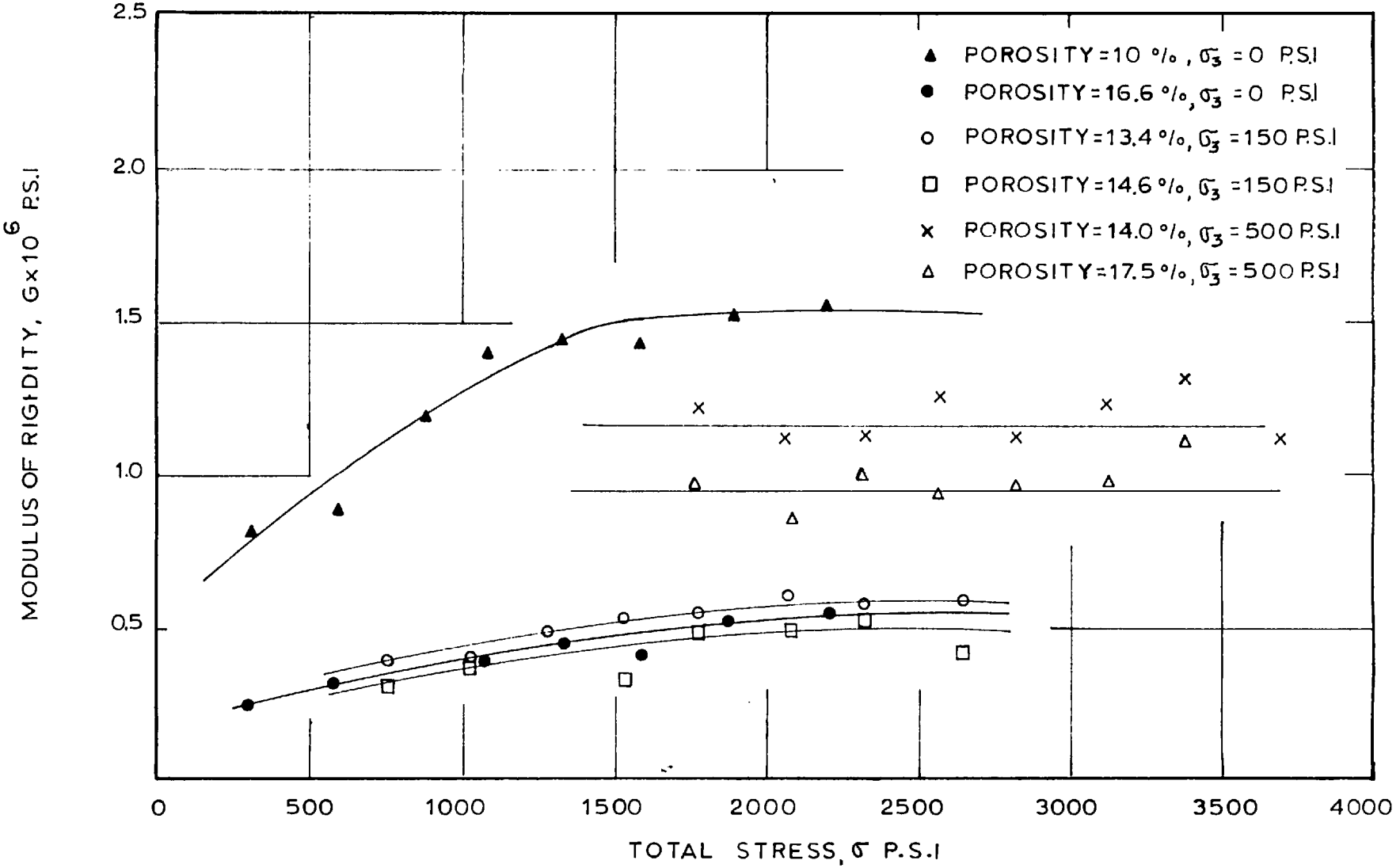
DRY TEST

FIG.4.27



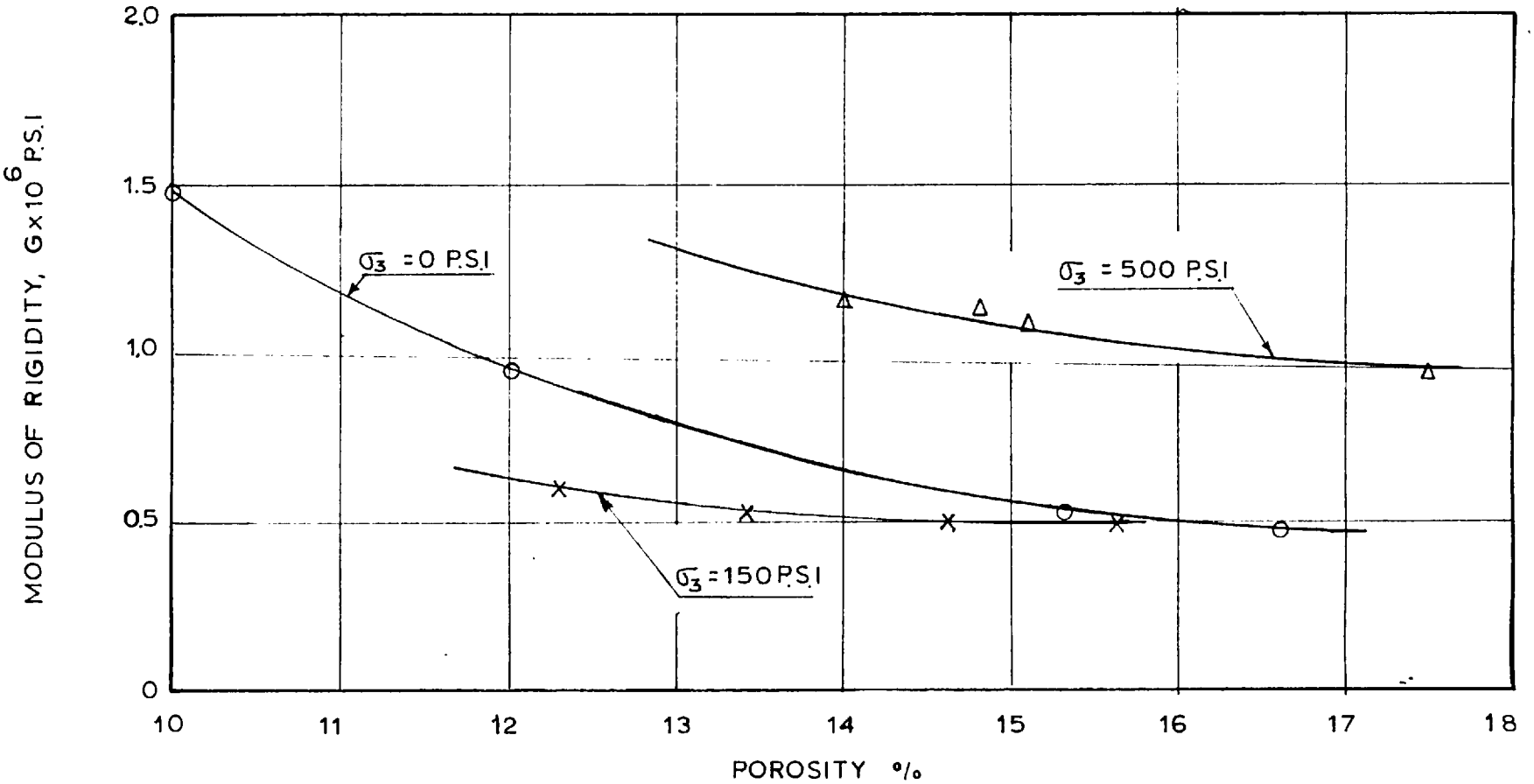
DRY TEST

FIG. 4.28



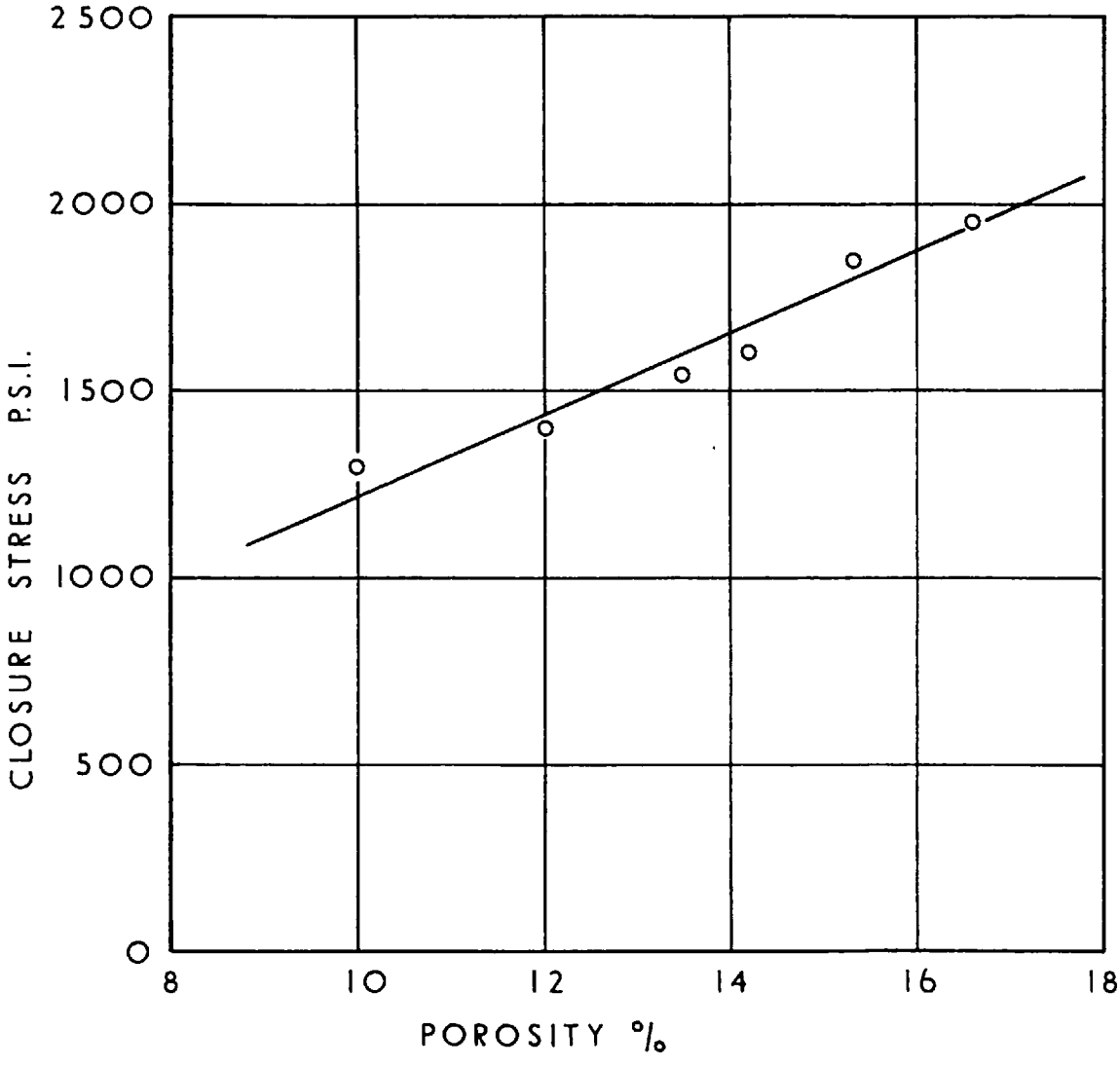
DRY TEST

FIG.4.29



DRY TEST

FIG. 4.30



VARIATION OF CLOSURE STRESS WITH POROSITY

FIG. 4.31

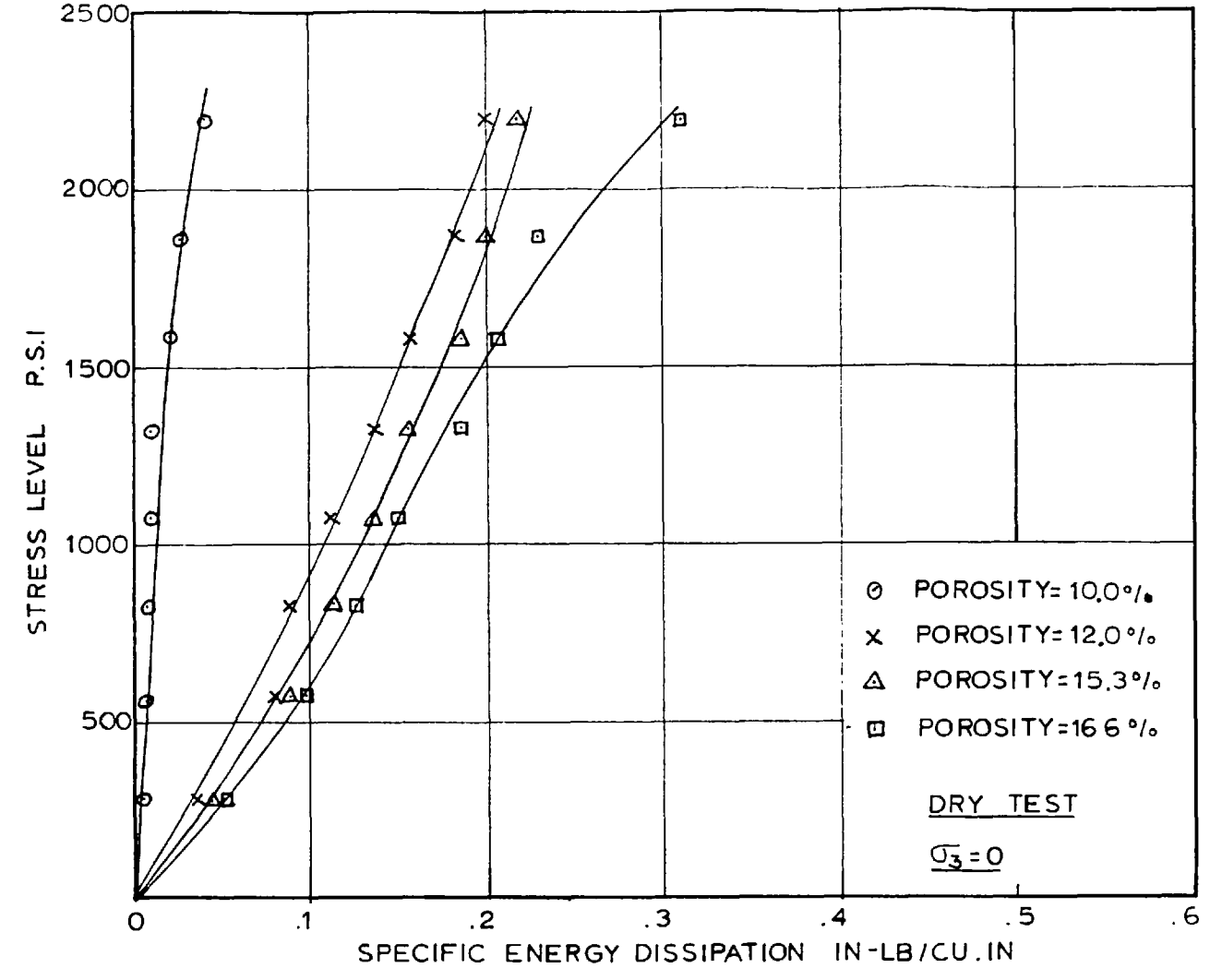


FIG.4.32(a)

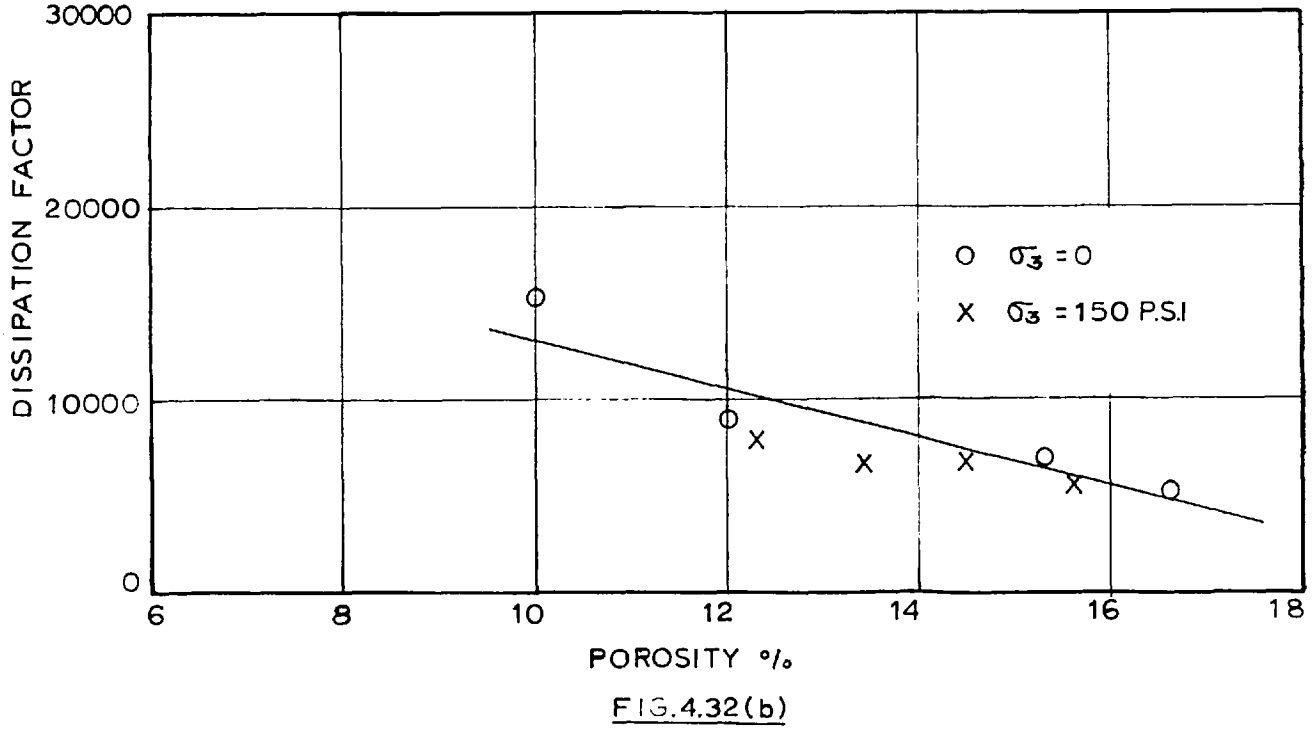
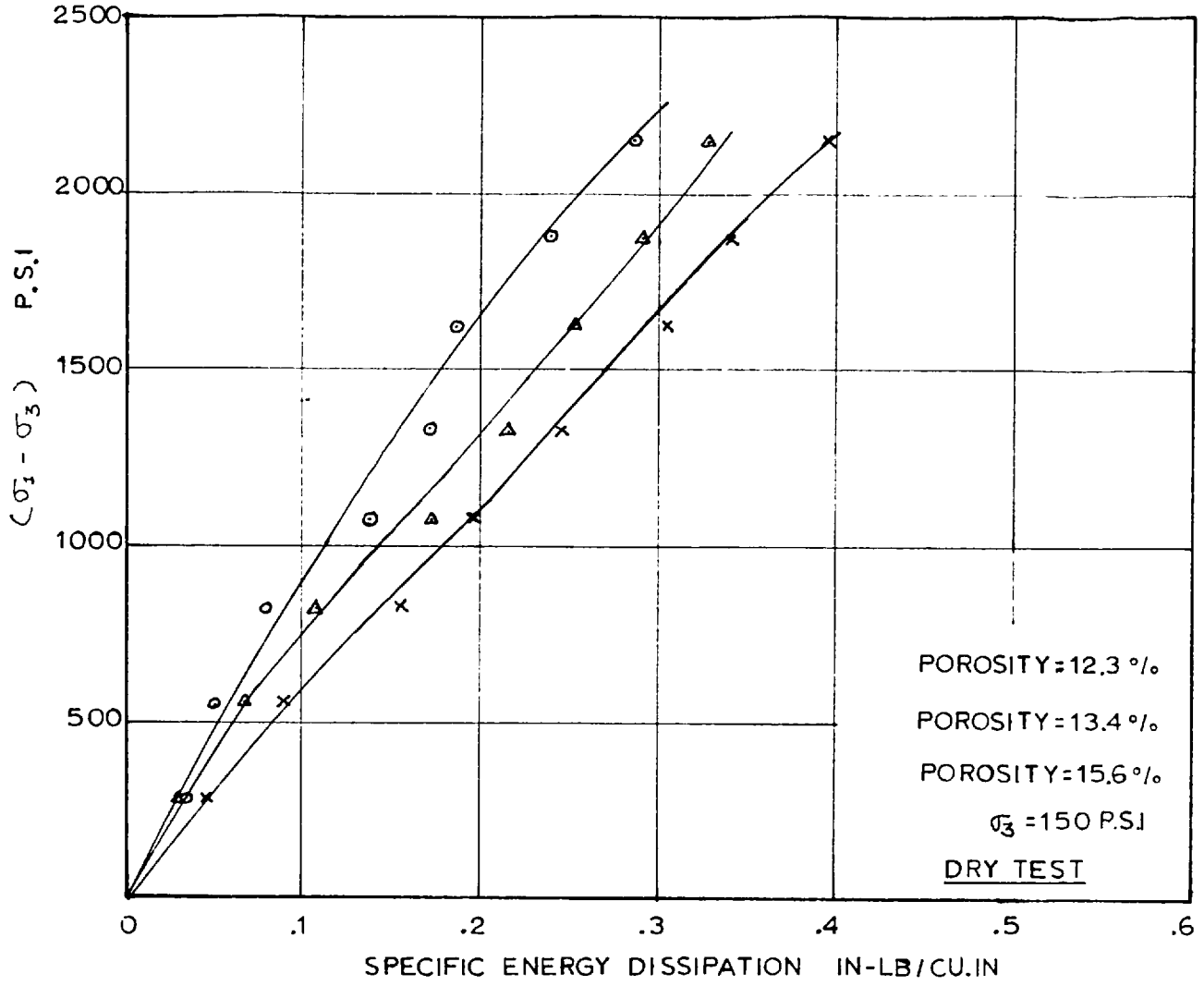


FIG.4.32(b)


2500
2000
1500
1000
500
(σ1 - σ3) P.S.I
0
.1
.2
.3
.4
.5
.6
SPECIFIC ENERGY DISSIPATION IN-LB/CU.IN
POROSITY = 12.3 %
POROSITY = 13.4 %
POROSITY = 15.6 %
σ3 = 150 P.S.I
DRY TEST

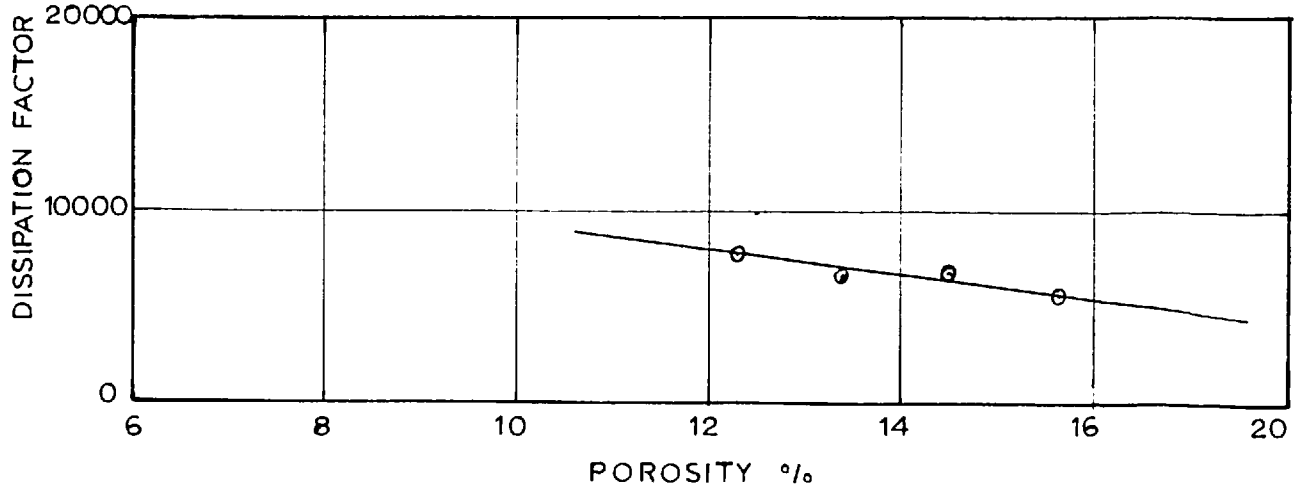

20000
10000
0
DISSIPATION FACTOR
6
8
10
12
14
16
20
POROSITY %

FIG. 4.33

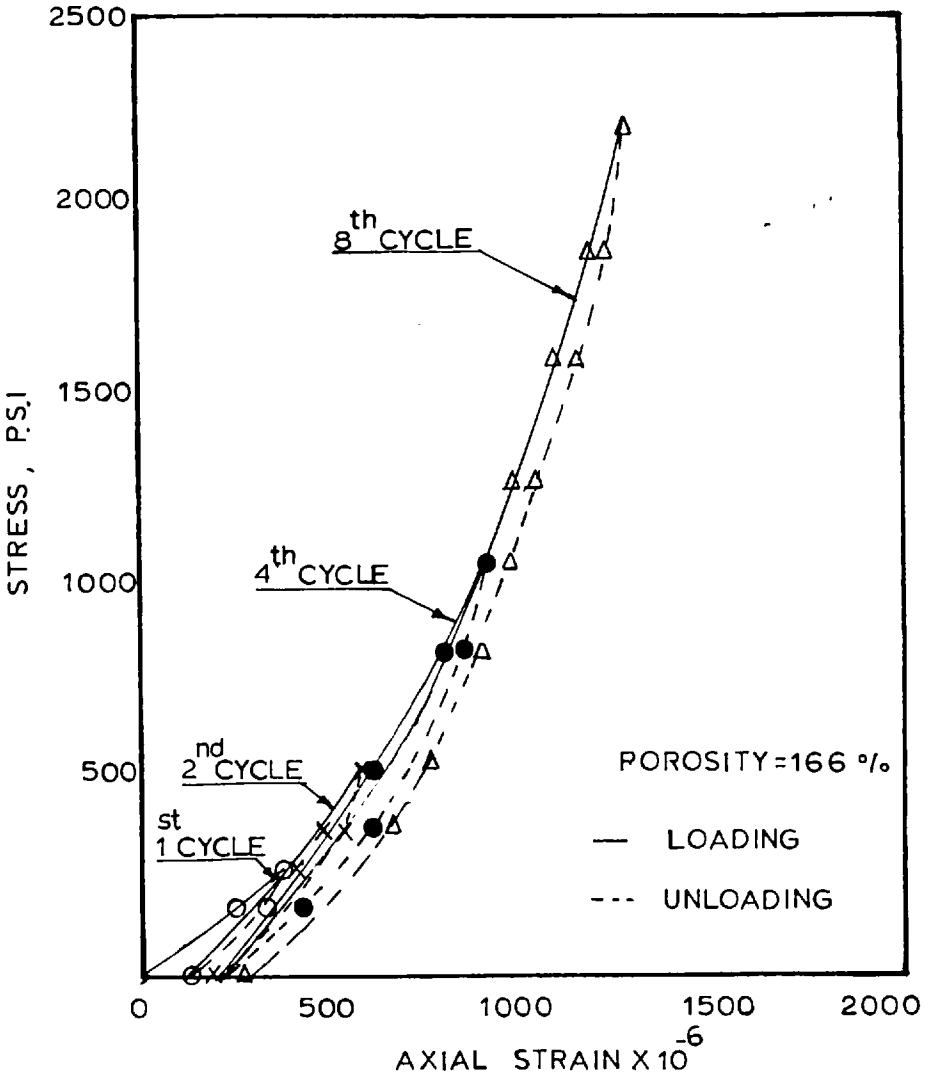
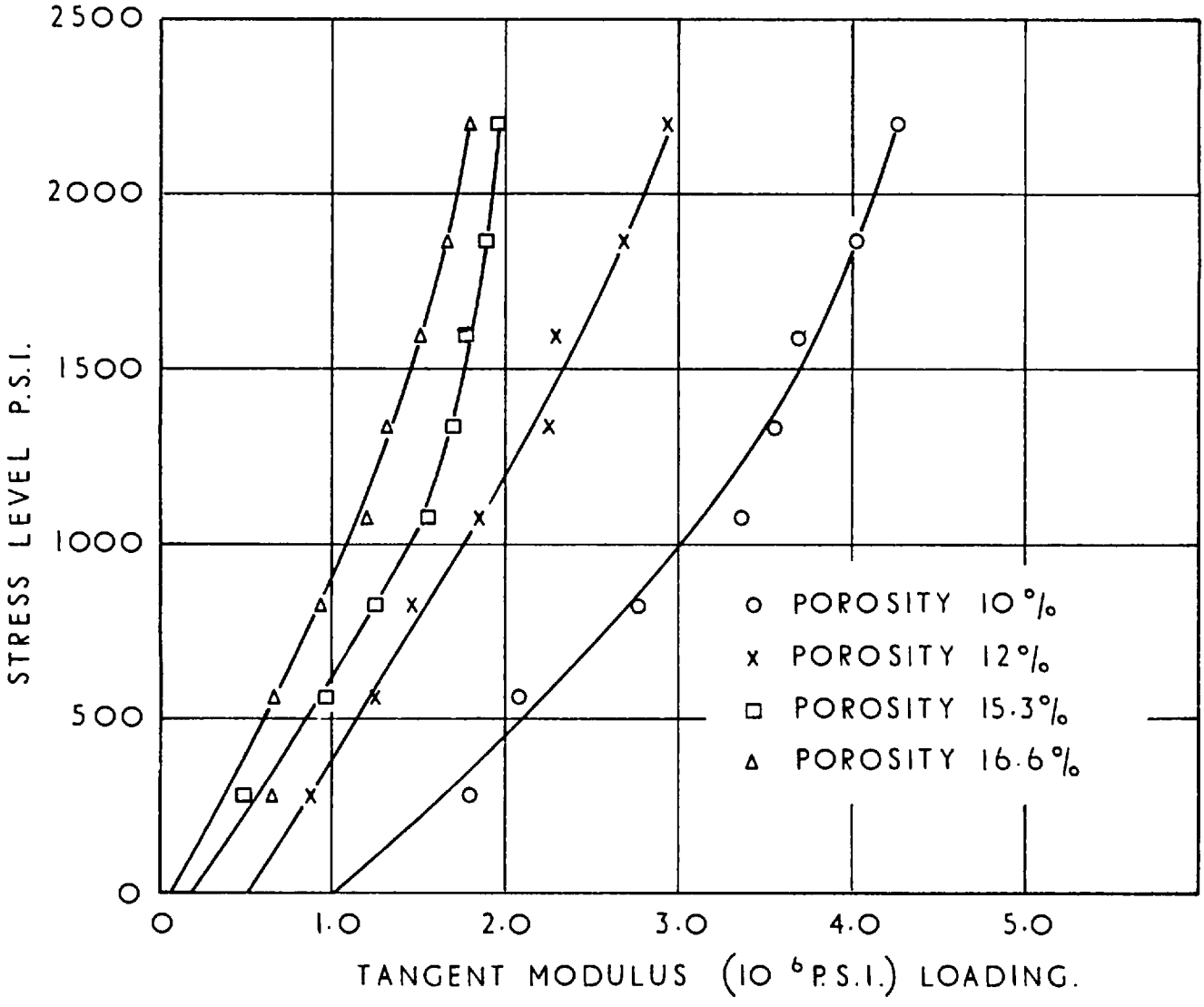
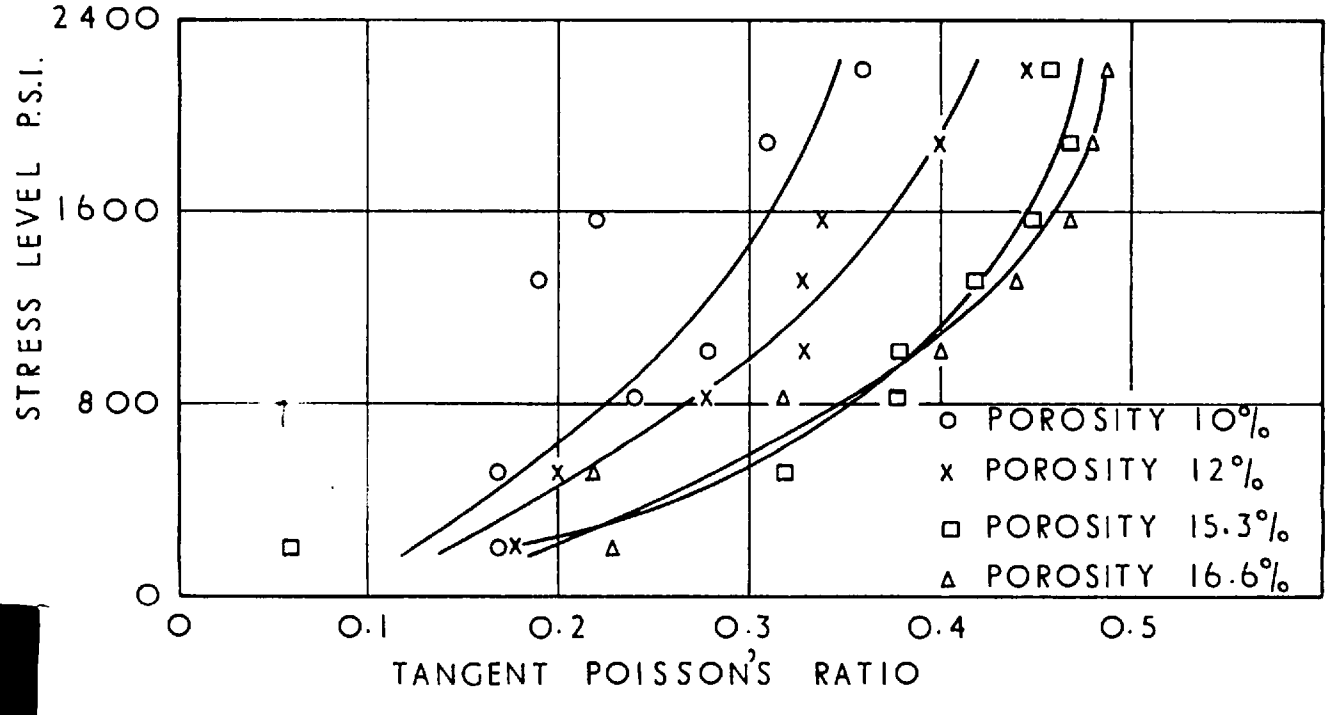


FIG. 4.34 RETESTING OF DRY SPECIMEN

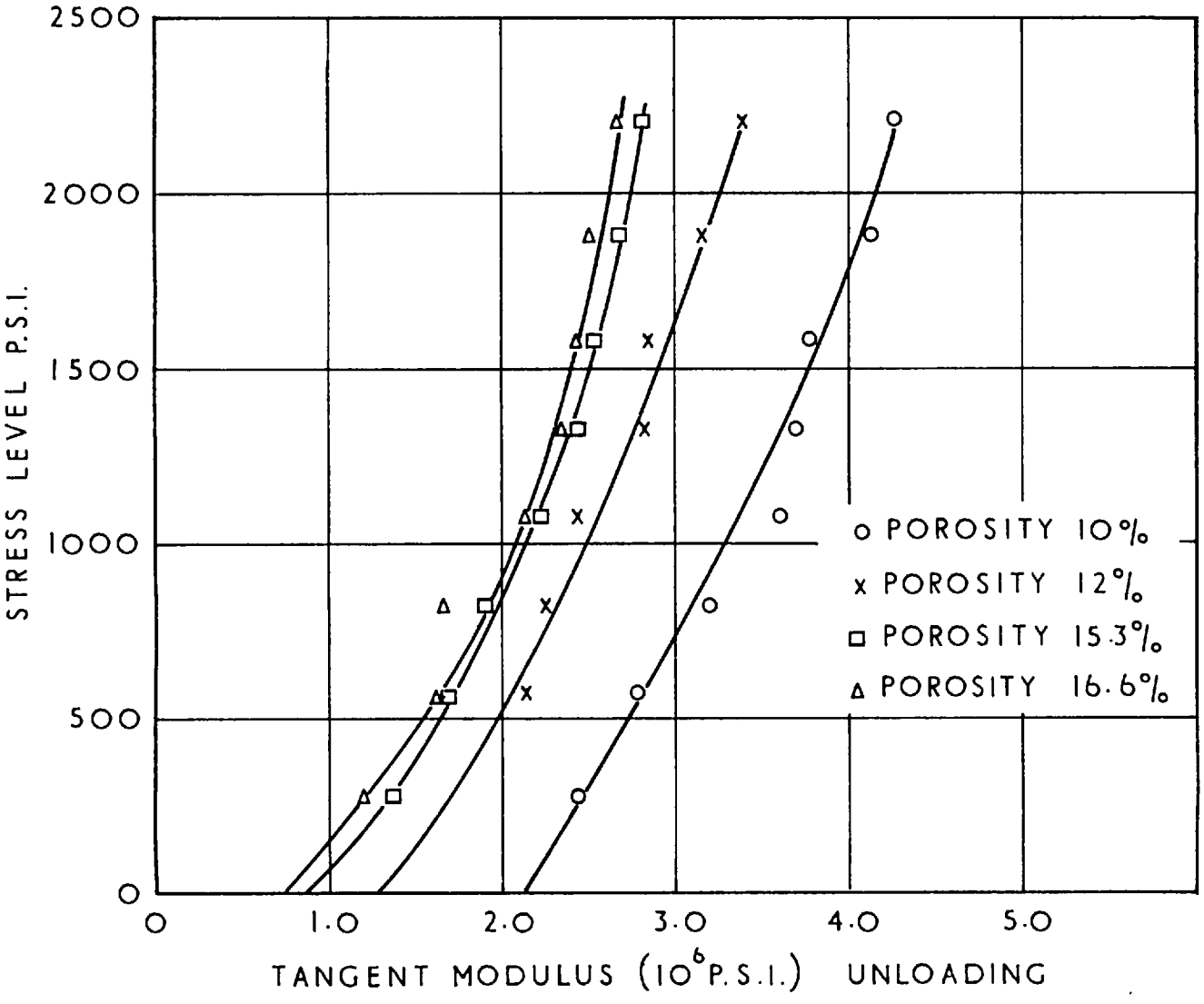
(UNIAXIAL COMPRESSION TEST)

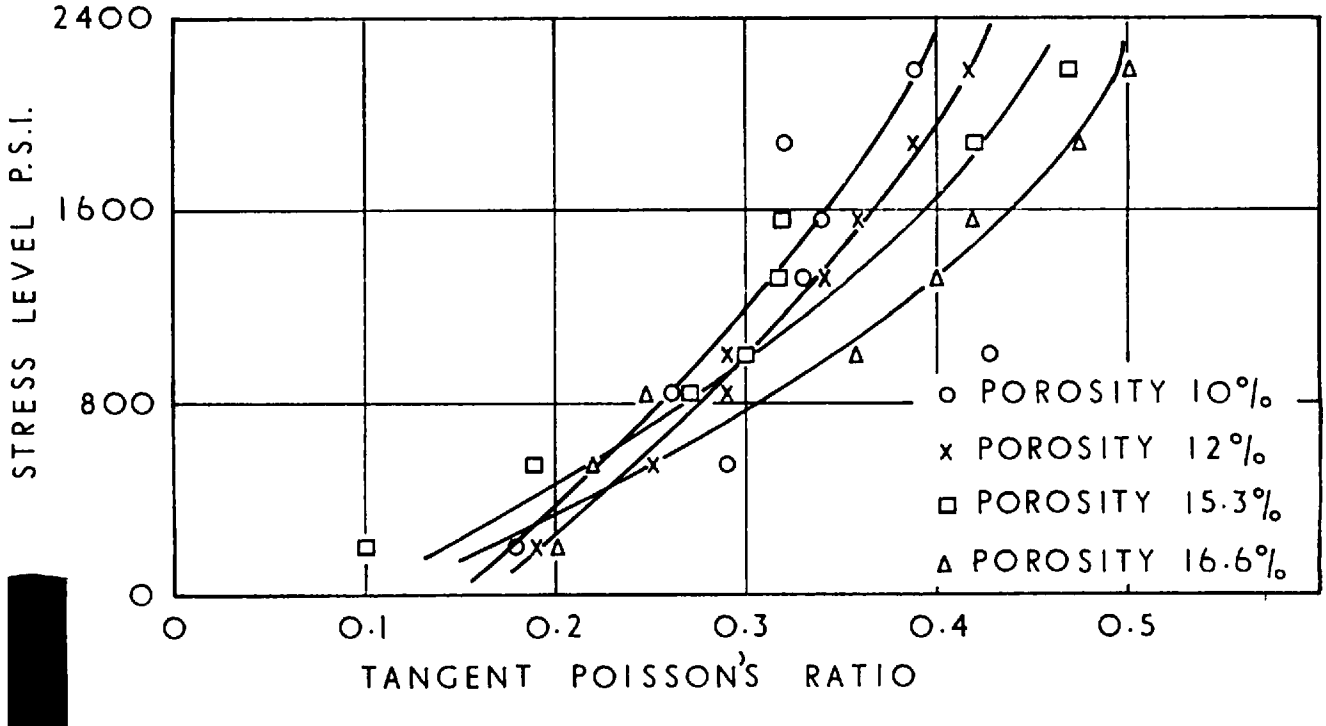




VARIATION OF TANGENT PARAMETER ON LOADING.

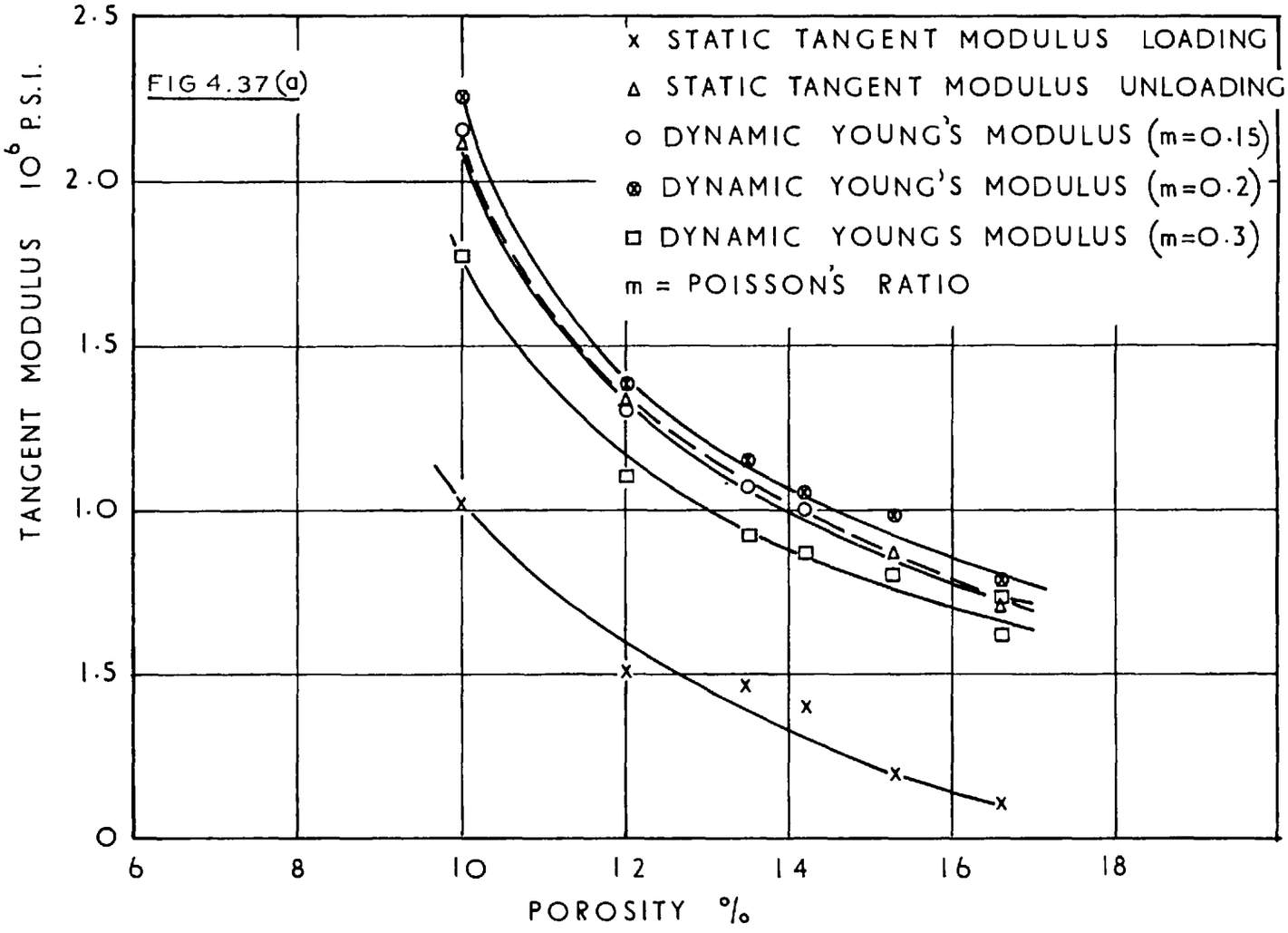
FIG.4.35

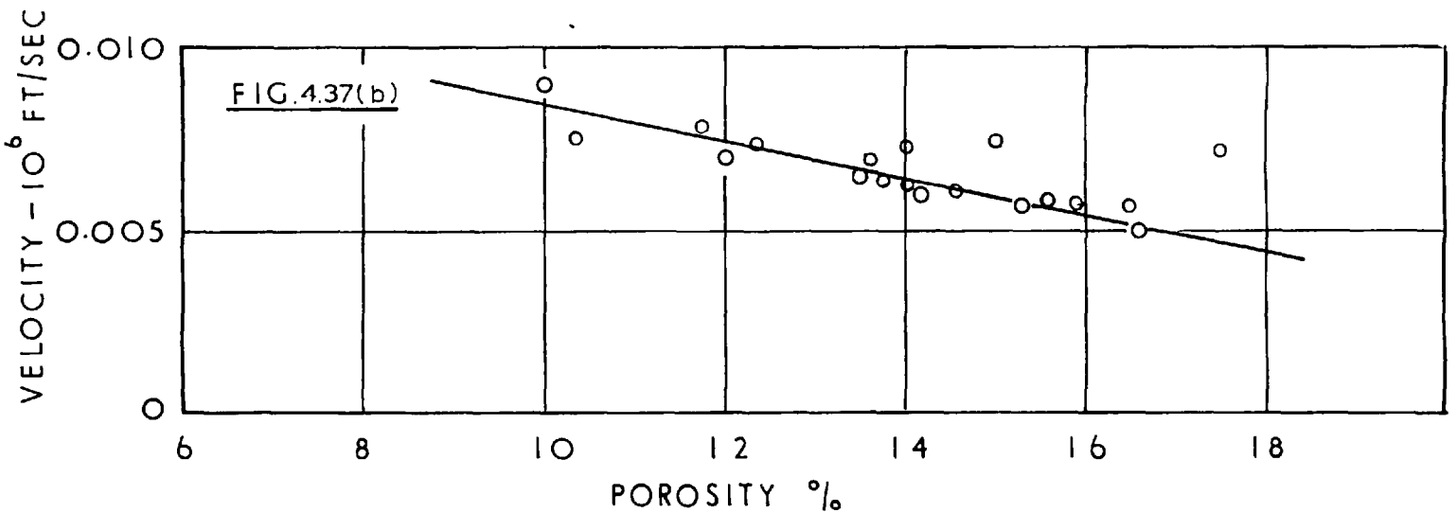




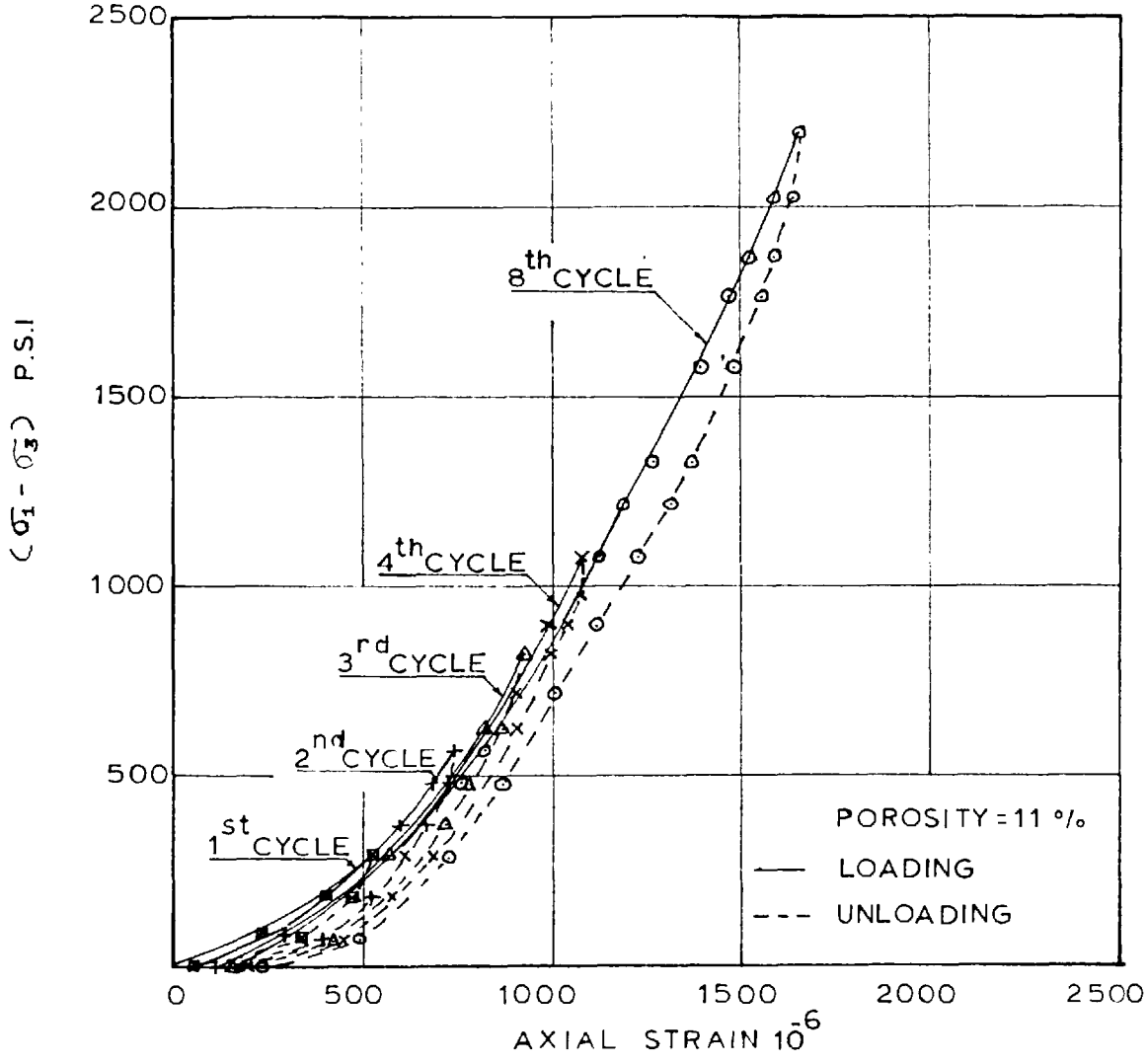
VARIATION OF TANGENT PARAMETERS ON UNLOADING

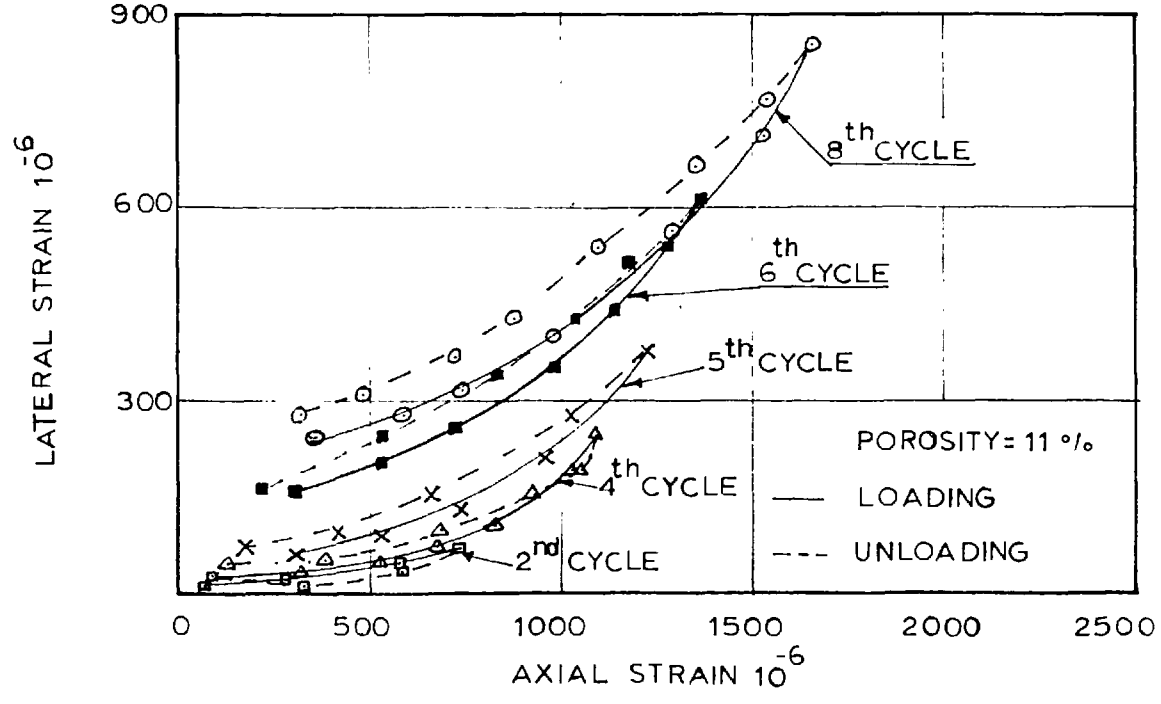
FIG. 4.36





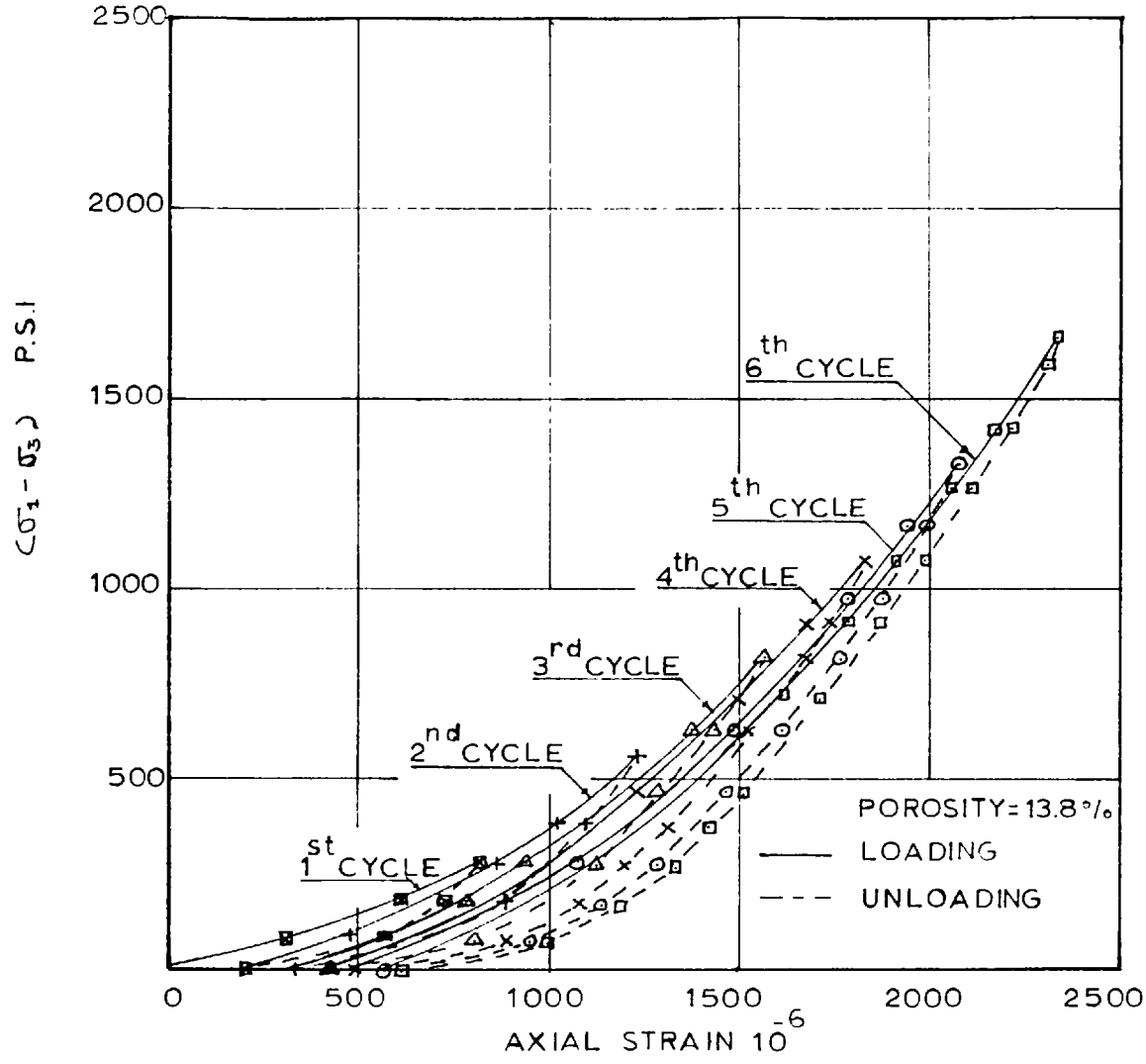
COMPARISON BETWEEN STATIC & DYNAMIC MODULI.

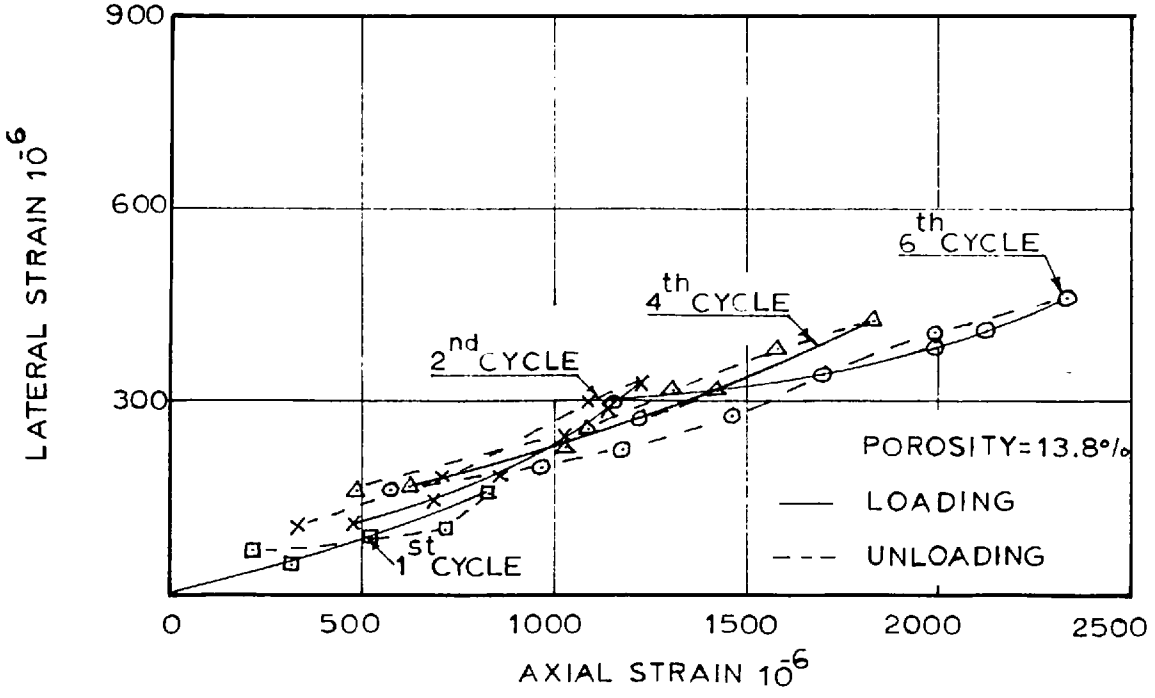




WET TEST $\sigma_3 = 0$

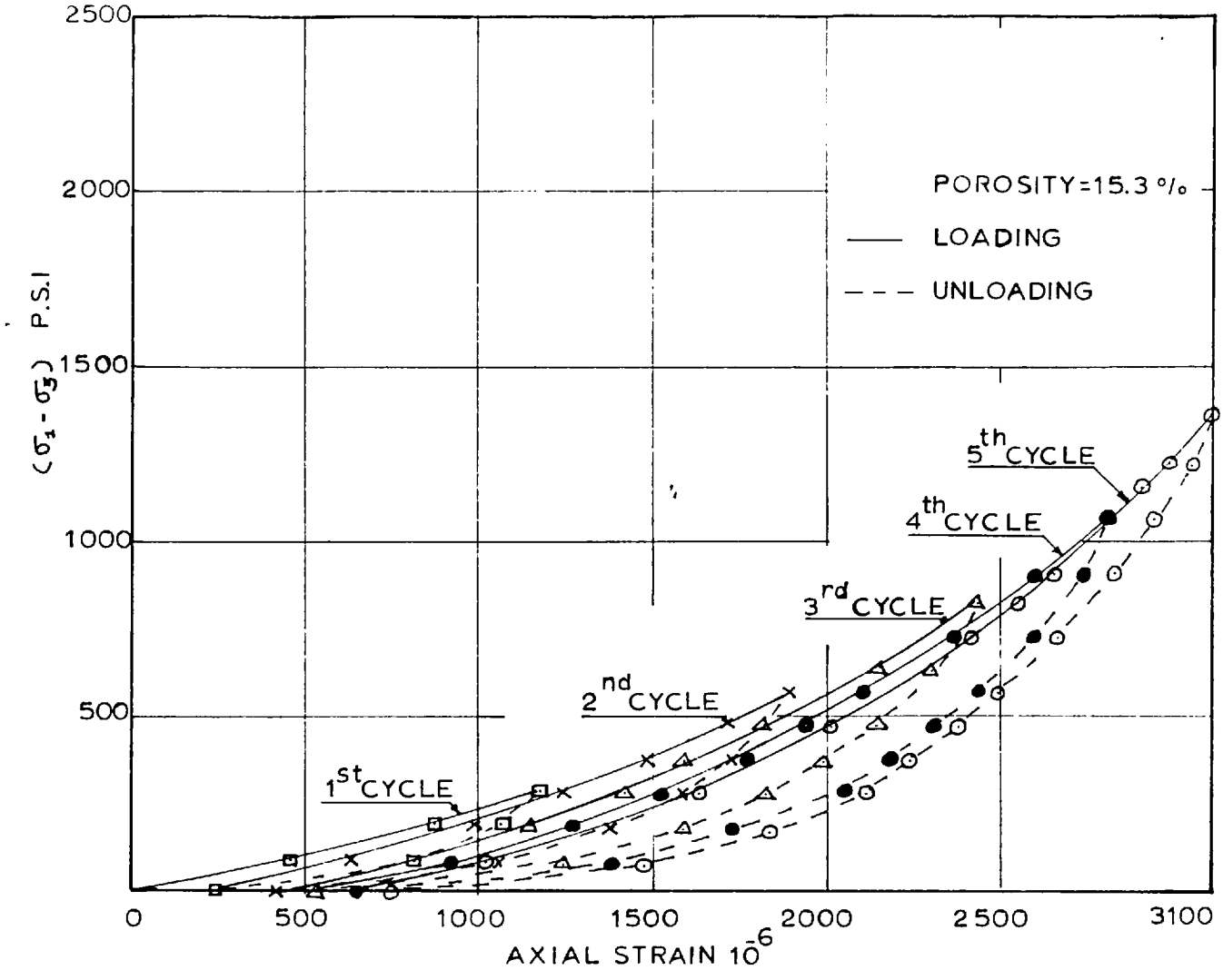
FIG. 4.38

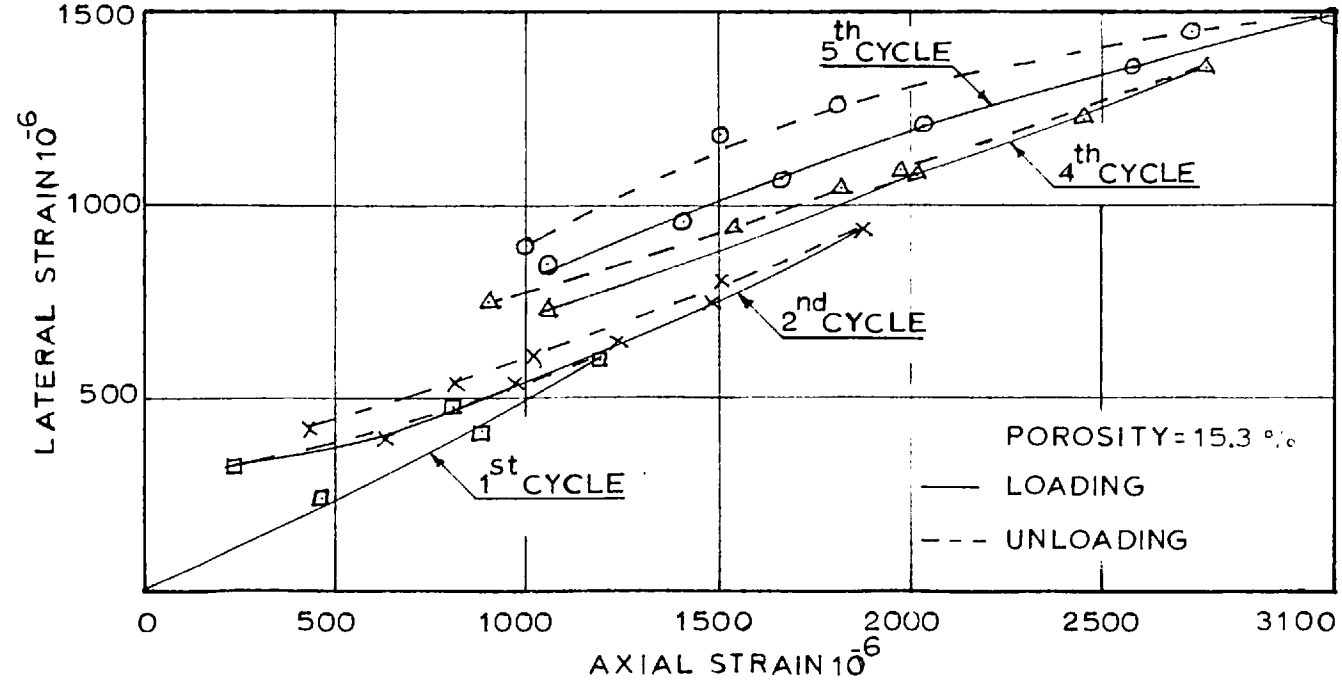




WET TEST $\sigma_3 = 0$

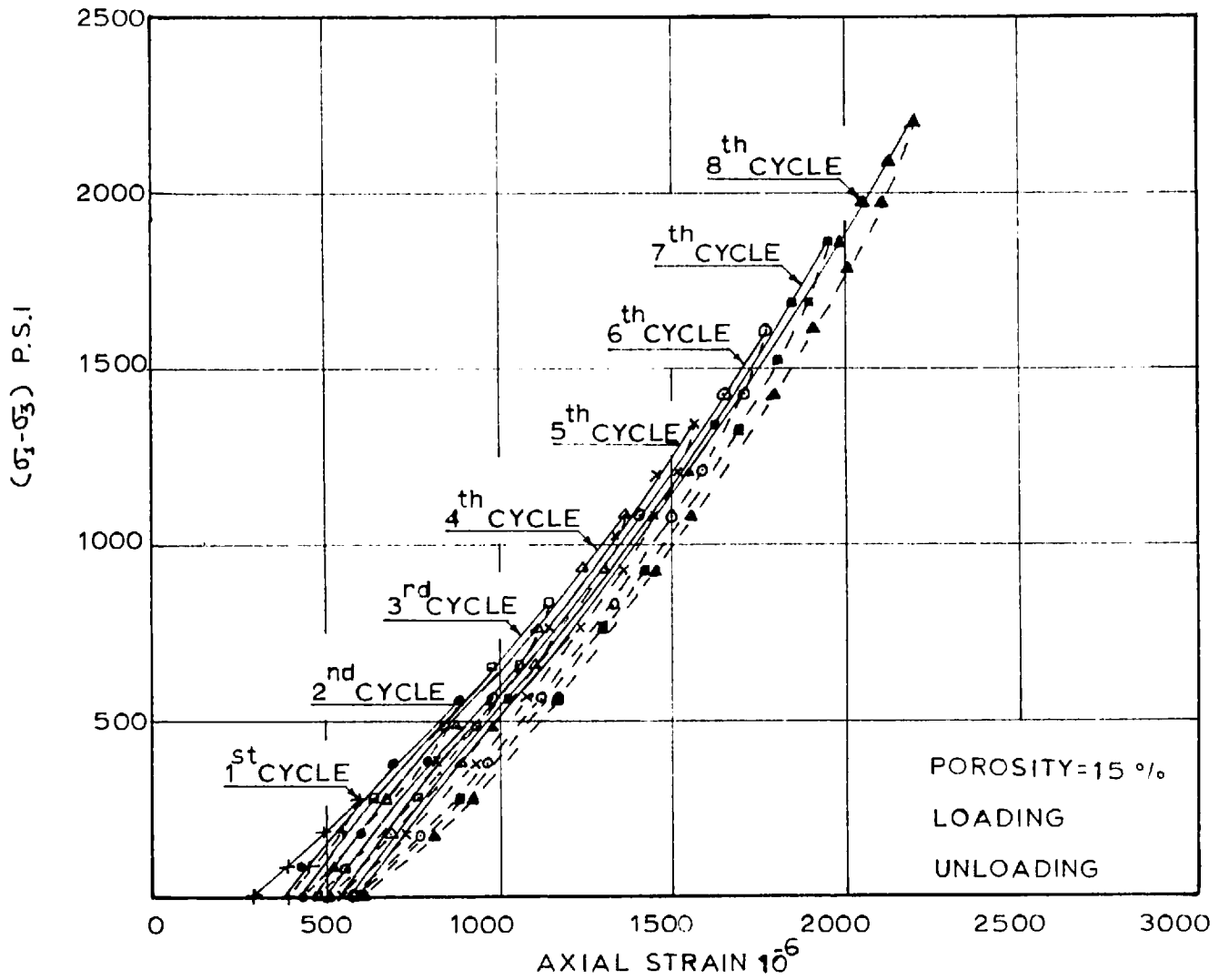
FIG.4.39

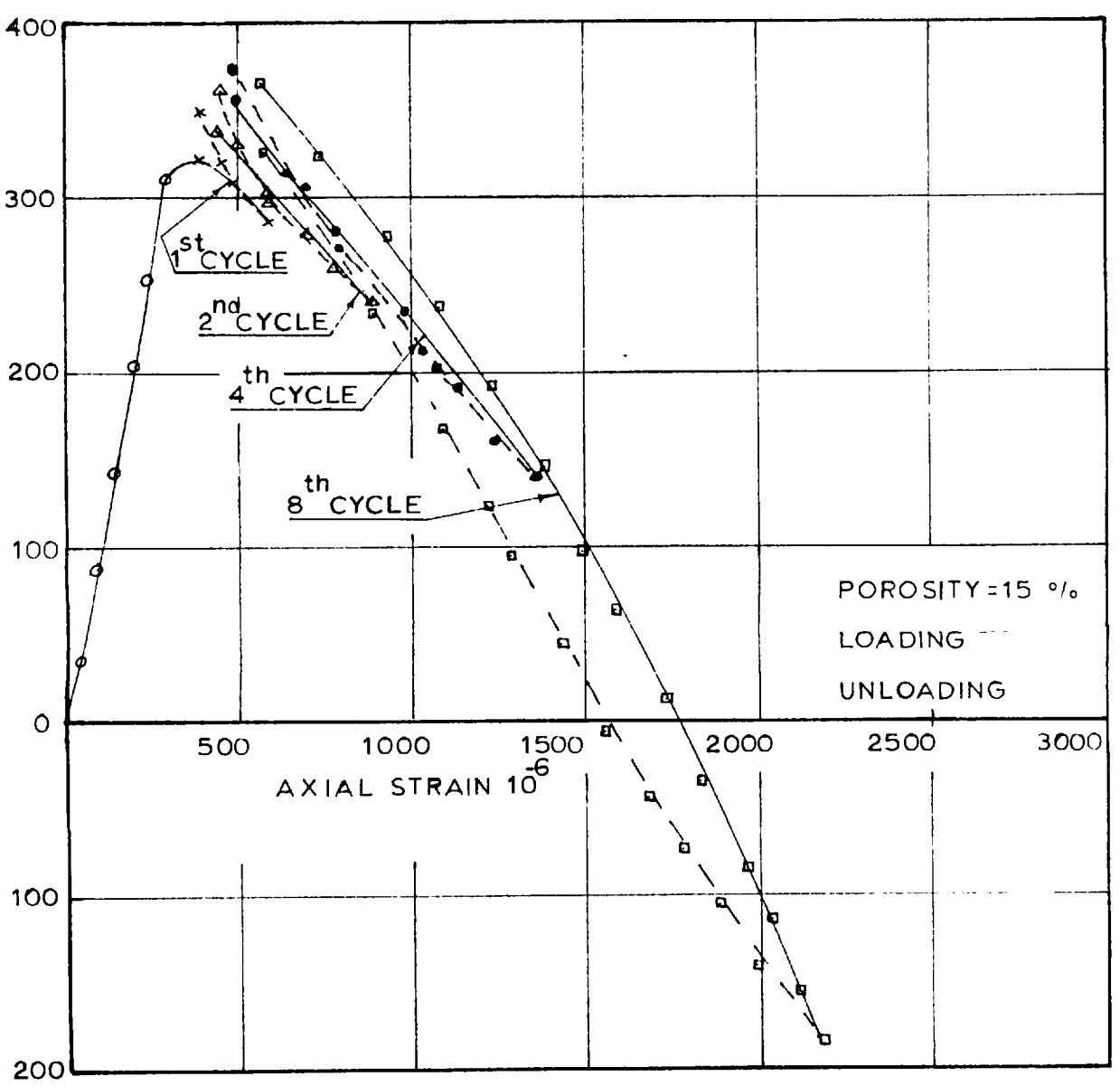


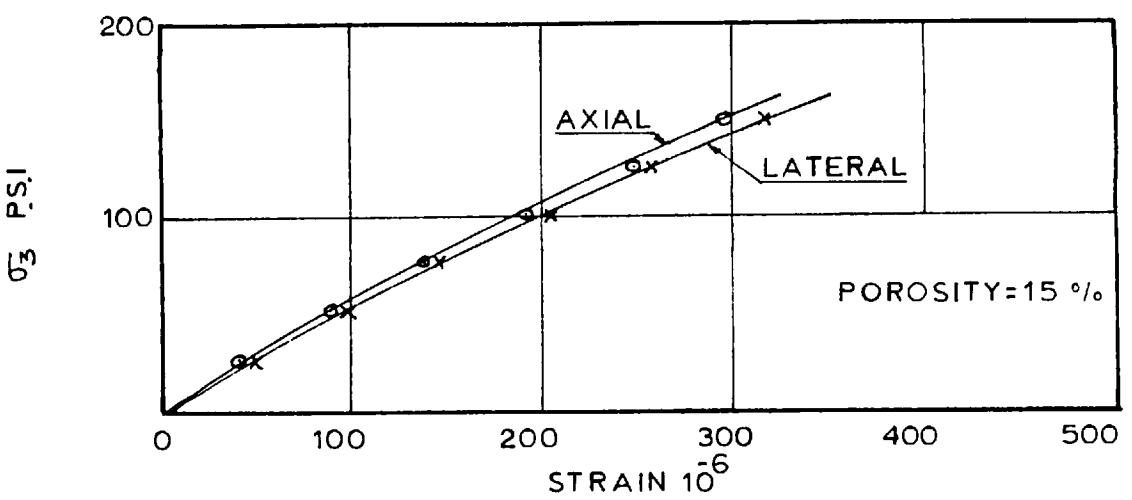


WET TEST $\sigma_3 = 0$

FIG.4.40



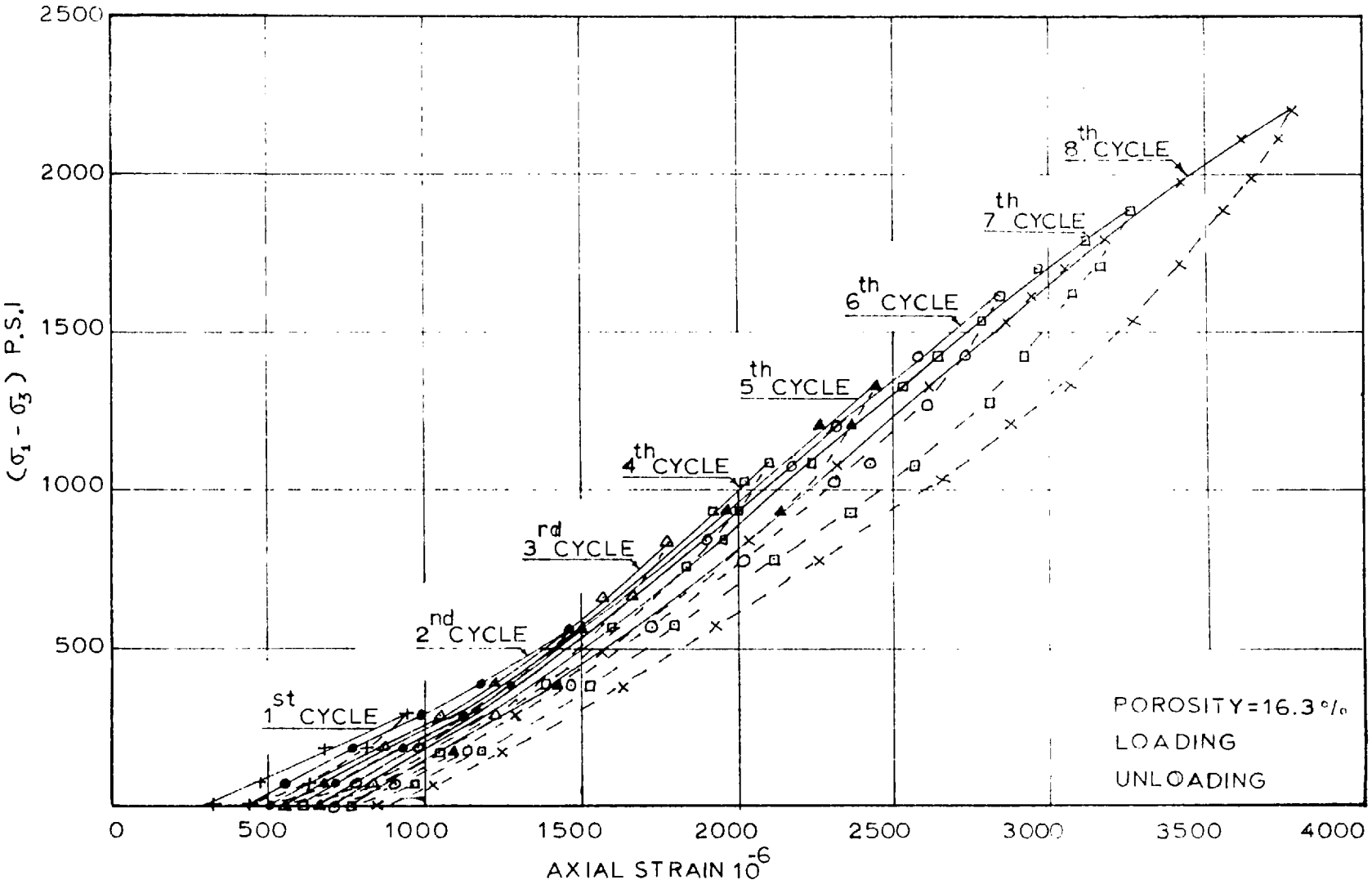


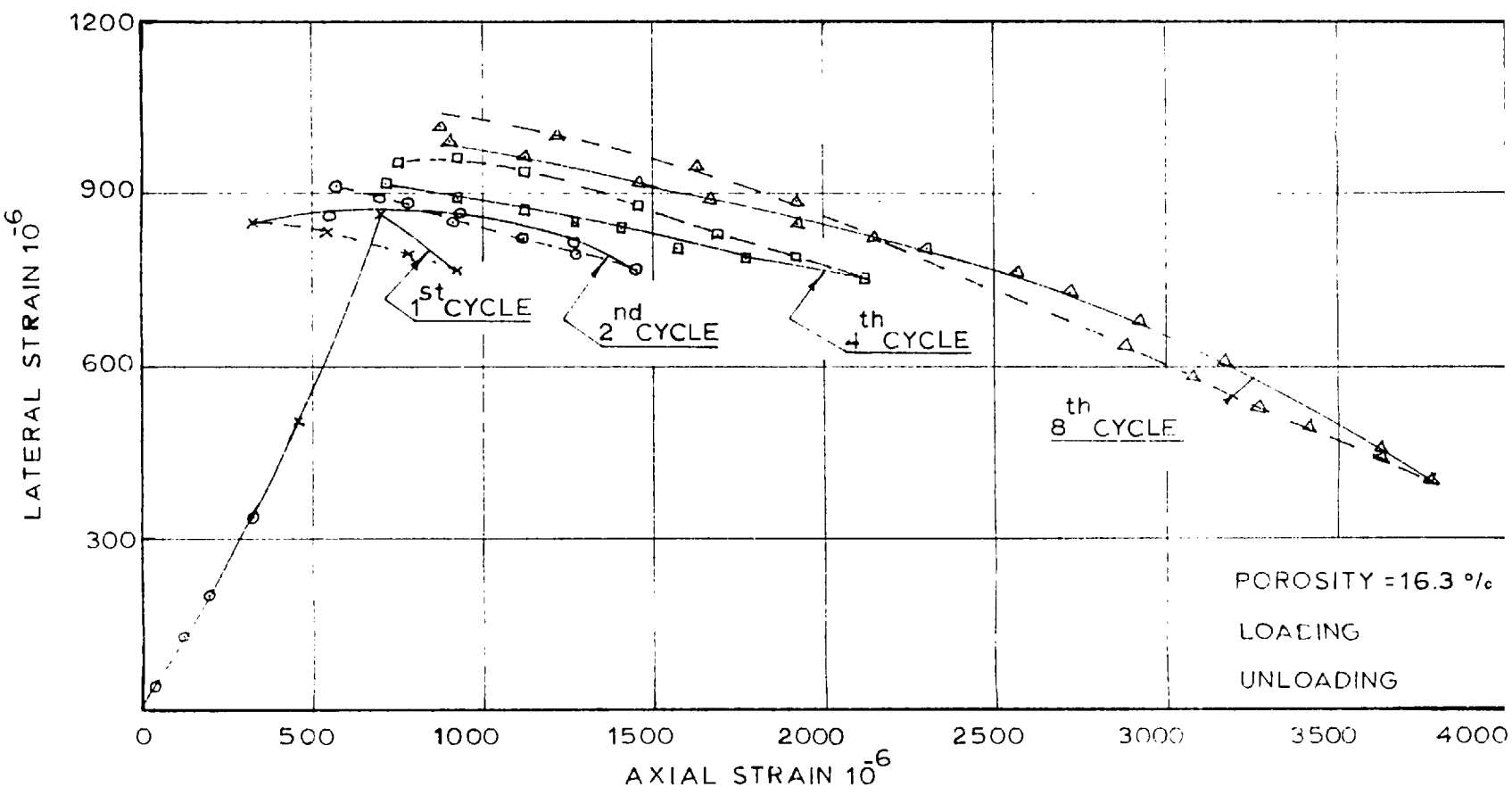


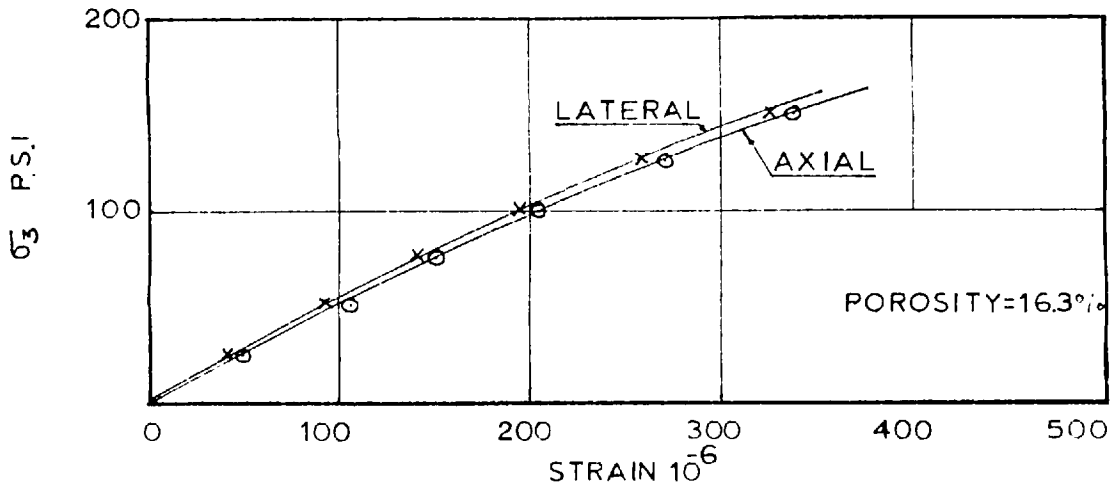
WET TEST

σ_3 = 150 P.S.I

FIG. 4.41



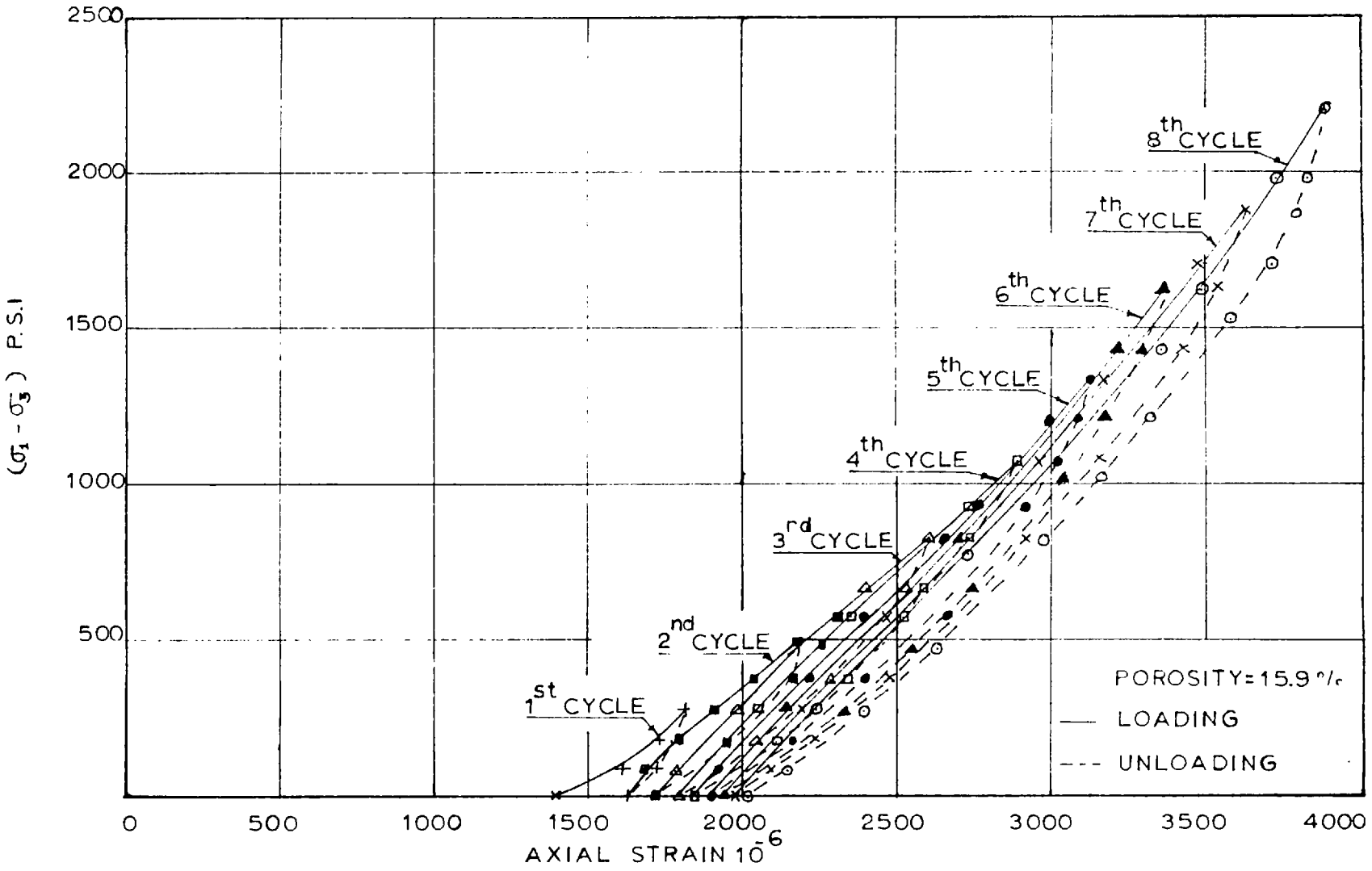


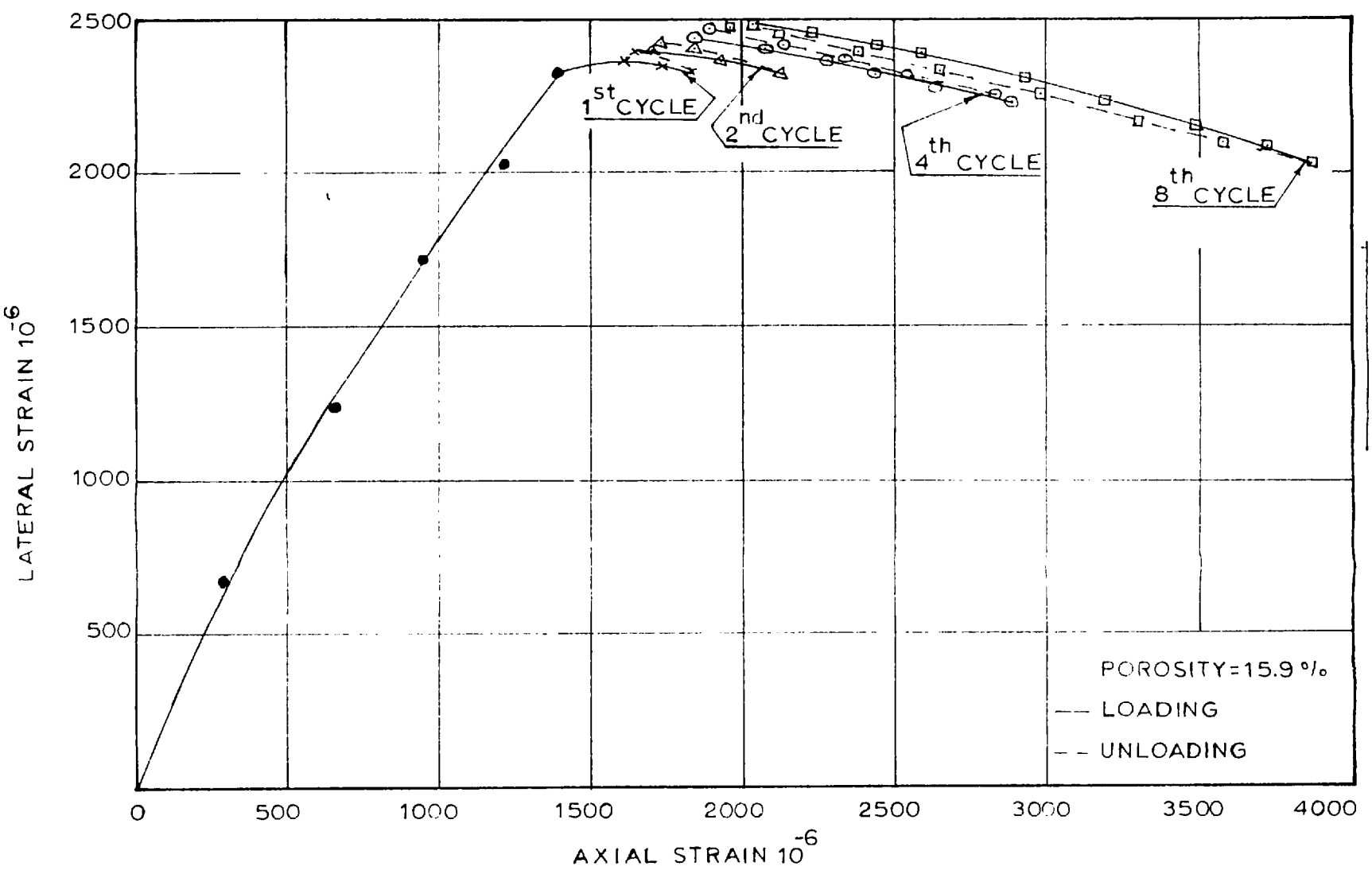


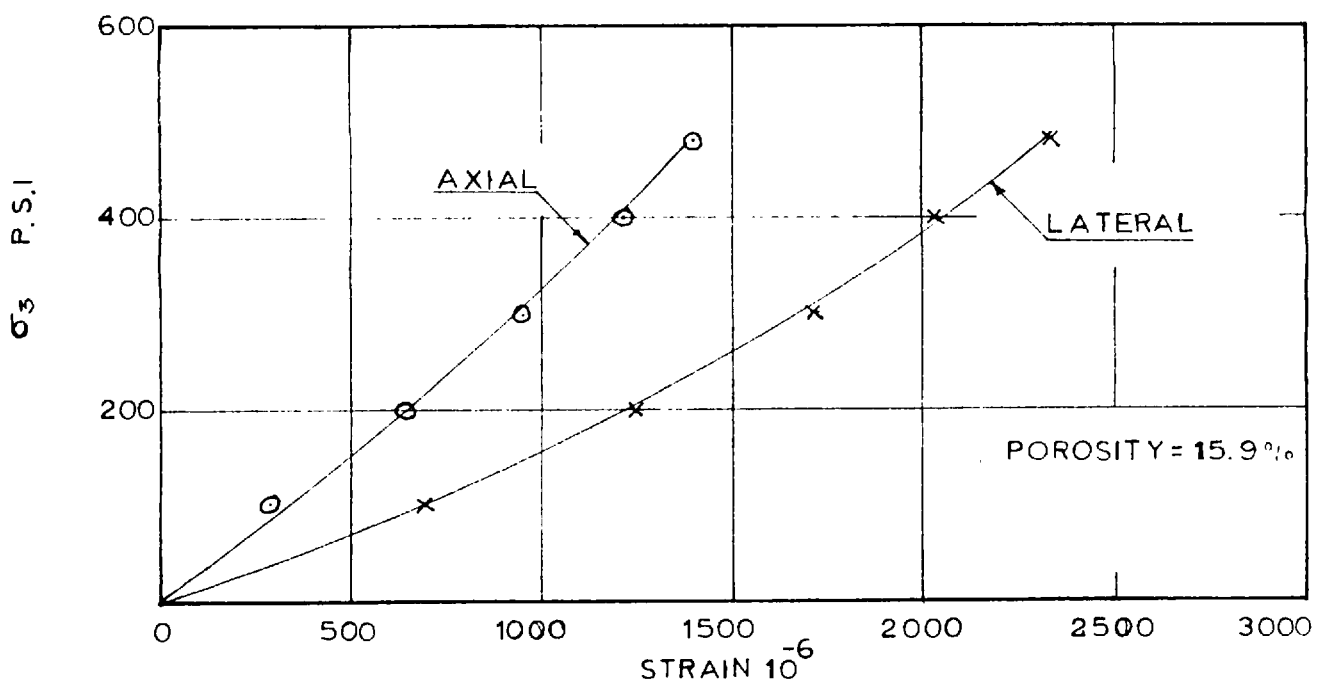
WET TEST

σ_3 = 150 P.S.I

FIG. 4.42







WET TEST

σ_3=500 P.S.I

FIG.4.43

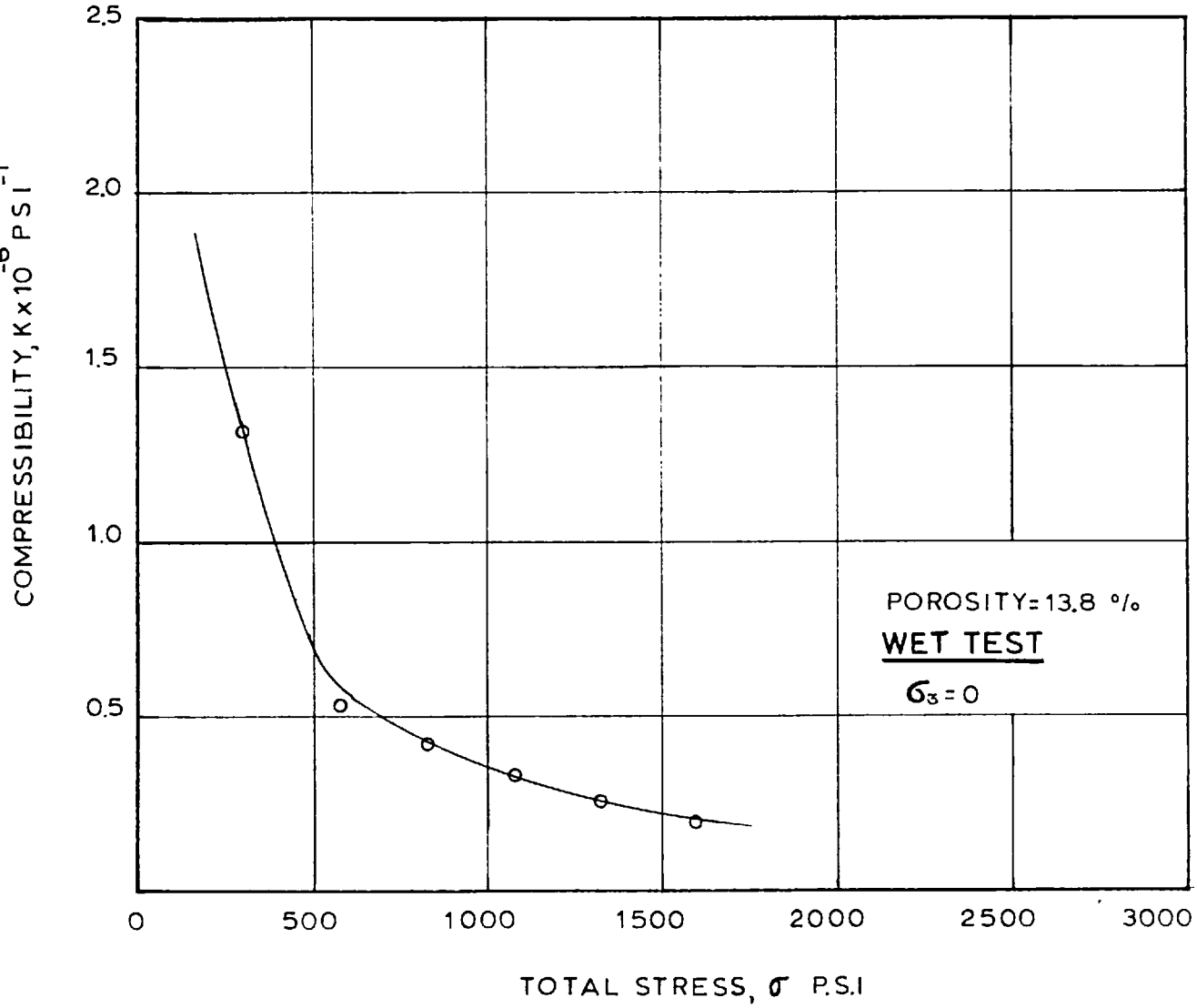

COMPRESSIBILITY, K x 10^-6 PSI^-1
2.5
2.0
1.5
1.0
0.5
0
500
1000
1500
2000
2500
3000
TOTAL STRESS, σ P.S.I
POROSITY = 13.8 %
WET TEST
σ3 = 0

FIG. 4.44

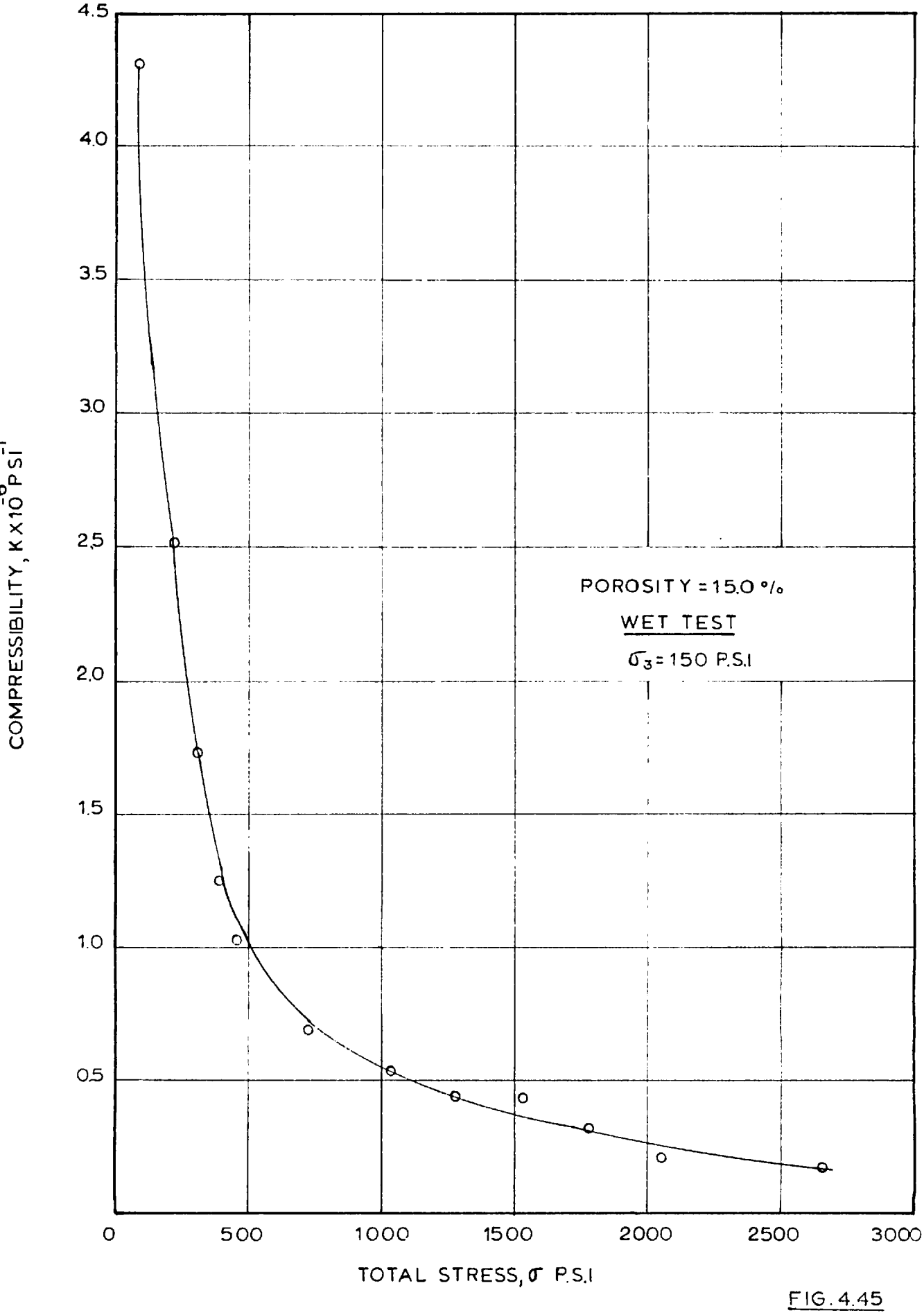
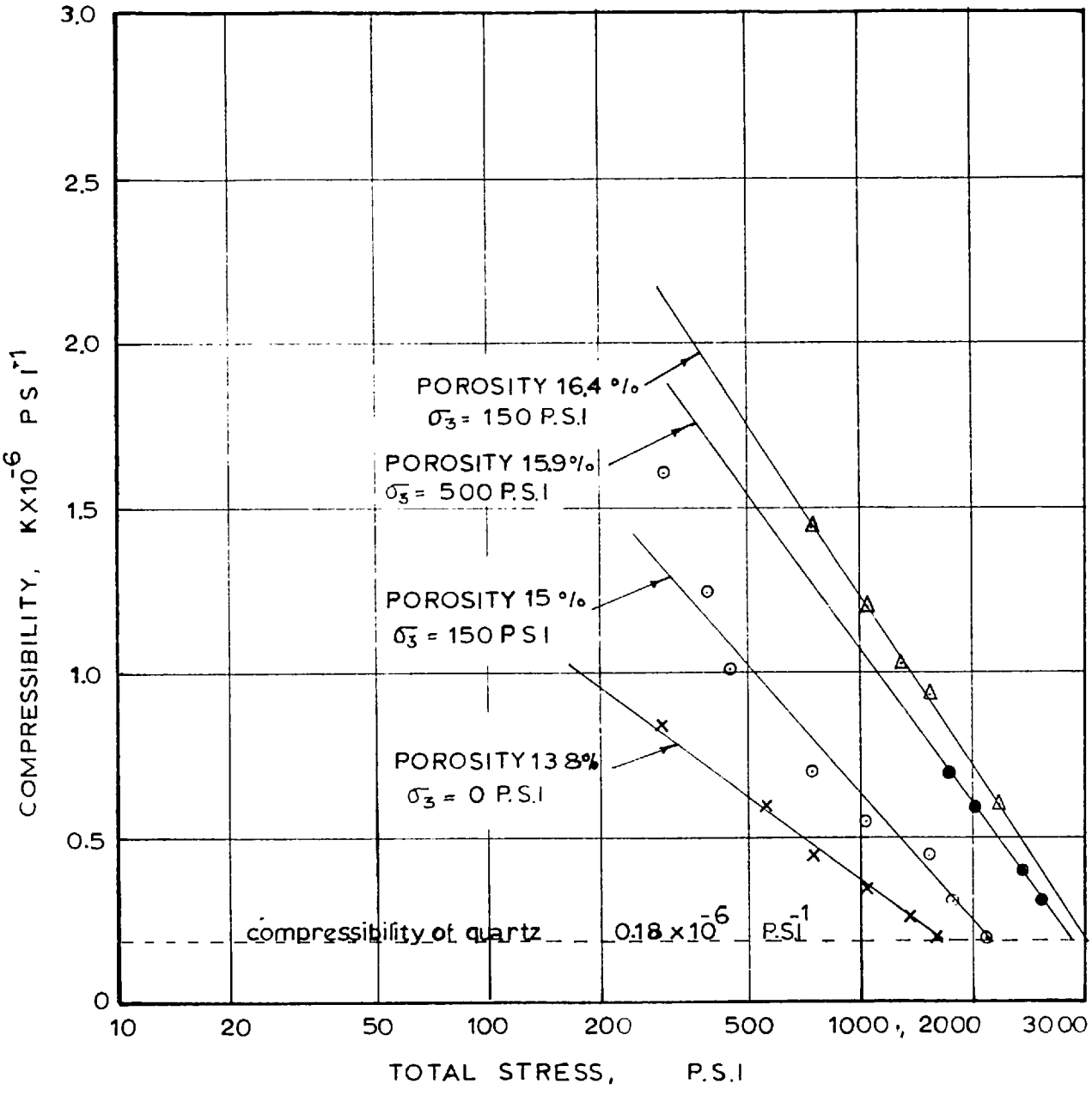
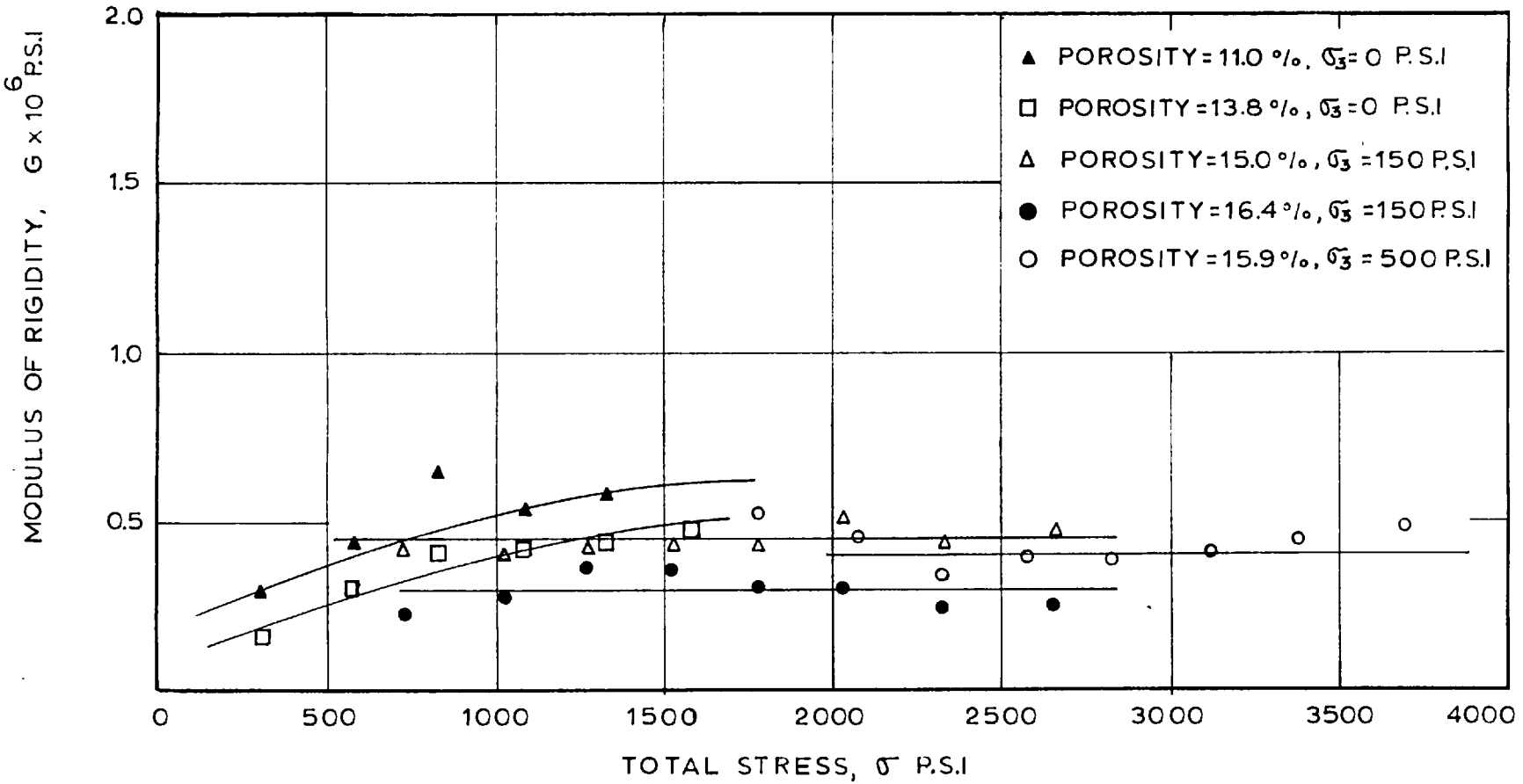

4.5
4.0
3.5
3.0
2.5
2.0
1.5
1.0
0.5
0
500
1000
1500
2000
2500
3000
COMPRESSIBILITY, K X10 $^{-6}$ PSI $^{-1}$
TOTAL STRESS, σ P.S.I
POROSITY = 15.0 %
WET TEST
σ_3 = 150 P.S.I

FIG. 4.45



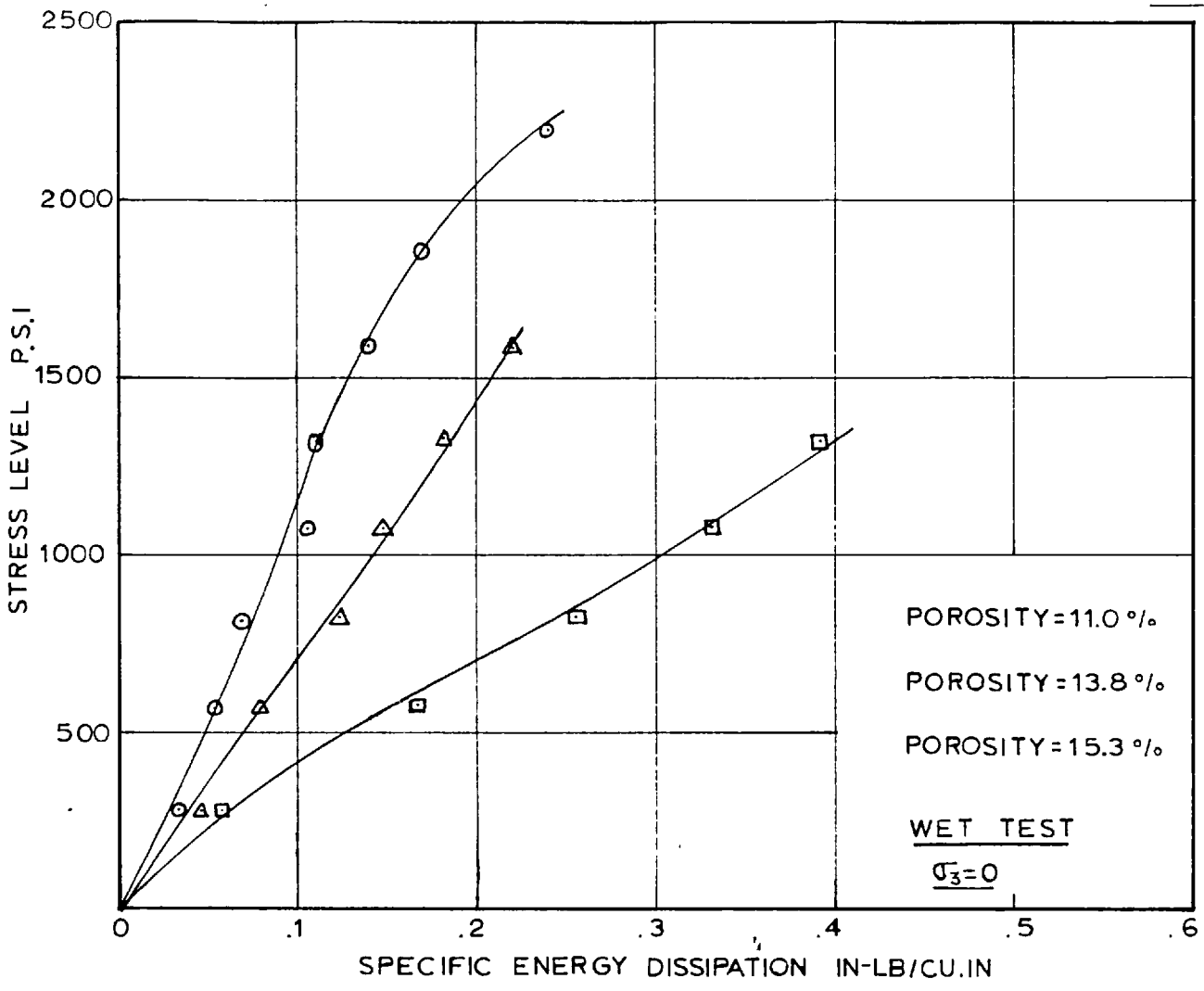
WET TEST

FIG. 4.46



WET TEST

FIG. 4.47


2500
2000
1500
1000
500
STRESS LEVEL P.S.I
0
.1
.2
.3
.4
.5
.6
SPECIFIC ENERGY DISSIPATION IN-LB/CU.IN
POROSITY = 11.0 %
POROSITY = 13.8 %
POROSITY = 15.3 %
WET TEST
$\sigma_3 = 0$

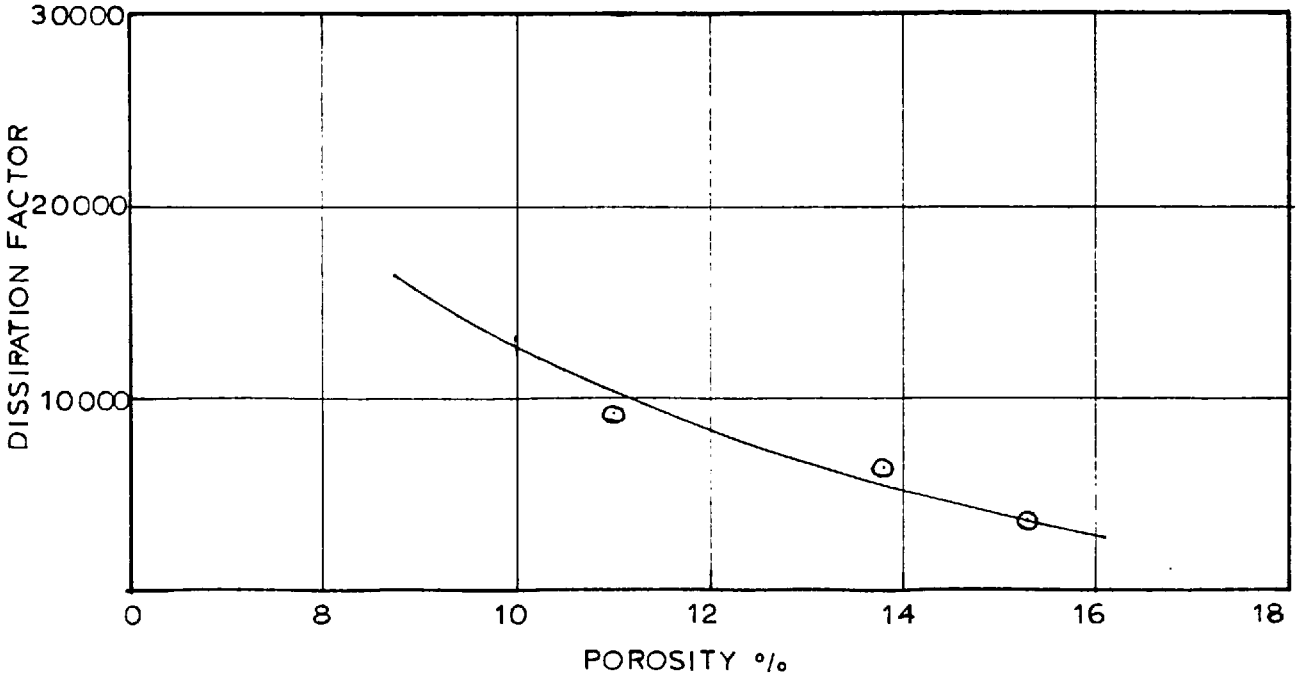
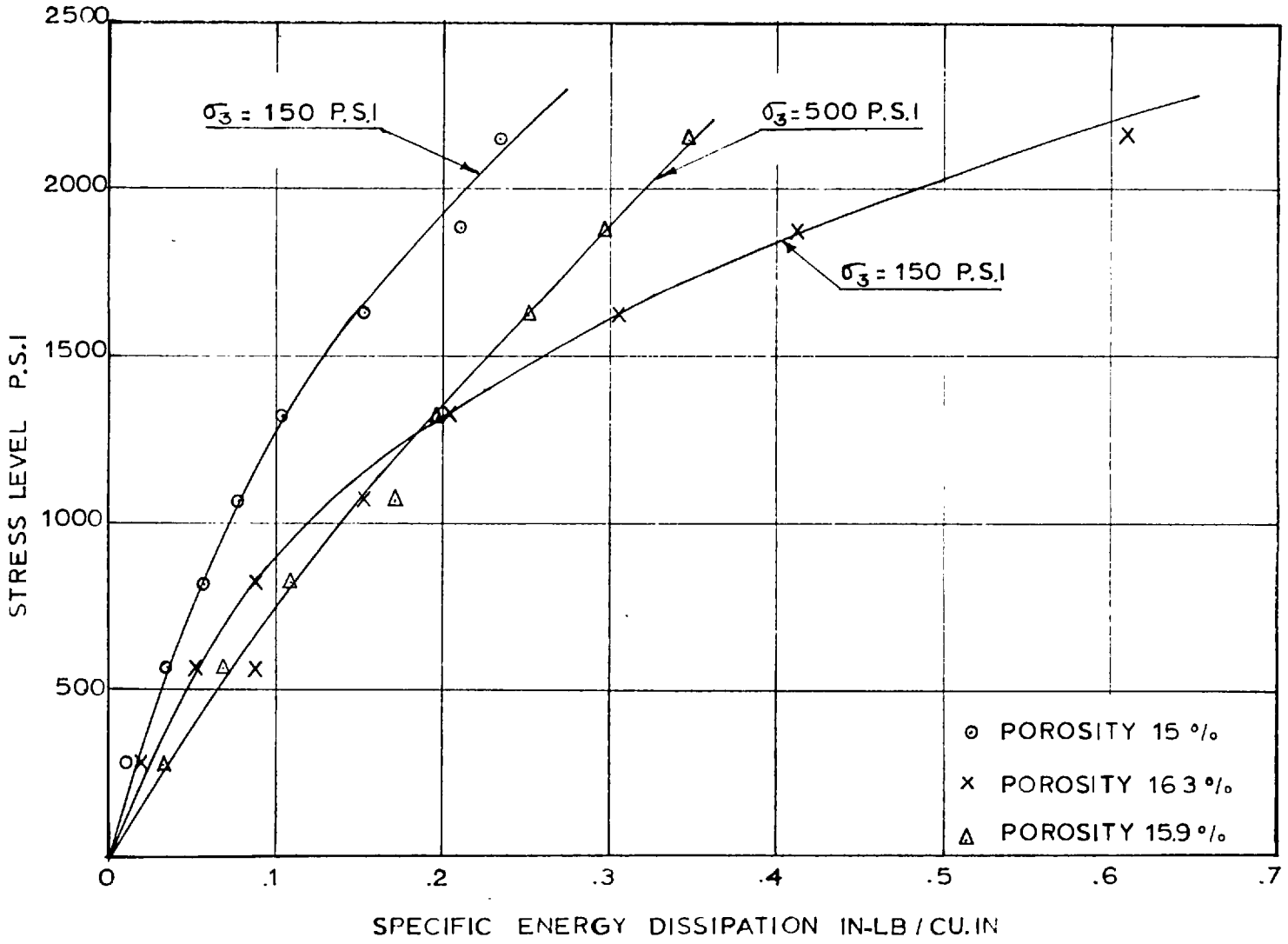
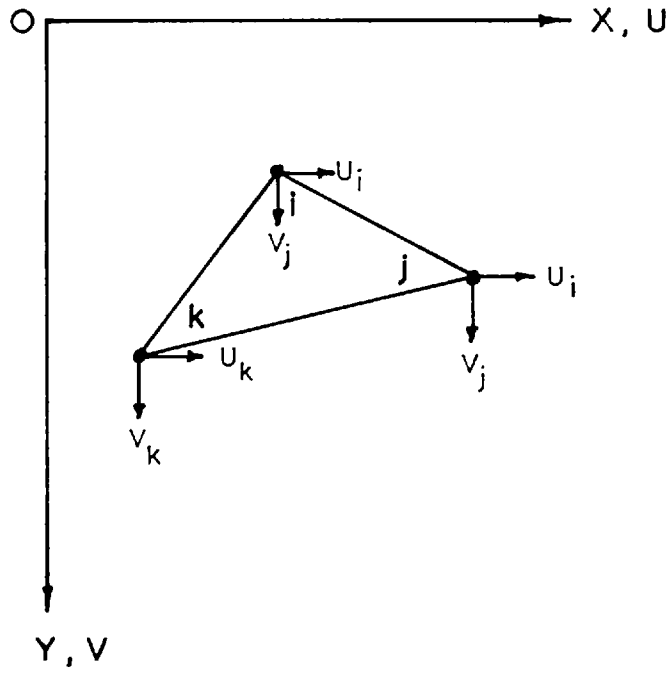

30000
20000
10000
DISSIPATION FACTOR
0
8
10
12
14
16
18
POROSITY %

FIG.4.48

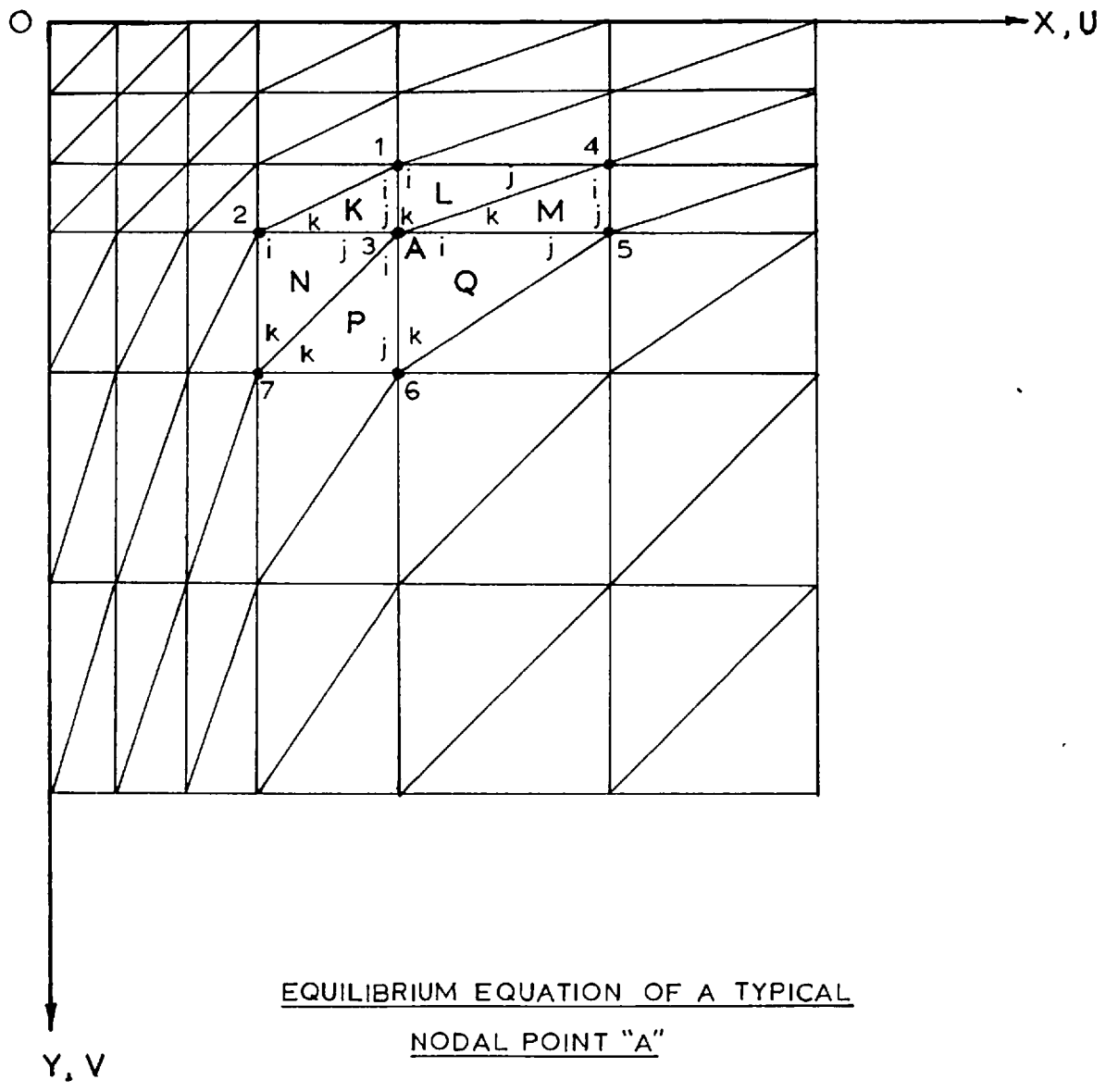


WET TEST FIG. 4.49



TRIANGULAR ELEMENT

FIG.5.1



EQUILIBRIUM EQUATION OF A TYPICAL NODAL POINT "A"

FIG.5.2

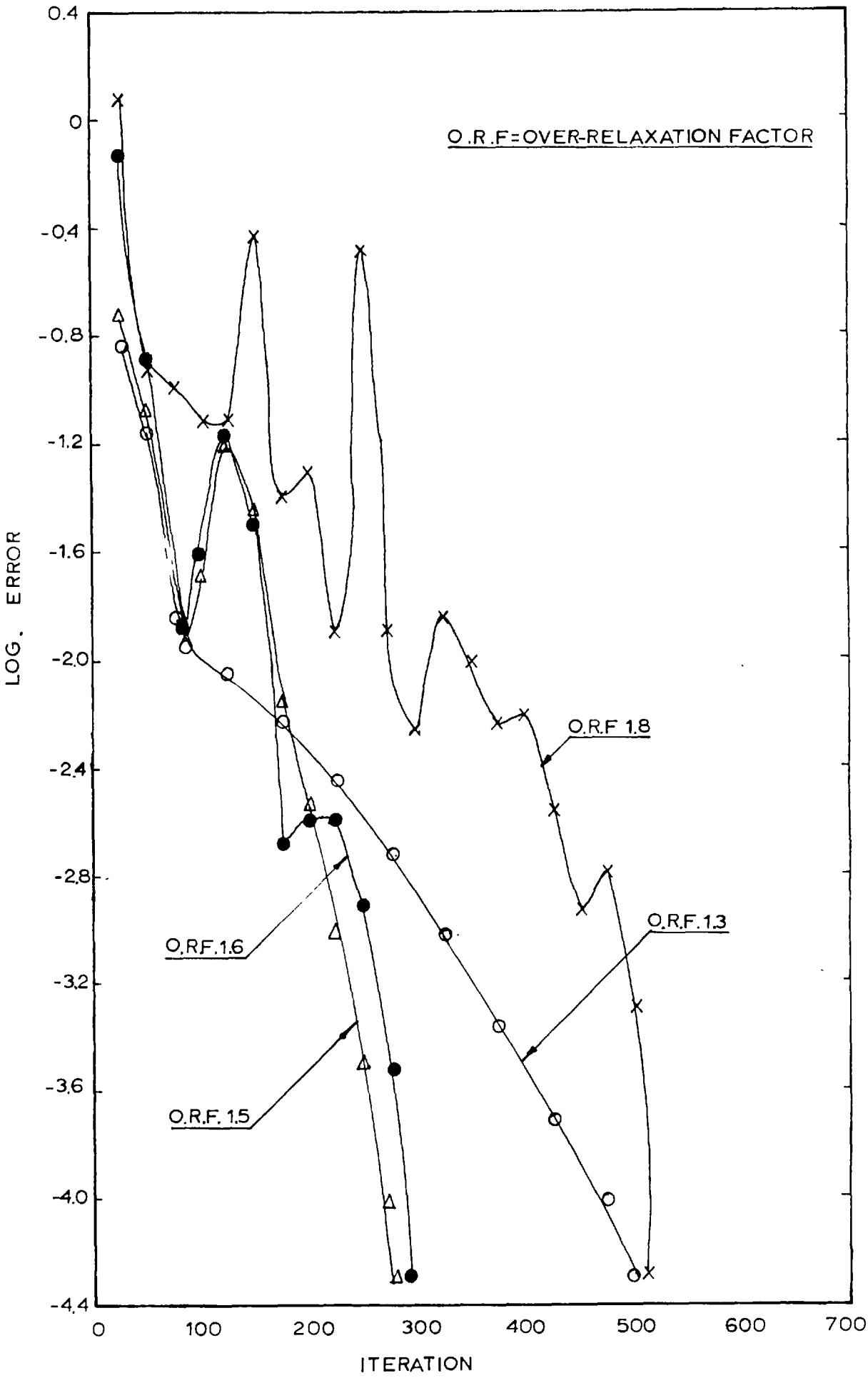
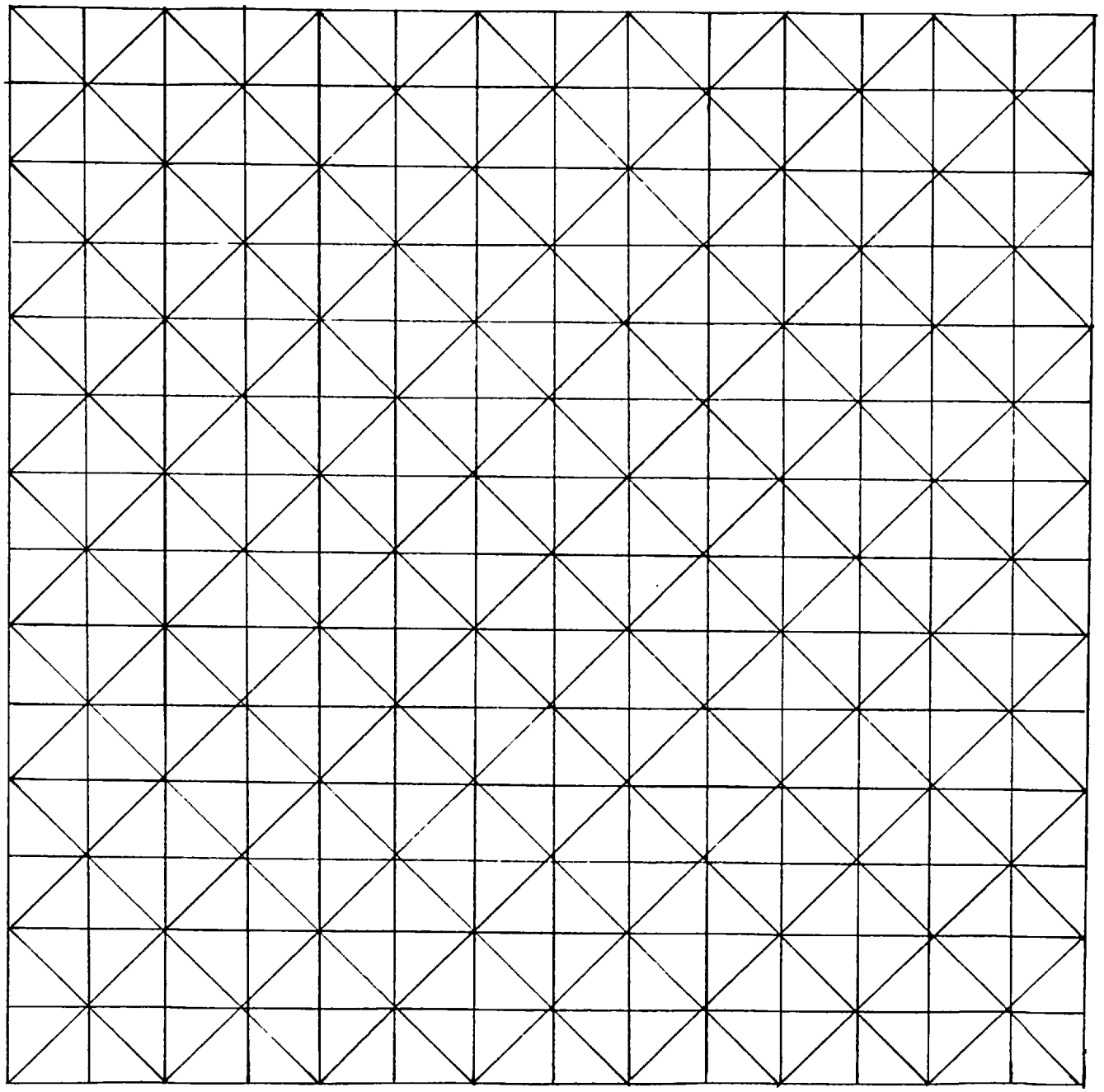

O.R.F=OVER-RELAXATION FACTOR
O.R.F 1.8
O.R.F. 1.6
O.R.F. 1.3
O.R.F. 1.5
LOG. ERROR
ITERATION
0.4
0
-0.4
-0.8
-1.2
-1.6
-2.0
-2.4
-2.8
-3.2
-3.6
-4.0
-4.4
0
100
200
300
400
500
600
700

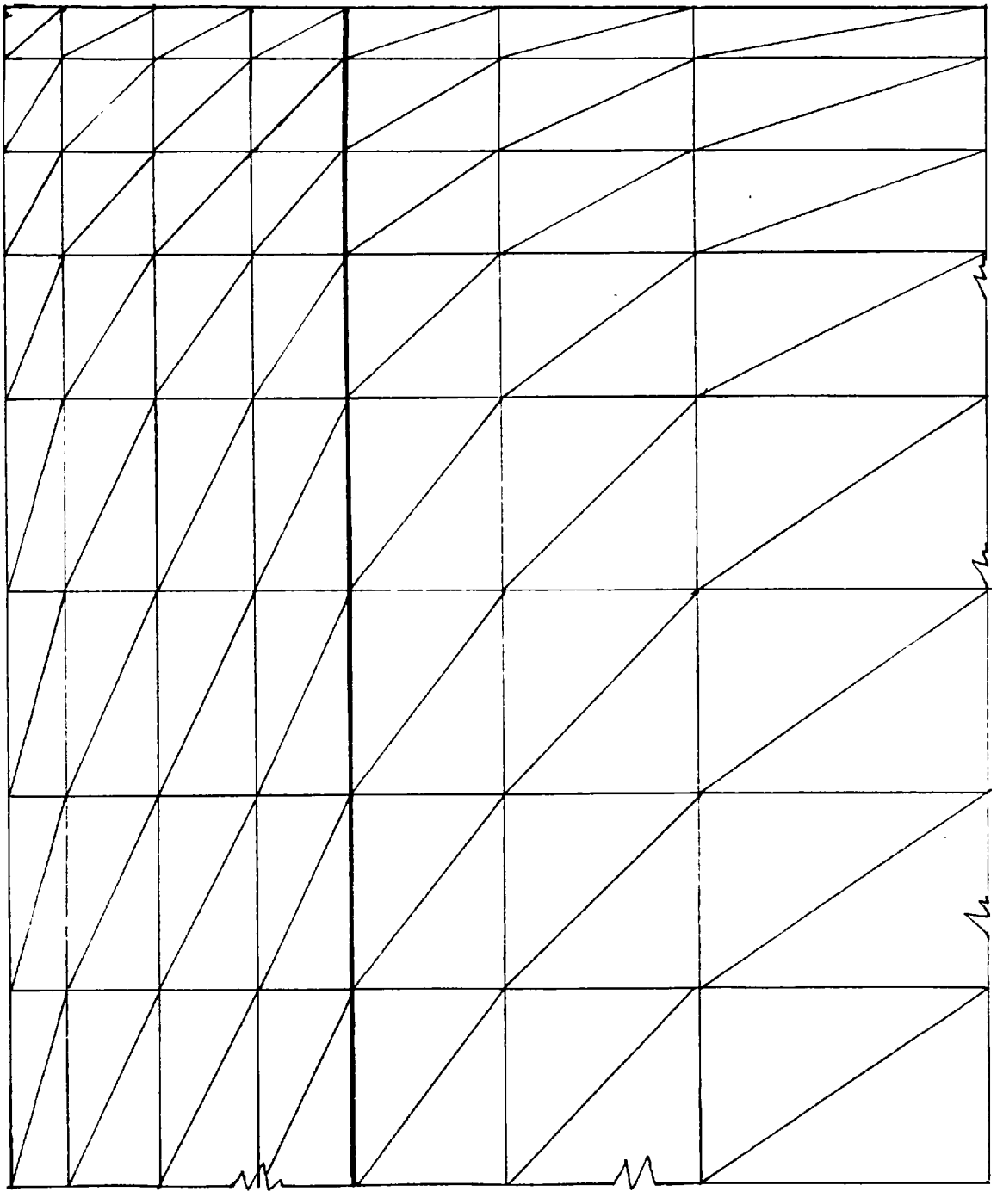
FIG. 5.3



MESH "A"

ELEMENTS OF UNIFORM AREA

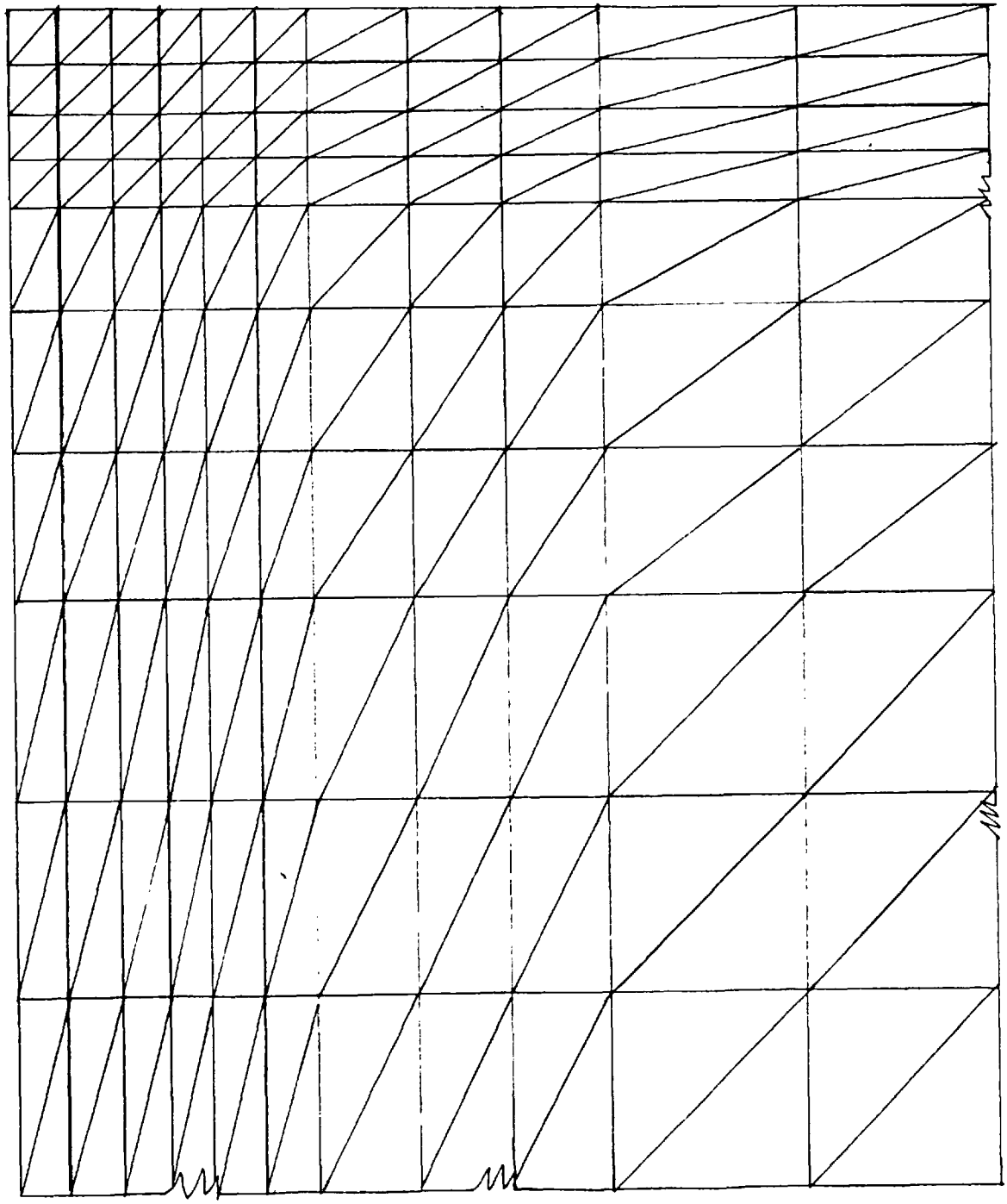
FIG 5.4a



MESH "B"

GRADED ELEMENTS

FIG. 5.4b



MESH "C"

FINE GRADED ELEMENTS

FIG. 5.4c

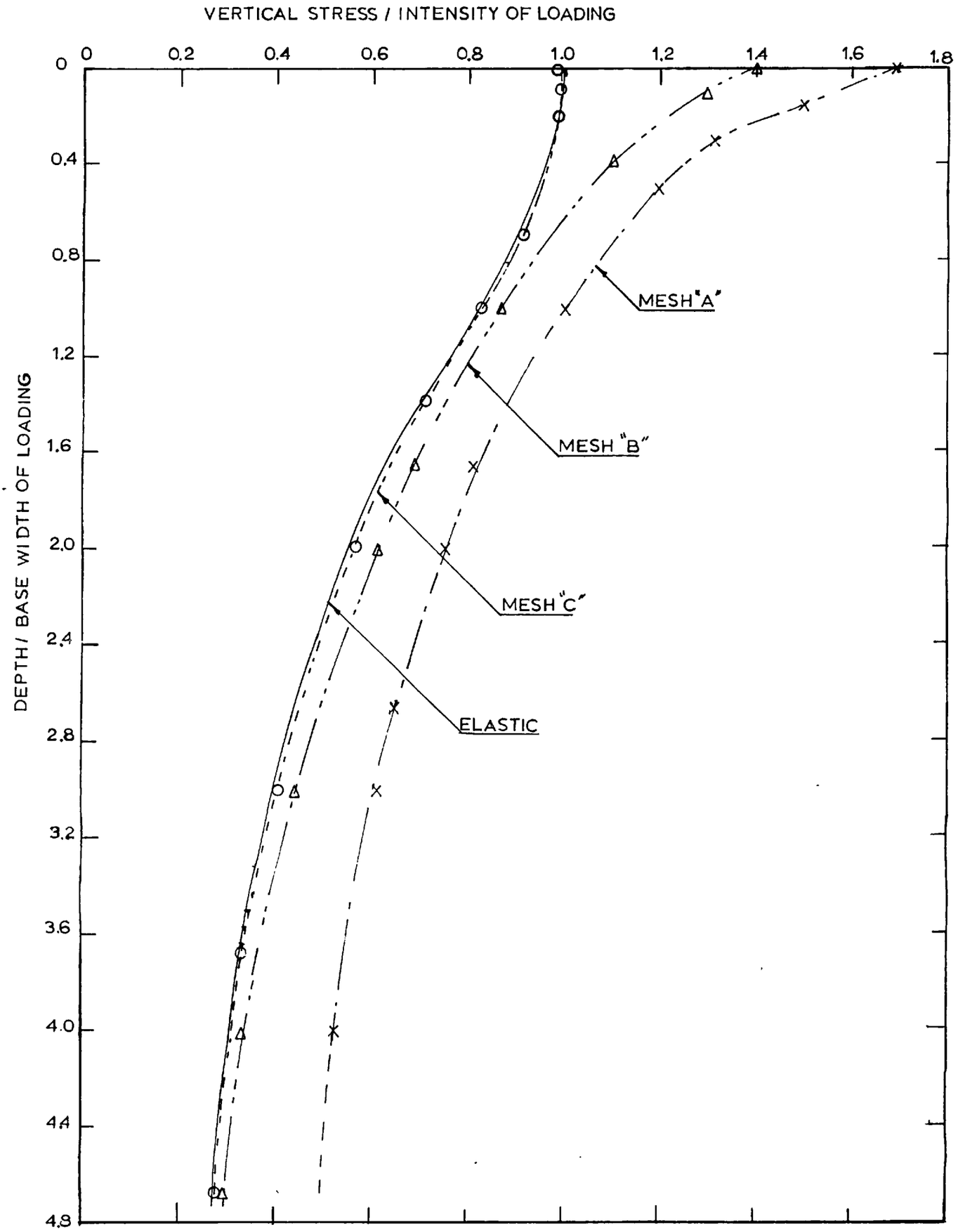
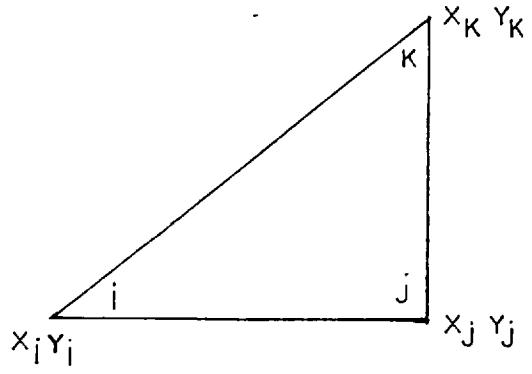

VERTICAL STRESS / INTENSITY OF LOADING
0
0.2
0.4
0.6
0.8
1.0
1.2
1.4
1.6
1.8
0.4
0.8
1.2
1.6
2.0
2.4
2.8
3.2
3.6
4.0
4.4
4.8
DEPTH / BASE WIDTH OF LOADING
MESH "A"
MESH "B"
MESH "C"
ELASTIC

FIG. 5.5



TYPICAL ELEMENT n ATTACHED TO NODAL POINT i

FIG.5.6

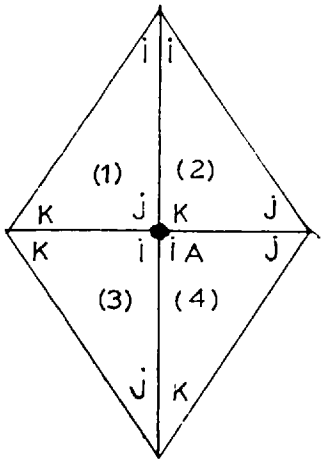
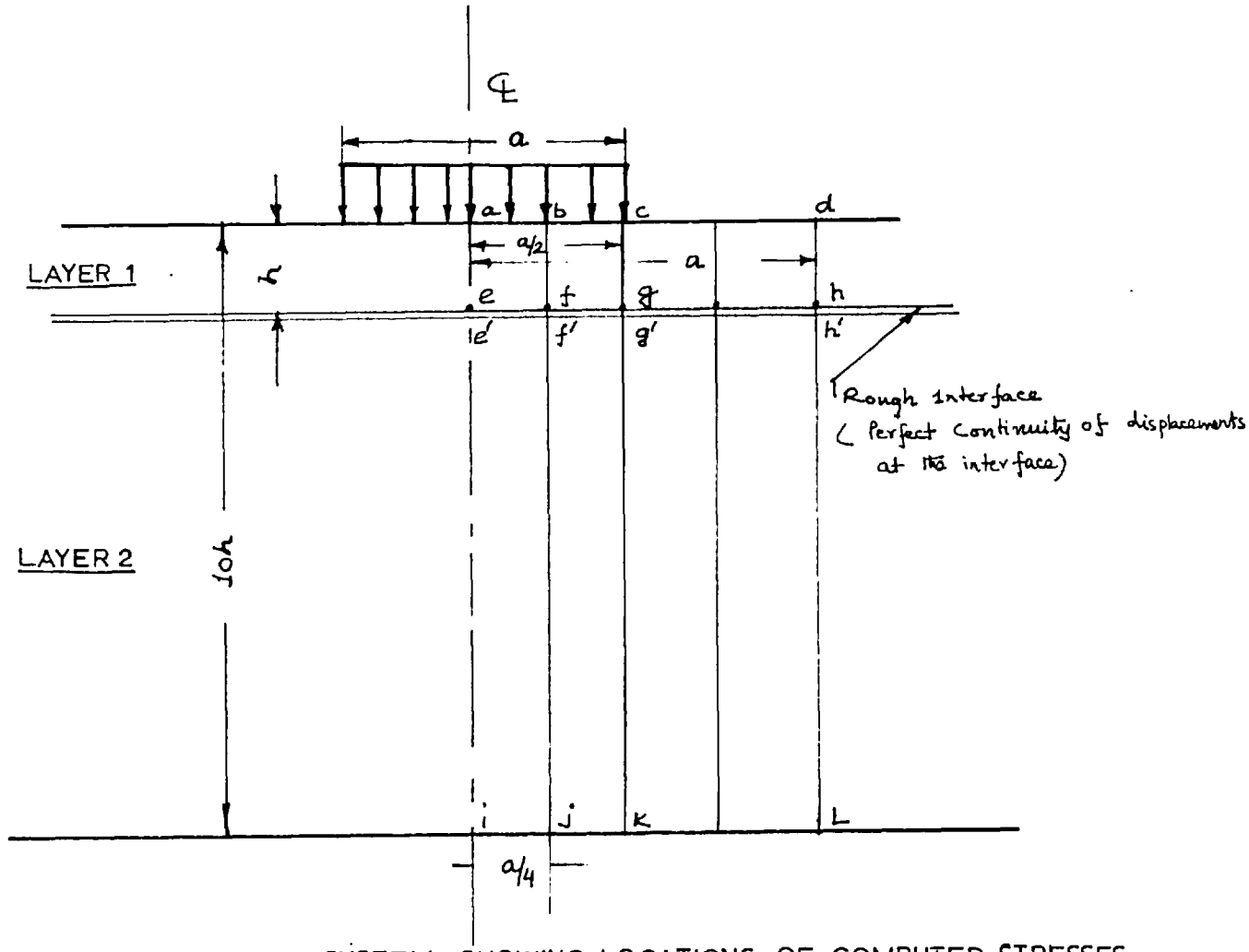


FIG.5.7



TWO LAYER SYSTEM SHOWING LOCATIONS OF COMPUTED STRESSES

FIG. 5.8a

PROBLEM: E_1 / E_2 = 0.02 ; a/h = 1 ; POIS = 0.25

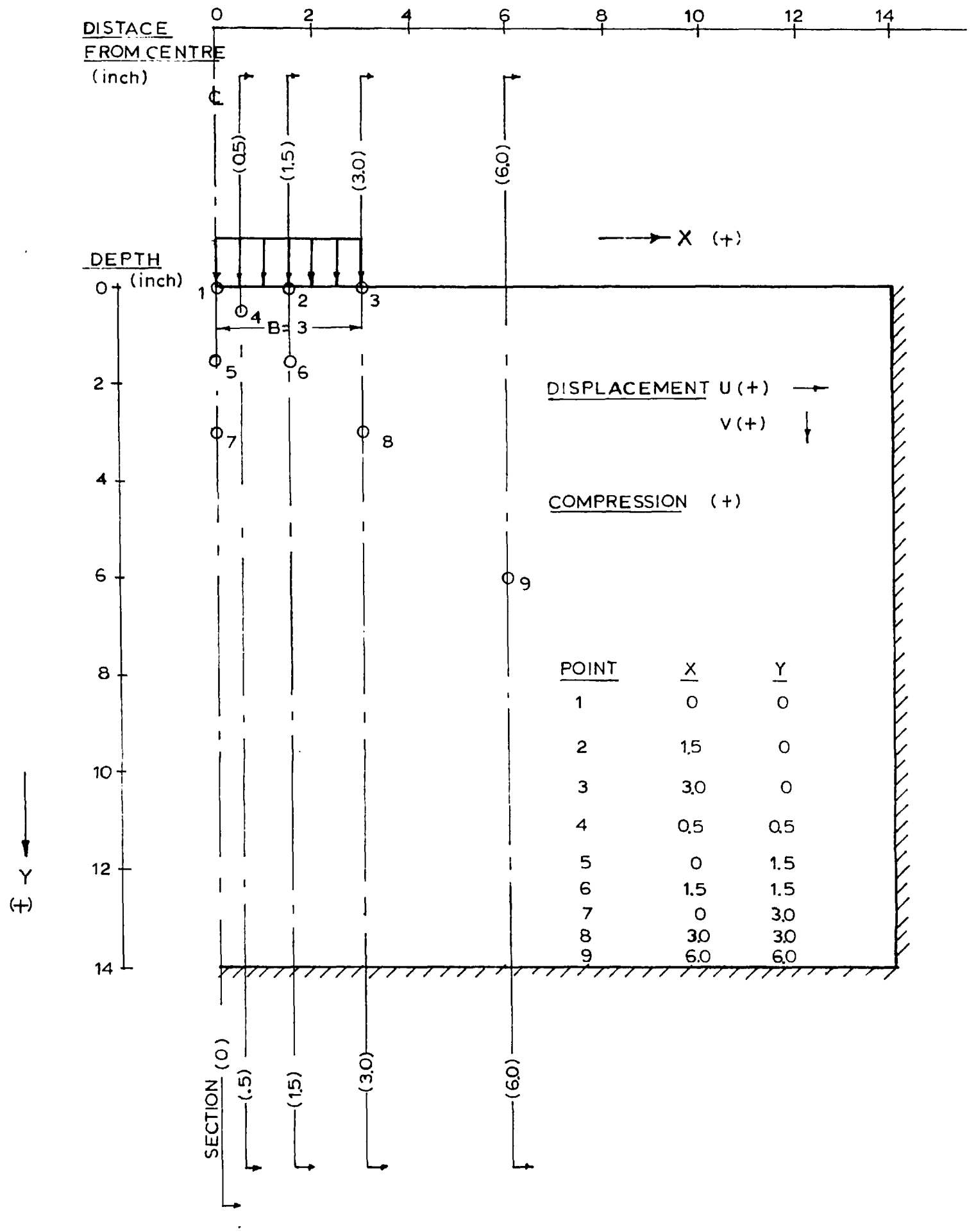
LOCATION	A.S	F.E.S	A.S	F.E.S	A.S	F.E.S
	σ_x / LOAD INTENSITY		σ_y / LOAD INTENSITY		τ_{xy} / LOAD INTENSITY	
a	- 4.5925	- 4.0391	- 1.000	-0.92	0.0	- 0.044
b	- 4.3034	-	-1.000	-	0.0	-
c	-3.6033	-3.1612	-1.000	-0.91	0.0	-0.360
d	-2.3651	-0.6220	0.00	0.0	0.0	- 0.132
e	2.8802	2.810	-0.2048	-0.2251	0.0	-0.061
f	2.7259	-	-0.2013	-	-0.0175	-
g	2.2978	1.866	-0.1925	-0.2031	-0.0311	-0.175
h	1.2979	0.672	-0.1612	-0.0930	-0.0448	-0.576
e'	-0.0078	0.0064	-0.2048	-0.2251	0.0	-0.061
f'	-0.0104	-	-0.2013	-	-0.0175	-
g'	-0.0161	-0.0067	-0.1925	-0.2031	-0.0311	-0.1750
h'	-0.0265	-0.0293	-0.1612	-0.0930	-0.0448	-0576
i	0.0040	0067	-0.0514	-0.0546	0.0	- 0.0008
j	0.0040	-	-0.0514	-	-0.0011	-
k	0.0038	0.009	-0.0513	-0.0540	-0.0022	-0.0011
L	0.0035	0.002	-0.0507	-0.0520	-0.0044	-0.0060

A.S = ANALYTICAL SOLUTION (LEMCOE, 1960)

F.E.S = FINITE ELEMENT SOLUTION

- VE COMPRESSION

FIG. 5.8b

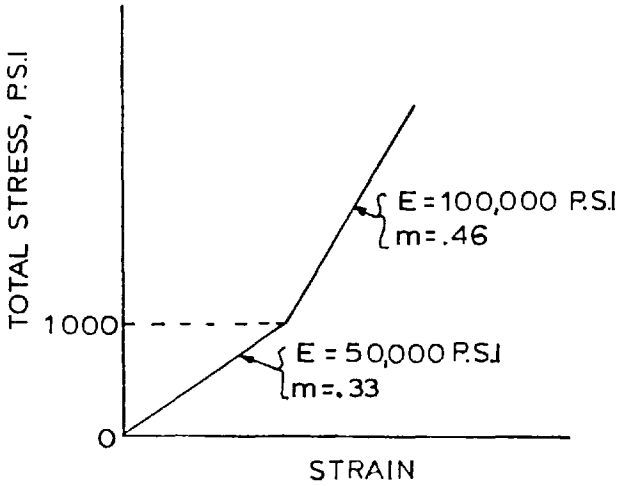


POINT	X	Y
1	0	0
2	1.5	0
3	3.0	0
4	0.5	0.5
5	0	1.5
6	1.5	1.5
7	0	3.0
8	3.0	3.0
9	6.0	6.0

FLEXIBLE STRIP LOADING SOLUTION

LOCATION OF SECTIONS AND SELECTED POINTS

FIG. 6.1



FIG(6.2 a) BILINEAR MODEL(1)

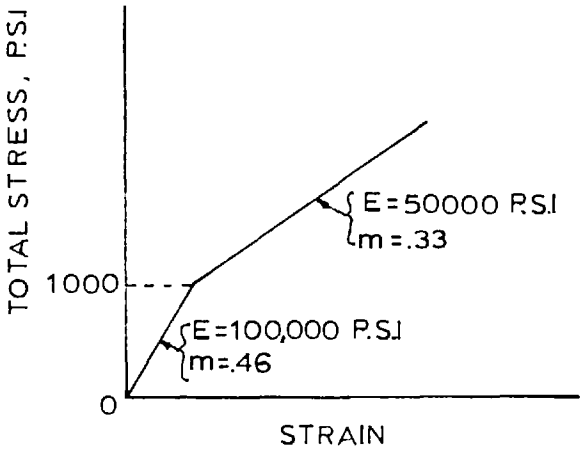


FIG.(6.2b) BILINEAR MODEL(2)

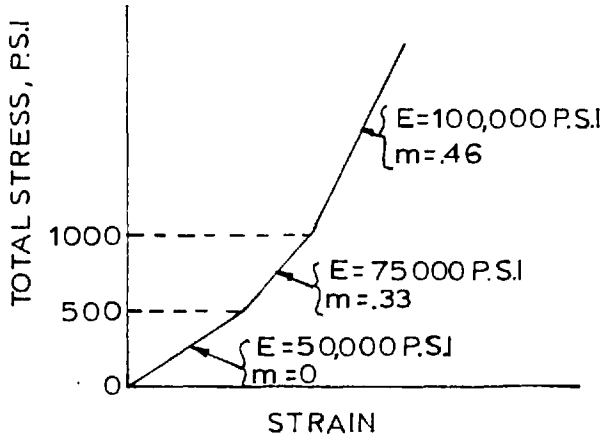


FIG.(6.2c) TRI-LINEAR MODEL(3)

DIFFERENT MODELS WITH ELASTIC PARAMETERS



FIG.6.3a

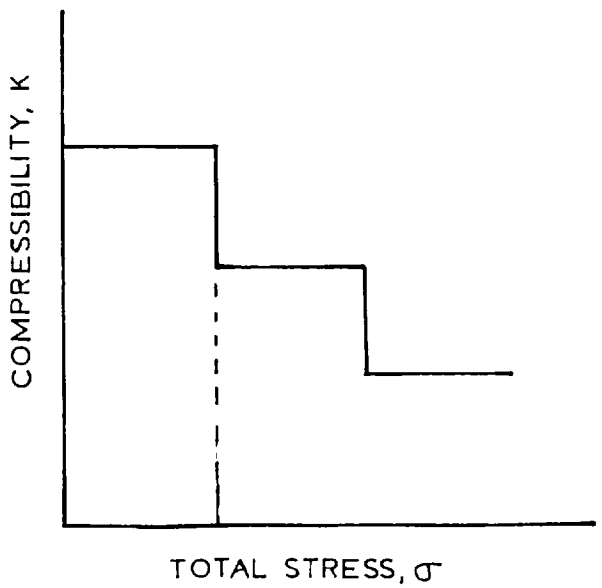


FIG.6.3b

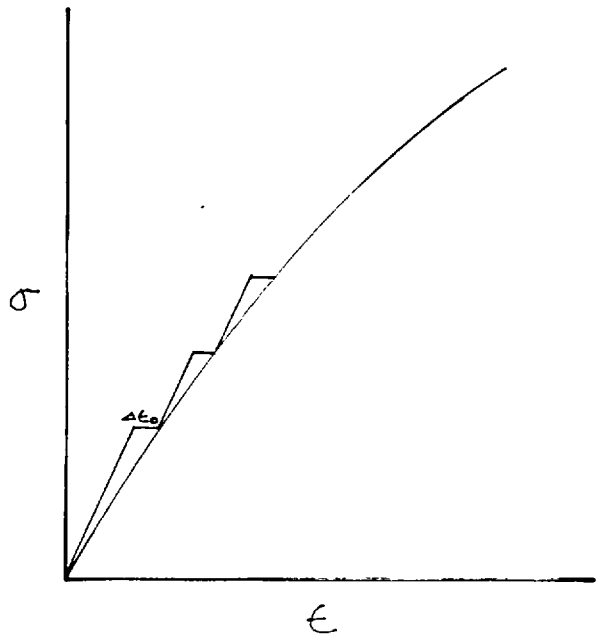


FIG.6.3c INCREMENTAL - INITIAL STRAIN PROCESS

DEPTH (INCH)	LOAD	SECTION 1 U	SECTION 1 V	SECTION 2 U	SECTION 2 V	SECTION 3 U	SECTION 3 V	SECTION 4 U	SECTION 4 V	SECTION 5 U	SECTION 5 V
0	L1	0	0.059	-0.0007	0.059	-0.0022	0.055	-0.0044	0.041	-0.0041	0.013
	L2	0	0.082	-0.0006	0.082	-0.0017	0.078	-0.0025	0.059	-0.0041	0.020
	L3	0	0.103	-0.0006	0.103	-0.0018	0.098	-0.0017	0.074	-0.0032	0.026
	L4	0	0.130	-0.0002	0.129	-0.0006	0.123	0.0006	0.090	0.0013	0.027
	L5	0	0.145	0.00002	0.144	0.0002	0.137	0.0028	0.097	0.0066	0.022
	L6	0	0.188	0.00010	0.188	0.0006	0.177	0.0037	0.122	0.0114	0.026
0.5	L1	0	0.058	-0.0002	0.057	0.0002	0.054	0.0003	0.040	-0.0019	0.013
	L2	0	0.081	0.0003	0.081	0.0014	0.077	0.0044	0.067	-0.0010	0.020
	L3	0	0.102	0.0005	0.102	0.0016	0.097	0.0063	0.072	0.0064	0.026
	L4	0	0.127	0.0012	0.127	0.0046	0.120	0.0118	0.088	0.0064	0.028
	L5	0	0.142	0.0018	0.141	0.0066	0.133	0.0164	0.093	0.0124	0.022
	L6	0	0.184	0.0024	0.183	0.0089	0.172	0.0222	0.117	0.0188	0.020
1.0	L1	0	0.057	0.0002	0.056	0.0012	0.052	0.0027	0.038	0.0007	0.013
	L2	0	0.079	0.0011	0.079	0.0039	0.074	0.0080	0.055	0.0017	0.020
	L3	0	0.100	0.0015	0.099	0.0054	0.094	0.0109	0.077	0.0041	0.026
	L4	0	0.124	0.0025	0.123	0.0086	0.101	0.0175	0.085	0.0110	0.028
	L5	0	0.137	0.0034	0.136	0.0115	0.127	0.0232	0.090	0.0179	0.022
	L6	0	0.178	0.0046	0.176	0.0155	0.164	0.0313	0.112	0.0260	0.020
1.5	L1	0	0.054	0.0008	0.053	0.0025	0.049	0.0043	0.036	0.0016	0.013
	L2	0	0.077	0.0017	0.076	0.0057	0.071	0.0093	0.054	0.0040	0.020
	L3	0	0.097	0.0023	0.096	0.0076	0.090	0.0137	0.068	0.0070	0.026
	L4	0	0.119	0.0036	0.118	0.0115	0.111	0.0210	0.082	0.0150	0.026
	L5	0	0.131	0.0047	0.130	0.0148	0.121	0.0271	0.086	0.0226	0.023
	L6	0	0.170	0.0063	0.168	0.0200	0.155	0.0366	0.108	0.0321	0.023
2.0	L1	0	0.050	0.0011	0.049	0.0032	0.046	0.0053	0.035	0.0030	0.013
	L2	0	0.074	0.0022	0.073	0.0069	0.068	0.0101	0.051	0.0059	0.020
	L3	0	0.093	0.0029	0.092	0.0089	0.086	0.0155	0.066	0.0094	0.026
	L4	0	0.114	0.0043	0.113	0.0182	0.105	0.0232	0.079	0.0183	0.029
	L5	0	0.124	0.0055	0.123	0.0187	0.114	0.0295	0.083	0.0264	0.023
	L6	0	0.160	0.0075	0.158	0.0225	0.145	0.0395	0.103	0.0374	0.021
3.0	L1	0	0.043	0.0013	0.042	0.0037	0.039	0.0061	0.031	0.0049	0.013
	L2	0	0.065	0.0024	0.064	0.0066	0.060	0.0103	0.047	0.0083	0.020
	L3	0	0.084	0.0034	0.084	0.0049	0.078	0.0168	0.061	0.0123	0.026
	L4	0	0.101	0.0050	0.100	0.0144	0.094	0.0249	0.073	0.0229	0.029
	L5	0	0.109	0.0061	0.108	0.0178	0.100	0.0309	0.075	0.0319	0.024
	L6	0	0.140	0.0082	0.138	0.0237	0.126	0.0408	0.093	0.0434	0.020
6.0	L1	0	0.026	0.0010	0.026	0.0029	0.024	0.0051	0.021	0.0061	0.011
	L2	0	0.039	0.0015	0.039	0.0045	0.037	0.0079	0.031	0.0095	0.017
	L3	0	0.052	0.0022	0.052	0.0065	0.050	0.0112	0.042	0.0131	0.022
	L4	0	0.066	0.0037	0.065	0.0125	0.061	0.0216	0.053	0.0228	0.026
	L5	0	0.067	0.0047	0.066	0.0137	0.062	0.0247	0.049	0.0331	0.018
	L6	0	0.084	0.0060	0.083	0.0175	0.077	0.0313	0.061	0.0406	0.018
11.0	L1	0	0.007	0.0004	0.007	0.0014	0.007	0.0026	0.006	0.0035	0.004
	L2	0	0.011	0.0007	0.011	0.0021	0.011	0.0038	0.010	0.0053	0.006
	L3	0	0.015	0.0009	0.015	0.0028	0.014	0.0052	0.013	0.0072	0.009
	L4	0	0.015	0.0029	0.015	0.0084	0.014	0.0120	0.013	0.0122	0.010
	L5	0	0.017	0.0025	0.016	0.0074	0.015	0.0136	0.013	0.0177	0.008
	L6	0	0.020	0.0032	0.020	0.0092	0.019	0.0166	0.016	0.0229	0.008

U = HORIZONTAL DISPLACEMENT

V = VERTICAL DISPLACEMENT

LOAD

L1 = 500 P.S.I

L2 = 750 P.S.I

L3 = 1000 P.S.I

L4 = 1500 P.S.I

L5 = 2000 P.S.I

L6 = 3000 P.S.I

NOTE: REF. FIG (6-1) ALSO

RESULT OF DISPLACEMENTS BILINEAR MODEL.1 (B.M.1)

FIG 6.4

DEPTH (INCH)	LOAD	SECTION 1 U	SECTION 1 V	SECTION 2 U	SECTION 2 V	SECTION 3 U	SECTION 3 V	SECTION 4 U	SECTION 4 V	SECTION 5 U	SECTION 5 V
0	L_1	0	0.023	-0.0006	0.023	-0.0013	0.020	-0.0018	0.011	0.00028	0
	L_2	0	0.043	-0.0014	0.042	-0.0040	0.038	-0.0053	0.020	-0.0010	0.007
	L_3	0	0.067	-0.0023	0.066	-0.0067	0.061	-0.0100	0.033	-0.0030	0.002
	L_4	0	0.124	-0.0043	0.123	-0.0123	0.114	-0.0189	0.067	-0.0081	0.013
	L_5	0	0.184	-0.0062	0.183	-0.0179	0.169	-0.0283	0.105	-0.0138	0.025
	L_6	0	0.309	-0.0098	0.307	-0.0282	0.285	-0.0461	0.185	-0.0249	0.052
0.5	L_1	0	0.021	-0.00008	0.021	0.00017	0.019	0.00098	0.011	0.0011	0
	L_2	0	0.040	-0.0005	0.039	-0.0012	0.035	-0.00013	0.019	0.0002	0.0005
	L_3	0	0.062	-0.0009	0.062	-0.0025	0.056	-0.0017	0.031	-0.0011	0.002
	L_4	0	0.117	-0.0019	0.116	-0.0052	0.106	-0.0046	0.064	-0.0042	0.012
	L_5	0	0.175	-0.0029	0.173	-0.0077	0.159	-0.0081	0.099	-0.0080	0.024
	L_6	0	0.294	-0.0046	0.293	-0.0121	0.270	-0.0139	0.176	-0.0151	0.049
1.0	L_1	0	0.020	0.00056	0.020	0.00140	0.018	0.0027	0.010	0.0018	0
	L_2	0	0.036	0.00014	0.036	0.00060	0.032	0.0026	0.018	0.0015	0.0005
	L_3	0	0.058	0.00005	0.057	0.00045	0.051	0.0023	0.030	0.0009	0.002
	L_4	0	0.109	-0.00019	0.108	0.00003	0.098	0.0024	0.062	-0.0002	0.012
	L_5	0	0.164	-0.00044	0.162	-0.00040	0.148	0.0024	0.096	-0.0022	0.023
	L_6	0	0.277	-0.00051	0.274	-0.00001	0.252	0.0029	0.169	-0.0058	0.048
1.5	L_1	0	0.018	0.00079	0.018	0.0021	0.016	0.0036	0.010	0.0025	0
	L_2	0	0.033	0.00059	0.032	0.0018	0.028	0.0041	0.017	0.0026	0.0006
	L_3	0	0.052	0.00076	0.052	0.0023	0.046	0.0047	0.028	0.0026	0.002
	L_4	0	0.101	0.00110	0.100	0.0034	0.090	0.0068	0.059	0.0030	0.012
	L_5	0	0.153	0.00140	0.151	0.0044	0.137	0.0087	0.093	0.0029	0.023
	L_6	0	0.259	0.00250	0.256	0.0081	0.234	0.0133	0.162	0.0026	0.048
2.0	L_1	0	0.017	0.00094	0.017	0.0026	0.015	0.0042	0.009	0.0030	0
	L_2	0	0.029	0.00082	0.029	0.0022	0.026	0.0051	0.016	0.0035	0.0007
	L_3	0	0.048	0.00110	0.047	0.0033	0.042	0.0063	0.027	0.0039	0.003
	L_4	0	0.093	0.00193	0.092	0.0055	0.083	0.0094	0.056	0.0056	0.012
	L_5	0	0.141	0.00260	0.139	0.0074	0.126	0.0126	0.089	0.0070	0.024
	L_6	0	0.240	0.00440	0.237	0.0131	0.217	0.0196	0.155	0.0102	0.049
3.0	L_1	0	0.014	0.00091	0.014	0.0026	0.013	0.0043	0.008	0.0036	0
	L_2	0	0.023	0.00095	0.023	0.0031	0.021	0.0057	0.014	0.0047	0.001
	L_3	0	0.038	0.00140	0.038	0.0039	0.034	0.0074	0.024	0.0056	0.003
	L_4	0	0.077	0.00260	0.076	0.0071	0.069	0.0116	0.051	0.0093	0.013
	L_5	0	0.118	0.00360	0.117	0.0101	0.107	0.0153	0.080	0.0130	0.025
	L_6	0	0.204	0.00610	0.202	0.0171	0.186	0.0252	0.140	0.0223	0.050
6.0	L_1	0	0.008	0.00060	0.008	0.0017	0.007	0.0030	0.005	0.0033	0.001
	L_2	0	0.014	0.00078	0.013	0.0024	0.012	0.0042	0.009	0.0050	0.002
	L_3	0	0.019	0.00110	0.019	0.0033	0.018	0.0064	0.014	0.0062	0.004
	L_4	0	0.040	0.00300	0.040	0.0062	0.039	0.0096	0.032	0.0123	0.013
	L_5	0	0.066	0.00280	0.065	0.0079	0.062	0.0131	0.052	0.0168	0.024
	L_6	0	0.118	0.00470	0.117	0.0135	0.111	0.0230	0.093	0.0294	0.047
11.0	L_1	0	0.002	0.00028	0.002	0.0008	0.001	0.0014	0.001	0.0017	0.006
	L_2	0	0.004	0.00046	0.004	0.0013	0.004	0.0024	0.002	0.0029	0.009
	L_3	0	0.005	0.00043	0.005	0.0012	0.005	0.0022	0.005	0.0035	0.004
	L_4	0	0.009	0.00086	0.009	0.0025	0.009	0.0046	0.008	0.0070	0.005
	L_5	0	0.015	0.00160	0.025	0.0048	0.015	0.0080	0.015	0.0093	0.011
	L_6	0	0.029	0.00360	0.029	0.0068	0.030	0.0107	0.028	0.0129	0.019

U = HORIZONTAL DISPLACEMENT

V = VERTICAL DISPLACEMENT

LOAD

L_1 = 500 P.S.I
L_2 = 750 P.S.I
L_3 = 1000 P.S.I
L_4 = 1500 P.S.I
L_5 = 2000 P.S.I
L_6 = 3000 P.S.I

NOTE: Ref fig 6.1

DISPLACEMENT RESULTS

BILINEAR MODEL 2 (B.M.2)

FIG. 6.5

DEPTH (INCH)	LOAD	SECTION 1 σx	SECTION 1 σy	SECTION 1 τxy	SECTION 2 σx	SECTION 2 σy	SECTION 2 τxy	SECTION 3 σx	SECTION 3 σy	SECTION 3 τxy	SECTION 4 σx	SECTION 4 σy	SECTION 4 τxy	SECTION 5 σx	SECTION 5 σy	SECTION 5 τxy
0.5	L_1	494.3	513.6	-12.0	402.5	476.1	7.0	425.0	437.0	19.0	164.8	242.8	145.0	14.0	4.3	7.6
	L_2	626.6	748.0	-12.3	541.6	715.3	-1.6	506.2	743.5	25.0	248.0	356.6	184.8	38.1	6.0	20.0
	L_3	814.6	997.6	-17.0	693.3	951.1	-2.0	642.5	990.6	36.8	337.8	515.6	217.5	59.1	8.0	25.8
	L_4	1101.3	1492.3	-24.3	900.6	1428.1	-4.1	880.8	1483.0	52.1	406.8	766.0	328.5	63.5	5.6	12.5
	L_5	1398.6	1982.0	-30.3	1185.6	190.2	-2.0	1094.3	1974.0	72.3	477.6	1005.3	457.3	91.0	11.8	26.5
	L_6	2154.0	2992.0	-43.0	1831.5	287.4	-1.3	1681.0	2975.8	111.5	716.5	1514.0	688.3	92.8	19.1	31.1
1.5	L_1	164.0	474.0	12.0	134.3	486.0	31.3	109.1	434.1	71.1	116.5	241.1	143.6	47.8	22.0	31.5
	L_2	402.0	711.0	5.3	323.6	686.1	25.8	287.0	664.3	80.0	196.0	344.1	242.3	87.0	56.6	53.8
	L_3	491.3	965.6	6.0	385.5	909.0	38.0	337.6	874.1	111.0	293.0	502.5	265.0	130.0	40.3	69.8
	L_4	640.3	1449.0	17.0	488.8	1368.6	52.3	419.6	1309.2	175.1	386.1	747.8	388.1	191.3	53.0	74.1
	L_5	800.6	1918.6	22.6	610.0	1821.0	73.8	517.3	1743.1	240.6	471.3	985.0	523.3	234.1	68.6	72.3
	L_6	1253.3	2896.0	35.3	965.6	2750.1	114.0	813.8	2626.5	369.0	779.3	1484.6	811.8	268.6	101.3	94.3
3.0	L_1	46.6	397.6	6.0	44.5	386.5	31.6	49.6	349.6	74.1	73.1	232.3	117.6	69.5	50.0	55.1
	L_2	20.0	685.0	33.3	42.0	590.1	61.1	50.3	532.3	131.0	106.0	335.0	189.8	110.0	76.0	87.3
	L_3	228.6	834.3	18.3	211.1	800.1	61.0	217.1	729.3	140.0	193.8	450.3	268.5	156.8	96.3	117.3
	L_4	247.0	1258.3	26.3	224.6	1209.6	84.2	232.3	1088.3	198.6	308.3	725.5	326.1	263.8	123.8	129.5
	L_5	289.0	1650.3	35.3	269.8	1593.3	118.6	281.3	1444.3	279.1	369.1	956.5	439.8	273.5	152.6	119.5
	L_6	466.3	2485.0	54.3	438.8	2401.1	184.0	451.0	2171.6	433.8	574.0	1437.5	694.1	390.3	297.5	225.3
6.0	L_1	10.8	169.8	3.0	17.1	262.1	16.3	22.6	245.6	40.5	38.3	199.1	65.3	63.0	91.8	55.1
	L_2	4.1	538.0	5.0	20.5	393.5	25.1	30.0	368.1	63.0	55.8	296.6	99.5	95.3	139.8	84.8
	L_3	1.8	578.0	3.5	15.0	533.3	36.1	30.5	497.3	92.8	72.0	407.1	142.3	129.3	182.8	118.6
	L_4	122.6	845.0	17.3	177.0	893.3	55.1	172.8	831.6	101.3	171.8	548.5	174.8	210.1	231.5	155.0
	L_5	184.0	1119.3	16.0	269.5	1103.0	68.3	277.6	1073.8	157.5	315.0	852.5	240.8	285.1	249.8	155.0
	L_6	278.0	1665.3	24.6	413.8	1717.0	106.0	425.3	1594.2	244.6	486.5	1264.8	374.3	513.6	571.5	253.3

LOAD

L_1 = 500 P.S.I
L_2 = 750 P.S.I
L_3 = 1000 P.S.I
L_4 = 1500 P.S.I
L_5 = 2000 P.S.I
L_6 = 3000 P.S.I

NOTE: REF. FIG. 6.1
+ve COMPRESSION

FIG. 6.6 BILINEAR MODEL 1 (B.M.1) RESULTS OF STRESSES

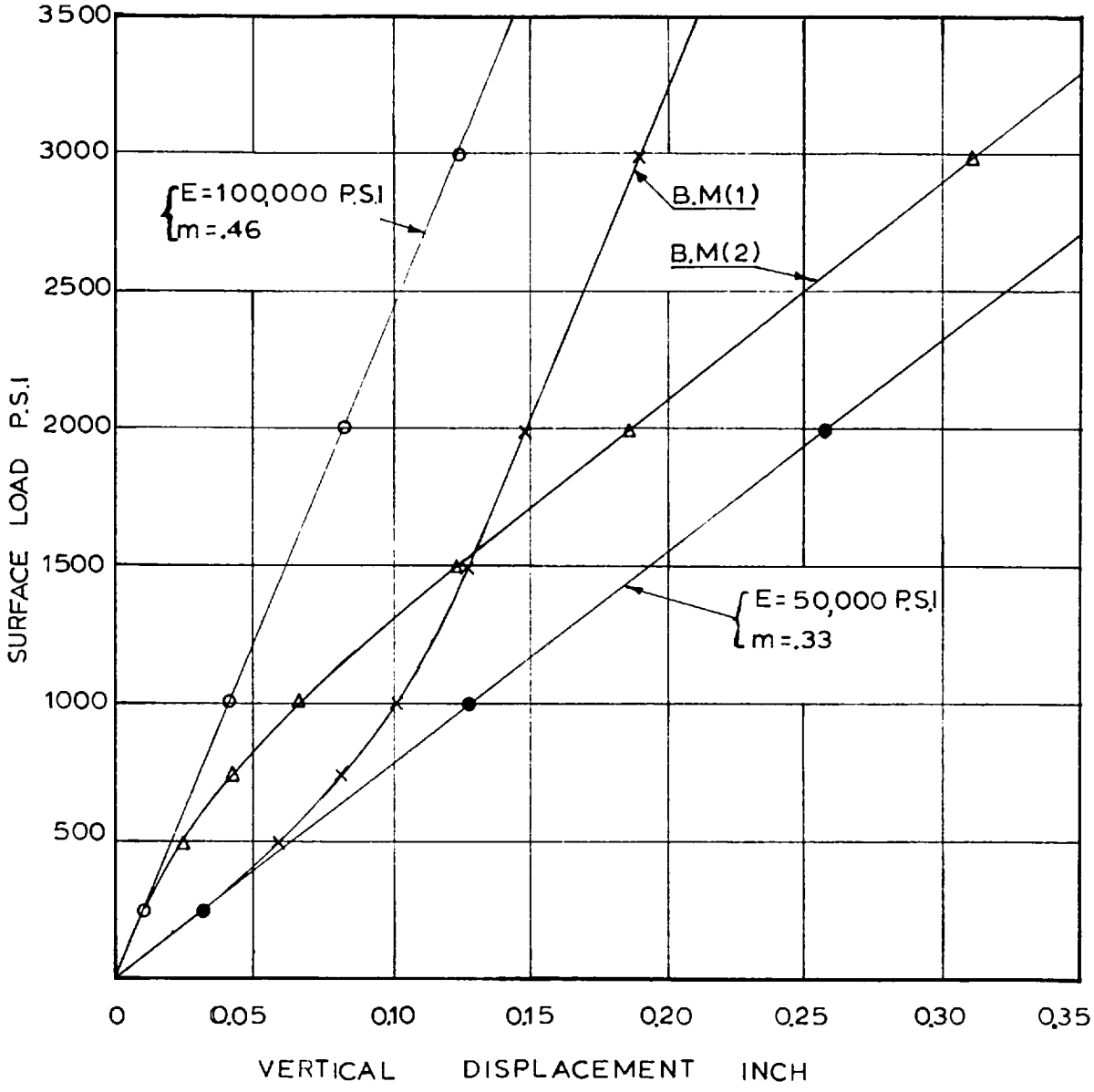
DEPTH (INCH)	LOAD	SECTION 1 σ_x	σ_y	τ_{xy}	SECTION 2 σ_x	σ_y	τ_{xy}	SECTION 3 σ_x	σ_y	τ_{xy}	SECTION 4 σ_x	σ_y	τ_{xy}	SECTION 5 σ_x	σ_y	τ_{xy}
0.5	L_1	226.0	450.6	23.3	272.1	501.1	11.1	250.3	467.0	76.0	130.6	226.3	101.5	6.8	1.5	1.0
	L_2	468.0	736.0	8.0	436.1	746.3	57.0	377.6	72.6	42.5	191.3	359.6	179.8	-24.6	-5.0	0.0
	L_3	663.6	986.6	6.6	614.3	992.1	11.5	544.0	978.1	49.1	333.1	539.1	269.3	-57.3	22.5	-3.6
	L_4	1049.0	1482.3	6.0	930.8	1482.1	35.0	859.1	1436.5	74.8	472.8	829.6	429.6	-92.6	1.3	2.5
	L_5	1430.3	1973.0	5.3	1310.0	1971.0	21.5	1164.8	1809.1	100.2	573.6	1082.6	583.6	-158.0	14.0	10.6
	L_6	2151.3	2971.0	3.6	1960.5	2953.1	27.3	1757.3	2944.5	138.1	803.3	1494.8	848.6	-248.3	5.8	44.3
1.5	L_1	169.5	484.0	2.6	222.6	524.6	20.1	190.0	470.1	59.1	160.5	234.6	127.6	76.3	26.3	16.6
	L_2	270.6	711.0	7.6	248.6	703.1	35.6	207.8	655.8	117.8	217.1	344.1	201.0	87.8	47.8	27.3
	L_3	386.3	951.0	10.1	350.3	943.1	45.0	300.6	870.1	145.8	302.1	391.5	276.0	111.8	58.5	33.3
	L_4	543.6	1423.3	27.3	543.6	1403.3	66.5	376.5	1305.3	214.1	465.5	831.6	459.6	172.5	88.6	80.5
	L_5	832.3	1895.0	21.6	739.0	1865.1	90.1	650.1	1732.6	289.3	649.5	1130.6	623.8	258.6	142.0	119.0
	L_6	1223.3	2851.0	33.1	1072.8	2795.5	131.6	928.5	2616.1	424.5	794.1	1511.0	961.0	268.1	83.8	162.1
3.0	L_1	51.8	394.6	2.0	113.1	403.0	25.5	116.3	371.3	78.0	139.0	241.3	121.5	111.6	53.3	40.5
	L_2	104.3	612.6	1.5	102.6	585.0	34.8	160.6	608.0	88.0	173.3	345.6	174.0	153.5	81.6	55.6
	L_3	153.0	818.6	6.3	148.3	787.3	51.5	165.5	710.5	146.8	240.3	516.0	240.3	270.0	346.0	185.3
	L_4	228.6	1215.6	14.0	218.5	1176.1	84.3	236.3	1048.8	229.6	336.8	822.1	377.8	330.8	167.8	170.5
	L_5	312.0	1613.0	21.0	295.6	1562.1	113.3	314.3	1342.1	302.6	358.2	1015.0	528.0	430.3	232.0	240.8
	L_6	431.6	2436.3	20.3	407.0	2350.5	177.5	436.5	2094.6	466.3	379.5	1484.6	722.3	603.6	297.5	365.0
6.0	L_1	69.3	276.3	4.0	91.8	283.5	17.6	94.0	263.5	42.8	104.0	207.6	66.5	111.6	92.8	43.5
	L_2	143.6	428.6	7.3	89.8	371.8	29.1	146.6	393.8	64.5	160.3	349.6	104.3	167.0	145.3	67.8
	L_3	190.3	588.3	4.3	138.6	318.3	31.1	121.0	496.6	81.5	203.0	488.1	136.1	231.1	210.5	99.3
	L_4	48.0	964.0	-3.0	64.0	832.5	22.6	91.3	730.1	94.3	193.8	640.8	164.0	318.6	312.5	172.3
	L_5	83.6	1150.0	8.3	112.0	1062.6	56.1	138.1	961.5	148.3	202.8	775.8	242.3	416.0	446.8	260.5
	L_6	112.6	1668.3	17.3	145.5	1568.3	96.3	183.0	1447.1	242.3	277.5	1155.6	384.0	553.0	709.8	414.3

LOAD

L_1 = 500 P.S.I
L_2 = 750 P.S.I
L_3 = 1000 P.S.I
L_4 = 1500 P.S.I
L_5 = 2000 P.S.I
L_6 = 3000 P.S.I

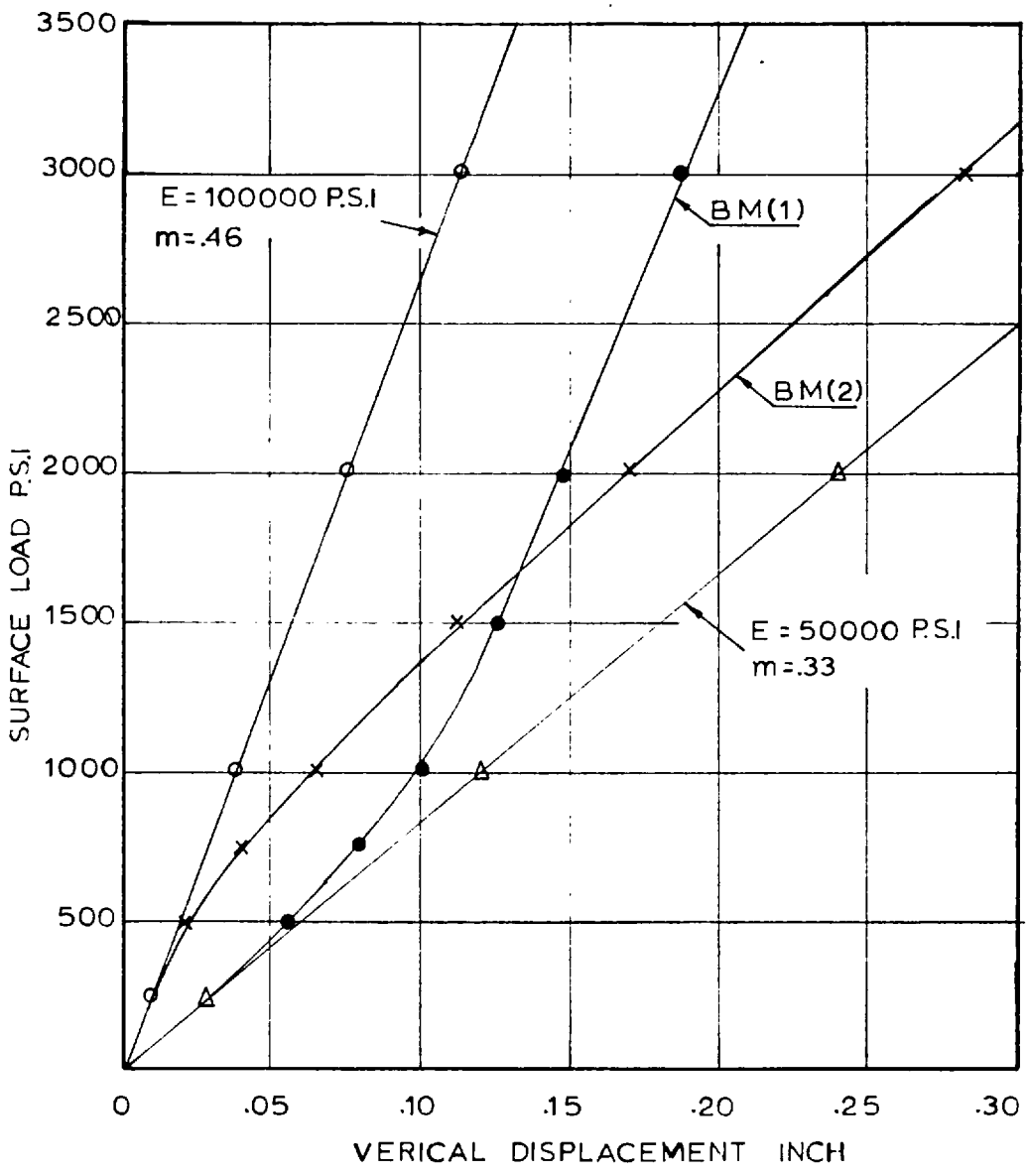
NOTE: REF. FIG. 6.1
+VE COMPRESSION

FIG 6.7 BILINEAR MODEL 2 (B.M.2) RESULTS OF STRESSES



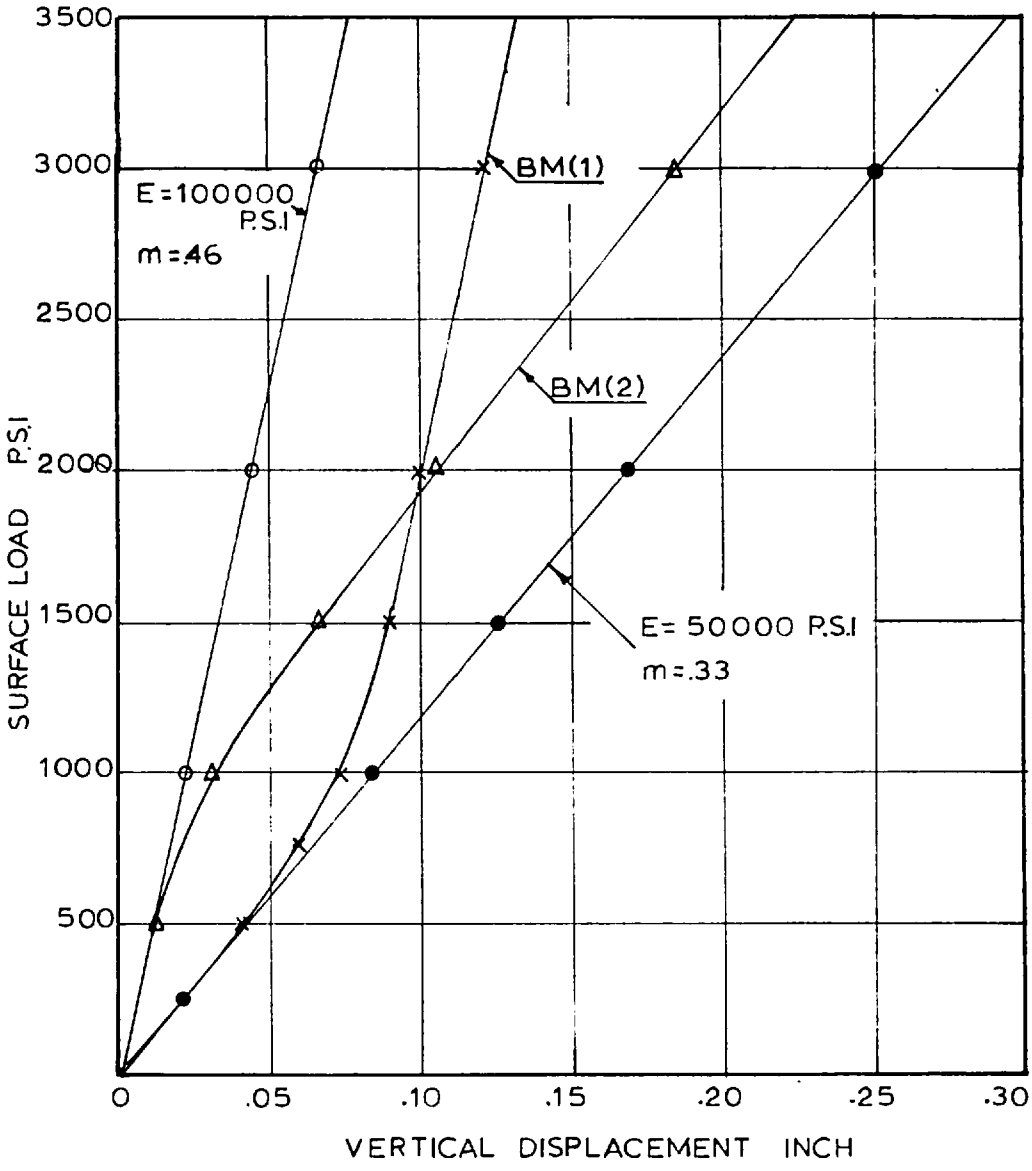
RELATIONSHIP BETWEEN SURFACE LOAD AND VERTICAL DISPLACEMENT OF POINT(1)

FIG.NO.6.8



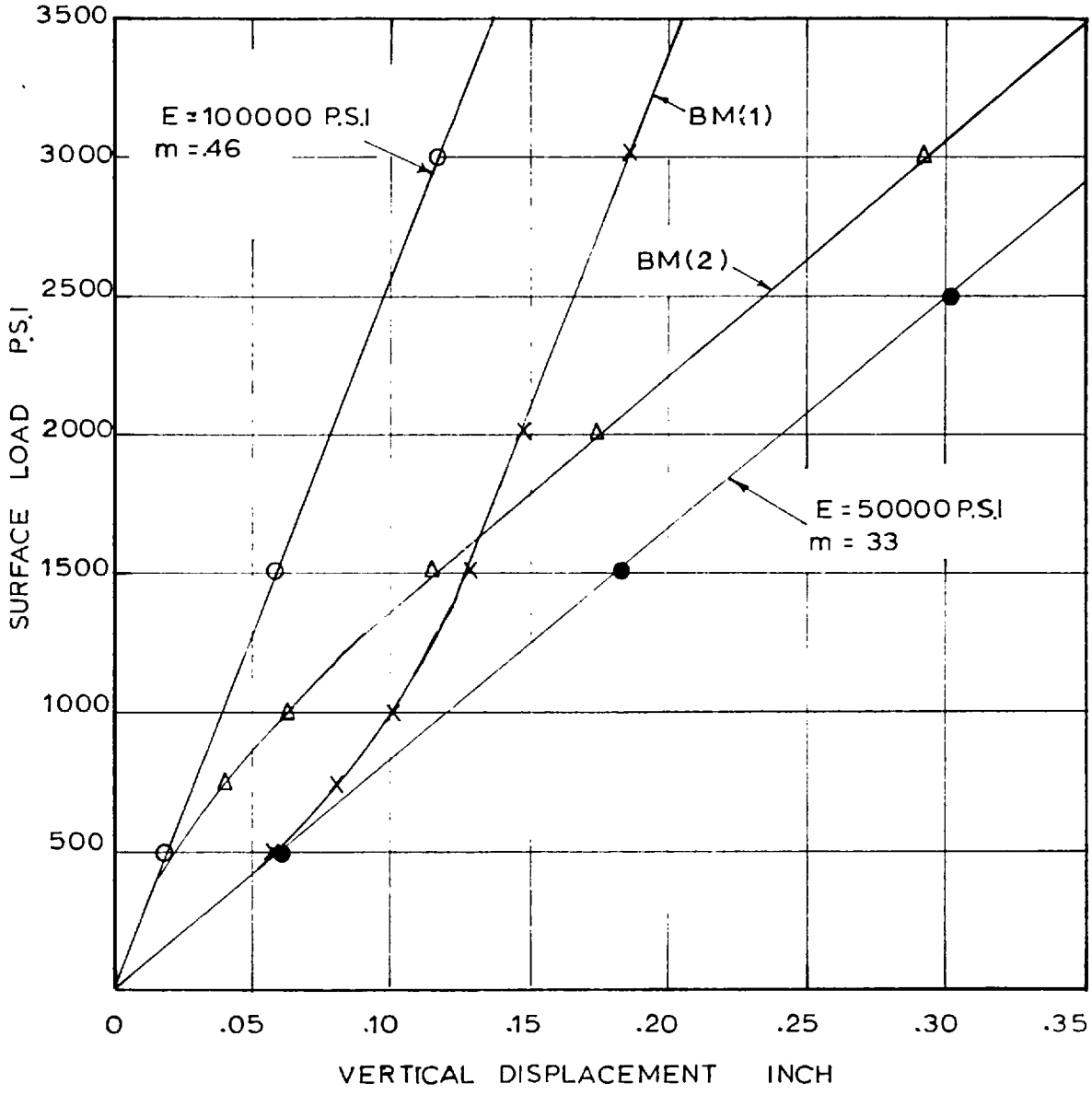
RESULTS OF POINT(2)

FIG.NO.6.9



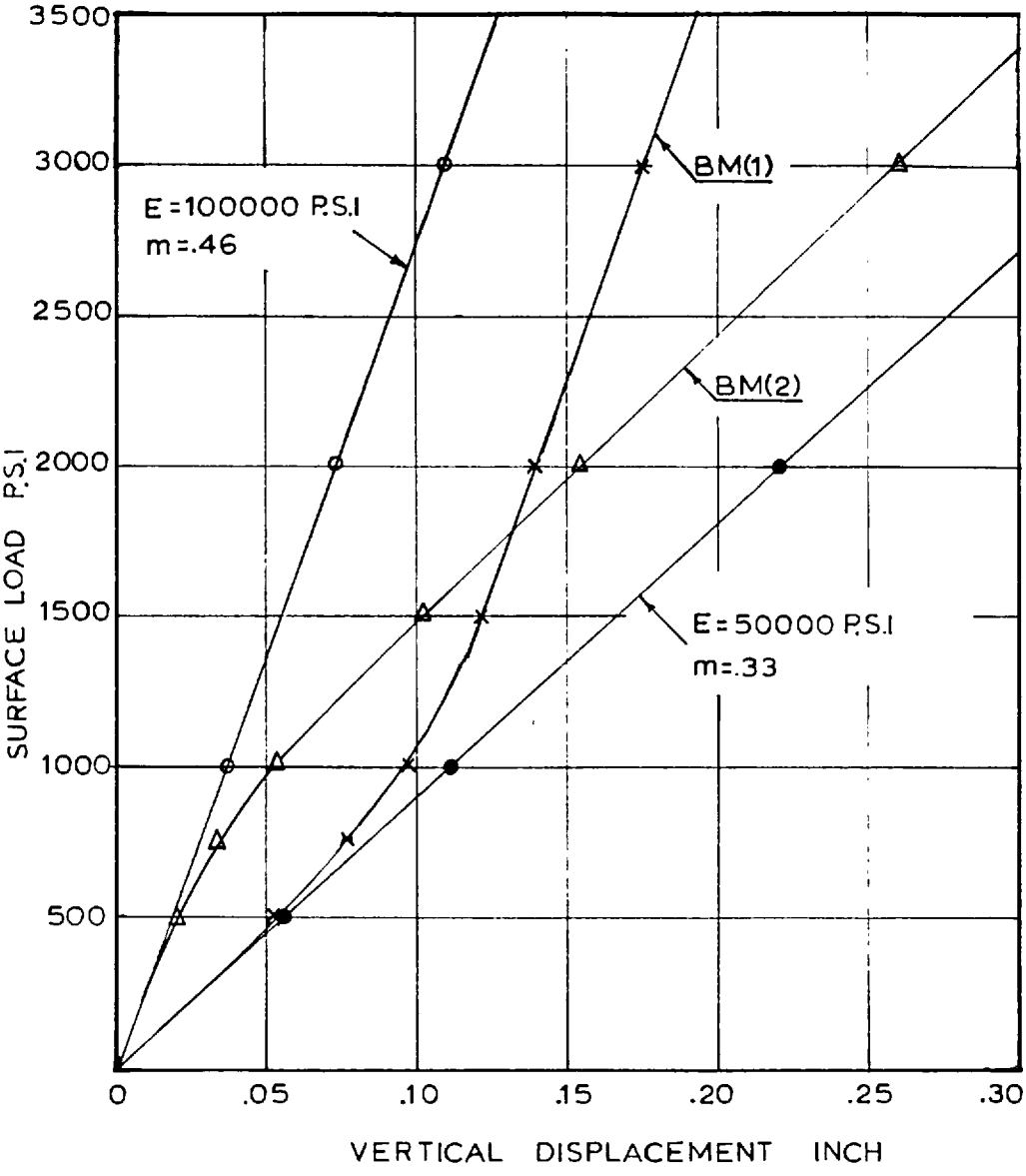
RESULTS OF POINT(3)

FIG.NO.6.10



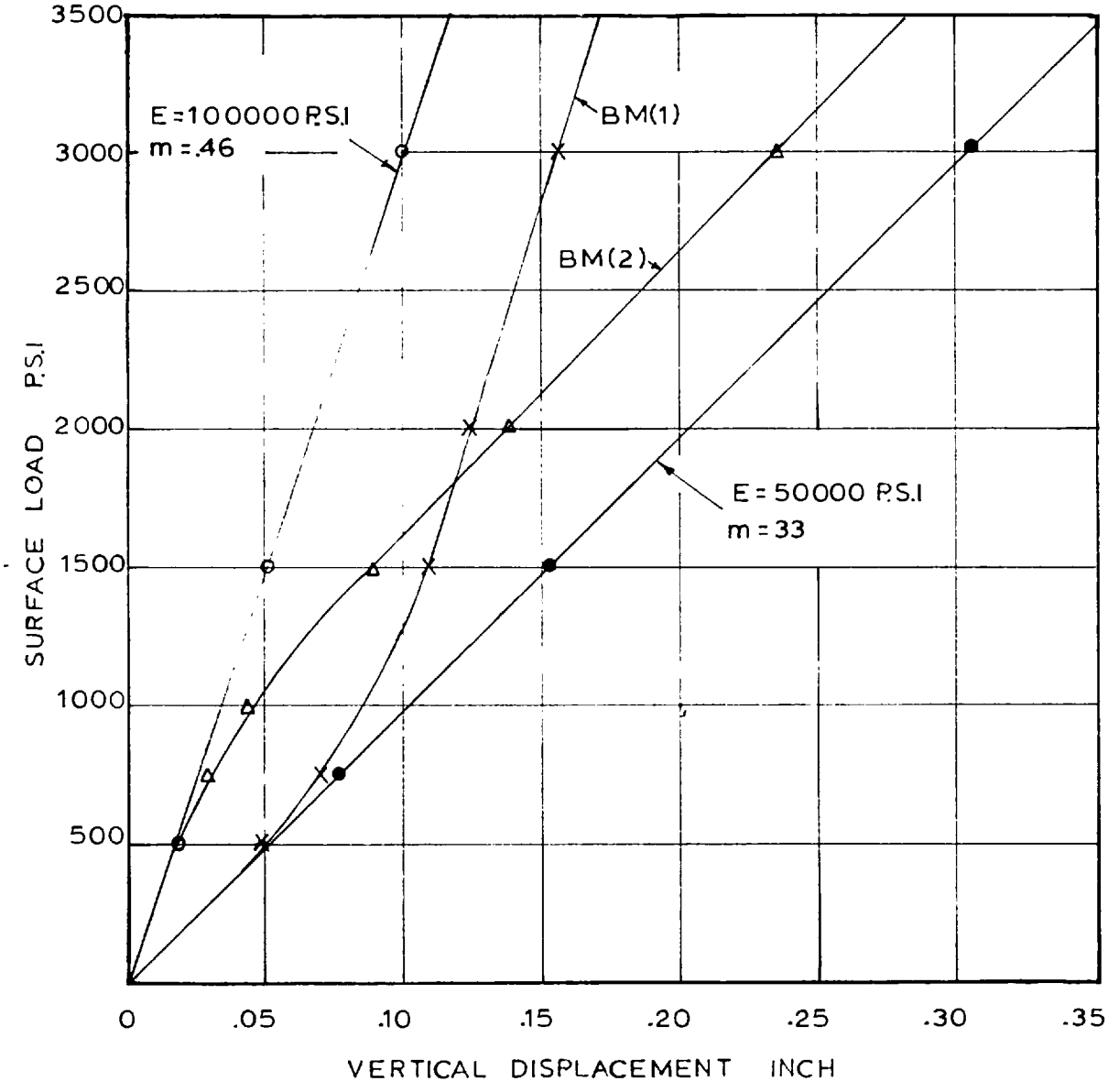
RESULTS OF POINT(4)

FIG.NO. 6.11



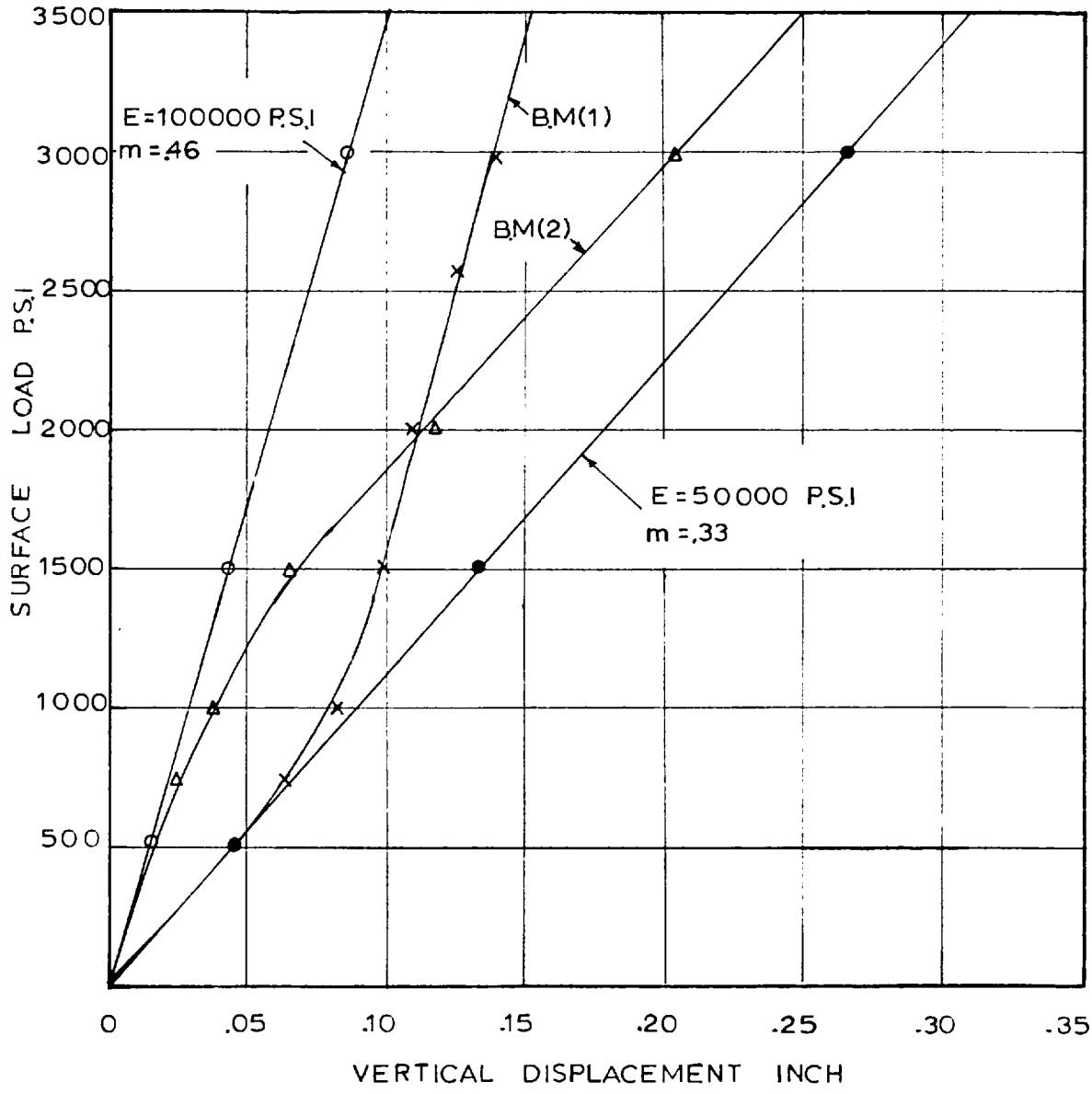
RESULTS OF POINT(5)

FIG.NO.6.12



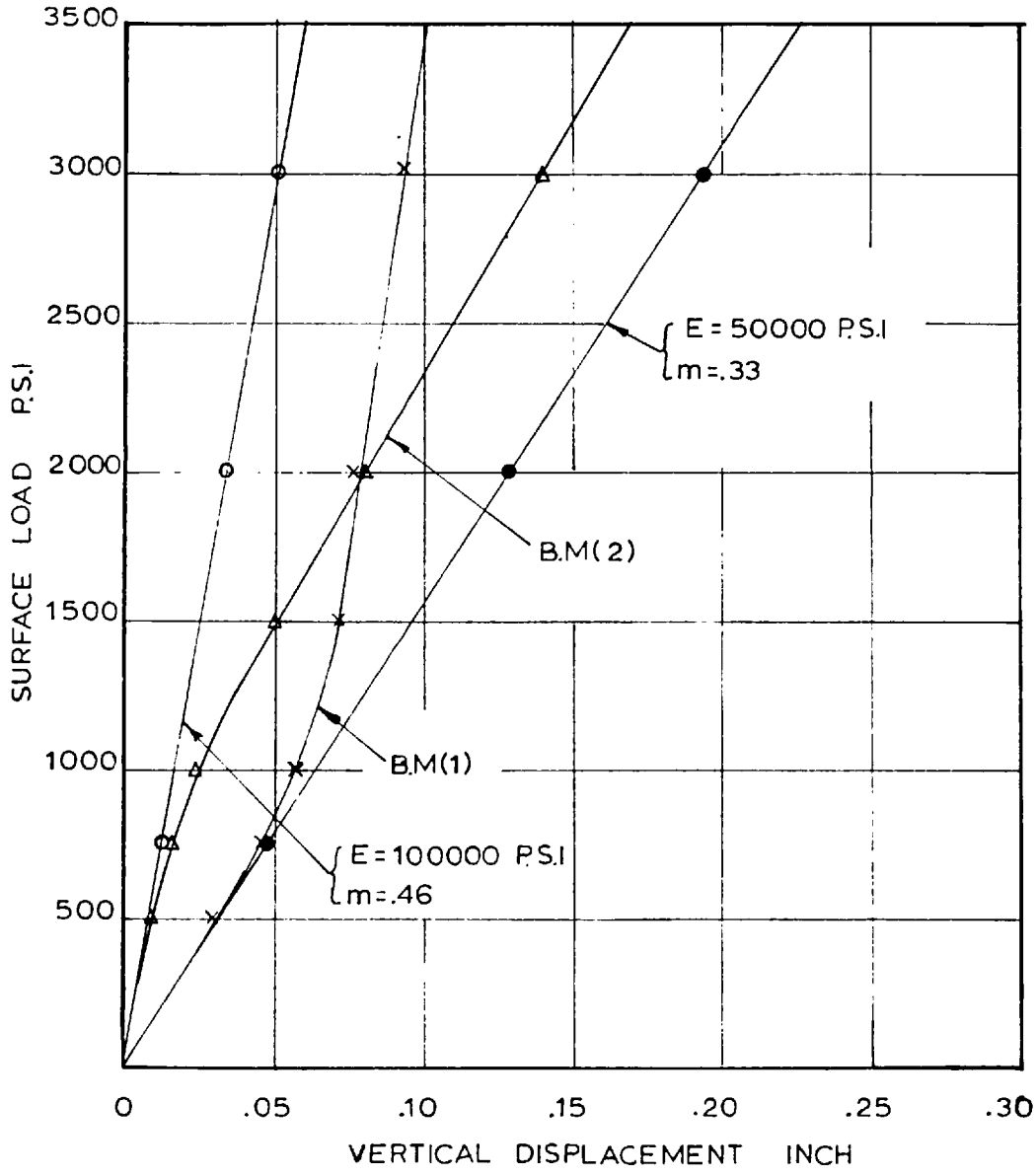
RESULTS OF POINT(6)

FIG.NO.6.13



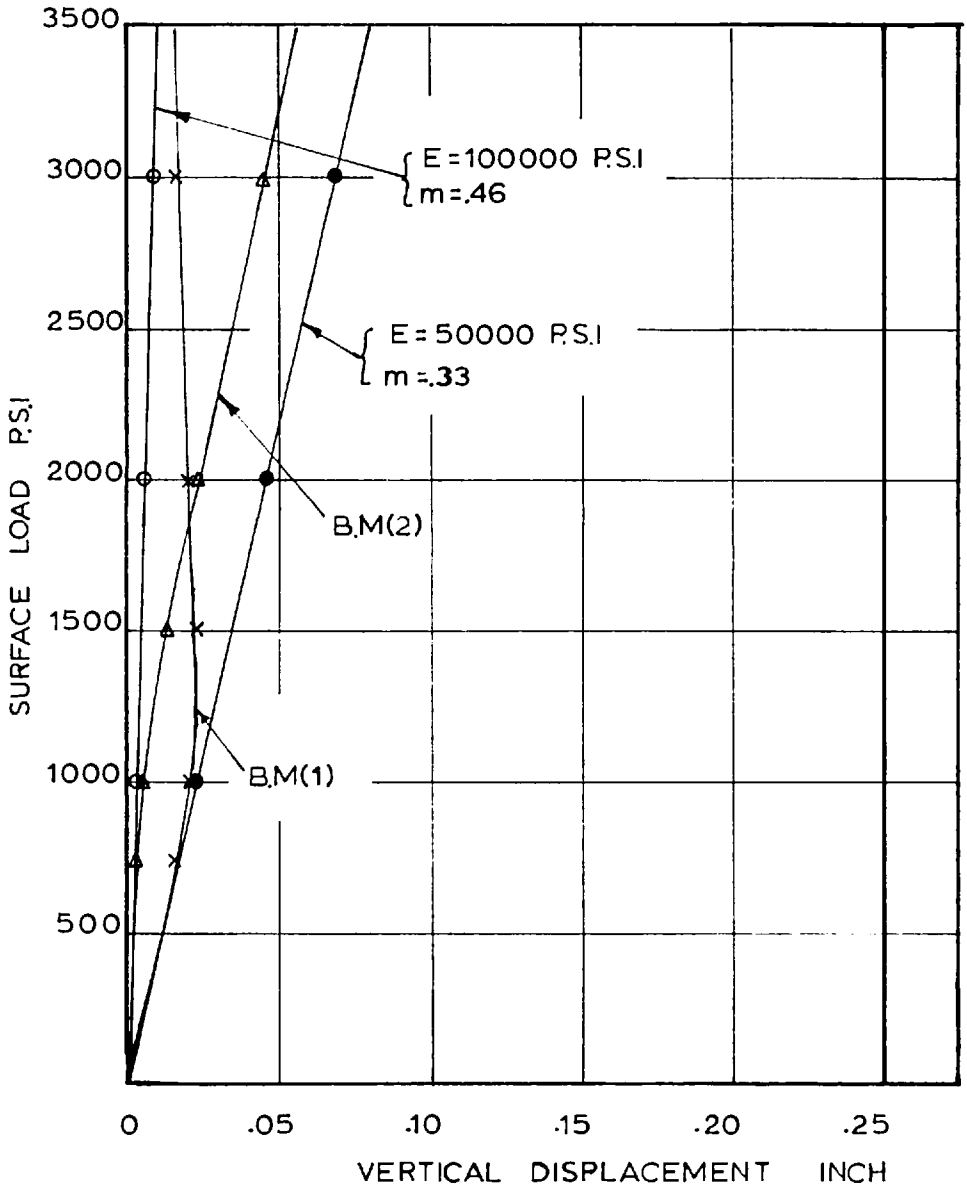
RESULTS OF POINT(7)

FIG.NO.6.14



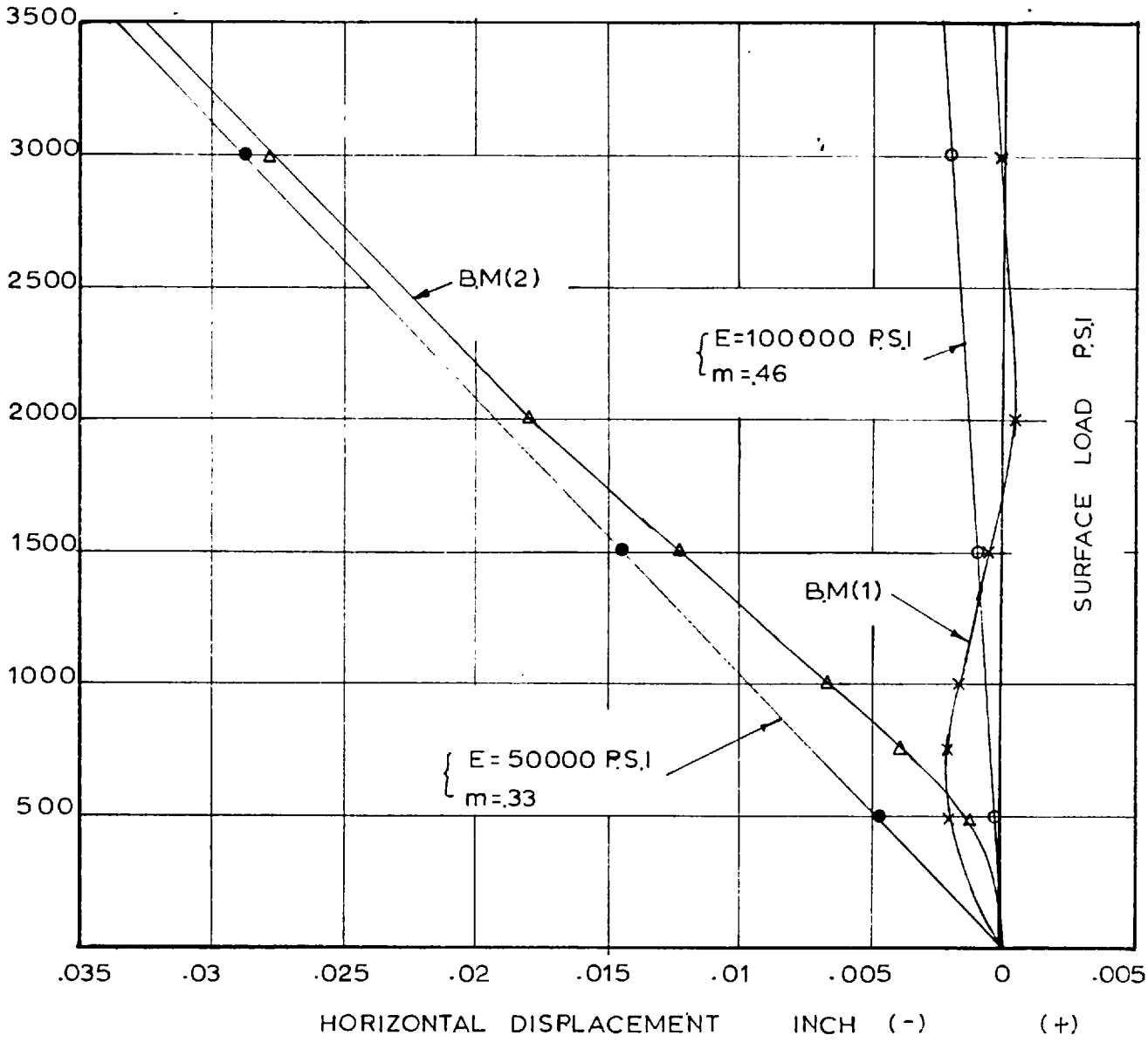
RESULTS OF POINT(8)

FIG.NO. 6.15



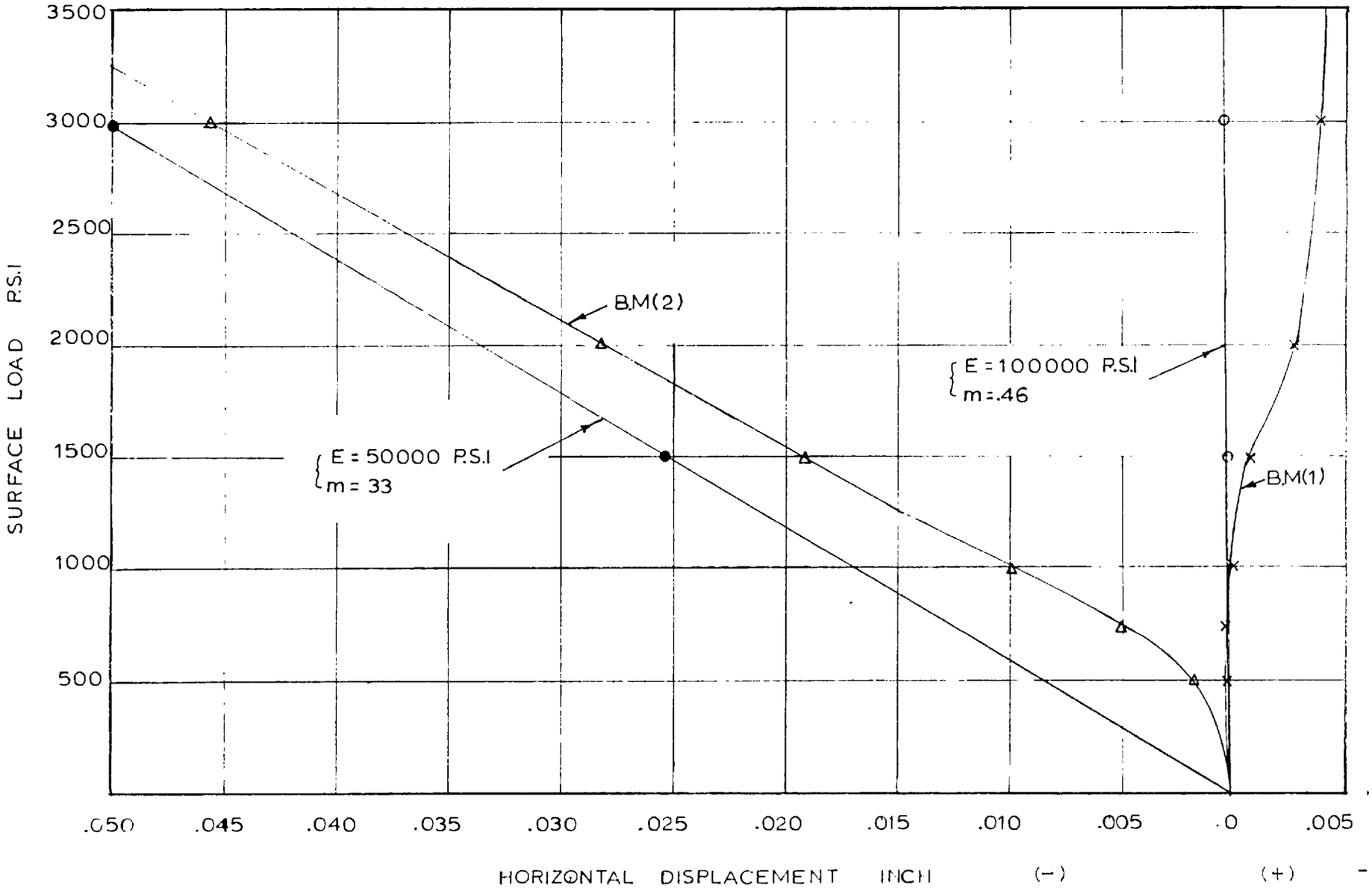
RESULTS OF POINT(9)

FIG.NO.6.16



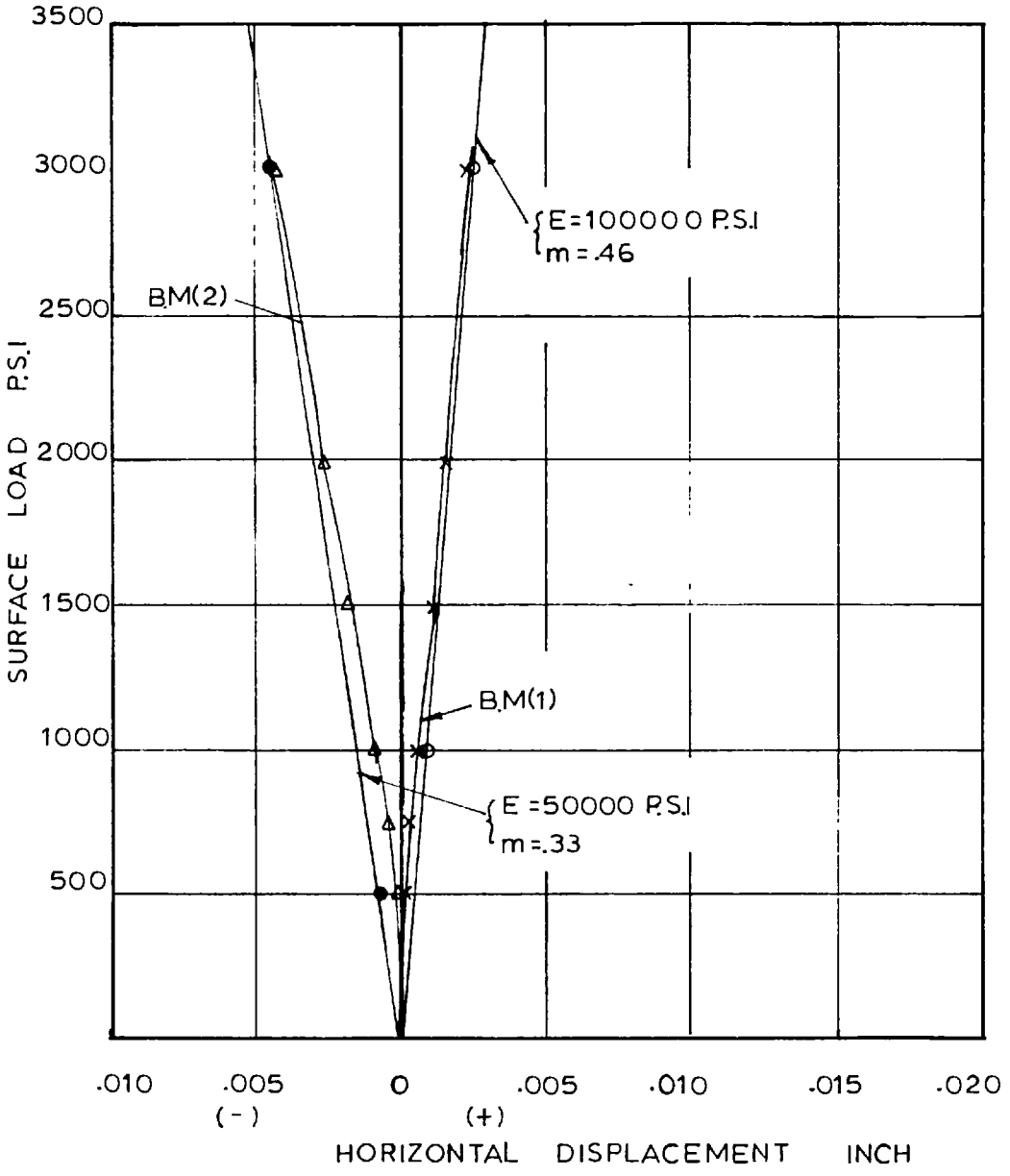
RESULTS OF POINT(2)

FIG.NO. 6.17



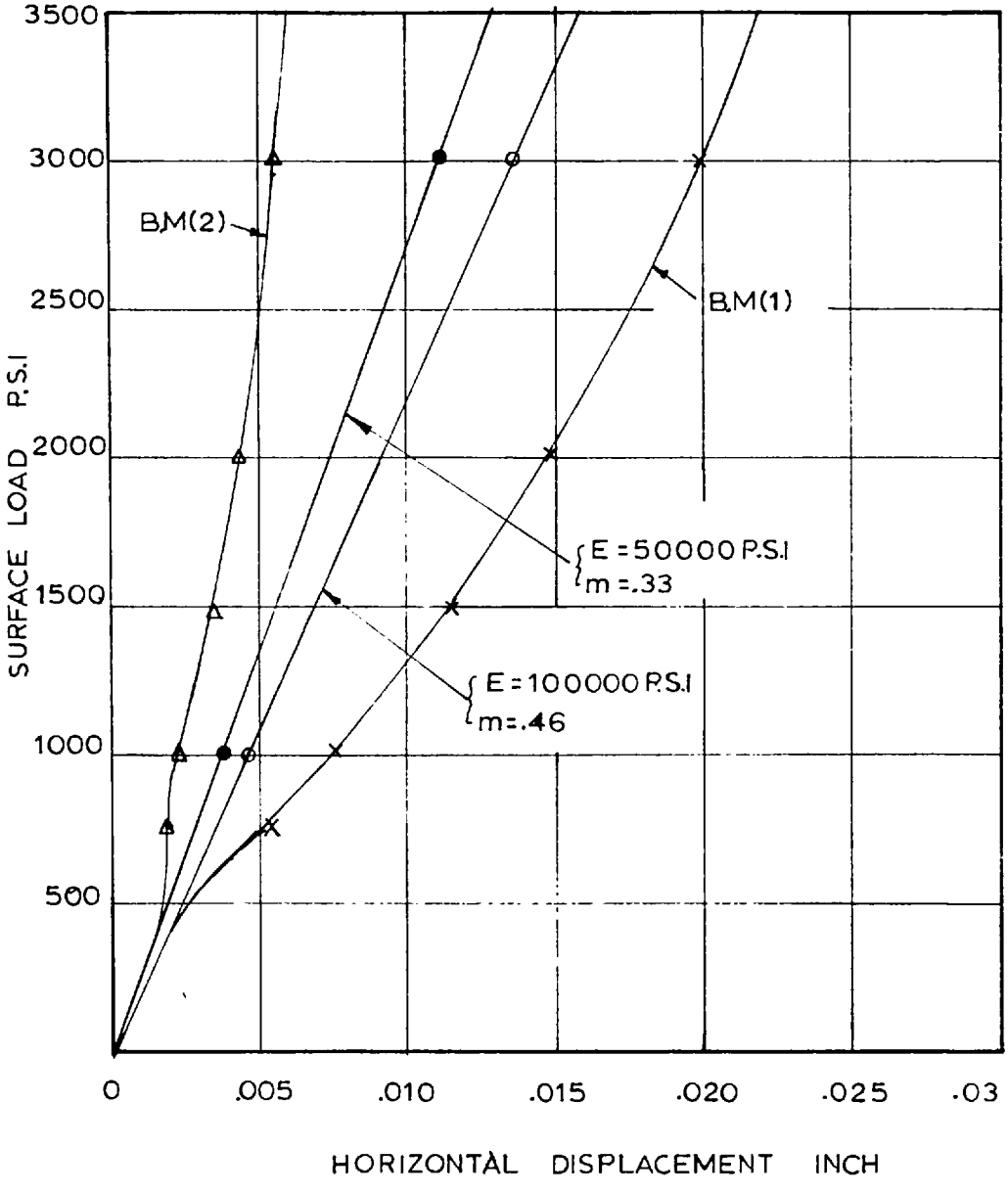
RESULTS OF POINT(3)

FIG.NO.6.18



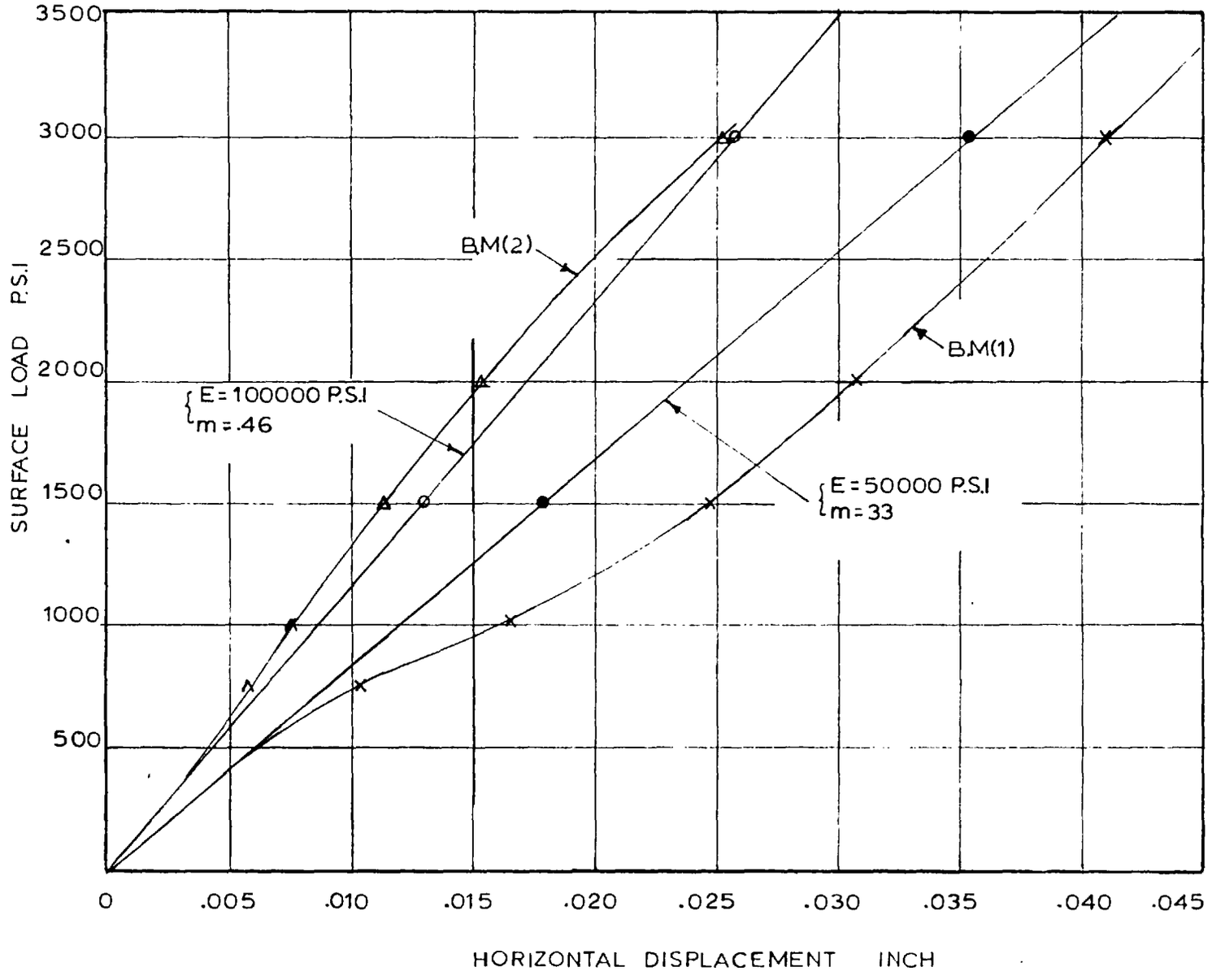
RESULTS OF POINT (4)

FIG.NO.6.19



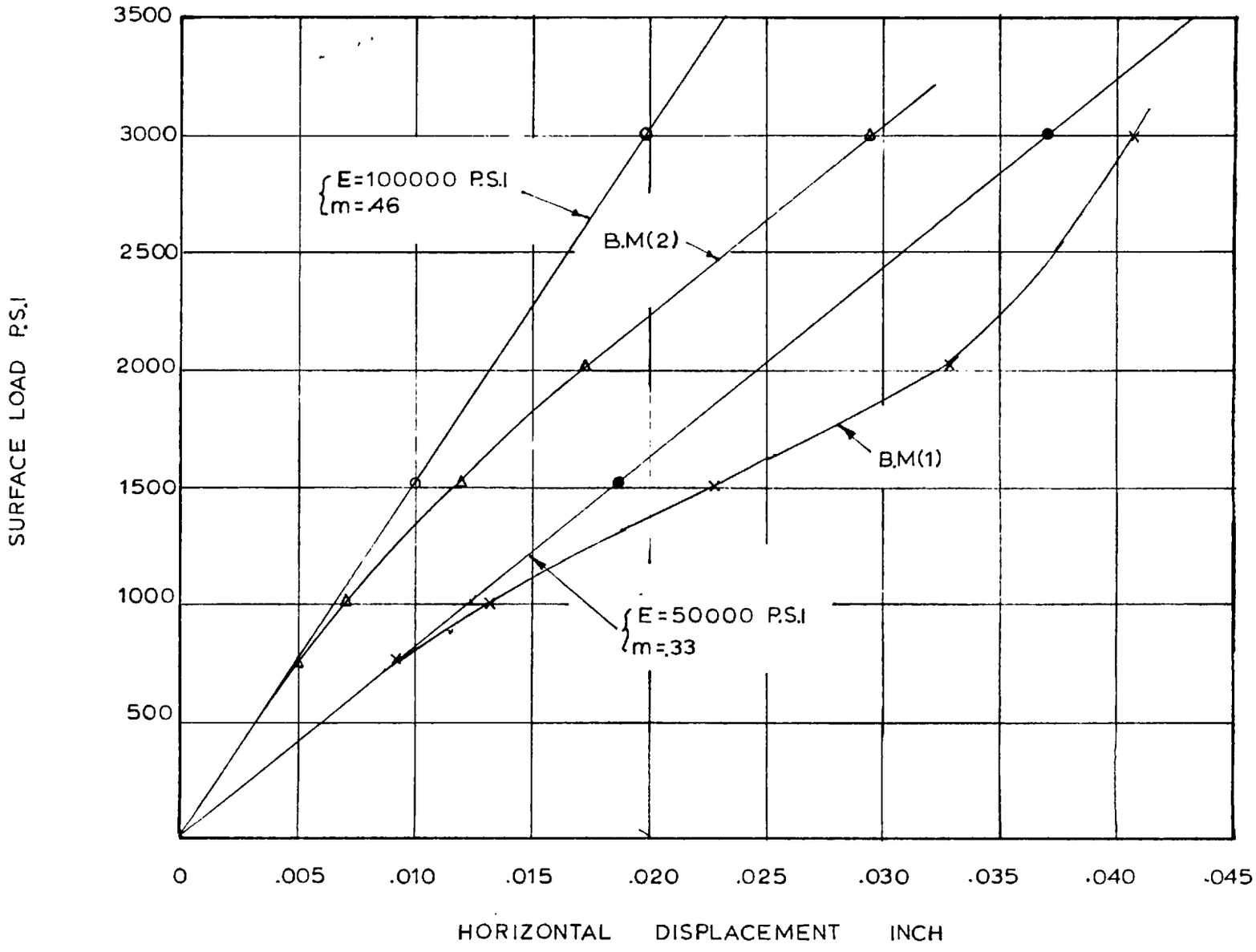
RESULTS OF POINT(6)

FIG.NO. 6.20



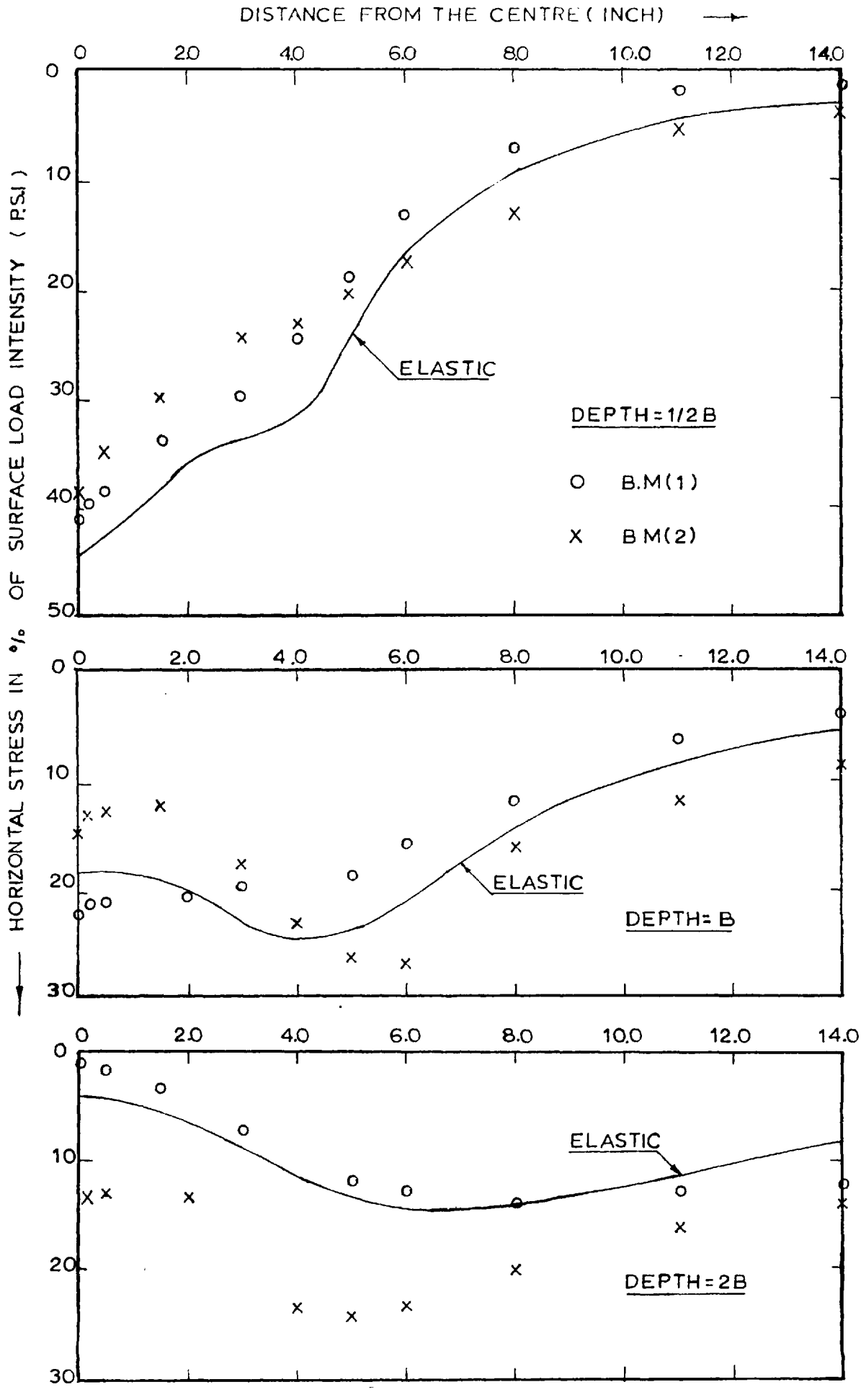
RESULTS OF POINT (8)

FIG.NO. 6.21



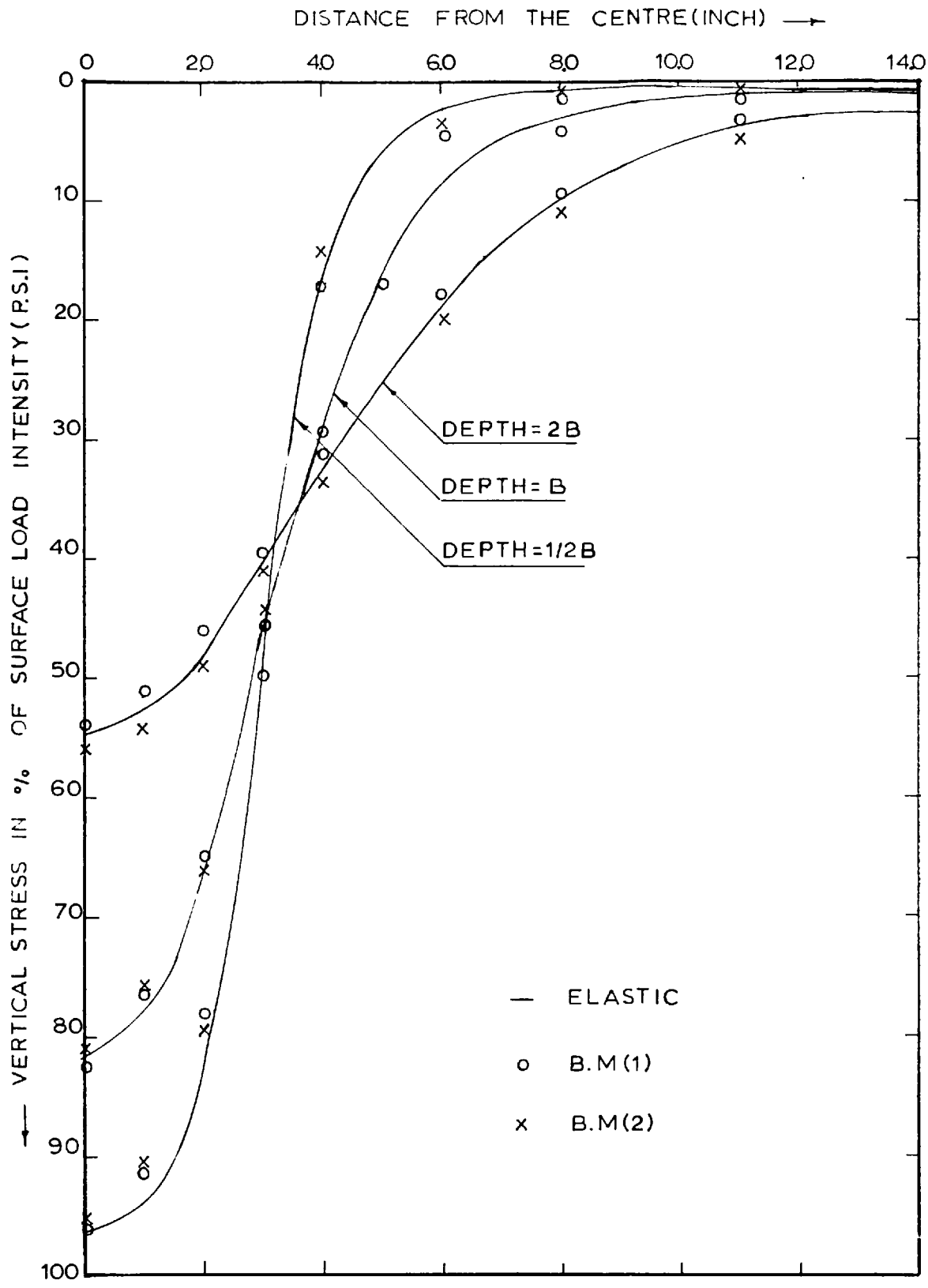
RESULTS OF POINT(9)

FIG.NO.6.22



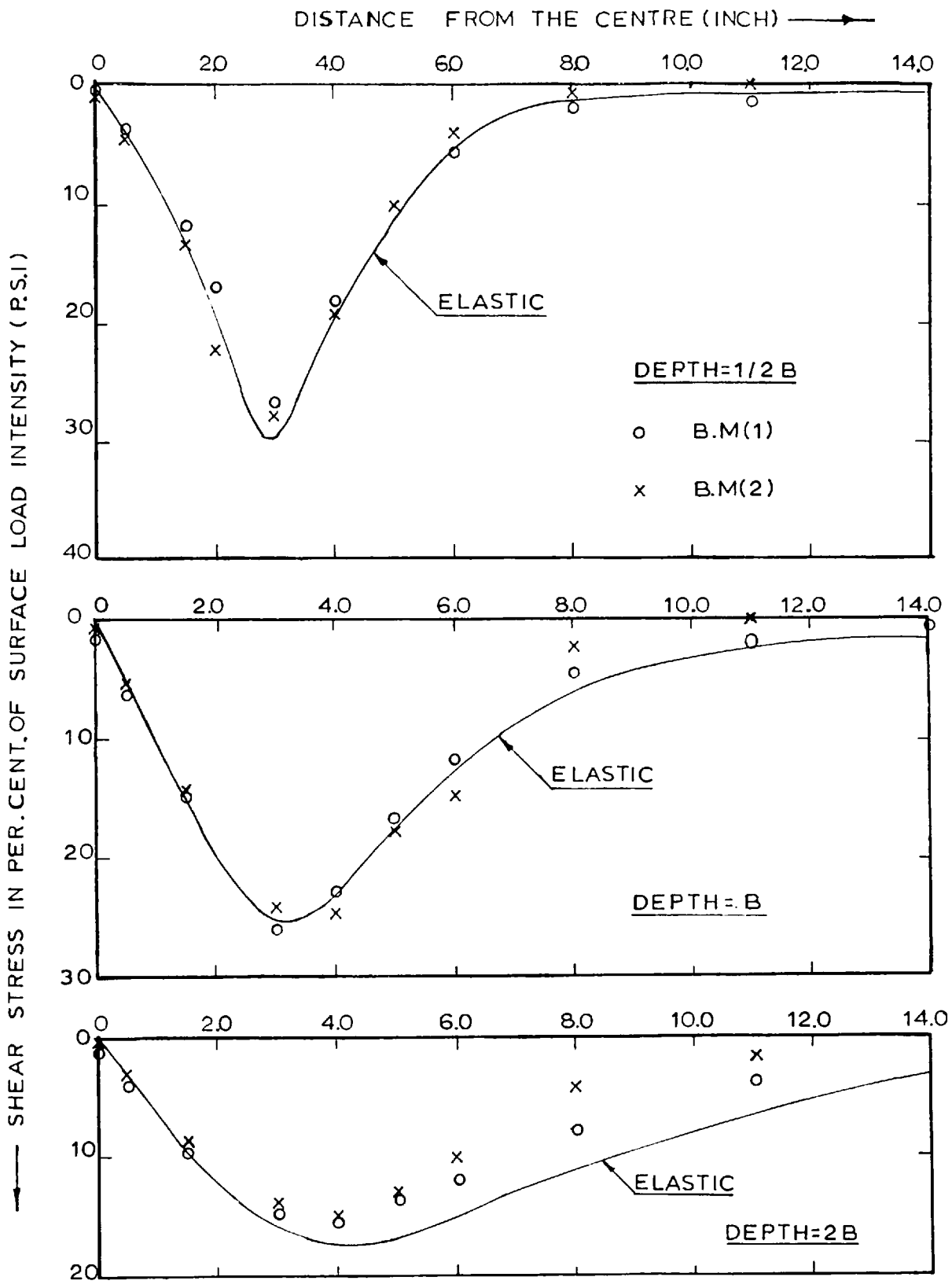
LOAD=1000 P.S.I

FIG.6.23



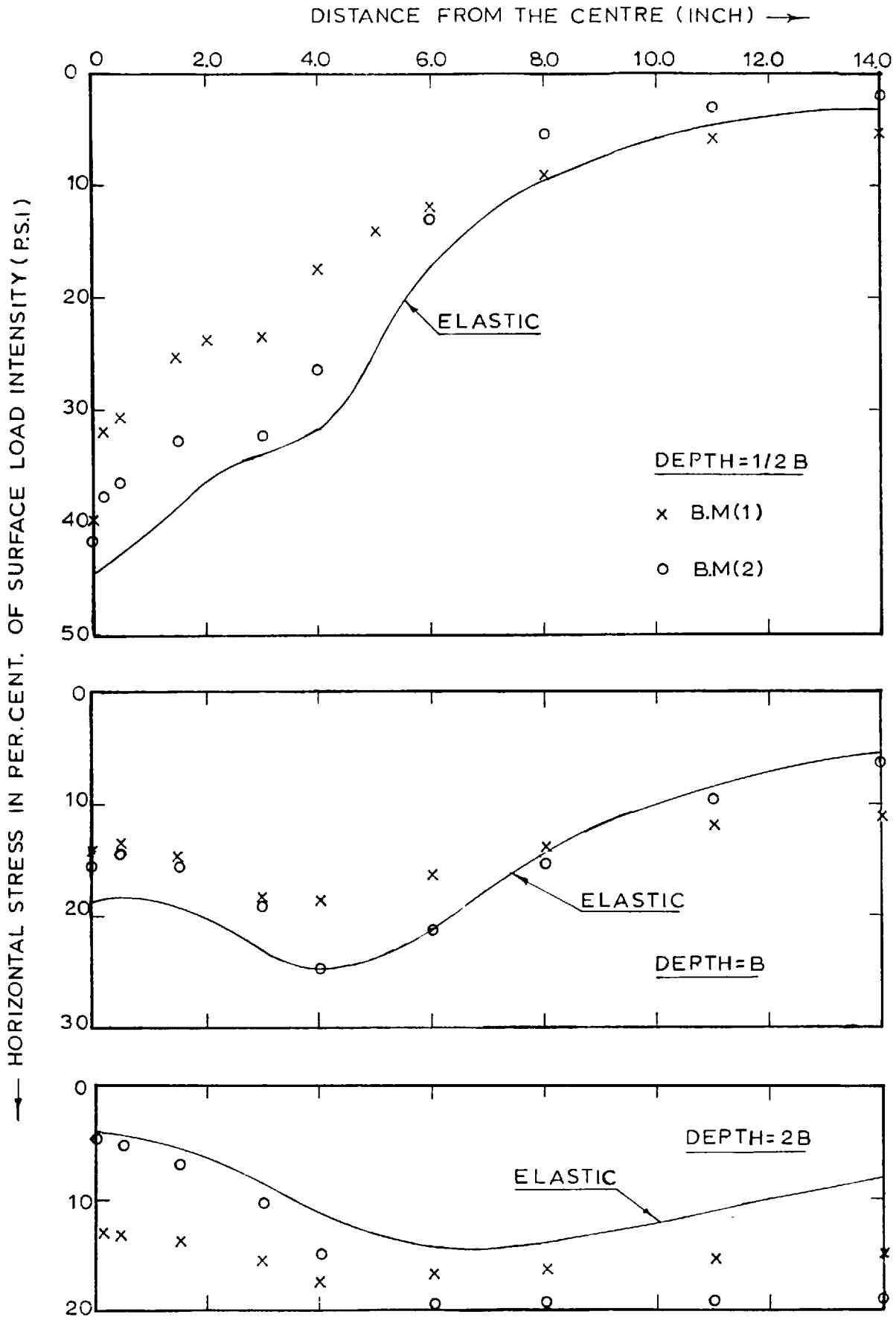
LOAD=1000 P.S.I

FIG. 6.24



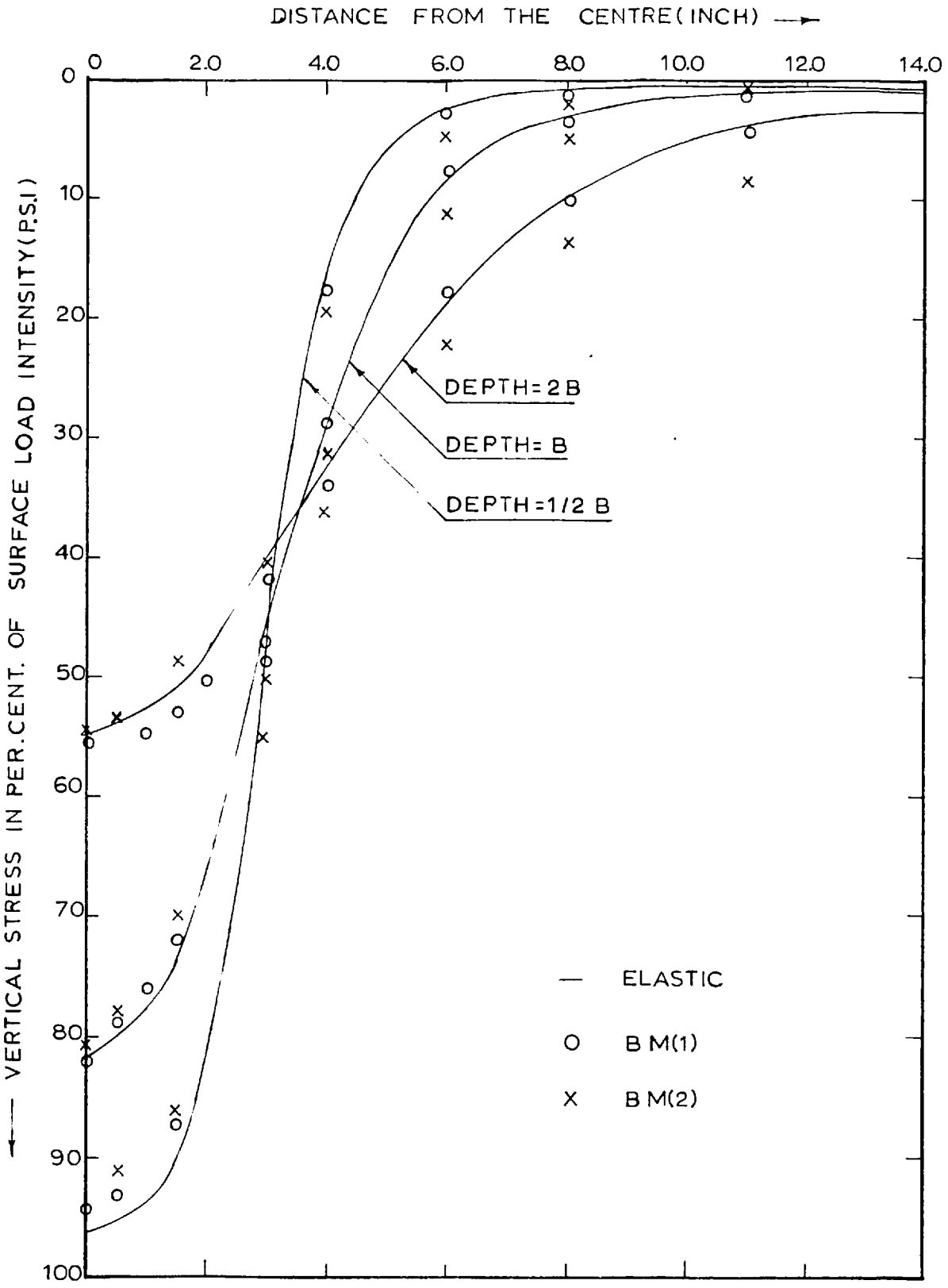
LOAD = 1000 P.S.I

FIG.6.25



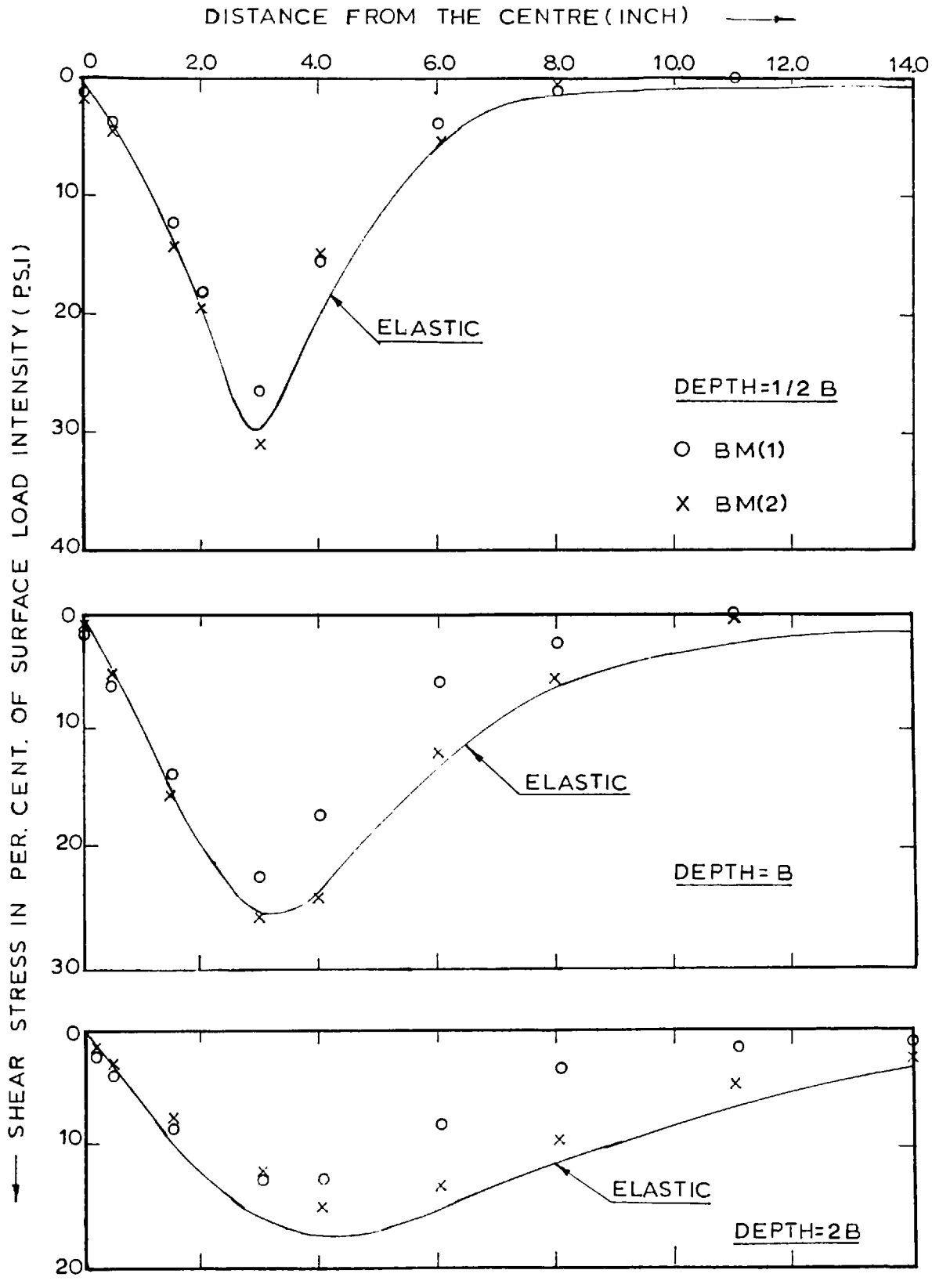
LOAD = 2000 P.S.I

FIG.6.26



LOAD=2000 P.S.I

FIG.6.27



LOAD= 2000 P.S.I

FIG.6.28

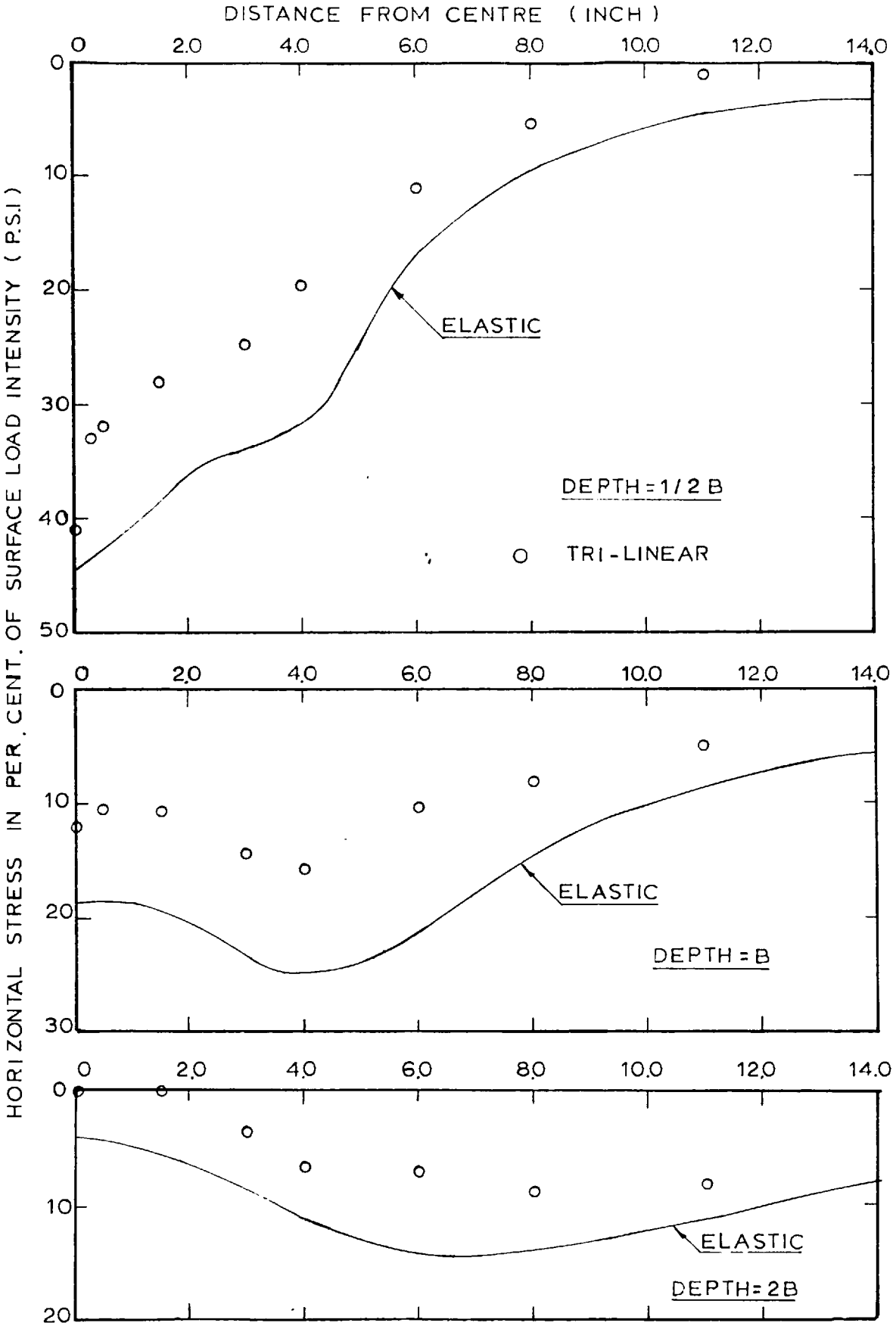

DISTANCE FROM CENTRE (INCH)
0
2.0
4.0
6.0
8.0
10.0
12.0
14.0
HORIZONTAL STRESS IN PER. CENT. OF SURFACE LOAD INTENSITY (P.S.I)
0
10
20
30
40
50
ELASTIC
DEPTH = 1/2 B
TRI-LINEAR
ELASTIC
DEPTH = B
ELASTIC
DEPTH = 2B

FIG. 6.29

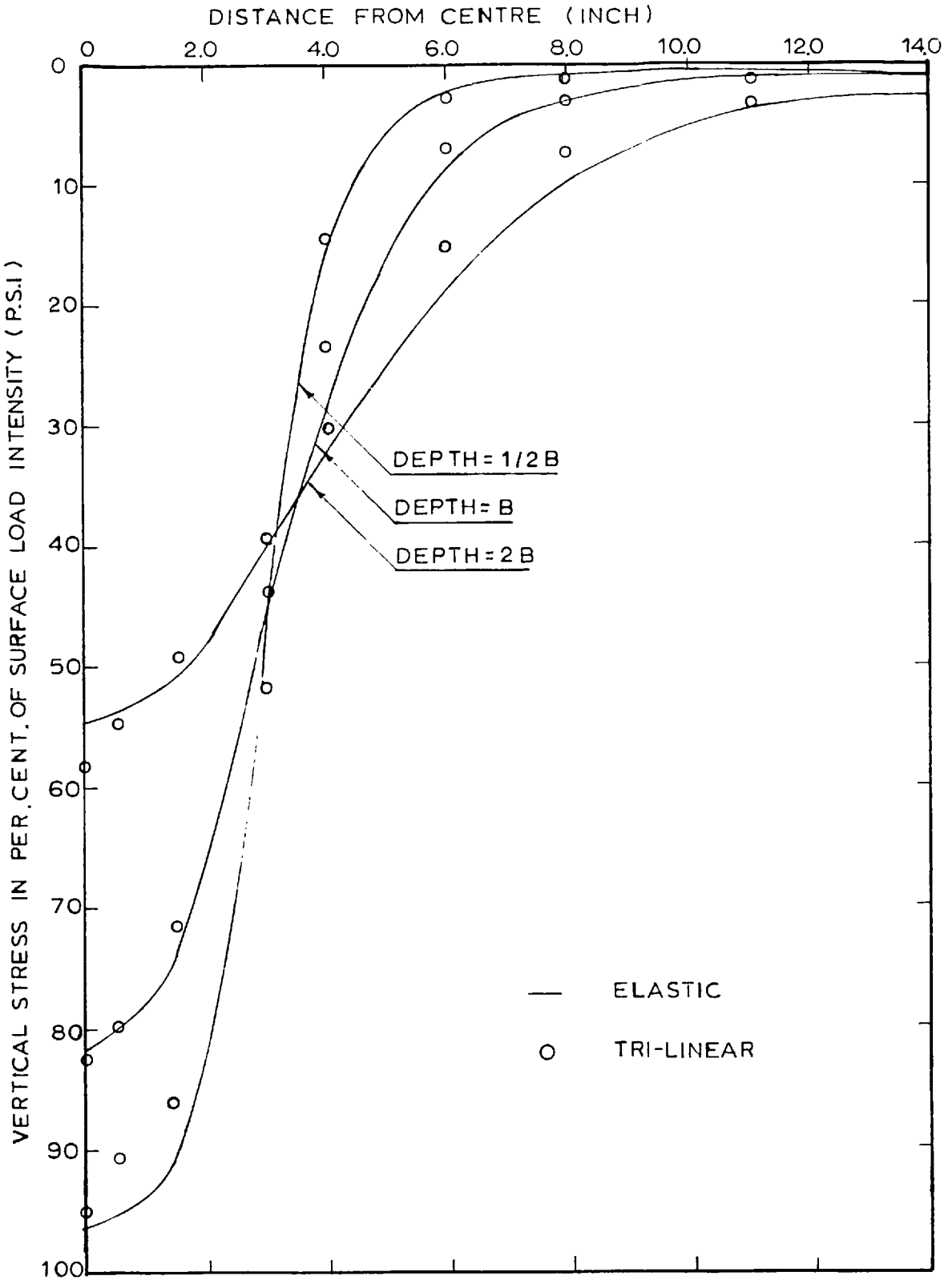

DISTANCE FROM CENTRE (INCH)
0
2.0
4.0
6.0
8.0
10.0
12.0
14.0
VERTICAL STRESS IN PER. CENT. OF SURFACE LOAD INTENSITY (P.S.I)
0
10
20
30
40
50
60
70
80
90
100
DEPTH = 1/2 B
DEPTH = B
DEPTH = 2 B
ELASTIC
TRI-LINEAR

FIG.6.30

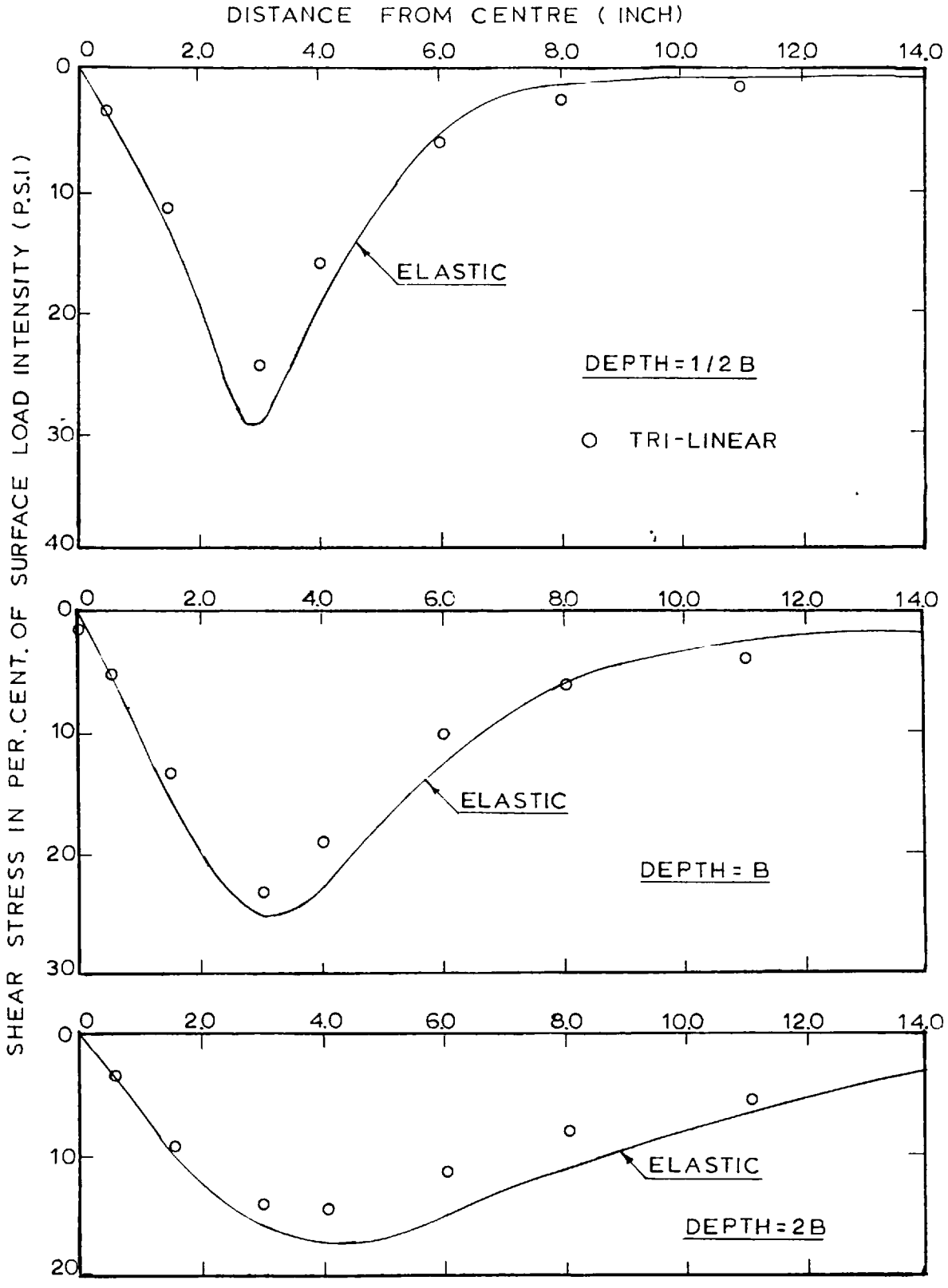

DISTANCE FROM CENTRE (INCH)
0
2.0
4.0
6.0
8.0
10.0
12.0
14.0
SHEAR STRESS IN PER.CENT. OF SURFACE LOAD INTENSITY (P.S.I)
0
10
20
30
40
ELASTIC
DEPTH=1/2 B
O TRI-LINEAR
ELASTIC
DEPTH = B
ELASTIC
DEPTH=2B

FIG. 6.31

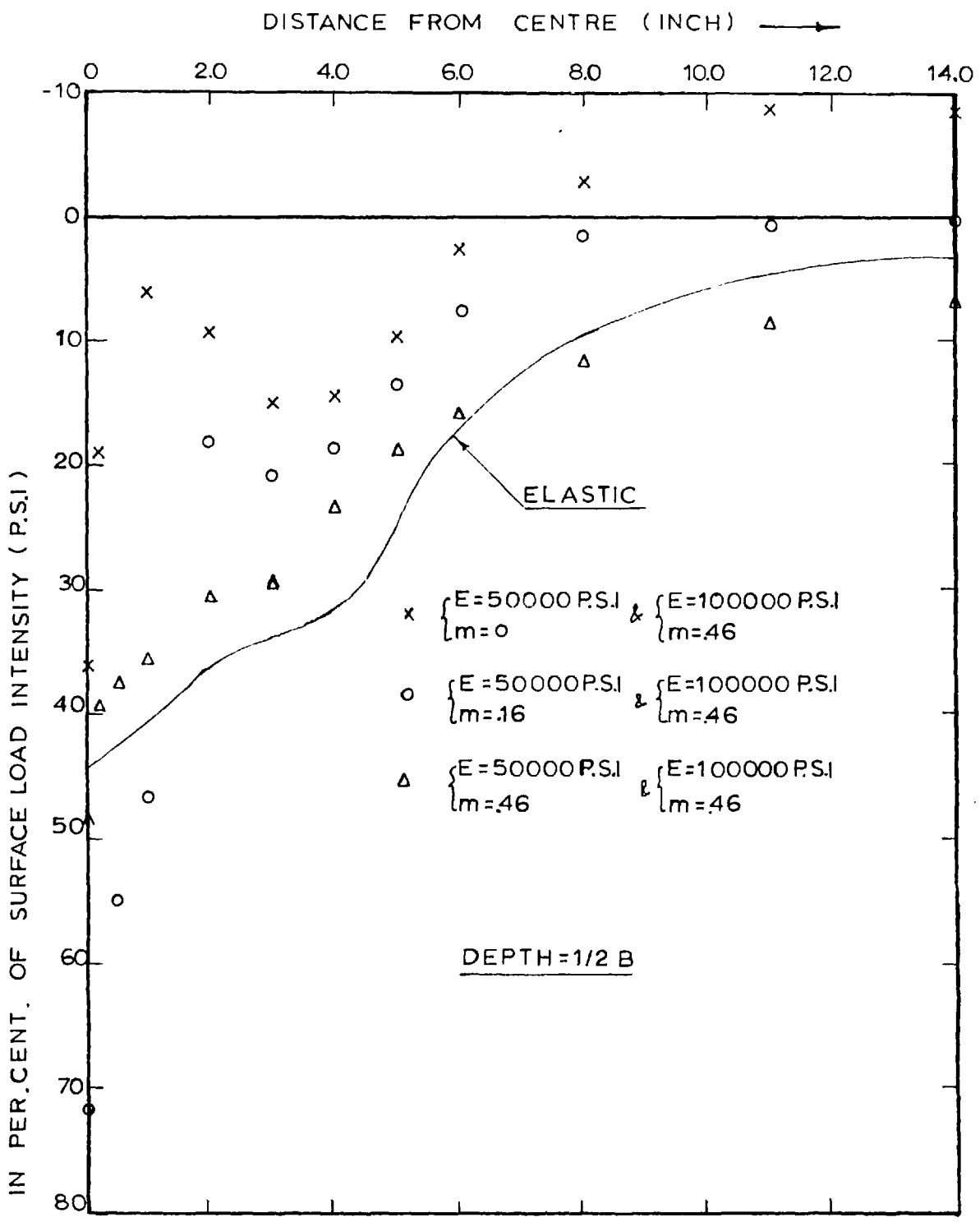

DISTANCE FROM CENTRE (INCH)
0
2.0
4.0
6.0
8.0
10.0
12.0
14.0
-10
0
10
20
30
40
50
60
70
80
HORIZONTAL STRESS IN PER.CENT. OF SURFACE LOAD INTENSITY (P.S.I)
ELASTIC
× {E=50000 P.S.I m=0 & {E=100000 P.S.I m=.46
o {E=50000 P.S.I m=.16 & {E=100000 P.S.I m=.46
Δ {E=50000 P.S.I m=.46 & {E=100000 P.S.I m=.46
DEPTH=1/2 B
ELASTIC
DEPTH=B
ELASTIC
DEPTH=2B

FIG. 6.32

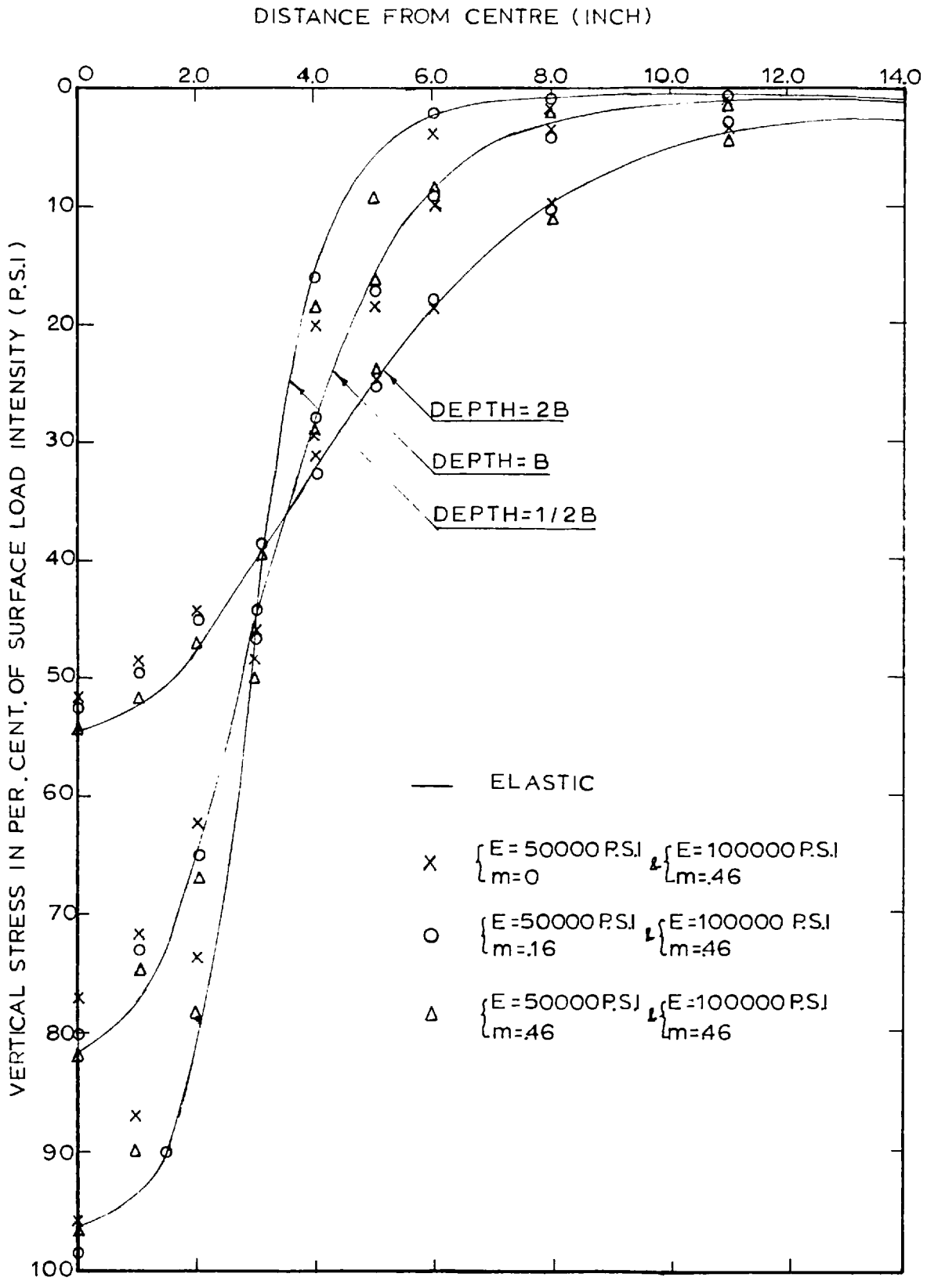

DISTANCE FROM CENTRE (INCH)
0
2.0
4.0
6.0
8.0
10.0
12.0
14.0
VERTICAL STRESS IN PER. CENT. OF SURFACE LOAD INTENSITY (P.S.I.)
0
10
20
30
40
50
60
70
80
90
100
DEPTH=2B
DEPTH=B
DEPTH=1/2B
ELASTIC
E=50000 P.S.I m=0 & E=100000 P.S.I m=.46
E=50000 P.S.I m=.16 & E=100000 P.S.I m=.46
E=50000 P.S.I m=.46 & E=100000 P.S.I m=.46

FIG. 6.33

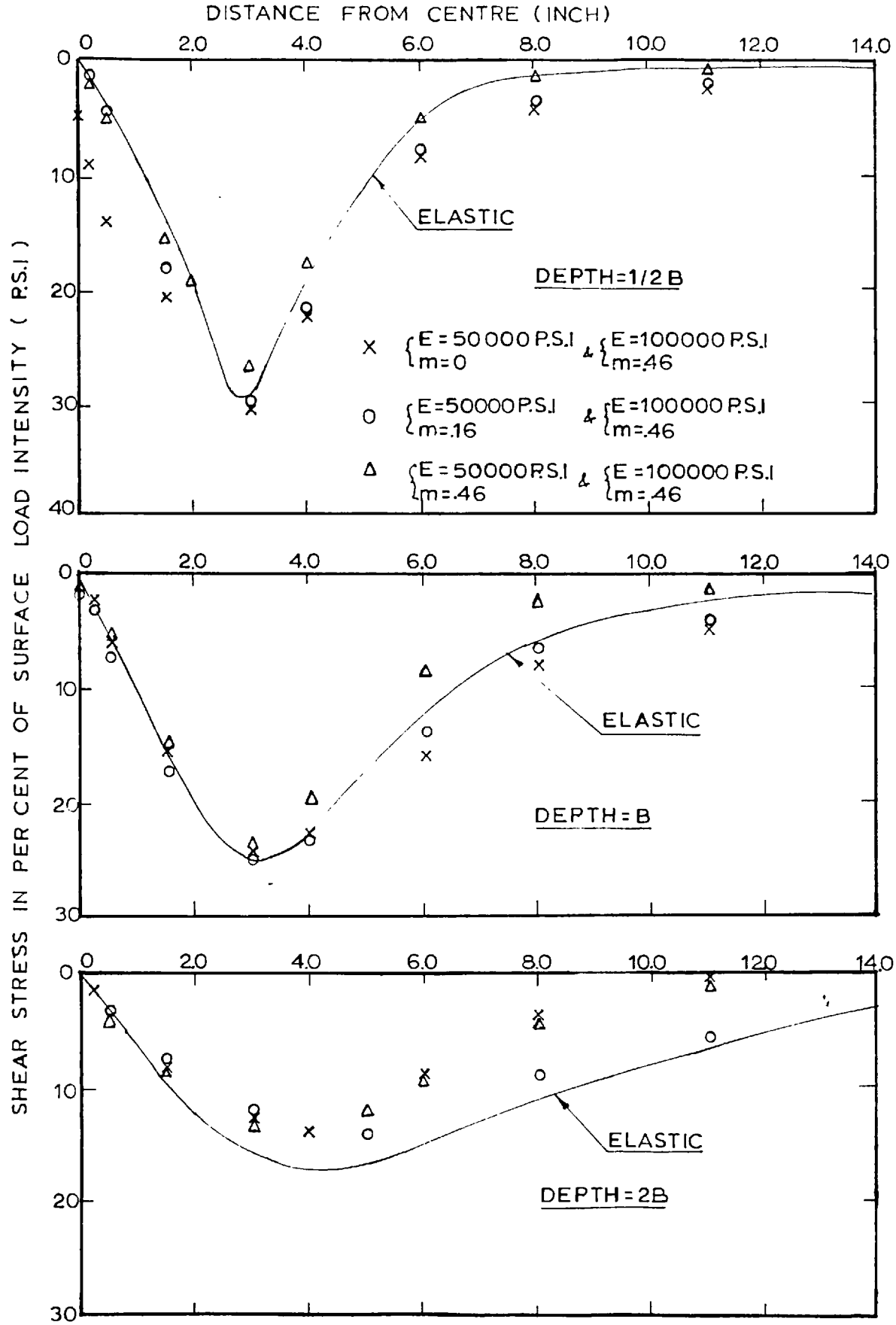
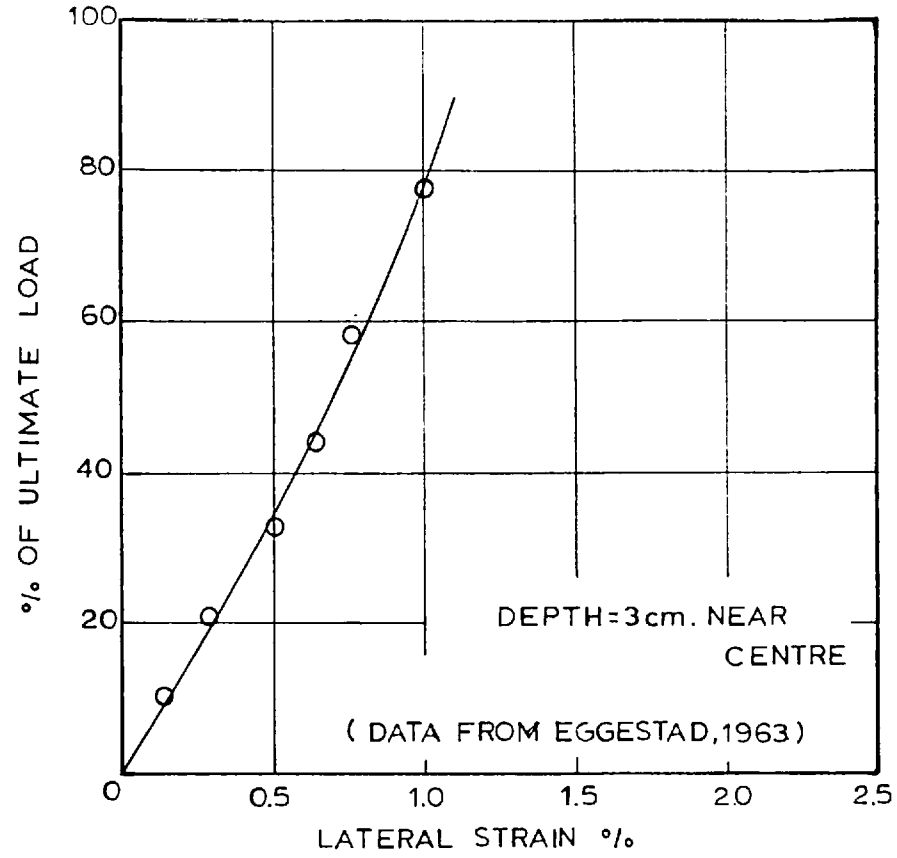

DISTANCE FROM CENTRE (INCH)
0
2.0
4.0
6.0
8.0
10.0
12.0
14.0
SHEAR STRESS IN PER CENT OF SURFACE LOAD INTENSITY (P.S.I)
0
10
20
30
40
ELASTIC
DEPTH=1/2 B
× {E = 50000 P.S.I m=0 & {E=100000 P.S.I m=.46
O {E=50000 P.S.I m=.16 & {E=100000 P.S.I m=.46
Δ {E = 50000 P.S.I m=.46 & {E =100000 P.S.I m=.46
ELASTIC
DEPTH=B
ELASTIC
DEPTH=2B

FIG. 6.34


100
80
60
40
20
0
% OF ULTIMATE LOAD
DEPTH=3cm. NEAR CENTRE
(DATA FROM EGGESTAD,1963)
0.5
1.0
1.5
2.0
2.5
LATERAL STRAIN %

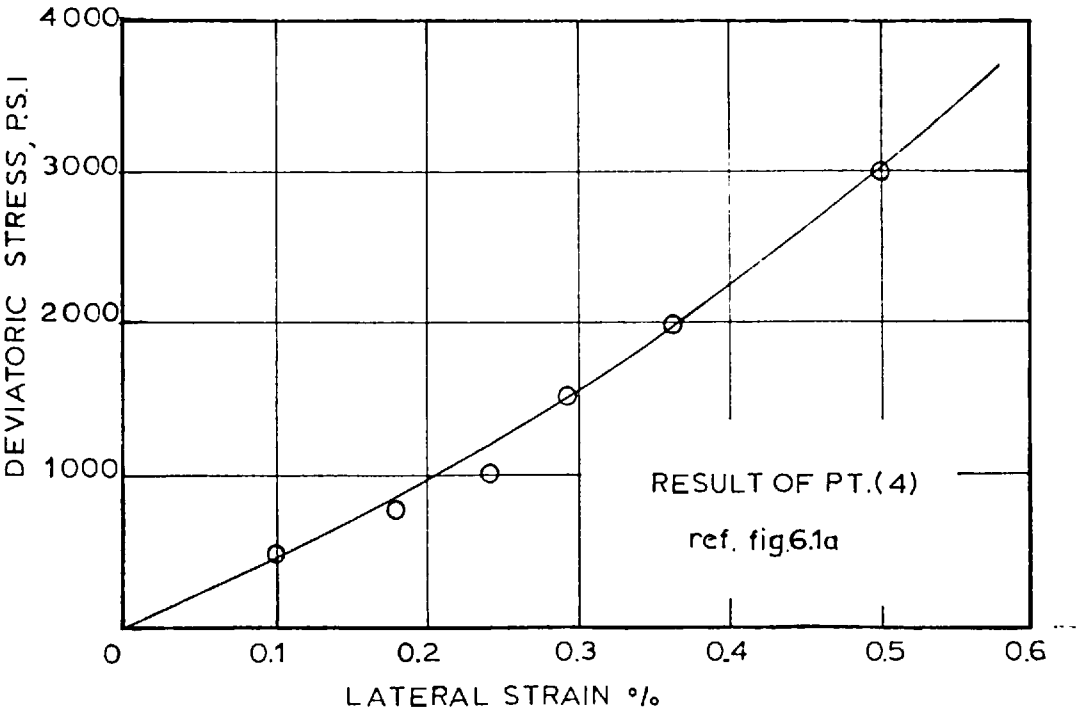
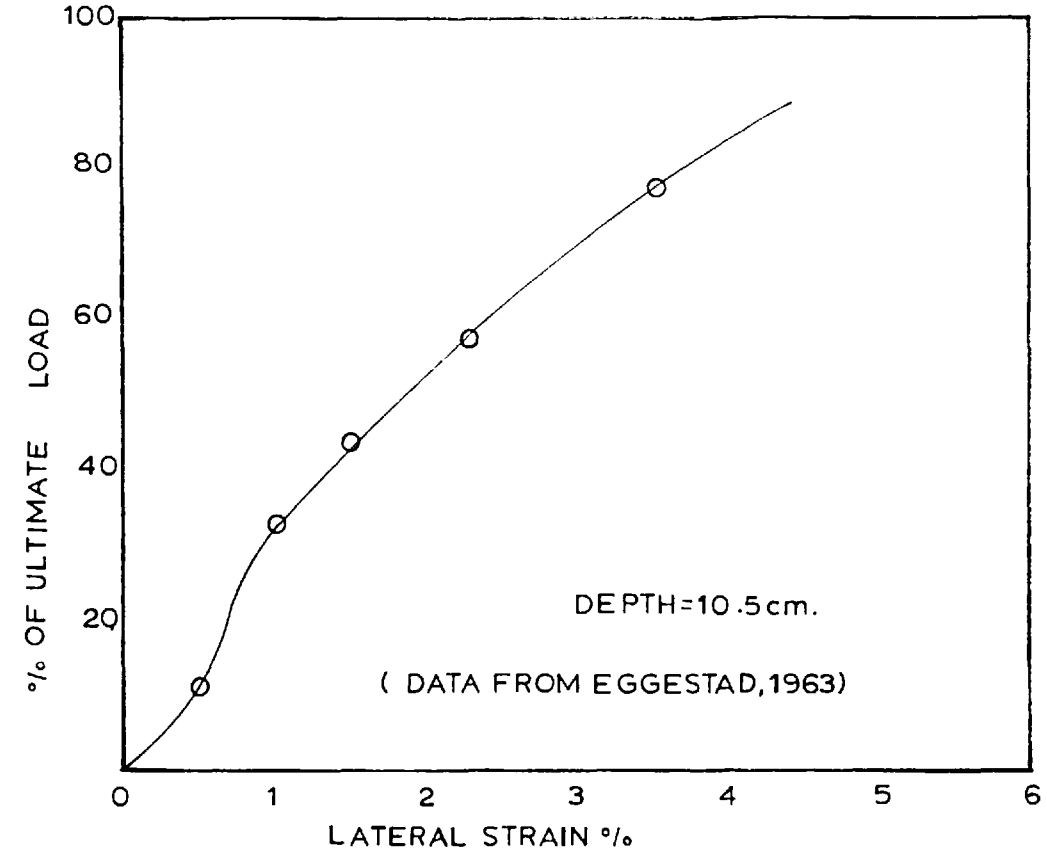

4000
3000
2000
1000
DEVIATORIC STRESS, P.S.I
RESULT OF PT.(4)
ref. fig.6.1a
0
0.1
0.2
0.3
0.4
0.5
0.6
LATERAL STRAIN %

FIG.6.35


100
80
60
40
20
% OF ULTIMATE LOAD
DEPTH=10.5cm.
(DATA FROM EGGESTAD,1963)
0
1
2
3
4
5
6
LATERAL STRAIN %

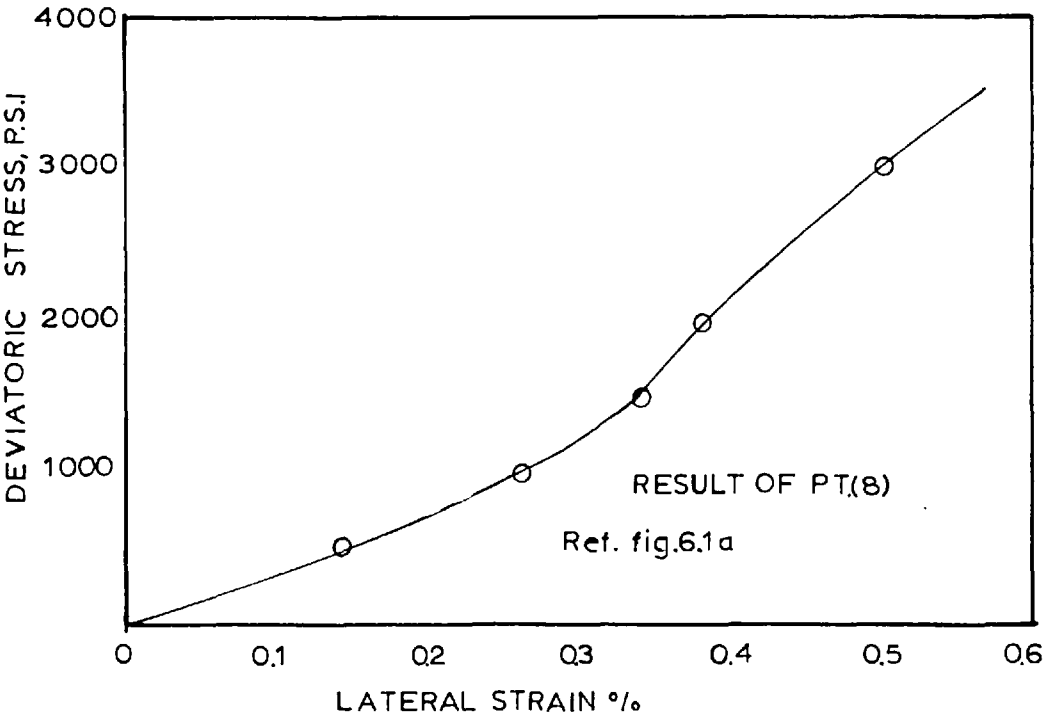

4000
3000
2000
1000
DEVIATORIC STRESS, P.S.I
RESULT OF PT.(8)
Ref. fig.6.1a
0
0.1
0.2
0.3
0.4
0.5
0.6
LATERAL STRAIN %

FIG.6.36

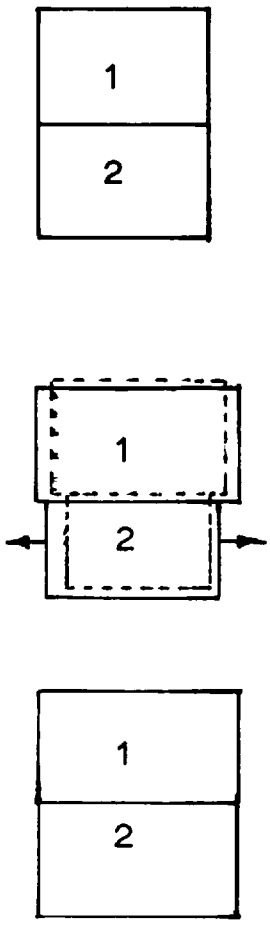
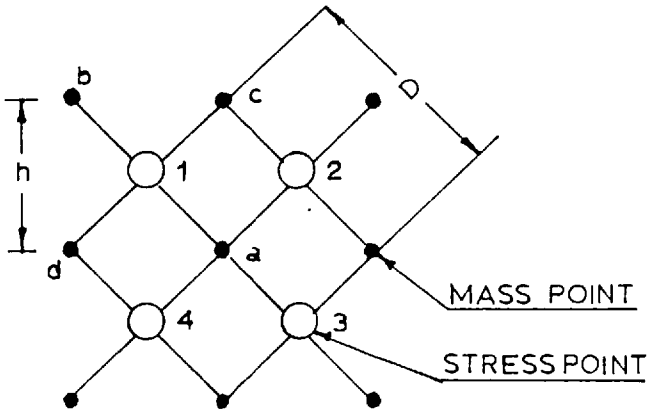


FIG.6.37





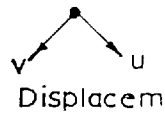
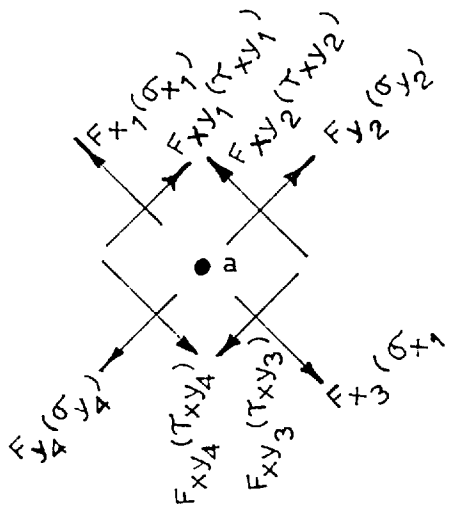


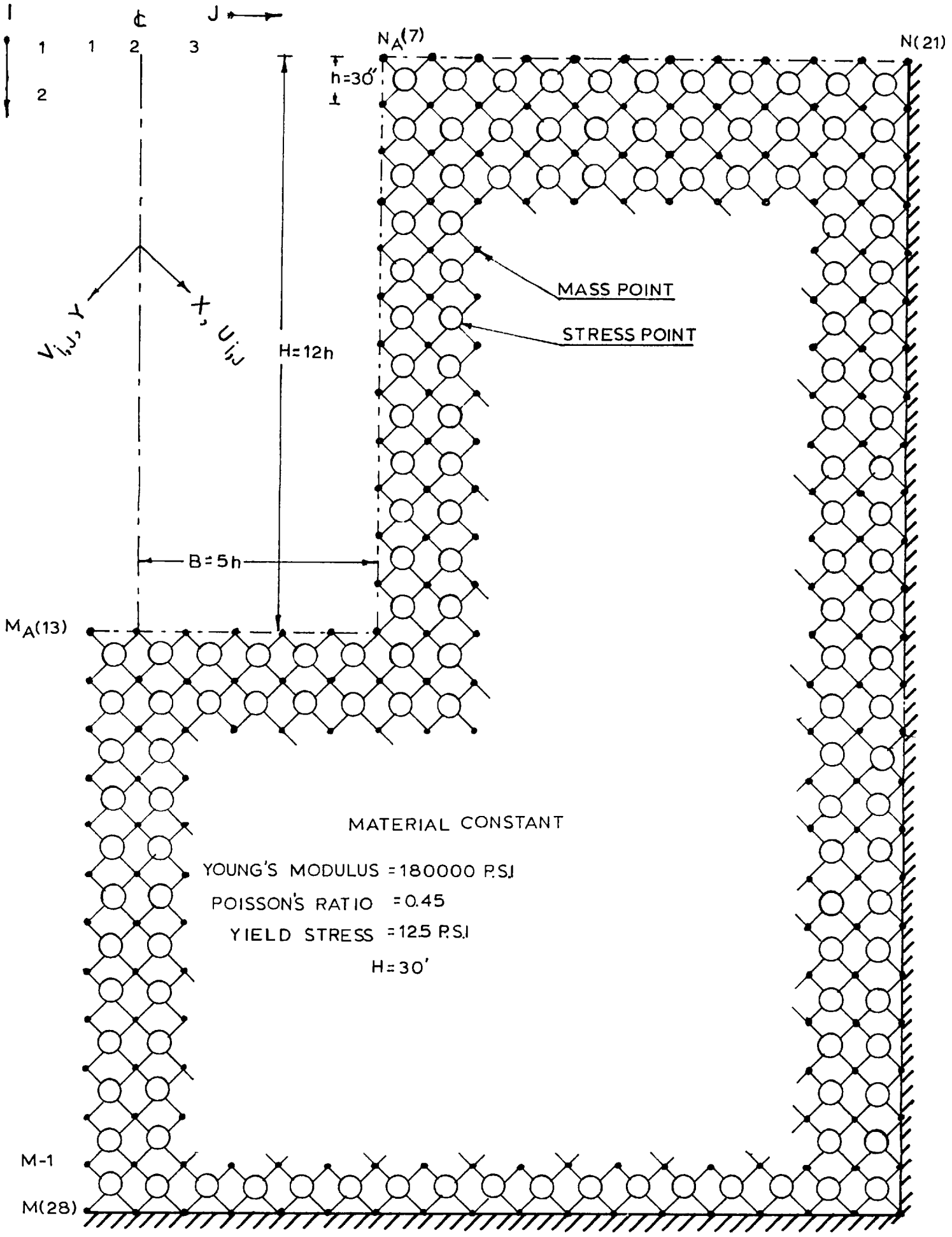
FIG. 7.1a



SIGN CONVENTION

stresses positive as shown on mass point

FIG. 7.1b FORCES (STRESSES) ACTING ON MASS POINT "a"



LUMPED PARAMETER MODEL

DIAGRAM SHOWING DIMENSIONS AND PROPERTIES OF MODEL USED IN PROBLEM

FIG. 7.2

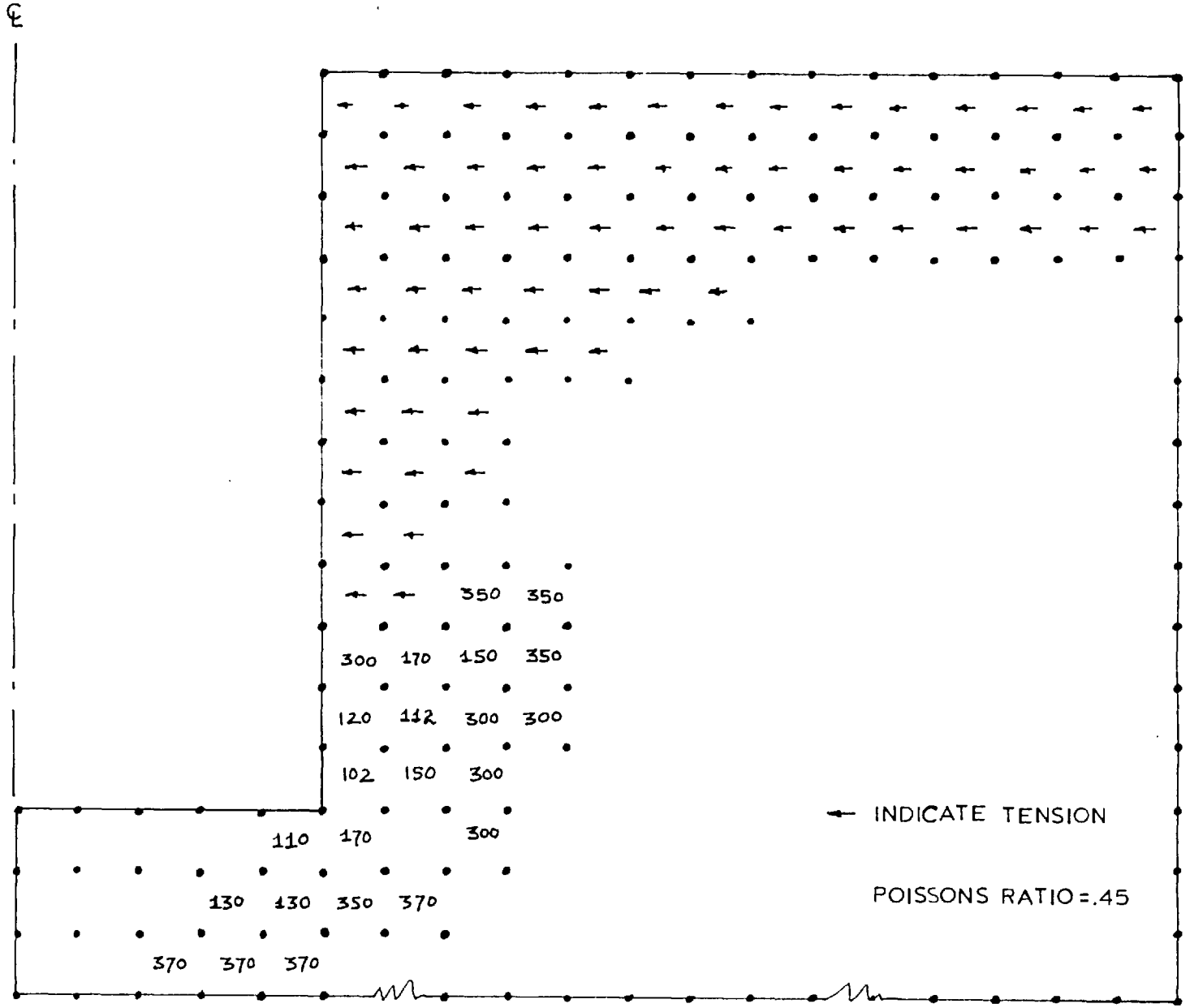


DIAGRAM SHOWING YIELDED STRESS POINTS AT DIFFERENT DENSITIES

FIG. 7.3

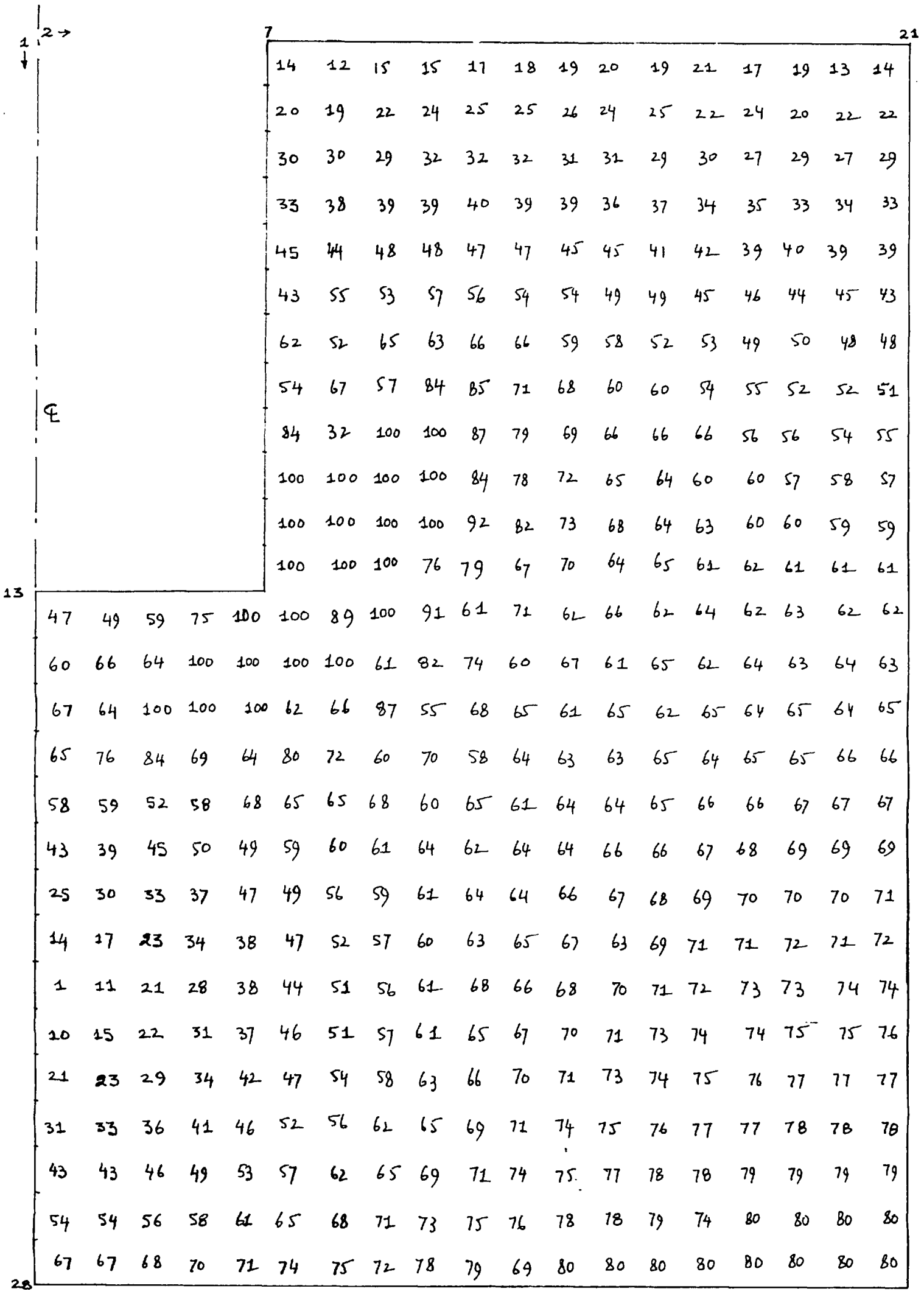


FIG.7.4 MAXIMUM SHEAR STRESS EXPRESSED AS % OF YIELD STRESS

(DENSITY = 370 LB./CU.FT.)

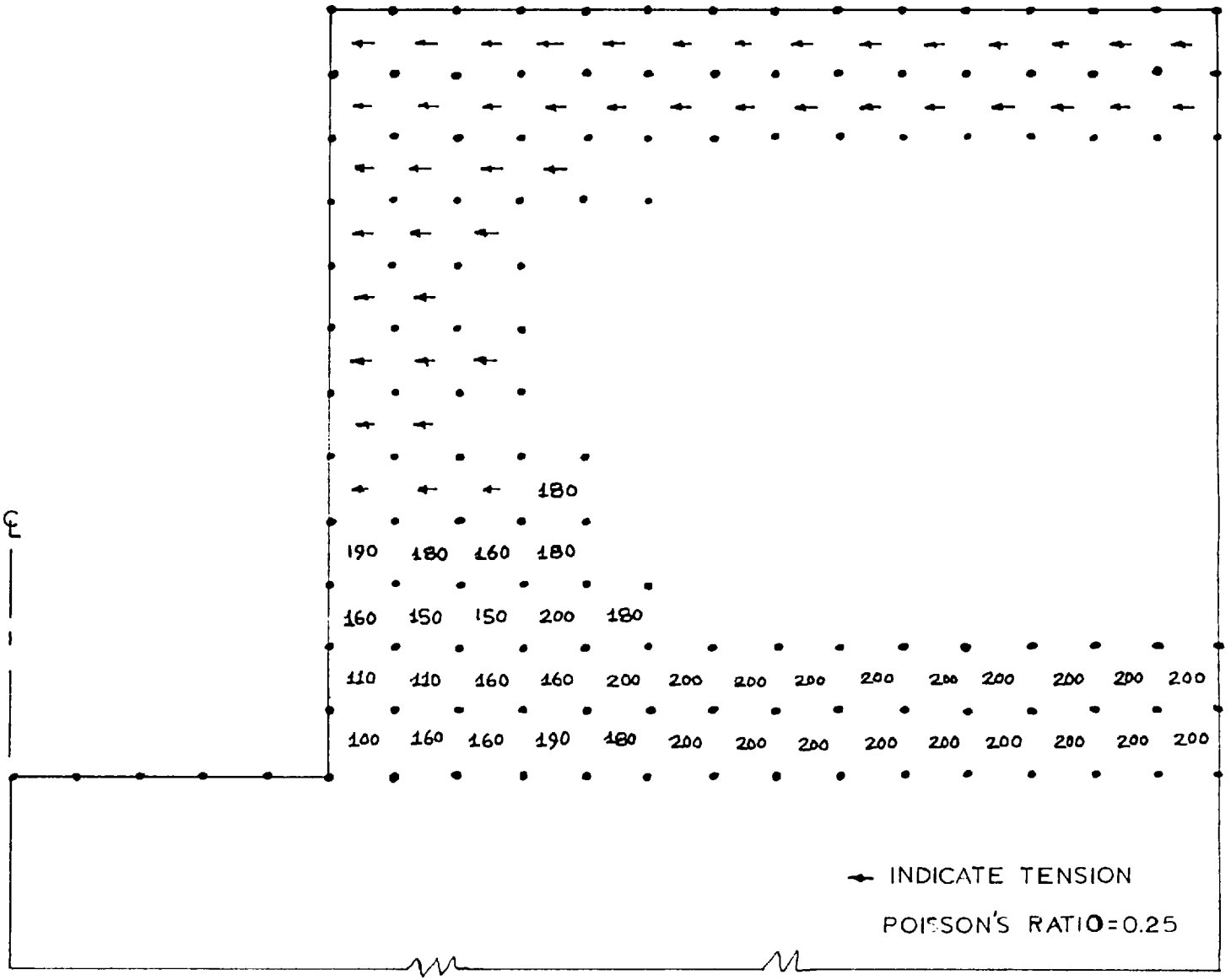


DIAGRAM SHOWING YIELDED STRESS POINTS AT DIFFERENT DENSITIES

FIG. 7.5

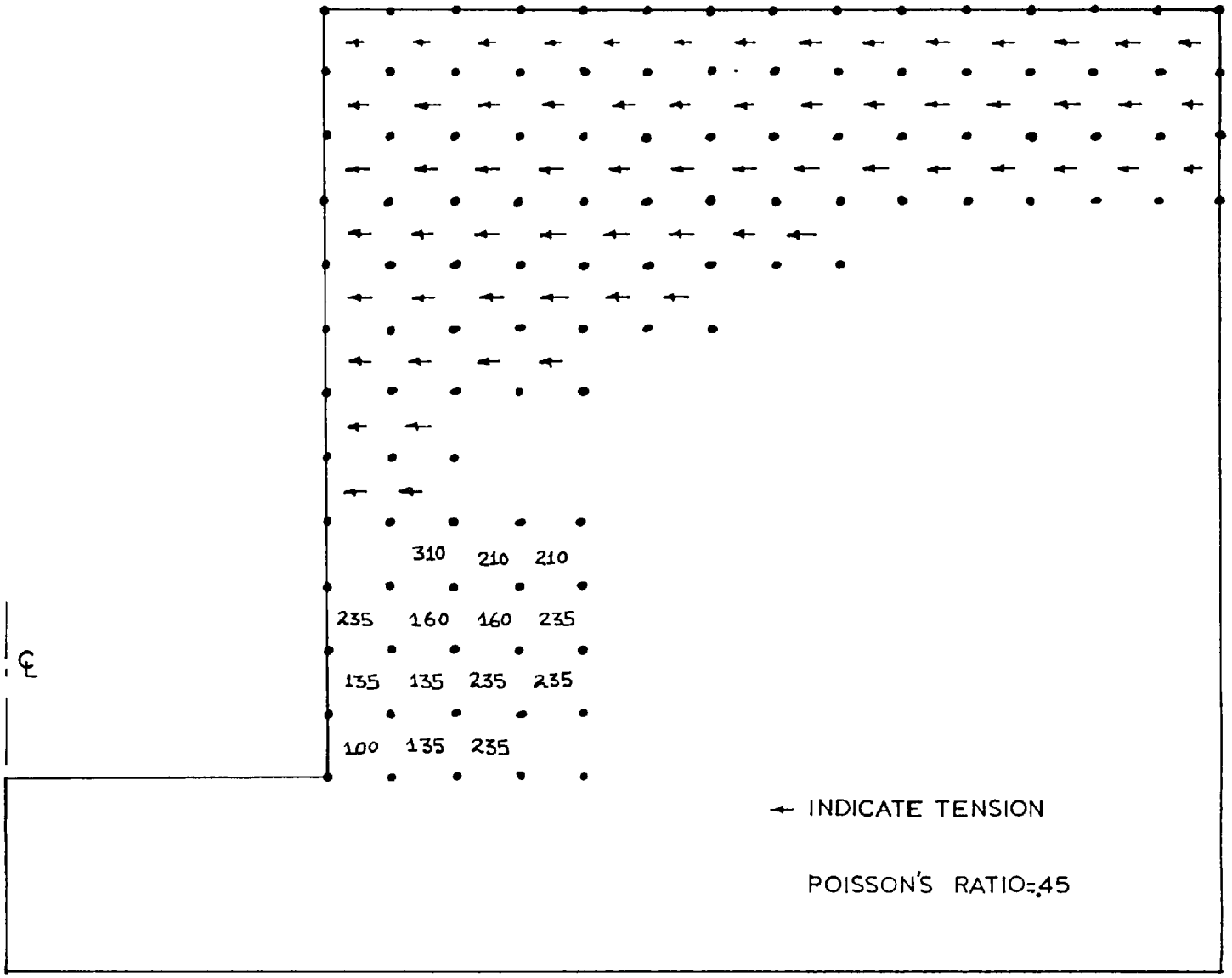


DIAGRAM SHOWING YIELDED STRESS POINTS AT DIFFERENT DENSITIES

FIG.7.6

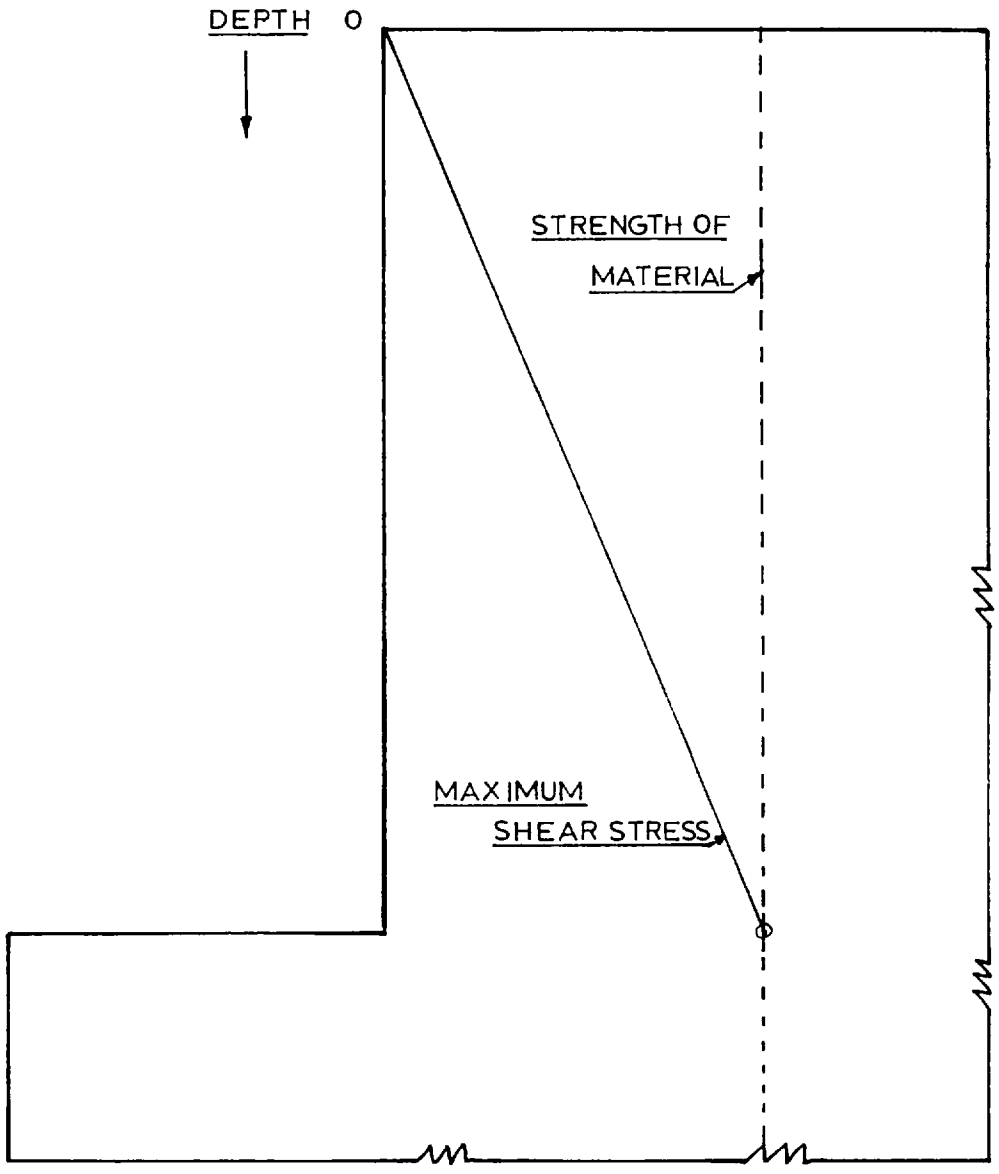
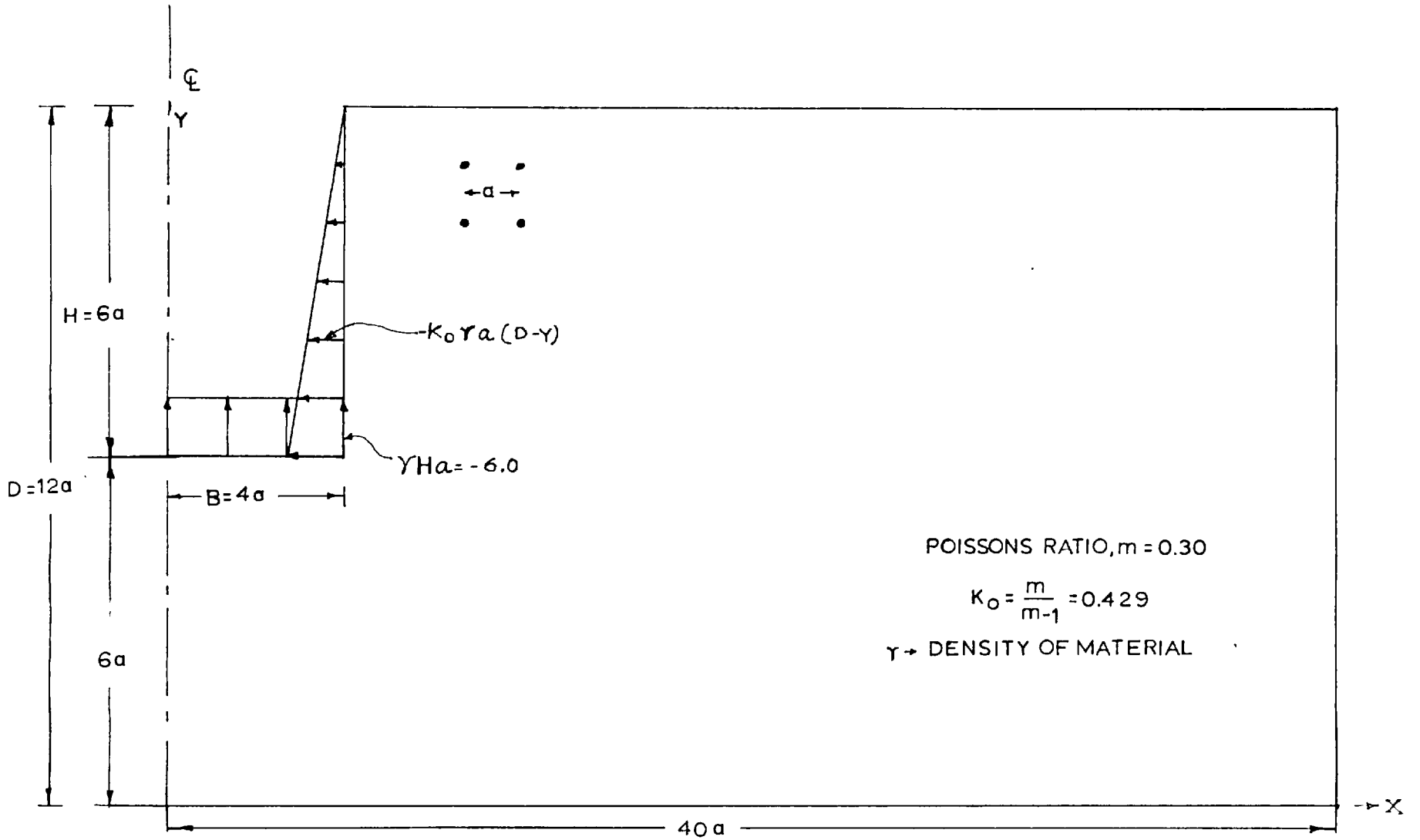
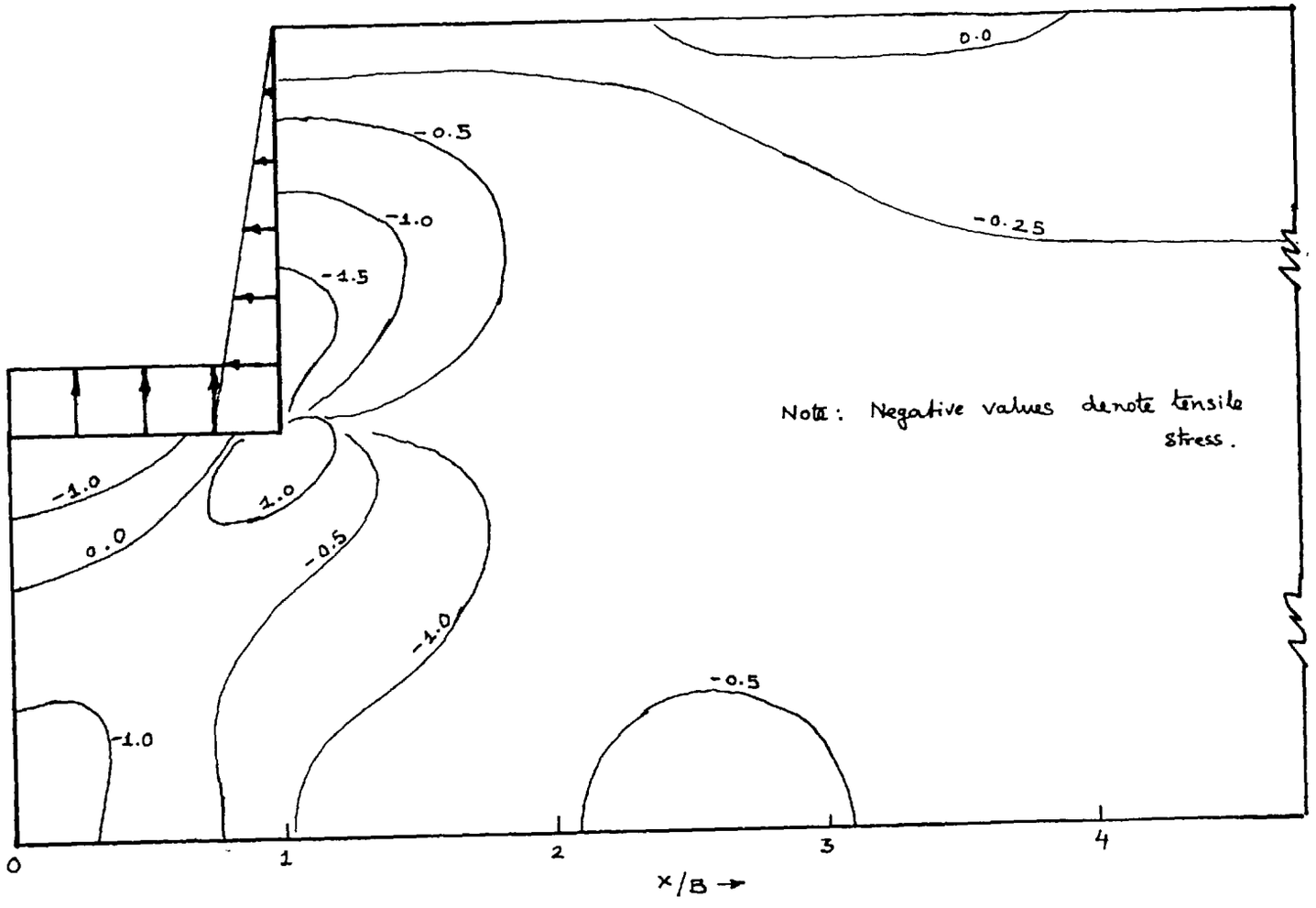


FIG.7.7



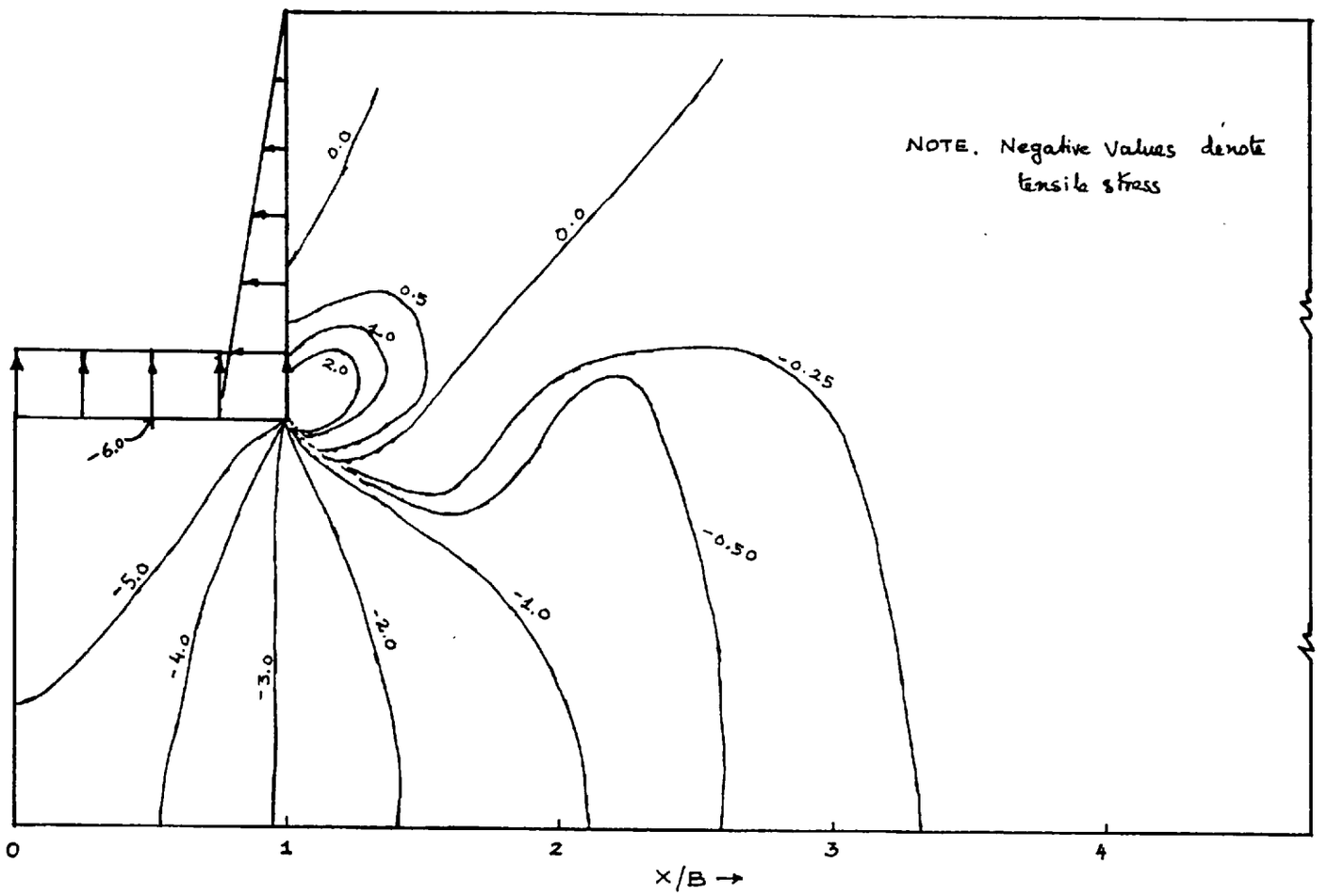
SAMPLE SOLUTION – PROBLEM GEOMETRY AND LOADING CONDITIONS

FIG. 7.8



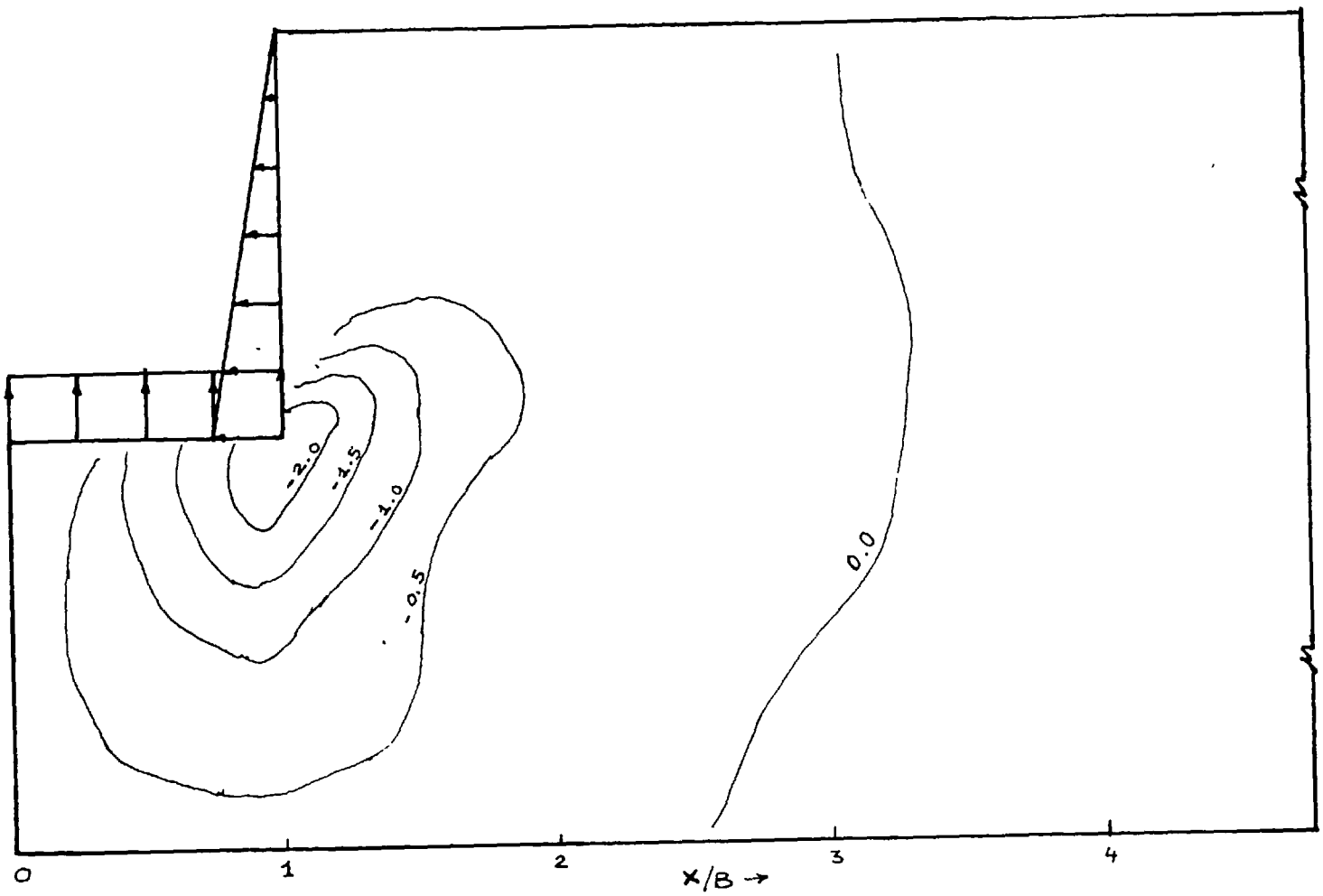
$\frac{\sigma_x}{\gamma a}$ STRESS due to loading shown in figure (7.8)

FIG 7.9



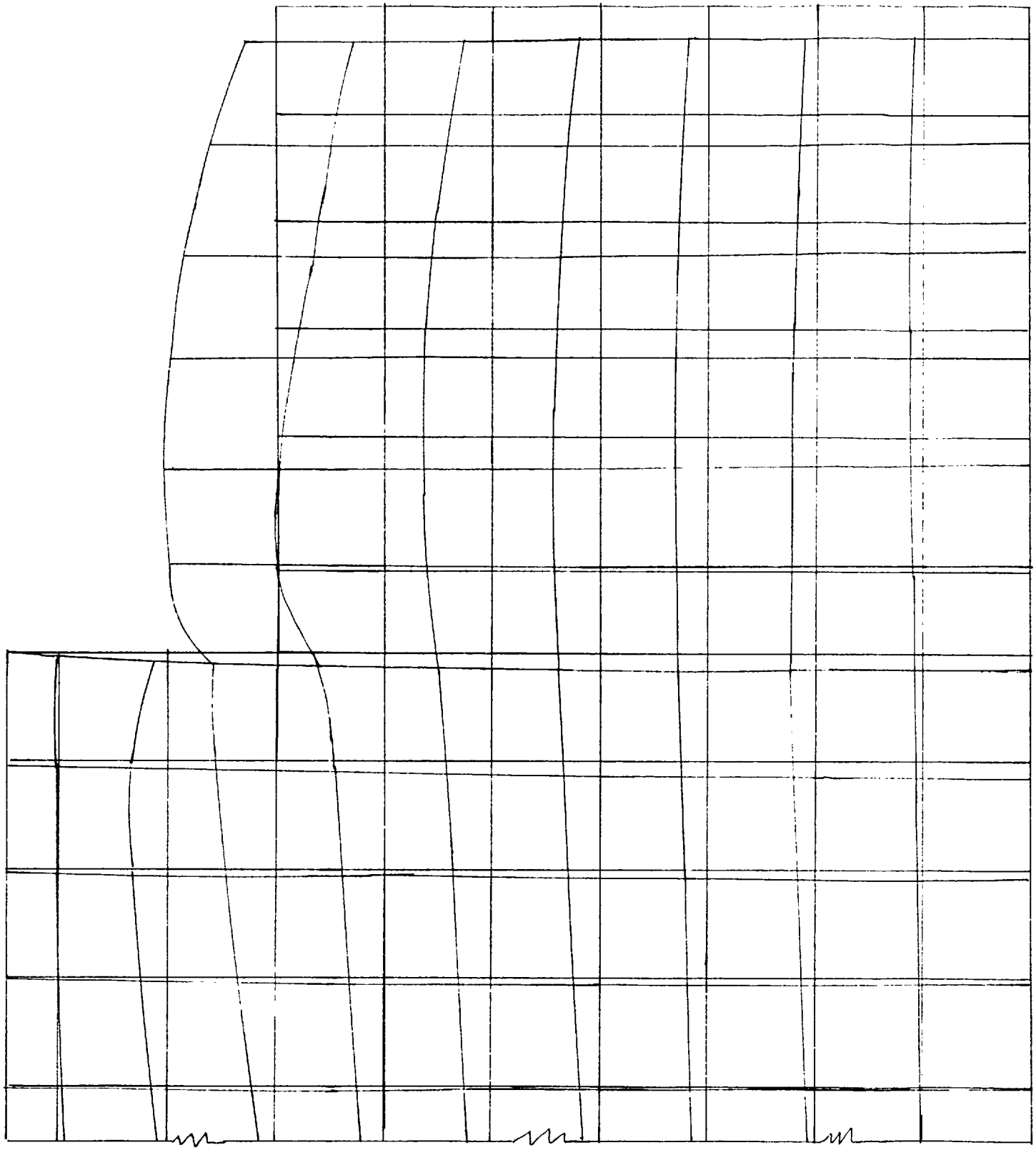
$\frac{\sigma_y}{\gamma a}$ STRESS due to loading shown in figure(7.8)

FIG. 7.10



$\frac{\tau_{xy}}{\gamma a}$ STRESS due to loading shown in figure (7.8)

FIG 7.11



SCALE:

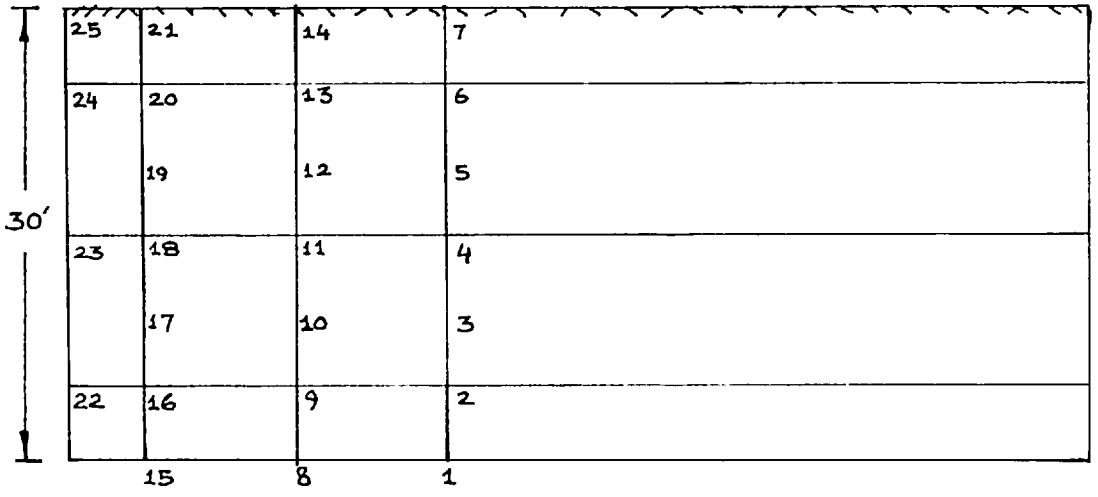
U/h 2×10^{-4}

V/h 2×10^{-3}

DISPLACEMENTS OF GRID POINTS

(expressed in dimensionless quantity)

FIG.7.12



MODULUS OF ELASTICITY = 10^7 P.S.I

POISSONS RATIO = 0.45

DENSITY = 100 LBS. PER. CU. FT

SAMPLE SOLUTION – GRAVITY STRESSES IN A SLOPE

FIG. 7.13

Node	σ_x (P.s.f)		σ_y (P.s.f)		τ_{xy} (P.s.f)	
	F.E.S.	L.P.S.	F.E.S.	L.P.S.	F.E.S.	L.P.S.
78	-1395.4	-1663.20	-2784.0	-2787.8	345.0	562.0
79	-1737.3	-1248.48	-2442.3	-2391.8	329.4	544.0
80	-1200.0	-858.24	-2024.7	-1984.3	233.1	562.0
81	-712.2	-514.08	-1563.9	-1546.5	138.3	512.0
82	-261.3	-214.00	-1070.0	-1080.0	58.8	436 0
83	176.0	198.00	-554.4	-599.0	8.7	288.0
92	-2217.6	-1684.8	-2886.3	-2724.4	534.0	518.4
93	-1565.4	-1144.8	-2463.9	-2433.6	494.4	643.6
94	-972.6	-653.76	-2113.8	-2085.1	298.8	714.2
95	-480.6	-325.44	-1674.3	-1622.8	113.7	648.0
96	-68.4	-115.2	-1092.9	-1111.6	-22.8	496 8
97	225.9	509.76	-546.6	-603.4	-63.3	326.8
106	-229.8	-2113.9	-3143.1	-2658.2	875.7	270 7
107	-1202.7	-604.8	-2838.6	-2620.6	691.8	1236.9
108	-233.1	-200.13	-1953.0	-2010.0	180.6	976 3
109	-113.7	-86.4	-1344.9	-1409.7	-46.5	660.9
110	-19.2	-17.2	-858.9	-953.2	-111.0	459.4
111	86.4	43.2	-424.1	-532.8	-79.8	267.8

NOTE : REF. FIG 7.13 FOR LOCATION OF NODES

F.E.S = FINITE ELEMENT SOLUTION (FINN, 1966

L.P.S = LUMPED PARAMETER SOLUTION

-VE COMPRESSION

FIG. 7.14 COMPARASION OF RESULTS - STRESSES IN A 30° VERTICAL SLOPE